THE GEOLOGY AND THE ALTERATION HISTORY OF THE GEITAFELL CENTRAL VOLCANO, SOUTHEAST ICELAND.

by

GUDMUNDUR OMAR FRIDLEIFSSON

A thesis presented
for the
Degree of Doctor of Philosophy

Grant Institute of Geology
Faculty of Science, University of Edinburgh

1983.

Declaration

I declare that all the work presented in this thesis is my own, except when stated otherwise, and that the thesis has been composed by myself.

TIL SIGRÚNAR

ABSTRACT

The Geitafell central volcano in SE-Iceland was formed within a rift zone in central Iceland, and was active for about 1 m.y. from approximately 6-5 m.y., slightly predating the SE-Iceland flexure zone.

The accumulated thickness of the tholeiite-suite strata, belonging to the volcano, is close to 2 km. The volcano consists primarily of tholeiitic lavas (~60%) and hyaloclastites (~30%) with less volumnious rhyolites (<10%). The hyaloclastites formed subglacially. The chronology of the stratigraphy, structure and intrusive events is provided and compared with the hydrothermal evolution of the volcano, which is evaluated by study of infilling sequences of mineral veins and amygdales, and their associated wall-rock alteration.

The volcano experienced 3 major structural events, (i) an uplift of the central region, (ii) a caldera subsidence, and (iii) a regional flexuring. Mapping of the intrusive rocks enabled the distinction of 12 major intrusive phases (I.P. 1-12), which include 2 gabbro intrusive events (I.P.2 and 10), 1 radial dyke swarm (I.P.3), 4 cone-sheet swarms (I.P.5,6,8,10), 2 acid intrusive phases (I.P.4 and 11) and 5 basaltic dyke swarms (I.P.1,7,9,10,12).

The establishment of a high-T hydrothermal system is found to relate to interactions between hot intrusive rocks and ground waters. The heat distribution into the hydrostatically controlled fluid system appears to have proceeded via supercritical and/or superheated hydrous fluids which existed within the hot intrusives, and also within gabbro contact aureoles.

A long period (possibly about 7-8 x 10^5 yrs) of cold ground water percolation predates the emplacement of the central gabbros (I.P.2),

prior to which a primitive low-T hydrothermal system was established due to a rise in the geothermal gradient within the volcano. A high-T hydrothermal system became active during I.P.2,3,4,5,6 and lasted until I.P.10 and 11 had been emplaced (estimated 2-3 x 10^5 yrs). Sanidinite facies hornfelses developed locally at I.P.2 gabbro margins, and were enveloped by aureoles of skarn mineral deposits. High-grade mineral assemblages, foreign to the host-rocks at shallow levels, similarly developed within the cone-sheets of I.P.5 and 6. A second major thermal boost accompanied the much later I.P.10, which resulted in new hornfelses and skarn deposits in gabbro aureoles, and extended the high-T hydrothermal activity within the volcano. After the relatively short intrusive episodes, the T-P of the fluid system was hydrostatically controlled and resulted in greenschist facies alteration, which principally involves two index mineral zones (i) an overlying epidote zone (fluid T ca. 230-300°C) and (ii) an actinolite zone (fluid T $\geq$ 300°C). The evolution of the high-T hydrothermal system is discussed in detail.

A low-T system (fluid T < 200°C) was established upon cooling after I.P.10 and 11. Flexuring of the volcano and I.P.12 accompanied the cooling period. The volcano and the flexure became buried by younger lavas erupted outside the volcano, and subsequently a regional zeolitization (fluid T $\leq$ 120°C) was superimposed upon all earlier formations.

CONTENTS

LIST OF FIGURES

LIST OF TABLES

MAPS

CHAPTER 1

GENERAL INTRODUCTION

1.1 Iceland

Icelandic geology has recently been reviewed in a special issue of Jokull (1979). The various topics of Icelandic geology are treated by several authors in this volume which was prepared in connection with the XXVI International Geological Congress in Paris, 1980 (to be published in the "Geology of Europe").

A summary of Icelandic geology relevant to the present study is presented below. This is largely based on papers by Saemundsson, and then Jakobsson; Simonarsson; Einarsson and Bjornsson; and Fridleifsson, I. B., in the review referred to above.

Iceland, located astride the Mid-Atlantic Ridge, is predominantly composed of basalt (80-85%) while intermediate and acid rocks constitute about 10% of the visible succession. Sediments, mainly of volcanic origin, account for some 5-10% in a typical Tertiary lava sequence , but are commonly much more abundant in Quaternary successions.

The exposed volcanic pile of Iceland ranges back in age to about 16 m.y. The oldest rocks are exposed in the extreme northwest and east, while the youngest rocks are located within the Neovolcanic Zones, which are separated into an axial rift zone and flank zones. The axial rift zone joins the Reykjanes Ridge in the southwest and the Kolbeinsey Ridge in the north. The stratigraphy of Icelandic rocks is conventionally divided into four principal groups: (i) Tertiary (Mio-Pliocene), 16-3.1 m.y.; (ii) Plio-Pleistocene, 3.1-0.7 m.y.; (iii) Upper-Pleistocene, 700.000-11.000±2000 yr.; (iv) Postglacial, 11.000 ±2.000 yr. - 0, (figure 1.1). The ages of these four groups are based on climatic evidence from interlava sediments or volcanic breccias and palaeomagnetic reversal patterns supported by radiometric age data.

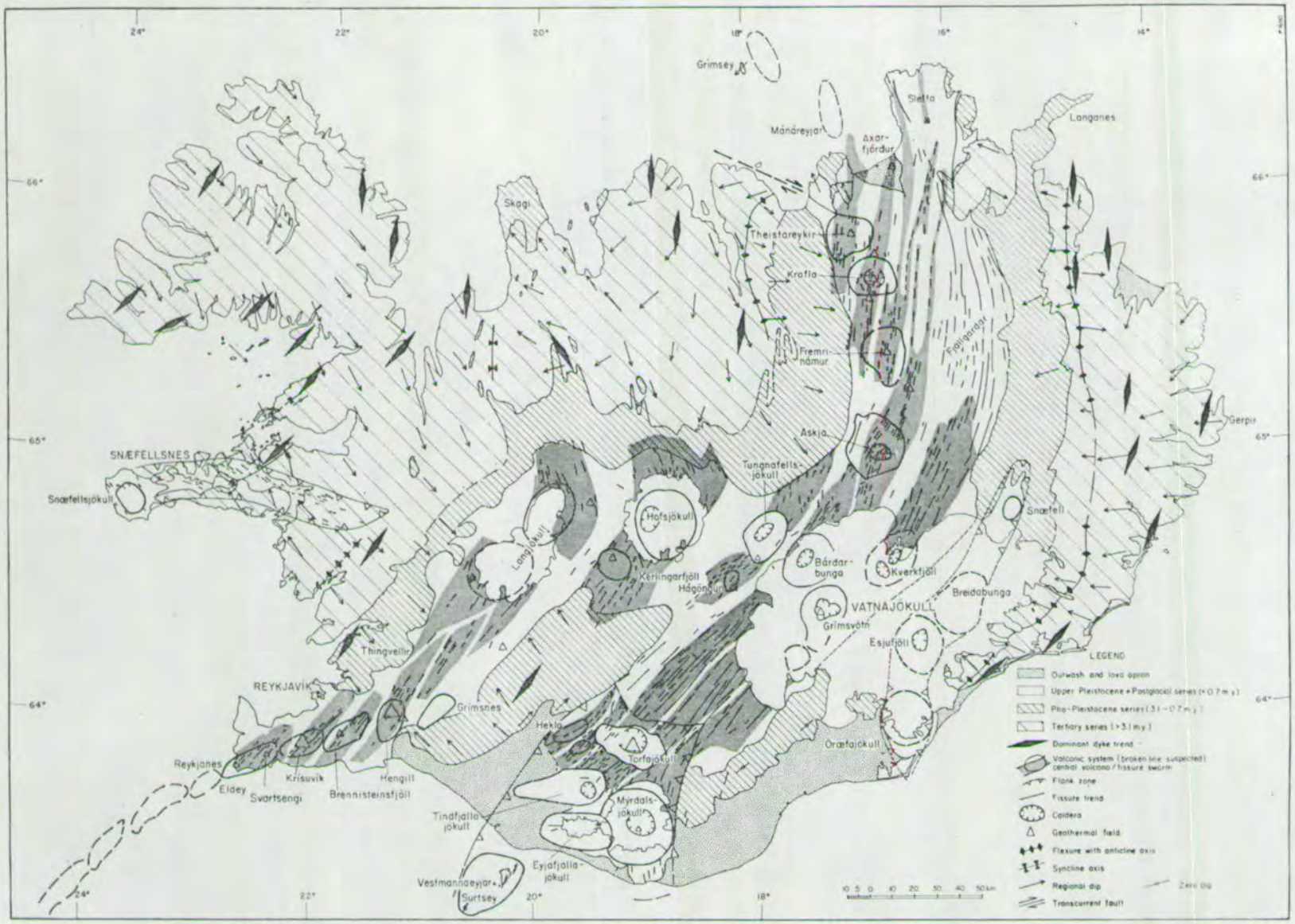

FIGURE 1.1. Stratigraphic and tectonic map of Iceland. From K.Saemundsson,1979.

Three main basic lava types are distinctive enough in the field to provide mappable stratigraphic units. These are: a) compound flows of olivine tholeiite, b) simple flows of tholeiite with little or no olivine, and c) plagioclase (and/or pyroxene) phyric flows (see Chapter 2.1). Some 60-70% of the acid rocks are found as lavas and intrusives while the rest is represented by pyroclastic material.

Throughout the Tertiary most of the basaltic eruptions can be classified among the three categories listed above. Intermediate and acid volcanism, as at present, is confined to central volcanoes; resulting ash-flow tuffs and airfall tuffs are interbedded in the plateau lava piles. Tertiary basic and acidic agglomerates or hyaloclastites are confined to the central volcano regions.

The boundary between Tertiary and Plio-Pleistocene rock series is somewhat arbitrarily fixed at the base of the Mammoth magnetic event (3.1 m.y. ago). At about this time, tillites first appear in the succession in southwestern and northeastern Iceland. The marked climatic cooling which occurred at this time is well documented in fossiliferous marine strata (Tjornes) and in interbasaltic lignite-bearing horizons elsewhere. During the formation of the Plio-Pleistocene series, tillites and fluvioglacial beds become frequent and subglacial volcanism produces pillow lavas and volcanoclastic breccias (hyaloclastites). These are interstratified with the lavas and indicate stages of cold periods during the Plio-Pleistocene. Studies of Tertiary plant remains indicate that the climatic changes that occurred at 3.1 m.y. were preceded by a period of cooling from upper Miocene into Pliocene (6-3 m.y.). Furthermore, it appears that in southeastern Iceland, ice-caps developed locally as early as 5 m.y. B.P. These probably formed on areas of high ground and high precipitation in the same way as e.g. the modern Vatnajokull.

The Upper Pleistocene Series is defined to include rocks formed during the Bruhnes magnetic epoch, from 0.7 m.y. ago, up to post-glacial times (9,000-13.000 yr. B.P.). The boundary with the underlying Plio-Pleistocene series is usually marked by an unconformity. The Upper Pleistocene volcanic rocks can usually be subdivided into, a) interglacial lavas, and b) subglacial pillow lavas and hyaloclastites.

The Postglacial Series includes lavas, pyroclastites, marine clays, fluvioglacial and fluvial outwash, off-shore hyaloclastites and soil formation. Some 24 volcanic systems have been active in postglacial time. One of these, the Krafla central volcano, located in the northeast axial rift zone, has been episodicly active since 1975. This volcanic episode has provided a unique opportunity to study the mechanism of rifting, the interplay between magmatic processes in the central volcano and associated fissure swarms, as well as the effects of magmatic/tectonic event on hydrothermal systems in two exploited hydrothermal fields.

Icelandic volcanic rocks predominantly belong to the tholeiite series. Volcanism throughout the Tertiary appears to have been fairly homogeneous genetically, as only rocks belonging to the tholeiite series have been observed. In the early Plio-Pleistocene only tholeiitic rocks appear to have been developed and then up to the present in the axial rift zone. The axial rift zone marks the trace of the plate boundaries where active plate growth is taking place. In the Pliocene, however (ca. 2.5 m.y. ago) three volcanic flank zones (Snaefellsnes, Vestmanneyjar-Tungna, Skagi) became active in addition to the axial rift zone. Early volcanism in these flank zones produced rocks belonging to transitionally alkalic series. In the

Snaefellsnes zone truly alkaline rocks succeed the "transitional" rocks from 0.7 m.y. to the present. In the Vestmann Islands alkalic rocks were produced during the Upper Pleistocene and Holocene.

The regional tectonics of Iceland have been drastically re-interpreted during the last decade or so. Synclines and anticlines (or flexures with anticlinal axes) occur in west, north and east Iceland (fig. 1.1). While these structural features have been used as evidence against ocean-floor spreading, the most recent ideas suggest that the synclines in west Iceland are remnants of a fossil axial rift zone. Some 6-7 m.y. ago, when volcanism ceased in the synclinal areas, a new rift zone may have formed further to the east and south at the site of the present-day Reykjanes-Langjokull axial rift zone. This shift of the rift zones resulted in the formation of an anticlinal structure in the Tertiary lavas in west Iceland (the Borgarnes anticline). In north and east Iceland a structural discontinuity occurs within the Tertiary basalts on both sides of the axial rift zone. The older sequence is downwarped (dips 20-30^{o}) below a younger unit (5 m.y.-present). In southeast Iceland the absence of such a discontinuity implies that the axial rift zone there remained unaffected. The monoclinal flexure in southeast Iceland crosses the field area under consideration and will be dealt with in later chapters.

The formation of the flank zones some 2.5 m.y. ago, accompanied by a change in the chemical composition of the volcanic products has already been mentioned.

The modern axial rift zones in Iceland exhibit structures, such as open fissures, grabens and crater rows on the surface with dykes and normal faults at deeper levels, while the flank zones are characterized by poorly developed rift structures. Fault patterns in a segment connecting the Reykjanes peninsula and the southern part of the

eastern volcanic zone indicate a component of sinistral shear (south Iceland seismic zone). The connection of the northeastern Iceland axial rift zone to the Kolbeinsey Ridge involves NW-SE trending wrench faults. One of these, the Husavik fault, has dextral shear and is regarded as showing true transform character. The active rift zone has N-S grabens and volcanic fissure swarms arranged in a dextral en echelon pattern (fig. 1.1). The transverse E-W zone across central Iceland has also been referred to as having transform character. The arrangement of fissure swarms and volcanic systems in the Snaefellsnes zone also indicates dextral shear. Furthermore the faults and fissures themselves suggest a component of extension.

The Mid-Atlantic-Ridge is characterized by high heat flow in the crestal region which decreases symmetrically away on either side until it reaches an average level for the oceans. Iceland, which forms a 500 km broad segment astride the ridge, falls entirely within the crestal anomaly. The regional heat flow ranges from some 80 mW/m^2 furthest away from the active volcanic zones, to about 300 mW/m^2 close to the margins of the axial rift zone. Geothermal gradients measured outside known geothermal fields vary from 37°C/km to 165°C/km.

Due to high heat flow and heavy precipitation in Iceland, extensive hydrothermal systems are formed. Conventionally the hydrothermal areas have been divided into two types based on the maximum temperature reached in the uppermost 1 km: low temperature areas <150°C and high temperature areas >200°C. The low temperature areas are located in the Tertiary and Plio-Pleistocene rocks, while the high temperature areas are located within the neovolcanic zones. Surface manifestations of the high temperature areas always occur within the volcanic systems and most often inside central volcanoes. Propylitization in the high temperature areas is often intense.

The high temperature areas are regarded as fed by fairly localized groundwater systems and are thought to receive heat from local heat-sources within the central volcanoes. By contrast the low temperature areas are fed by ground-water which percolates through porous rocks in the highlands and flows laterally along faults and pervious horizons for distances of tens of kilometres. These waters withdraw heat from the hot country rocks and some reappear on the surface along faults and dykes in the lowlands as hot springs.

Hydrogen isotope studies have shown that the waters in both types of hydrothermal areas are chiefly of meteoric origin. Notable exceptions occur in the Reykjanes peninsula where oceanic water is involved in two hydrothermal systems.

Mineral zones have been mapped from drill-holes and correlated with down-hole temperatures. In the low temperature areas, four zeolite zones are recognized; in order of increasing temperature: (i) chabazite; (ii) mesolite/scolecite; (iii) stilbite; (iv) laumontite (Kristmannsdottir and Tomasson, 1978). In the high temperature areas, four mineral zones have been mapped and correlated with down-hole temperature; in order of increasing temperature these are: (i) zeolites/smectites; (ii) mixed layer clay minerals; (iii) chlorite/epidote; and (iv) chlorite/actinolite (Palmason et al., 1979). General aspects of hydrothermal systems and the currently active hydrothermal fields in Iceland are discussed in Chapter 4 and 11.

Extensive mapping of earlier Tertiary and Plio-Pleistocene rocks initiated by the pioneering work of G. P. L. Walker in the 1950's in eastern Iceland, has revealed regional zeolite zones (fig. 1.2). These have a nearly horizontal disposition and are superimposed on tilted strata and their boundaries are believed to indicate geoisothermal surfaces. The zonal distribution, along with studies of dyke

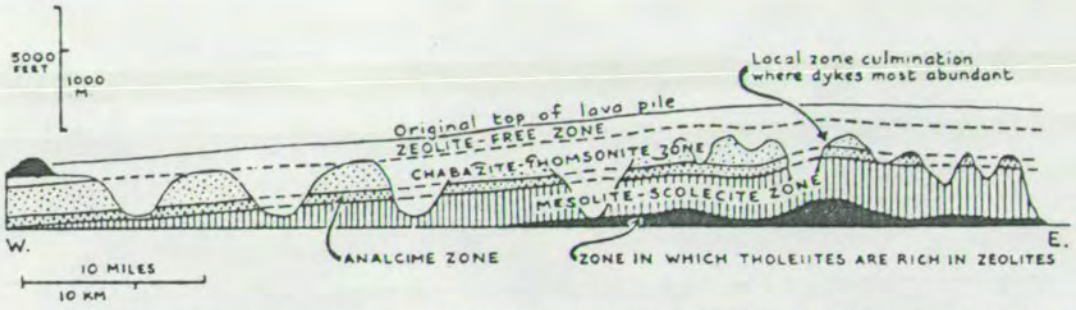

Diagrammatic section across the Tertiary lava pile in eastern Iceland showing the zonal distribution of amygdale minerals. The western end of the section corresponds to sections in upper Jökuldalur and Fljótsdalur; the eastern half corresponds to exposures in the Eastern Fjordlands. After Walker 1960.

FIGURE 1.2

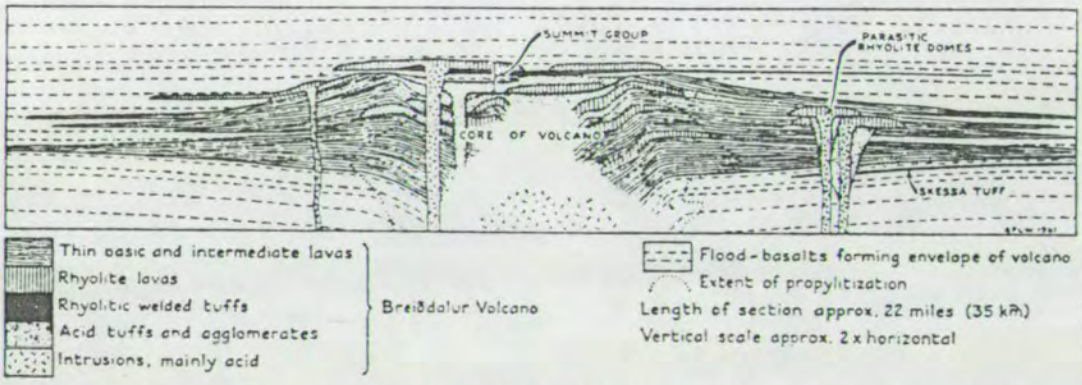

Schematic section through the Breiddalur Tertiary central volcano in eastern Iceland. Underlying and enveloping lavas are indicated. From Walker, 1963.

FIGURE 1.3

intensity, has made it possible to estimate the depth of the current erosional level below the original surface. Up to 1800 m may have been eroded in southeastern Iceland, some 1000 m in the eastern fjords and a few hundred metres on the northwest peninsula. The zeolite zones are, with increasing depth: (i) chabazite/thomsonite; (ii) analcime; (iii) mesolite/scolecite; and (iv) laumontite zone which is only visible at deep stratigraphic level where intrusive intensity exceeds some 10%.

The regional zeolite zones are disrupted in and near fossil central volcanoes by associated hydrothermal aureoles. More than 15 such volcanoes have been mapped, all showing propylitized cores. Intrusive rocks at shallow depth gave rise to hot water convection cells which result in hydrothermal alteration. The propylitized cores are thus regarded as the products of such localized thermal anomalies (or "hot spots") superimposed on the regional geothermal system. The study-area comprises one such palaeothermal anomaly associated with a former central volcano.

Structural relationships in Icelandic lava piles indicate that they grew as lenticular units from fissure eruptions fed by dyke swarms that were commonly localized about central volcanoes. The stratigraphic units thicken towards the central volcanoes and intermediate and acid rock become interbedded in the lava piles (fig. 1.3). The central volcanoes commonly develop calderas 5-10 km in diameter. Intrusive-dolerites (largely in the form of sheet swarms), gabbros and granophyres, are exposed in most of the eroded central volcanoes. Active periods of these volcanic systems have been found to vary from 300.000 years to over 1 m.y. They are preserved as entities in the regional volcanic pile, indicating that they grew, drifted off towards the margins of the current volcanic zones and then became extinct.

New ones replace them over the more or less stationary deep-seated zone of magma generation beneath the active rift zones.

1.2 South-East Iceland

The field area is located in SE-Iceland in the upper Hornafjordur region (fig. 1.5, map 1).

Knowledge of the regional geology of SE-Iceland has recently been reviewed and extended by Torfason (1979). The rocks are mostly older than 3.1 m.y. and central volcanoes are intercalated with plateau lavas as elsewhere in Iceland. In addition two prominent geological features occur in SE-Iceland. These are major intrusions of gabbro, granophyre and granite, some of which postdate the lava pile considerably, and a monoclinal flexure which runs from Breidamerkurjokull in the southwest, along the Vatnajokull ice-sheet some 250 km north to Vopnafjordur (fig. 1.4).

The major intrusions will not be discussed in any detail here, but Torfason (1979) suggests that some of them may be roots of off-axis stratovolcanoes superimposed on older rock formations. These stratovolcanoes may have been similar to the presently active Oraefajokull volcano in the off-axis zone of Snaefell-Oraefajokull (see fig. 1.1).

The monoclinal flexure crosses the present field area and its chronology is relevant to this study (Chapter 3). The regional dip in the eastern fjords is 6-8° at sea-level, diminishing upwards (Walker, 1959) and the flexure in southeastern Iceland is defined as the zone where dips of the lava pile are greater than 10° (Walker, 1964; Annels, 1967). Van Bemmelen et al. (1955) and Rutten et al. (1960), the first to describe the flexure, linked it to subsidence of the Neovolcanic zone (central graben). They assumed vertical

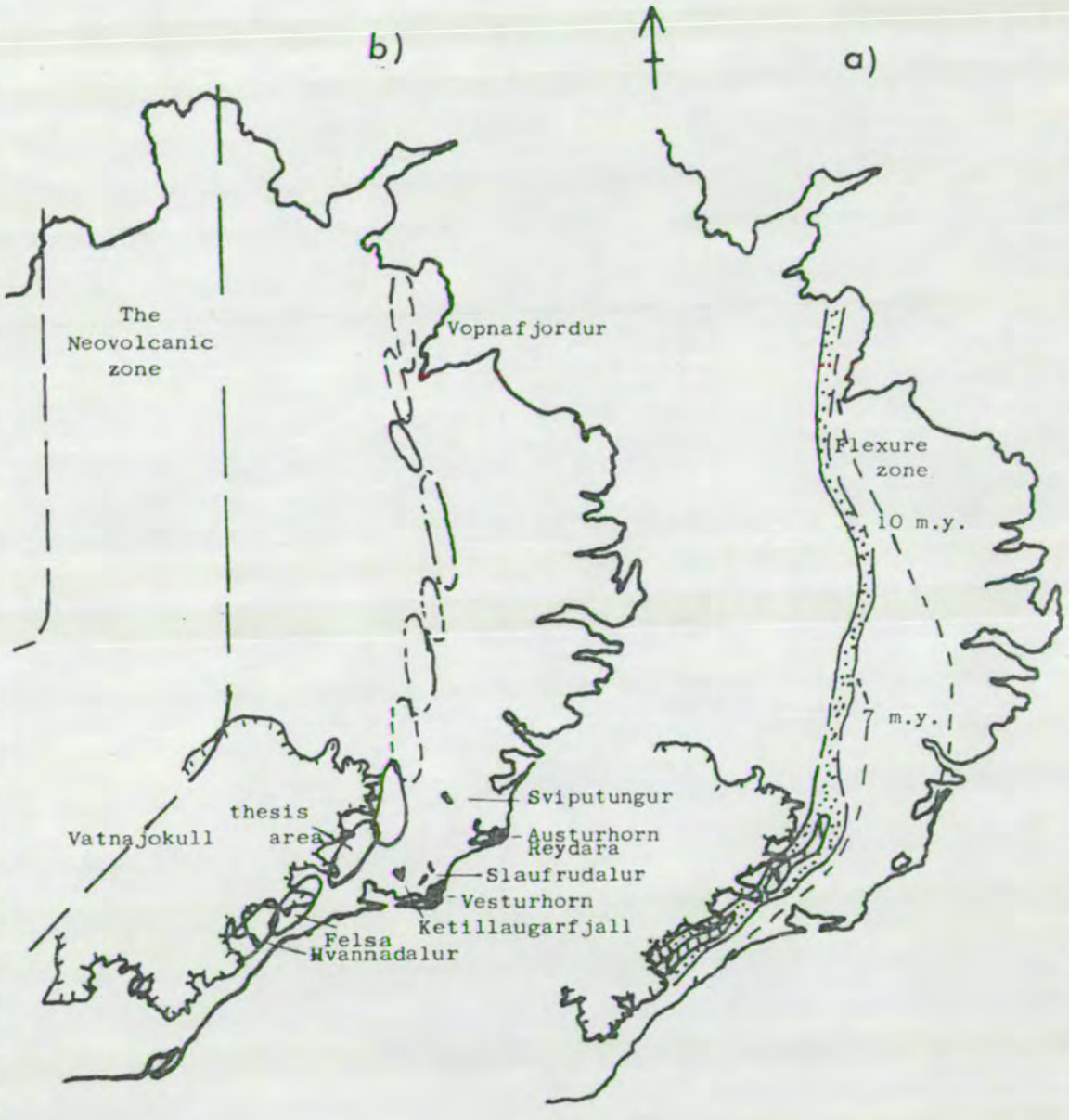

FIGURE 1.4. a) The flexure zone in eastern and southeastern Iceland, and b) the en echelon arrangement of it as proposed by Torfason, 1979.

The major intrusions in Sviputungur, Austurhorn, Reydara, Slaufrudalur, Vesturhorn, Ketillaugarfjall, Felsa and Hvannadalur are shown and the location of the thesis area. (Slightly modified from Torfason, 1979; lava isochrones from Saemundsson, 1979).

movements, but did not consider spreading. Walker (1964) believed the flexure was formed on the surface and that the abundant breccias and sediments were formed in a lake resulting on the downwarp side of the flexure. He also mentioned abundant major and minor intrusions occurring within the flexure zone and called it a tectonovolcanic flexure. Annels (1967) also agrees that the flexure had a surface expression and suggested that it was gradually overlapped by younger lavas from the west. He maps a 5° angular unconformity above the flexure zone and relates all the major and minor intrusions in the upper Hornafjordur region to this structural feature. Newman (1967) had a similar approach to Annels and concurred that both the flexure and the intrusions developed over the same period of the Tertiary. Ward (1971) and Saemundsson (1974) related the flexures to a shift in the volcanic rift zones from west to east at about 4 m.y. Walker (1974 , 1975b) and Watkins and Walker (1977) noted that the zeolite zones are themselves bent down in the flexure zone in eastern Iceland and could thus not have been expressed at the surface during accumulation of volcanics within the zone as was earlier suggested by Walker (1964). Walker (1974) suggested that the flexure zone was formed as a consequence of the increased density resulting from sheet swarms within the flexure zone, and stated that dips were less than 10° where sheets are scarce or absent, but commonly rise to 15-25° where sheets are abundant. Torfason (1979) in his regional review denied that there is any correlation between dip and intrusion intensity and referred to a number of places where dips exceed 20° although intrusive sheets compose less than 1% of the succession. However, Torfason emphasised Walker's (1974) evidence of zeolite zones bending into the flexure and agreed that the flexure could not have been formed on the surface during accumulation of the lava pile within it.

He also pointed out that the flexure is not parallel with the regional strike of the lava pile and that it shows an en echelon pattern (fig. 1.4). With evidence for some sheets postdating the flexure and age dates for the late Hvannadalur, Fellsa, Kjardalsheidi and Sviputungnahnukur major intrusions, which Torfason regarded as having formed some 40-60 km east of an active axial rift zone, he concluded that the flexure may have formed contemporaneously with these major intrusions at between 1.5 and 2.5 m.y. ago in Kalfafellsdalur area, and about 2.5-3.0 m.y. in Lonsoraefi,to the west and east of the present field area, but did not comment on its age further to the north. Torfason also considered that flexuring was accompanied by intense intrusive activity that gave rise to shallow dipping sheets in addition to the major intrusions referred to above.

Yet another interpretation of the flexure, as it affects the study area, will be given in Chapter 3.

1.3 Field Area

The field area is located in upper Hornafjordur region (fig. 1.5 and map 1). The volcanic pile is of Tertiary age (5-6 m.y. old) and was deeply eroded by glaciers during Pleistocene. Valley glaciers from the Vatnajokull ice-sheet are still present and one of them, Hoffellsjokull, dissects the field area. Two glacial rivers from this glacier split the area into three mountainous areas; (a) Vidbordsfjall-Graenafell, (b) Svinafell, and (c) Hoffellsfjall-Grasgiljatindur, separated by broad braided-rivers and fluviatile plains at 50-60 m altitude. The Vidbordsfjall-Graenafell in the SW has steep slopes up to some 400 m altitude with gentle slopes above, reaching up to 663 m in Graenafell. Svinafell (362 m) lies between the rivers. The Hoffellsfjall-Grasgiljatindur mountains in the NE rise steeply from

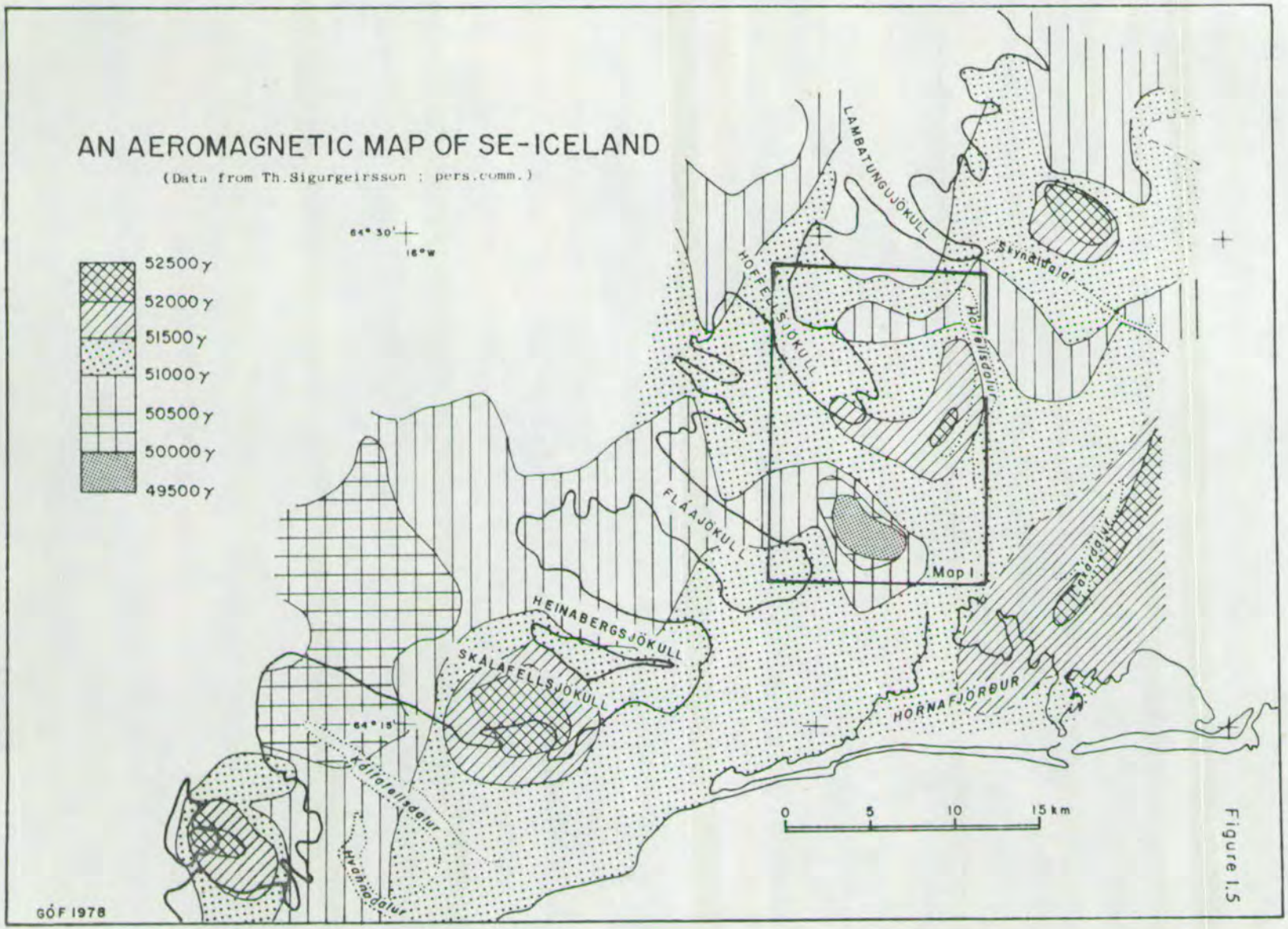
AN AEROMAGNETIC MAP OF SE-ICELAND
(Data from Th.Sigurgeirsson ; pers.comm.)
64° 30'
16°W
52500γ
52000γ
51500γ
51000γ
50500γ
50000γ
49500γ
LAMBATUNGUJÖKULL
Svínafellsjökull
HOFFELLSJÖKULL
Hoffellsdalur
FLÁAJÖKULL
Map I
Lónsdalur
HEINABERGSJÖKULL
SKÁLAFELLSJÖKULL
HORNAFJÖRÐUR
64° 15'
Kálfafellsdalur
Hrútárdalur
0
5
10
15 km
GÓF 1978

Figure 1.5

the plains. They form a N-S ridge, culminating at 1267 m, which is deeply incised on its western side by six NE-SW striking ravines. The northward striking valley of Hoffellsdalur bounds the ridge to the east. The mapped area covers some 150 km^2.

Apart from passing remarks on this area in older literature, the first serious geological study of the area was done by Jonsson (1954). His work, later supported by palynological studies (Jonsson, 1954, 1955, 1978; Schwarzbach, 1955; Schwarzbach et al., 1957) suggested that the Hornafjordur rocks are of Upper Miocene to early Pliocene in age. However, the first detailed maps of the area were presented by Annels (1967) and Newman (1967). Annels mapped the general geology, while Newman was mainly concerned with the major intrusions. Both of them also mapped a large area to the south (Ketillaugarfjall-Setbergsheidi) and a major intrusion in Hvannadalur, some 40 km away to the west. Their conclusion on the thesis area was that all the major and minor intrusions were formed more or less simultaneously with the flexure zone. Annels noted the difference in average lava flow thicknesses from Hoffell (8.3 m) and Setbergsheidi (10-10.8 m) and believed the difference was due to active flexuring during the eruption of the Hoffell lavas. He also regarded the hyaloclastites in the area to be formed within a depression caused by the flexure and noted that the onset of Pleistocene glaciation was recorded by tillites overlying the hyaloclastites.

Both Annels and Newman described extensive secondary alteration of the volcanic rocks. Annels mapped several mineral zones (calcite-, chlorite-, epidote- and garnet-zones), and Newman described the gabbro alteration and showed zonal arrangement of several minerals. Their work provided the impetus for the present study.

As noted above, both Annels and Newman associated the intrusive

complex with active flexuring. Whereas Annels also described and mapped two volcanic centres where felsitic intrusions are located (in Efstafell and in a ravine between Vidbordsfjall and Graenafell, map 1), he did not recognize that the whole area represented a deeply dissected central volcano comparable to others in the east and southeast of Iceland, like Breiddalur (Walker, 1963), Thingmuli (Carmichael, 1962, 1964, 1967) and Alftafjordur (Blake, 1964). It was, however, realized in the early stages of mapping the zones of alteration that the whole area, from Vidbordsfjall to Hoffellsfjall, is a collapse structure characterized by intense intrusive activity and propylitization, with associated rhyolitic/granophyric rocks, of the sort typically found in dissected calderas of the central-type volcanoes.

Torfason (1979) mapped large areas in SE-Iceland, including a central volcano in Kollumuli (NE of the present area) and reviewed earlier studies. Torfason, however, incorrectly cites Annels (1967) as having described a central volcano, which Torfason calls the "Hoffell central volcano". An important part of the present study is concerned with evaluating the two possibilities, whether the intrusives in Hornafjordur are (a) "related to" the flexure, or (b) a central volcano situated along the zone of weakness (deep-seated faulting?) either pre- or postdating the flexuring event.

Annels (1967) marked the onset of Pleistocene with tillites overlying the hyaloclastites in the region. According to the current chronological scale this meant that the rocks above the tillites were younger than 3.1 m.y. However, he contradicts his general conclusion, referring to age dating by Wensik (1960?) and Gale et al. (1966), stating: "It thus appears that this glaciation began at least 3.1 m.y. ago and probably near to 5 m.y. ago. A Pliocene glaciation may therefore have to be invoked" (Annels, 1967, p. 84). His general conclusion

however, on the onset of Pleistocene, has not been accepted. Torfason (1979) supports, by new radiometric dating, Jonsson's (1954) belief that Pliocene glaciation developed in SE-Iceland and gave rise to tillites back to ca. 5 m.y.

The present argument concerning the tillite chronological argument remains with the formation of local Early-Pliocene icecaps in SE-Iceland. The stratigraphic succession, however, has every characteristic of the Plio-Pleistocene rock series described by Saemundsson (1979) with interbedded tillites and hyaloclastites. It was shown in section 1.1 that the four main stratigraphic rock series in Iceland, "Tertiary, Plio-Pleistocene, Late Pleistocene and Postglacial", have their distinctive characteristics. The boundary between Tertiary and Plio-Pleistocene rock series was somewhat arbitrarily fixed at 3.1 m.y. at the Mammoth magnetic event, at the time where tillites appear in southwestern and northeastern Iceland (Saemundsson, 1979). From the chronological point of view this boundary has to be drawn as in figure 1.1 for SE-Iceland. From the stratigraphical point of view, however, it would be natural to draw this boundary back to the lowest tillites and regional hyaloclastites. That would necessitate that the whole Pliocene period (back to ca. 5 m.y.) is included within the Plio-Pleistocene rock series; in other words, that the boundary between the two series cannot be fixed at 3.1 m.y.

Moving the boundary back to 5 m.y. receives some support from other regions in Iceland. Climatic cooling is recorded from Late Miocene-Early Pliocene (6-3 m.y.) plant remains in west Iceland (Simonarson, 1979). Apparent fluvioglacial deposits are also found in west Iceland in strata older than 3.1 m.y. (Johannesson, 1975 and pers. comm.). A local glaciation in SE-Iceland during the whole Pliocene period, due to elevated topography and heavy precipitation

similar to the present situation is, therefore, by no means the only alternative explanation. Preglacial topography in Iceland must have been considerably different from the present. Assuming drift, the tillite and hyaloclastite succession in SE-Iceland was located near the middle of Iceland above a productive axial rift zone. Elevated topography over at least a part of the axial rift zone, would then have to have been the case. It is therefore suggested that the Icelandic stratigraphic chronological scale be modified to four general categories:

a) Miocene (from 16-5 m.y.) instead of Tertiary (16-3.1 m.y.)

b) Plio-Pleistocene (from 5.0-0.7 m.y.)

c) Late Pleistocene (from 0.7 m.y. - 11.000 ± 2.000 years)

d) Postglacial (last 9.000 - 13.000 yrs.).

Descriptions of hypabyssal intrusions (sheets and dykes) are provided by both Annels (1967) and Newman (1967). Annels noted at least two sets of cone-sheets centred about the main gabbro intrusions, and observed that they vary from aphyric basalt (or dolerite) to highly porphyritic types. He commented also on the contrasted behaviour of basic sheets according to whether they intrude lavas or fragmental rocks (particularly hyaloclastites). In the former they tend to be regular but in the hyaloclastites their form and directional trends are highly irregular. Newman, too, recognized at least one dolerite cone-sheet swarm intimately associated with the gabbro intrusions. Newman claimed that, while most of the sheets and dykes are tholeiitic, some dykes contain some olivine (both modal and normative) and are therefore olivine tholeiites. No clear age relationship was recognized between the tholeiite and olivine tholeiite intrusions. It is, however, difficult in the field to distinguish the one from the other and he therefore classified the sheets on grain size and

relative abundance of plagioclase phenocrysts into three groups: 1) dolerites, 2) porphyritic dolerites, and 3) basalts. He concluded that they were intruded in the age sequence 1)-3). Description of the petrography, mineralogy and (some) chemistry are also provided by Newman (1967). However, despite the abundance of detail listed by both Annels and Newman, their descriptions of the overall chronological relationships are quite inadequate to be used as a basis for this study of the hydrothermal processes that affected the rocks. Consequently, the volcanic complex had to be partly remapped. The boundaries of the gabbros remain more or less unchanged from those shown on Newman and Annels' maps; Annels' mapping of the higher parts of the flank areas has also been accepted without modification. The main changes in the present map include the introduction of two hyaloclastite units instead of one (Annels, 1967) with a basalt lava unit between them, and most significantly, the introduction of a caldera fault.

The field work was done from mid-June to early September in 1977, 1978 and 1979. Most of the time was spent on the Hoffellsfjall-Grasgiljatindur mountain ridge on which the deeply dissected ravines provide excellent sections into the complex. Use was made of topographical maps (U.S. army sheets 6120 I and II), aerial photographs (R.A.F. 1945, U.S.A.F. 1961, and L.I. 1975), and geological maps (Annels, 1967 and Newman, 1967).

The principle aims of the study were, a) to establish the general aspects of the hydrothermal system and the nature of the hydrothermal alterations, and b) to interpret the physico-chemical aspects of the alteration (propylitization). However, as a preliminary, it was necessary to revise the stratigraphy, to establish the chronological sequence of eruptive and tectonic events, and to determine the overall pattern of faulting and jointing.

Some 500 thin sections were used to study the rock alteration and about 1000 microprobe analyses to support mineral identification and to study the mineral chemistry.

The general result of the study shows that the volcanic complex occurs within a central volcano. This volcano, Geitafell Central Volcano, is named after an early gabbro intrusion in Geitafell, which shows much of the volcano's evolutionary history. Late in the volcano's history a caldera collapse occurred, attended by intrusion of gabbro and felsite and eruption of rhyolitic flows. Hydrothermal activity ceased after the caldera event, and flexuring followed. Emplacement of thick (2-10 m) brown dolerite dykes followed the rhyolite eruptions near the end of the flexural event. The volcano was subsequently buried by tholeiite, olivine tholeiite, and porphyritic lava flows, which subsequently became zeolitized. Sometime during the Pleistocene, a glacial valley was carved down to deep levels in the middle of the volcano; the valley was subsequently filled by fluvioglacial sediments covered by hyaloclastites, which include pillows and brecciated columnar-jointed lava masses. These late volcanics are presumably erupted from sites outside the central volcano. Later glaciers eroded the volcano further down to sea-level, with the residual high-ground masses being largely erosional remnants of the volcano's flanks.

CHAPTER 2

STRATIGRAPHY

2.1 Introduction

The main aspects of Icelandic central volcanoes was presented in Chapter 1. Apart from the rock types encountered in these volcanic centres, geochemical studies hitherto have shown the Tertiary volcanic rocks to be of tholeiitic affinity (olivine tholeiite, tholeiite, basaltic andesite , andesite (icelandite), dacite and rhyolite).

Annels (1967) and Newman (1967) studied the geochemistry of volcanics in the Geitafell Central volcano and concluded that these rocks also belonged to the tholeiite family. They noted the bimodality of the rock types, predominantly tholeiite and rhyolite. Rocks of intermediate composition were found forming a few dykes, "lava masses" in hyaloclastite in Efstafell and Sandmerki and one lava flow at a low stratigraphic level in Hoffellsfjall are mentioned.

No further petrochemical studies have been made during this research. However, from field characteristics, it is clear that rocks of intermediate composition become increasingly abundant in the upper stratigraphic units of the volcano. The presence of such intermediate rocks lends support to a model of a central volcano.

The field key used to distinguish lava types in Icelandic strata was initially presented by Walker (1959) and later supported and modified by geochemical studies (Carmichael, 1964). Three basic lava types are distinguished:

1. Compound flows of olivine tholeiite
2. Simple flows of tholeiite with little or no olivine
3. Plagioclase (and/or pyroxene) porphyritic flows.

Gradations exist between the three. The olivine tholeiites often produced lava shields which are seen as thick pahoehoe flows consisting of thin flow units. The olivine-poor tholeiites are commonly fissure-

erupted as lavas. Central volcanoes erupt both types but the latter are more abundant, forming unusually thin flows (central-type tholeiites). The porphyritic lavas (3) are commonly erupted from fissures and are often the most voluminous flows erupted in single eruptions (Saemundsson, 1979).

Basaltic andesites lie compositionally between tholeiite and andesite (icelandite). Basaltic andesites are commonly thicker than tholeiites, are finer grained and often have bimodality of grain-size of the Fe-Ti oxide minerals (Carmichael, 1964).

Field characteristics of andesitic lavas (icelandites) were described by Walker (1959, 1963) as being transitional in character between rhyolite and tholeiite. They are dense, dark rocks with more or less conchoidal fracture and have a prominent flow structure. A distinct sheen is seen on fractured surfaces owing to parallelism of minute plagioclase crystals. While flow structure of the tholeiites is normally parallel to the base of the flows, the flow structure in the andesites is often conspicuously folded or contorted.

Studies of pillow lava sequences in Iceland (Fridleifsson, I. B. et al., 1982) have shown that magma chemistry affects the pillow dimensions greatly. Pillows of dacite to rhyolite composition are larger than basaltic pillows and show irregular (often lobe-like) bodies with a diameter of up to several tens of metres.

Rhyolite lavas are easily distinguishable in the field on colour basis alone. They show prominent flow banding, most often folded and contorted. Pitchstone at the base and top of these flows is common.

The revised stratigraphic map (Map 1, backcover) also shows the general structure of the volcano and the generalized setting of minor intrusions. The strata young to the NW.

Panoramic photos of the field-area can be seen in figs. 2.1 and 2.2 where the position of topographical localities referred to in the

Figure 2.1. View from Vidbordsfjall to the NE. Hoffellsjökull (glacier) from the Vatnajökull icesheet. The Svinafell area is the "island" in the sandur outwash plain, extending into the glacier along Öldutangi (ridge). Jökulfell (green hyaloclastite underneath the light brown rhyolite) is seen furthest to the left. In the background the ridge Hoffellsfjall - Grasgiljatindur is seen. The location of the ravines are marked with arrows on the overlay, from right : Kraksgil, Midfellsgil, Geitafellsgil, Efstafellsgil, Thverargil and Austurgja, separated by : Tungufell, Midfell, Geitafell and Efstafell (incl.Thverargil) respectively.

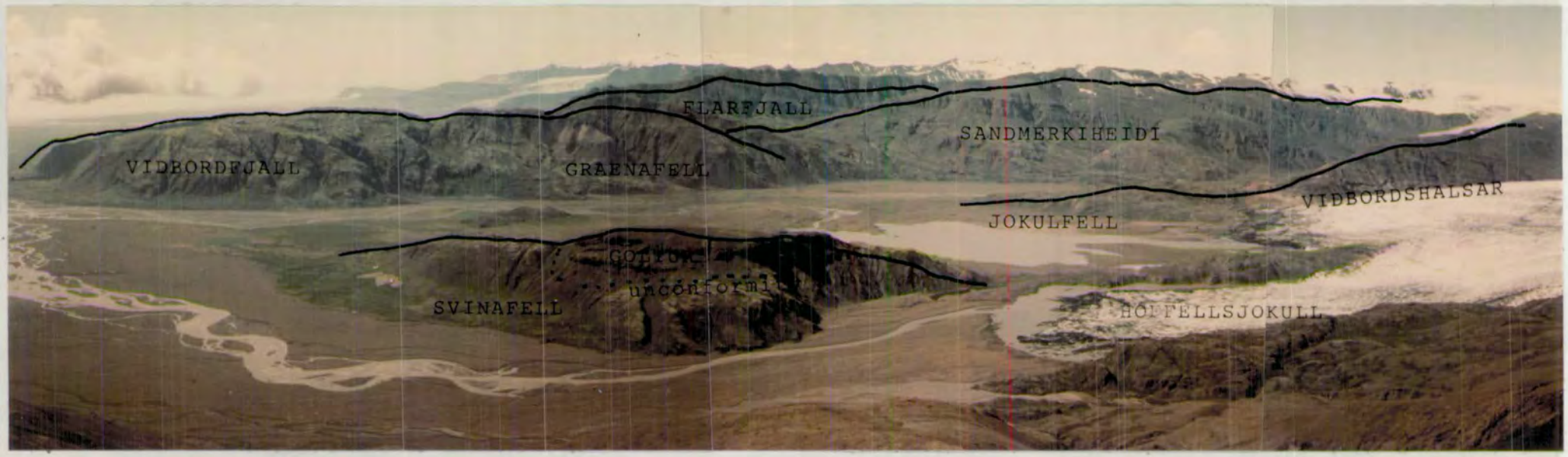

Figure 2.2. View from Hoffellstindar to the west. The Svinafell area is in the middle including the unconformable Svinafellgoltur formation. The Vidbordsfjall - Graenafell ridge followed by Sandmerkiheidi are seen in the near distance. Flarfjall ridge is seen behind. Oraefajokull (2119 m), the highest peak in Iceland, is seen in the background middle, covered by an icesheet. The cliff exposures in Vidbordsfjall are the gabbros. The Geitafell gabbro is seen along the margin of Hoffellsjokull and its terminal lake (lower right).

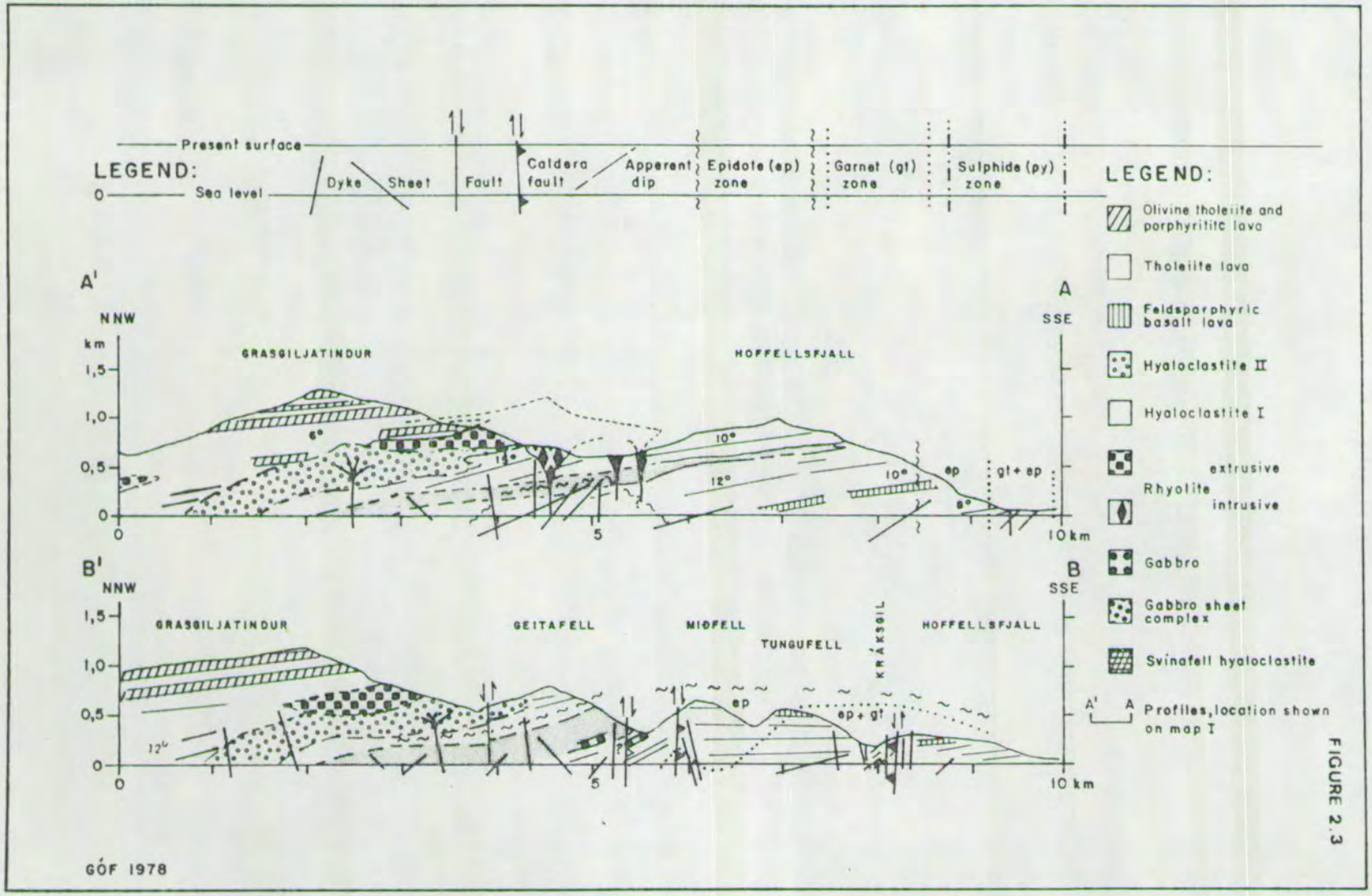
Present surface
LEGEND:
0 Sea level
Dyke
Sheet
Fault
Caldera fault
Apparent dip
Epidote (ep) zone
Garnet (gt) zone
Sulphide (py) zone
LEGEND:
Olivine tholeiite and porphyritic lava
Tholeiite lava
Feldsporphyric basalt lava
Hyaloclastite II
Hyaloclastite I
extrusive
Rhyolite
intrusive
Gabbro
Gabbro sheet complex
Svinafell hyaloclastite
Profiles, location shown on map I
A'
NNW
km
1,5
1,0
0,5
0
GRASGILJATINDUR
HOFFELLSFJALL
6°
12°
10°
12°
10°
8°
ep
gt + ep
0
5
10 km
A
SSE
B'
NNW
GRASGILJATINDUR
GEITAFELL
MIÐFELL
TUNGUFELL
KRÁKSGIL
HOFFELLSFJALL
12°
ep
ep + gt
B
SSE
GÓF 1978

FIGURE 2.3

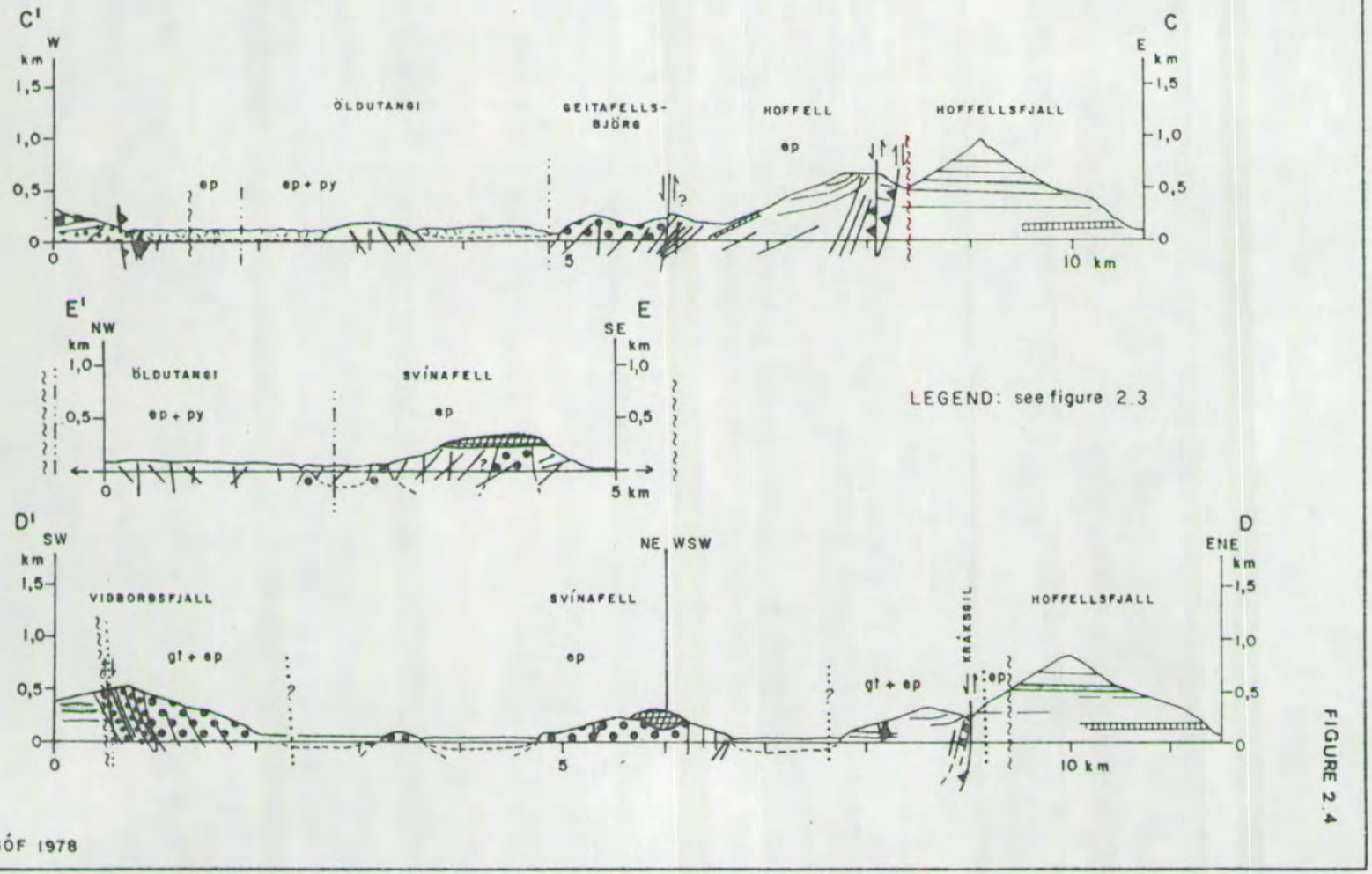
C'
W
km
1,5
1,0
0,5
0
ÖLDUTANGI
GEITAFELLS-
BJÖRG
HOFFELL
HOFFELLSFJALL
ep
ep + py
0
5
10 km
C
E
km
1,5
1,0
0,5
0
E'
NW
km
1,0
0,5
ÖLDUTANGI
ep + py
SVÍNAFELL
ep
0
5 km
E
SE
km
1,0
0,5
LEGEND: see figure 2.3
D'
SW
km
1,5
1,0
0,5
0
VIÐBORÐSFJALL
gt + ep
NE, WSW
SVÍNAFELL
ep
gt + ep
KRÁKSEIL
ep
HOFFELLSFJALL
0
5
10 km
D
ENE
km
1,5
1,0
0,5
0
GÓF 1978

FIGURE 2.4

text are given. The characteristic greenish grey colour of the propylitized rocks can be seen in these photos.

Figures 2.3 and 2.4 show stratigraphical profiles through the volcano. Their position is shown on Map 1.

The main stratigraphic units are listed below, from top to bottom:

Basalt lava unit III, min. thickness 700 m

Rhyolite unit II ca. 150 m

Earliest tillite, age ca. 5 m.y.

Hyaloclastite unit II, min. thickness 300 m, but variable

Basalt lava unit II, max. thickness 500 m, but variable

Hyaloclastite unit I, ca. 300 m, variable

Rhyolite unit I, max. thickness 50 m, variable

Basalt lava unit I, max. thickness 750 m.

2.2 Stratigraphic Units

The general strike of the succession is NE-SW, dipping from 6-50° to the NW. On the flank of the volcano both in Hoffellsfjall and Grasgiljatindur, the strike/dip relationships are somewhat variable, but a general deflection of strike towards E-W suggests an original "constructional surface" indicating the original position of the summit area (Map 1). The stratigraphic units are presented below, beginning with the oldest rock unit.

Basalt Lava Unit 1: 700-750 m of basaltic lavas compose this unit. The lavas are predominantly tholeiites. At the base of this unit (east of Hoffellsfarm) a rhyolite lava outcrops which is connected to the Setbergsheidi rhyolite. Lava Unit I can be divided into three sub-units (a), (b) and (c) (fig. 2.5).

Sub-unit (a): The base of this sub-unit is poorly exposed, but it is partly underlain by a rhyolite lava which is connected to the

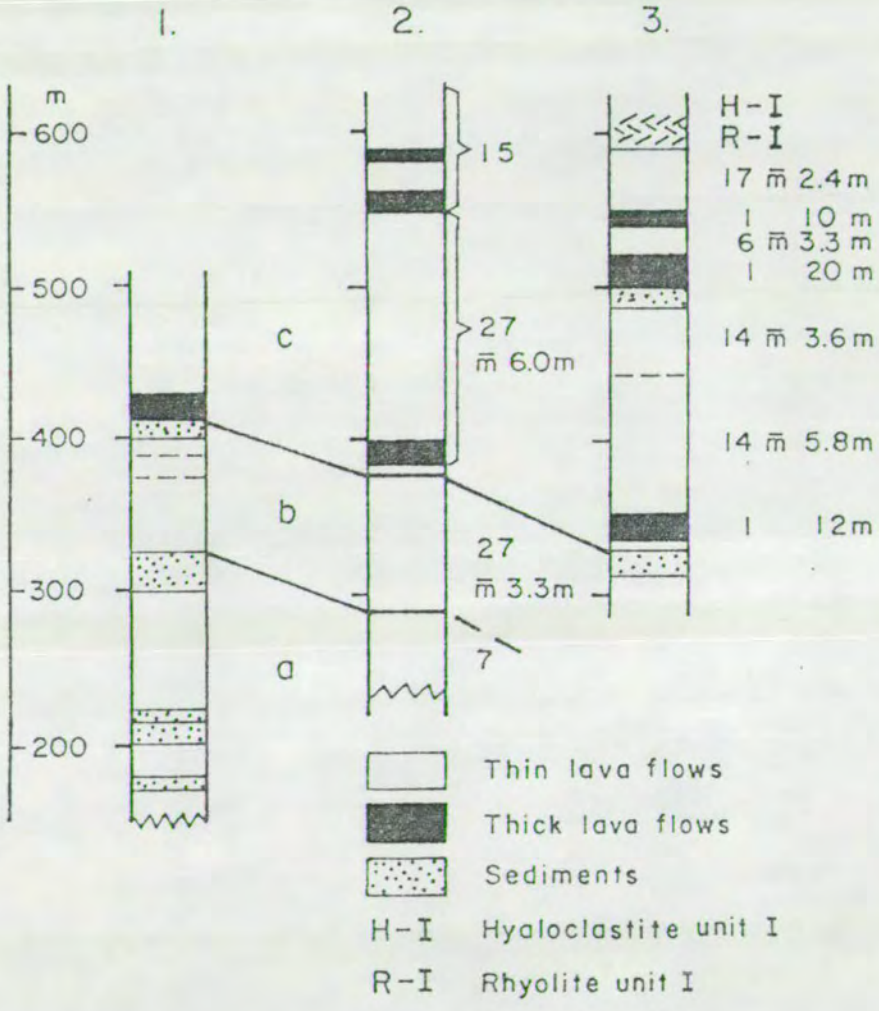

FIGURE 2.5. Simplified stratigraphic profile though Basalt lava Unit I in Hoffellsfjall.

1. Above farms.
2. Between Storuskridugil and Urdaskridugil
3. Ofaeruhjallar (Skora)

Sub-units marked: a, b, c
Number of lava flows in sub-units b and c are given and mean thickness. Mean value of sub-unit c is ca. 5.0 metres.

Setbergsheidi rhyolite in the southeast. Several sedimentary beds, some including air-born tuff, are interbedded with the lavas. The acid tuffs may have emanated from Setbergsheidi like the rhyolite below. The sediments are mainly of aeolian origin but partly of fluvial origin (Annels, 1967). The mean thickness of lava flows within this sub-unit is close to 6 m.

Sub-unit (b): This sub-unit includes sparsely-feldsparphyric lavas (Map 1). Two or three feldsparphyric flows and one pyroxene-phyric flow are seen amongst thin, aphyric, often highly vesicular lava flows in profile 1, fig. 2.5. Due to internal variance within the porphyritic lavas, with respect to phenocryst content, or to localized extent of the feldsparphyric flows, this generally porphyritic sub-unit makes a rather poor marker horizon. In profile 2 (fig. 2.5) this sub-unit is composed of 27 thin scoriaceous compound flows whose mean thickness is 3.3 m. The compound flow character, where boundaries between individual flows are unclear, resembles that of shield-type olivine tholeiites.

In profile 3 (fig. 2.5) only the top of sub-unit (b) is exposed, comprising sparsely-feldsparphyric and highly-vesicular lavas. Lavas within sub-unit (b) wedge out up-dip.

A 15-20 m-thick bedded conglomerate separates sub-units (b) and (c). This contains a pebbly-silt at the base, sub-rounded scree deposits in the middle and a fluviatile pebble bed near the top. The conglomerate can be traced across the mountain towards Kraksgil (caldera fault) and is probably related to a conglomerate bed occurring at a low level inside the Kraksgil ravine.

Sub-unit (c): This sub-unit comprises 3 thick lava flows (>10 m), 52 thin flows (< 10 m) and one 10-15 m thick conglomerate containing a lot of scoriaceous basalt (profile 3, fig 2.5). The thick lava at the base of this sub-unit is probably the lava described by Annels (1967)

to be of intermediate composition. The mean thickness of lavas in this sub-unit is 5 m. The profile shows two compound lava units of thin flows, near the middle (14 flows, mean 3.6 m) and close to the top (17 flows, mean 2.4 m). These compound flow units are regarded as "central-type tholeiites" and are more distinct than those in sub-unit (b). Lava flows wedge out up-dip in sub-unit (c) just as in sub-unit (b).

Basalt Lava Unit I thickens towards the middle of a hypothetical NE-SW striking fissure-swarm crossing the Geitafell central volcano. The average flow thickness is 5-6 metres. Basalt Lava Unit II (see later) also comprises thin flows with an average thickness of some 4-6 m. The mean thickness of lavas in Hoffellsfjall is some 2 m less than the 8.3 m mean value proposed by Annels (1967).

Inside the caldera in Tungufell and Midfell (see Map 1), it is mainly sub-unit (c) which occurs. Lack of marker horizons within this sub-unit make correlation across the caldera fault difficult. One acid tuff bed occurs, exposed at low levels in Midfellsgil and up-dip in Tungufell. The acid tuff is partly overlaid by a basaltic conglomerate (seen in Midfellsgil), but neither horizon could be traced across the fault. Some 150-200 m higher in the strata several feldsparphyric lavas occur (second feldsparphyric horizon, Map 1). Traced down-dip, several densely feldsparphyric lavas in Tungufell become only sparsely feldsparphyric as seen in Midfell and Geitafellsgil. This porphyritic lava group is therefore a poor marker and seems to be of local extent as it was not found outside the caldera fault in Hoffellsfjall.

A marked difference exists between the two sparsely feldsparphyric lava groups in Basalt Lava Unit I and the densely porphyritic flows in Basalt Lava Unit III (see below). The feldsparphyric flows in Lava Unit I contain small phenocrysts (<0.5 cm) while the densely porphyritic

flows in Lava Unit III contain larger (>0.5 cm) feldspar phenocrysts and sometimes also pyroxene and olivine phenocrysts. This difference is indicated on Maps 1 and II and in figs. 2.3 and 2.4.

Annels (1967) came to a similar conclusion concerning the local extent of the feldsparphyric flows in Lava Unit I and suggested that the upper group might have emanated from the Hauksheidi area (in the Svinafell area), and suggested a genetic connection to the Valagil gabbro in Hauksheidi. A correlation between the Valagil gabbro and the feldsparphyric lavas would affect the chronological model for the intrusives and will be discussed in Chapter 3.

Above the feldsparphyric lavas in Midfell, inside the caldera, tholeiitic lavas continue up to 500 m altitude where two (conglomeratic) hyaloclastite beds occur. The lower of these shows fragments of acid and basic material similar to Hyaloclastite Unit I (see below). A correlation is proposed between these sediments in Midfell and Hyaloclastite Unit I outside the caldera. This would involve a maximum of some 200 m subsidence near the caldera fault. However, towards the central area of the caldera strike/dip relationship suggests a total subsidence of up to 500 m (see Chapter 3.2).

Above the hyaloclastite beds in Midfell there are both tholeiite lavas and lavas of more intermediate appearance. Exposures are poor but these flows can perhaps be correlated with those overlying Hyaloclastite Unit I outside the caldera (i.e. belonging to Lava Unit II).

Rhyolite Unit I: This acid unit occurs at the base of, and within Hyaloclastite Unit I. An altered pitchstone layer, a granophyric intrusion and an acid tuff are found on the east side of Hoffellsfjall (Map 1). One rhyolite flow is found in Geitafellsgil (Map 1). These scattered occurrences suggest a source of rhyolitic volcanism within the mapping area. The Hyaloclastite Unit I above shows a mixed

composition, in particular near its base. An altered pitchstone layer is also found near the base of Hyaloclastite Unit I in Geitafell. The thickness of Rhyolite Unit I is estimated at some 50 m.

Hyaloclastite Unit I: This hyaloclastite unit is of mixed composition. Predominantly, however, it is composed of aphyric basalt clasts (20 cm down to microscopic particles). Locally, acid clasts also occur, preferentially near the base of the unit. The acid material may be derived from Rhyolite Unit I. A crude bedding is seen in places, showing clasts of basic and acid material, which may indicate a reworked nature of the mixed breccias.

Basic pillow lavas have not been found within this unit, but pillow fragments occur, as in Efstafellsnes. Locally (Hoffellsfjall east), fragments of feldsparphyric basalt and scarcer gabbro xenoliths are found.

The hyaloclastite is heavily intruded and further brecciated by sheets.

The best exposures of this unit are seen in Geitafell and Geitafellsgil, where it reaches a thickness of some 300 m. The unit wedges out up-dip in Hoffellsfjall, but continues across the valley, Hoffellsdalur, to the NE into Vatnssteinafell and may be equivalent to - or contemporaneous with - the hyaloclastites in the Kollumúli central volcano (Torfason, 1979). To the SW the hyaloclastite unit becomes thinner, as seen in Vidbordsfjall. Within the sheet-swarm, intimately associated with the gabbros in Vidbordsfjall (Map 1), hyaloclastite material is common. Exposures, however, of both country-rocks and gabbro/country-rock contacts are poor in Vidbordsfjall, and more detailed mapping is needed to evaluate the relationship between hyaloclastites and the gabbro complex and its associated sheet swarm.

In the middle of the volcano, hyaloclastite crops out from the Valagil gabbro into Oldutangi, to the NW, up to the glacier. Most

of this hyaloclastite is regarded as belonging to Unit I, but the upper part may belong to Hyaloclastite Unit II. Such a correlation implies that the hyaloclastites were thickest in the middle of the volcano where the two units may combine. Reworked hyaloclastite, including sparse fragments of sub-rounded gabbro, are found in the NW most exposures in Oldutangi. The hyaloclastite in Oldutangi has survived glacial erosion due to the high intensity of hypabyssal intrusions.

On a regional scale, it can be seen that Hyaloclastite Unit I extends from Flarfjall (Map 1) through the Geitafell central volcano (in the middle of which it may have been thickest), to Geitafell (ca.300 m) and through Hoffellsfjall (ca.150-200 m thick in the central part). A reconnaissance survey to the NE suggests that this unit continues in Vatnssteinafell until it disappears unconformably below the Dalsheidi formation (see Svinafellsgoltur formation), to reappear unconformably below the Mulatindur formation (Torfason, 1979) on the flank of the Kollumuli central volcano.

Torfason (1979) suggested that the Kollumuli and the Geitafell volcano (his Hoffell central volcano) hyaloclastites were local formations formed within calderas. However, as far as the Geitafell central volcano was concerned, a caldera stage had not been reached when the hyaloclastites were formed and it appears that Hyaloclastite Unit I extends between these two central volcanoes. A regional glaciation (Mio-Pliocene?) to account for the Hyaloclastite Unit I formation cannot be excluded. Annels (1967) noted that sediments thicken towards the NW and suggested that some of the hyaloclastites might have been formed within a depression caused by the flexure. However, it will be shown in Chapter 3 that the flexural event postdated the hyaloclastites in the Geitafell central volcano. Lava Unit I also wedges out up-dip to the SE; i.e. thickens to the NW and apparently also thickens towards the middle of the volcano as seen in lavas in Midfell and

Tungufell, some of which are of local extent (i.e. sub-unit (c) thickens inwards). Therefore, the Geitafell central volcano seems to have marked the site of a topographical rise, not a depression. It is concluded that a regional glaciation accounts for Hyaloclastite Unit I.

Basalt Lava Unit II: The topographical relief of Hyaloclastite Unit I resulted in the irregular distribution of Lava Unit II. Local unconformities are common as Basalt Lava Unit II banks against the underlying hyaloclastite. Interbedded, reworked hyaloclastite beds are common within Lava Unit II and a fluvioglacial boulder bed is found at high altitude levels in Geitafell in Lava Unit II.

The aggregate thickness of the unit is estimated at between 400-500 m. Most of the lavas are thin, highly vesicular, central-type tholeiites, but several thick lava flows of more intermediate composition also occur. Three to four basaltic andesites are found outside the caldera in Midfellsbotn overlying Hyaloclastite Unit I. These are followed by some 200 m of thin central-type tholeiites up to the top of Hofellstindar. In Graenafell, to the west, just below Hyaloclastite Unit II, a characteristic icelandite flow with contorted and folded flow-banding is found. Intermediate lavas therefore occur both at the top and bottom of this lava unit. A few intermediate flows also appear to be present in Efstafell and Efstafellsnes, but exposures are inadequate due to high intrusive intensity. Distribution of Lava Unit II is shown on Map 1; the intermediate lavas do not form a mappable horizon and their only occurrence is that referred to above. While Lava Unit II buries Hyaloclastite Unit I on the flank of the volcano, this unit is not present in the middle of the volcano in Oldutangi.

Hyaloclastite Unit II: This hyaloclastite unit, as well as part of Unit I, are described at length by Annels (1967, p. 48-86). The minimum thickness of Unit II is 300 m. The unit dips steeply (20-40°) to the NW. As seen in Efstafell, the hyaloclastite has accumulated in

several eruptions and, while most of the Unit is composed of aphyric basalt fragments (some as recognisable lava pillows), reworked, porphyritic, boulder beds also occur, as does some feldsparphyric tuff. Blocks (sometimes pillows) of intermediate lavas also occur. In addition, some highly vesicular interbedded lava flows may be found.

In Jokulfell in the west, a porphyritic pillow breccia is found within otherwise aphyric hyaloclastite, and one porphyritic lava unit comprising several flows is found within the hyaloclastite. The porphyritic lavas (Map 1) are of localized extent and outcrop within fault blocks which show subsidence to the SE into the caldera. Feldsparphyric boulders are found in the hyaloclastite above these lavas suggesting erosion within the Unit. In Graenafell, further to the west, porphyritic tuff lenses are found within aphyric tuff.

The feldsparphyric lavas in Jokulfell and the porphyritic hyaloclastite elsewhere, may be related to the same eruptive event that produced the early gabbro intrusion in Geitafell (intrusive phase 2) and Valagil. Hyaloclastite Unit II is intruded by intrusive phases 5 and 6 and all later intrusive phases (Chapter 3).

Tillite bed - showing poorly sorted material including rounded boulders up to 2 m across, separates this unit from Rhyolite Unit II above. This tillite is earliest found in the field area. It overlies the eroded surface of a columnar jointed branching basalt intrusion on the top of Hyaloclastite Unit II in Efstafellsgil and can be traced across the mountain to Grasgil. Its maximum thickness is 8 m in Grasgil, but is thinner (<1.5 m) in Efstafellsgil.

Rhyolite Unit II: This unit comprises some 3 rhyolite lavas, the lowest of which is 50-100 m thick, and acid tuff beds with two thinner rhyolite lavas interbedded in the base of Lava Unit III. Altogether, Rhyolite Unit II is some 150 m thick.

In Grasgil (Map 1) Hyaloclastite Unit II is absent and Rhyolite

Unit II overlies an 8 m thick tillite resting directly on Basalt Lava Unit II. Above the tillite is a 25 m thick layered tuff of mixed composition (acid and basic pumice layers) overlain in turn by a rhyolite lava, ca. 70 m thick.

The distribution of this rhyolite horizon (both flows and intrusions) is shown on Map 1. Rhyolite Unit II is associated with intrusive phase 11 (see Chapter 3) which may have accompanied the caldera event. In Geitafell a 20-30 m thick, highly porphyritic, lava overlies the rhyolite. The porphyritic lava has a typical olivine basalt weathering surface. In addition to large (up to 2 cm) neatly zoned bytownite phenocrysts, the lava contains smaller pyroxene and partly iddingsitised olivine phenocrysts. This unusually thick porphyritic olivine tholeiite may correlate with intrusive phase 10 (which overlaps intrusive phase 11, Chapter 3). The late gabbros in Kraksgil and Vidbordfjall are contemporaneous with intrusive phase 10 (Chapter 3). Part of the late gabbros in Vidbordfjall show modal olivine like the lava described above and they may be related to the same eruptive event. A similar lava also outcrops in Efstafell, immediately above Hyaloclastite Unit II (in Grjotbotn). Both of these lavas are of local extent. It is only the overlapping intrusive phase 10 and the succeeding intrusive phase 12 which cross-cut the Rhyolite Unit II formations.

Basalt Lava Unit III: This lava unit is at least 700-800 m thick as estimated from a reconnaissance field survey up to the Vatnajokull ice-cap in the north. The mapping of this unit is adopted unchanged from Annels (1967). The Lava Unit comprises thick tholeiite, olivine tholeiite and feldspar porphyritic basalt flows, some of which also contain phenocrysts of pyroxene and olivine. Most of the lavas are regarded as having been erupted outside the Geitafell central volcano. Annels mapped a 5° structural unconformity within Lava Unit III, which has

been confirmed by dip measurements on Gjanupstindur (Map 1). Lavas above the unconformity were extruded after the flexure.

Mainly the basal part of Lava Unit III was studied. The two highly porphyritic lavas from Geitafell and Efstafell, which may be contemporaneous with intrusive phase 10, were described with Rhyolite Unit II. Both of these lavas show reverse palaeomagnetism. Immediately above the porphyritic lava in Efstafell a thick coarse-grained lava occurs. In Austurgja, but now immediately above the rhyolite lava, some 8 coarse-grained lavas occur. These lavas are distinctively brown weathered. Both the weathering and petrographic similarities with intrusive phase 12 (Chapter 3), which Annels, for instance, named "brown dolerite dykes", suggest a possible correlation between the two. The brown lavas show normal palaeomagnetism like many members of intrusive phase 12. The coarse-grained lavas in Austurgja have a dip of some 10-12° NW and form an 80 m thick unit, while only one lava was found in Efstafell.

A magnetostratigraphic profile was taken from the brown lavas in Austurgja up Vesturmuli (near the glacier's margin). Three thick marker horizons are found in the succession whose positions are indicated in profile 4 (fig. 2.6). The lowest is of volcanic origin occurring at 320-350 m, poorly exposed. In ascending sequence this shows (i) pitchstone, (ii) vesicular rhyolite, (iii) acid tuff, (iv) basic pyroclastic layer, and (v) tholeiite scoria. In a general sense this "acid bed" is included in Rhyolite Unit II, which implies that rhyolite volcanism overlaps intrusive phase 12 (and its extrusive phase).

The second marker horizon occurs at 450-480 m and forms an erosional platform, a 20-30 m thick sediment with a tillite at the top. The 5° dip unconformity mapped by Annels occurs near this horizon. This marker bed is indicated as conglomerate in profile 4, fig. 2.6.

The third marker bed (610-645) which also forms an erosional platform is a conglomerate (possibly including a tillite). The marker horizons aid in the correlation of the magnetostratigraphic profile in Vesturmuli with that of Lambatungnatindur (Torfason, 1979) as is discussed in section 2.3.

Three porphyritic lava sub-units are also found in the profile in Vesturmuli. Their position is shown on Map 1. Six porphyritic lavas form the lowest sub-unit (365-400 m). Three porphyritic lavas interbedded with tholeiite lavas form the second sub-unit (570-610 m). The third porphyritic sub-unit, only partly exposed in the profile, begins at 700 m with a 15 m thick porphyritic lava followed by a thick olivine tholeiite lava.

In Vidbordshalsar west of Hoffellsjokull (Map 1) two porphyritic lava sub-units are shown.

The interesting aspects of these porphyritic lavas with respect to the flexure zone are two-fold. (1) They were extruded subsequent to the flexural event, and (2) they are zeolitized - showing three zeolite zones. The zeolite zones are tilted and are discordant to the stratigraphy. East of Hoffellsjokull, analcime is common in amygdales from 400-600 m in Vesturmuli (near the glacier), and from 400-1000 m in Efstafell. Above, in both places, only chabazite and thomsonite occur in amygdales along with opaline silica. These zeolite occurrences form, in accordance with Walker's (1960) zeolite zones, a) an analcime zone, and b) an overlying chabazite-thomsonite zone (see general scheme in fig. 1.3). In Vidbordsdalur (at 300 m) and in Vidbordshalsar, however, in and above the lower porphyritic sub-unit (500-600 m) (Map 1), mesolite, scolecite, thomsonite, mordenite, stilbite and heulandite are common and clearly indicate the mesolite-scolecite zone of Walker (1960).

These stratigraphically discordant zeolite-zones are superimposed on post-flexural lavas and not bent into the flexure-zone in this area, as is the case in an older succession in eastern Iceland (Walker, 1974).

The present observation is in accordance with post-propylitization and post-flexural formation of low-grade zeolite assemblages within the volcano and its lower flank area (Chapter 4). No evidence was found for pre-propylitization zeolite-formation within the volcano.

Structural unconformity within Lava Unit III, general strike/dip relationships between Lava Unit III and underlying units (Chapter 3), the possible connection of late intrusive phases to lava flows below and at the base of Lave Unit III and zeolite zone arrangements seem to suggest that the major part of Lava Unit III postdates the volcanological/structural/high-grade hydrothermal evolution of the Geitafell central volcano and the flexural event.

The Svinafellsgoltur Palagonite Formation

An unconformable Pleistocene tillite and a palagonite breccia within the volcanoare seen in Svinafellsgoltur (Map 1). These formed in a valley, eroded into the middle of the Geitafell volcano down to the 150 m altitude level. The tillite and breccia formation has been mentioned by Thorarinsson (1952) and Annels (1967), and described in some detail by Jonson (1952, 1954). Walker et al. (1966) described a similar formation in Dalsheidi (in the NE) which they suggested was formed by a subglacial eruption, to the west of the region, from which a lava flowed beneath a valley glacier to its present position. Walker et al. (1966) noted that the Svinafellsgoltur formation contains porphyritic basalt while that in Dalsheidi shows aphyric basalt suggesting that these formations were not necessarily strictly contemporaneous (or at least not formed from the same eruption). At many localities the Dalsheidi formation rests directly on striated basement, while elsewhere, a thin layer of tillite intervenes. The formation on

Svinafellsgoltur, however, shows a thick sediment, possibly formed under subaerial fluvioglacial conditions. Torfason (1979) mapped a similar formation within the Kollumuli central volcano. The formation on both Dalsheidi and Kollumuli were shown by Torfason to be reversely magnetized and thereby at least older than Bruhnes epoch (0.7 m.y. - present), i.e. early Pleistocene. The formation on Svinafellsgoltur is also reversely magnetized and may have formed during the same palaeomagnetic period as the others.

The formation shows a 2 m thick, brown, fine-grained sediment at the base, followed by a brown, 8 m thick boulder bed (largest boulders 1.5 m^3; grading down to silt). The chaotic boulder bed grades into a grey, ca. 50 m thick silt sediment which includes some pebble and stone (glaciofluvial outwash), fine-grained sand and pebble lenses (stream deposits). The exposure referred to is seen in the southern part of the formation, but the sediments thin towards the north (up valley), where they are only 23-25 m thick (Jonson, 1954). The sediments may have formed under subaerial conditions. Resting directly on the fluvioglacial sediments is a feldsparphyric basalt lava which shows well developed columnar jointed basalt blocks and pillow basalt, intermixed with coarse to fine fragmental rocks. The lava may possibly have flowed over water-saturated fluvioglacial outwash (or into a glacial lake?). It is deposited nearly horizontally and can be separated into two units, the lower from 210-280 m and the upper from 280-360 m. It is mainly the sediment which suggests that the valley was not being carved by a glacier during the formation of the mixed lava- and fragmental mass, and hence, that the igneous formation was not formed subglacially as was the Dalsheidi formation.

Two interesting features were observed within the Svinafellsgoltur formation: (1) There is some evidence suggesting a N50°E fault

affecting the boulder bed, and (2) a porphyritic dyke (0.5-0.7 m), striking N60°E, cuts the top of the fluvioglacial sediment. The dyke is discernible in the overlying lava for some 20 m. Since this dyke could not be traced into the basement rock it does not appear to be a feeder for the flow, but may have flowed downwards into a fissure. The dyke and the fault, however, suggest some active tectonic movements within the central volcano during the emplacement of the Svinafellsgoltur formation.

2.3 Palaeomagnetic Stratigraphy

Torfason (1979) used geomagnetic polarity reversals supported by new age dates to relate the lava-palaeomagnetism to a geomagnetic polarity time-scale from Watkins and Walker (1977). Torfason suggested that the lava pile in Lambatungnatindur was of similar age to those in Grasgiljatindur.

Three more or less continuous geomagnetic profiles were taken from Lava Units II and III and correlated to Torfason's (1979) profile and the polarity time-scale of Watkins and Walker (1977). These profiles are shown in fig. 2.6. One profile is from Lava Unit II in Hoffellsfjall, extending from the top of Hyaloclastite Unit I up to the middle of Lava Unit II. Geomagnetism at the top of Lava Unit II was also tested. All showed reverse polarity. There are, however, problems regarding geomagnetic studies within altered rocks. Lavas may have demagnetised and secondary magnetism may have built up. Fluxgate magnetometer-studies from propylitized rocks are unreliable. The palaeomagnetic data gathered from Lava Unit II were from zeolitized lavas only. The other profiles were from Lava Unit III, one from part of the Efstafell-Grasgiljatindur succession and the other from the Mular succession (Vesturmuli).

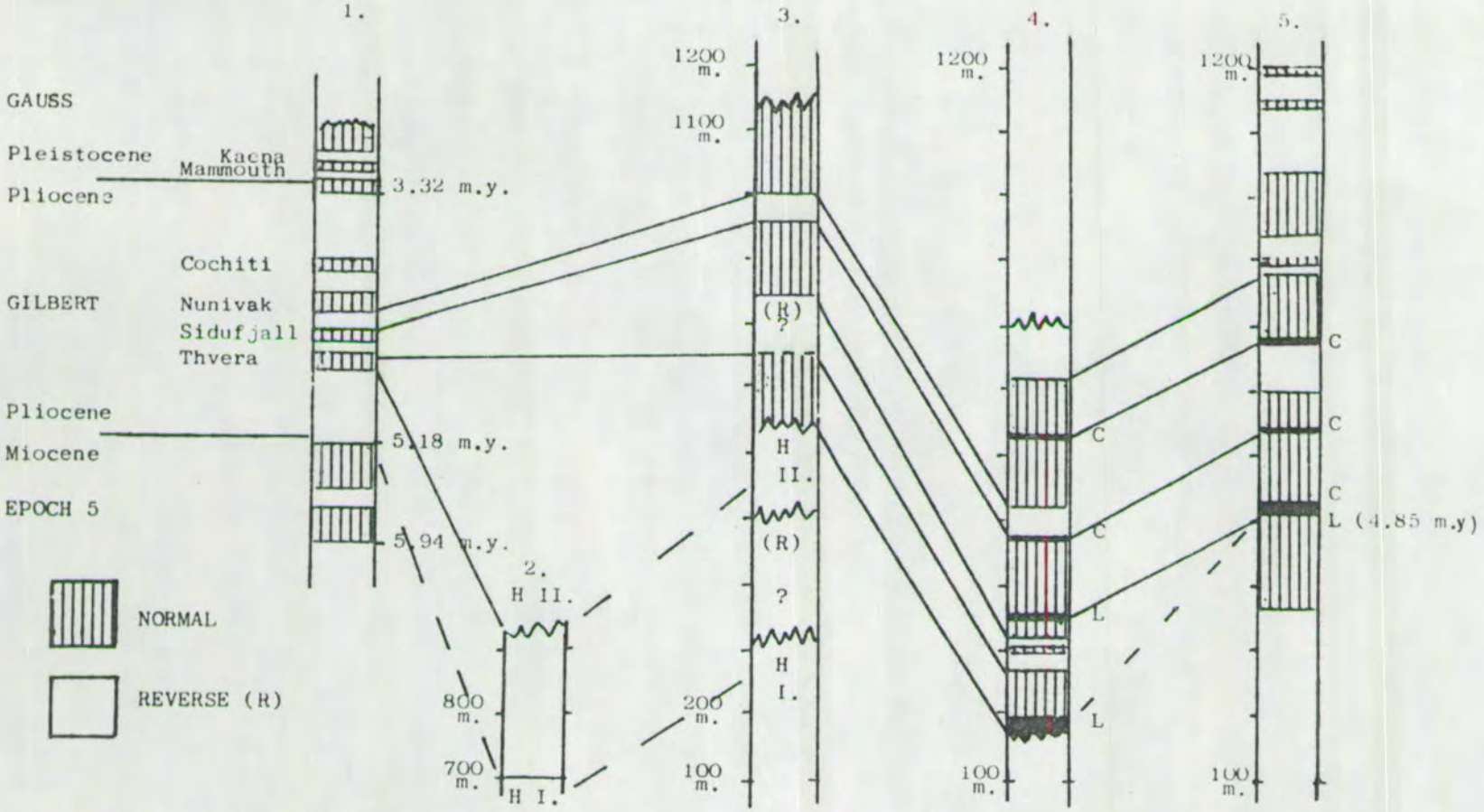

FIGURE 2.6. Magnetostratigraphic profiles. 1. Geomagnetic polarity time scale (Watkins and Walker, 1977) 2. Hoffellstindar (Lava Unit II). 3. Efstafell (Lava Unit III). 4. Mular (Lava Unit III) and 5. Lambatungnatindur (from Torfason, 1979). C : conglomerates (tillites?); L : Rhyolite and acid tuff. H I.: Hyaloclastite Unit I; H II.: Hyaloclastite Unit II.

Profile 4 can be correlated with profile 5 through the discernible marker horizons described along with Lava Unit III. This correlation implies an interesting relationship between stratigraphic evolution and the palaeomagnetic succession, suggesting that the lava succession was built up somewhat differently in the two areas.

The relationship of the profiles to the geomagnetic polarity time-scale (Watkins and Walker, 1977) suggests that Basalt Lava Unit II, Hyaloclastite II and the base of Lava Unit III were extruded during the Early Gilbert magnetic epoch, i.e. Early-Pliocene. A profile from Vidbordsfjall (Torfason, 1979), the position of which is not precisely known but which, from field relations, has to be from Lava Unit I, shows three reversals. This profile is not shown in fig. 2.6, but can fit magnetic epoch 5 (see fig. 2.6). The stratigraphic succession studied (Basalt Lava Units I-III) appears to have accumulated from epoch 6 through the Nunivak magnetic event, or from some 6.0 m.y. to ca. 4 m.y. While detailed magnetostratigraphic studies are needed from this rather unfavourable (altered) succession, a lifespan of 2 m.y. for the succession may be realistic. If so, the lifetime of the Geitafell central volcano can be estimated to be some 1 m.y. (i.e. from sub-unit (b) in Lava Unit I through Rhyolite Unit II). A possible figure for the lifespan of the intrusive and high-grade hydrothermal activity in the volcano also emerges as being only 0.2-0.3 m.y. Most of Hyaloclastite Unit II was present when the Geitafell gabbro (intrusive phase 2) was injected and when high-grade hydrothermal activity began (Chapter 4), while hydrothermal activity ceased after the Rhyolite II phase, the end of which is reckoned (Torfason, 1979) to have occurred at 4.85 m.y.

Several samples from intrusive phases 2, 11 and 12 are currently being dated by K. Albertsson, and obviously new data may or may not support these estimates for the lifespans of the various events.

However, in conclusion, the lifespan of the Geitafell central volcano is thus estimated as close to 1 m.y. and the intrusive and high-grade hydrothermal activity may have taken place over some 0.2-0.3 m.y.

2.4 Summary

Chapter 2 is summarized in Table 2.1. The stratigraphic units are shown, their thicknesses, age estimates and the lifespan of the Geitafell central volcano. The time relations of the major structural events and the position of intrusive phases are also shown, while the intrusive and structural aspects are treated in Chapter 3.

BASALT LAVAS III (ca. 700 m), lower 600 m before Cochiti magnetic event (c.4 m.y.)

lowest 100 m

AGE:

5.0.m.y. ?

flexural event

------ GEITAFELL VOLCANO

RHYOLITE UNIT II (ca. 150 m)

-----caldera event

Intr.phases 10 - 12

---

earliest tillite

Intr. phases 2 - 10

HYALOCLASTITE II (min. 300 m)

BASALT LAVAS II (ca. 400 m)

HYALOCLASTITE I (min.300 m)

glaciation; Pliocene/Miocene ?

Intr. phase 1

RHYOLITE UNIT I (ca. 50 m)

BASALT LAVAS I (ca. 700 m)

Magnetic epoch 5 ?

subunit c

subunit b

subunit a

------ GEITAFELL VOLCANO

6.0.m.y. ?

TABLE 2.1.

CHAPTER 3

INTRUSIVES AND STRUCTURE

3.1 Introduction

Intrusive rocks in the Geitafell volcano include several gabbro, granophyre and felsite intrusions, together with dyke-and sheet-swarms. Their general field relations are shown on Map 1.

A chronological sequence is established for the intrusive rocks. The term dyke is used for tabular intrusive bodies generally dipping from 60° to vertical, while the term "sheet" is used for "identical" intrusions generally dipping less than 60° down to horizontal. The basaltic dykes and sheets range from aphyric fine-grained basalts, porphyritic basalts to aphyric and porphyritic dolerites. The petrographic differences, coupled with cross-cutting relationships, show that at least 12 major intrusive phases are separable in the field.

The age relationships of the intrusive rocks, their petrographic character, distribution and the apparent connection to extrusives and structural evolution are described below. Mineralogical and petrological descriptions, however, are kept at a minimum, as these have been given by Annels (1967) and Newman (1967) for all the intrusive types concerned. Maps of the strike/dip relationships for intrusive phases 3, 5, 6, 7, 8, 9, 10, 11 and 12 are shown in figures 3.2, 3.5, 3.6, 3.7, 3.10, 3.11, 3.14, 3.15 and 3.17 respectively. These figures also include stereographic projections showing the pole directions of the intrusives considered. The lower hemisphere is used in the stereographic plots.

3.2 Intrusive Phases

Intrusive Phase 1: This intrusive phase is regarded as a feeder dyke system to Basaltic Lava Units I and II, Rhyolite Unit I, Hyaloclastite Unit I and possibly as a part of a feeder system to Hyaloclastite Unit

II. Members belonging to this intrusive phase are fine grained basaltic dykes. The only available criterion to distinguish this intrusive phase from younger basaltic phases with reasonable assurance, is a cross-cutting relation with the widely distributed, highly characteristic doleritic cone-sheet swarm of intrusive phase 5.

Acid intrusives regarded as belonging to intrusive phase 1 are only found within Rhyolite Unit I on the east side of Hoffellsfjall.

Intrusive Phase 2: The Geitafell and other contemporaneous gabbros constitute intrusive phase 2. Their distribution is shown in Map 1. As with most of the other gabbros, the Geitafell gabbro has hypidiomorphic granular texture ranging in grain-size from 2-4 mm in the central portion. The mineral phases are bytownite-labradorite, calcic augite and titanomagnetite, with occasional olivine (up to 2% modal, Newman, 1967) and sparse orthopyroxene (hypersthene analysed). Olivine and orthopyroxene are most often completely pseudomorphed, mainly by talc, chlorite and magnetite.

The NE margin of the Geitafell gabbro comprises an irregular zone (ca. 50-70 m wide, Newman, 1967) of marginal finer-grained gabbro which ranges from feldsparphyric to aphyric fine-grained gabbro ("doleritic gabbro"). Towards the north, porphyritic fine-grained gabbro dykes extend from the main gabbro body across Efstafellsgil.

Locally, pegmatitic gabbro veins occur in coarse grained gabbro at the western side of the body, near the ice-marginal lake of Hoffellsjokul. The veins consist of large (up to 10 cm) augite and labradorite crystals. The whole gabbro body is net-veined by felsitic and granophyric veins (intrusive phase 4) grading to a felsite intrusion breccia at the southern end. The felsitic material is unchilled against the gabbro and is regarded as having been emplaced while the gabbro was still hot. The acid material ranges from fine-grained

quartz-feldspar rocks with a minor content of ferromagnesian minerals, to well-developed granophyre. Occasionally phenocrysts of andesine (zoned to albite) and augite (replaced partially by actinolite) are also present.

Time Relation to Other Gabbros: Other gabbros in the area include the Valagil gabbro, Hauksheidi gabbro-sheet complex and Oldutangi gabbro, (all occurring in the Svinafell area), Stora-Dima and Litla Dima gabbros (outcropping in the sandur plain between the Svinafell area and the Vidbordsfjall-Graenafell ridge), Kraksgil gabbro, and the Vidbordsfjall gabbro complex, which shows four separate gabbro units (A, B, C and D). Annels (1967) and Newman (1967) also described a fine-grained gabbro near the Hoffell farm (Hoffellsdalur gabbro). This latter body, however, was not found by the present author, although dolerite sheets belonging to intrusive phase 5 are common at Hoffell farm, sometimes showing small gabbro clots typical of intrusive phase 5. The discrepancy may be due to a semantic difference regarding the distinction between "fine-grained gabbro" and "coarse-grained dolerite". All the exposures near the Hoffell farm showed shallow dipping dolerite sheets and the "Hoffellsdalur gabbro" is therefore excluded from the present map. The new finding of gabbro in Litla Dima, however, near Jokulfell in the sandur plain, is shown on Map 1. The Litla Dima gabbro consists of fine-grained gabbro grading through diorite into granophyric rock.

As described by Annels and Newman, the gabbros are primarily quartz gabbros with subordinate olivine gabbros. Porphyritic and doleritic marginal facies are commonly developed. A range in colour index from melano- to leucocratic gabbros also exists (Newman, 1967). In some cases the leucocratic part of the gabbros shows well-developed granophyric texture, with quartz (<10%) and sodic feldspars (oligoclase-andesine), but a fairly high content of titanomagnetite and prismatic

pyroxenes, the latter largely replaced by ferroactinolite and chlorite. Newman and Annels called these relatively rare varieties 'amphibole rocks', or 'amphibole gabbros'. This leucocratic rock type is mainly found associated with the late gabbros in Kraksgil and Litla Dima and is better described as diorite. As with the Geitafell gabbro, many of the other gabbros are net-veined by acid material. A magmatic evolution from olivine gabbro, through quartz gabbro, diorite and finally granophyre appears to be indicated.

A crude time relation between the gabbros is presented in Annels (1967) and Newman (1967). Both regarded the Geitafell and Svinafell gabbros as the oldest, with the possibility that the Stora Dima and Vidbordsfjall gabbro unit A were contemporaneous with them. Annels labelled the four gabbro units in Vidbordsfjall as A, B, C and D, and believed them to have been injected in that order (fig. 3.1). Newman agreed with this age relation but indexed the same units as D, A, B and C. Gabbro unit B of Annels (Newman's unit A), was described as olivine gabbro, while the other units consist of quartz gabbro, ranging in grain size from marginal dolerite, through porphyritic gabbro to coarse grained gabbro in the centre. Annels' gabbro unit A (Newman's unit D) only showed the coarse-grained gabbro facies, while all the other units also showed the marginal fine-grained facies.

To avoid further confusion regarding the Vidbordsfjall gabbro units Annels' nomenclature of A, B, C, D is used in this work (fig. 3.1). In addition to unit B, an olivine gabbro is also present at the northernmost margin of unit D. A new time sequence for the gabbro units is postulated. Gabbro unit C is regarded as the oldest and contemporaneous with intrusive phase 2, while units A, B and D are younger.

The evidence of gabbro unit C being oldest emerges from the fact that unit C is cut by intrusive phases 5 and 6 while the others are not. Both intrusive phases 5 and 6 are metamorphosed by unit B; hence B

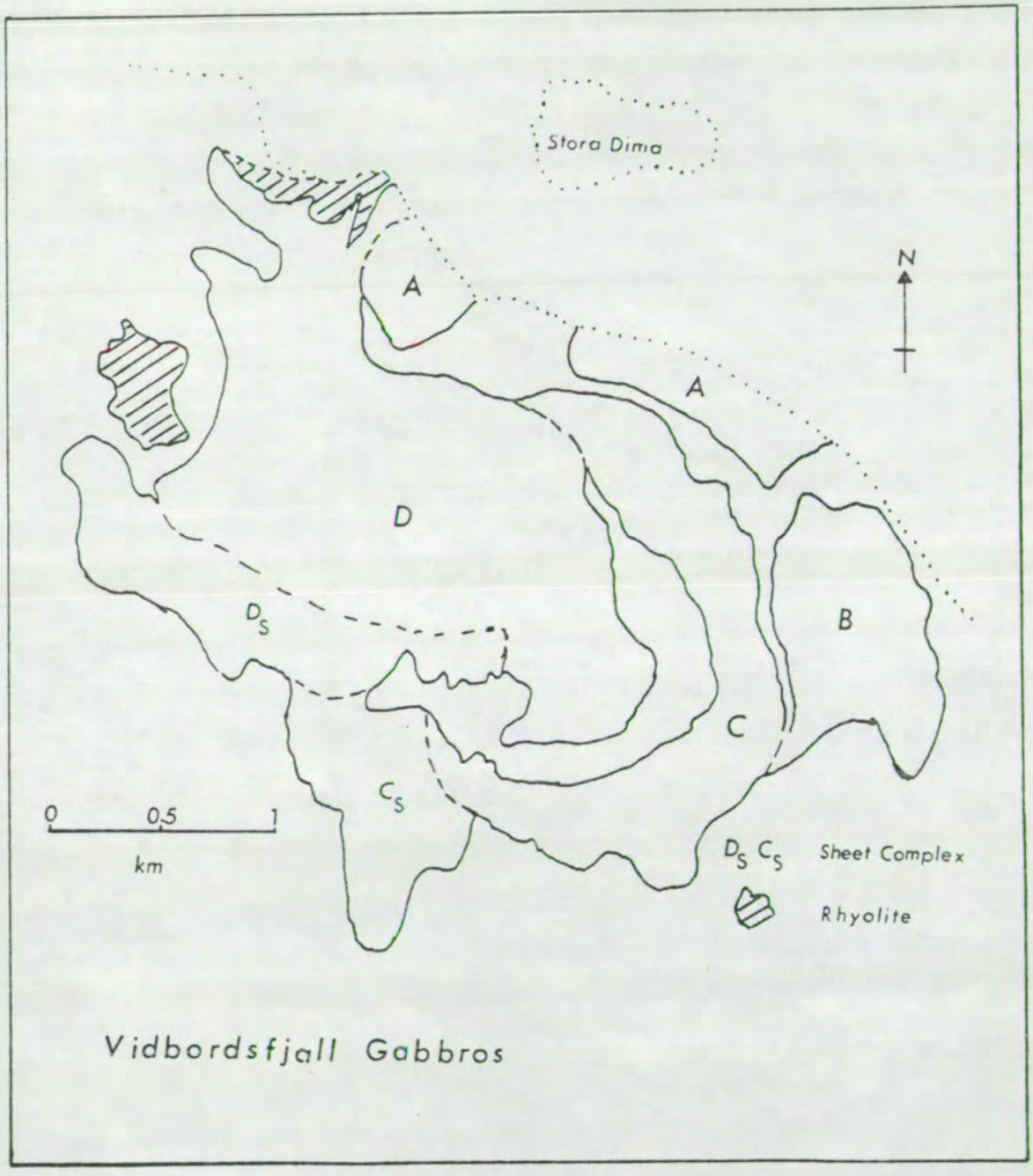

FIGURE 3.1. Gabbro units A, B, C and D in Vidbordsfjall.
(from A.E.Annels, 1967).

clearly postdates C. Unit B, like units A and D, is only cut by intrusive phases 11 and 12, suggesting that these three units have a roughly similar age: the precise chronology of B, A and D, however, remains unknown. They may be roughly contemporaneous with intrusive phase 10.

The Stora Dima gabbro was not studied. The Kraksgil gabbro and the gabbro-diorite in Litla Dima are also regarded as belonging to intrusive phase 10.

In summary, gabbros belonging to:

a) intrusive phase 2, are those of Geitafell, Svinafell and unit C in Vidbordsfjall, and

b) intrusive phase 10, are those of Kraksgil, Litla Dima, and units A, B and D in Vidbordsfjall.

The present study therefore suggests two major gabbro injection pulses. As will be shown later, intrusive phase 10 overlaps intrusive phase 11, and the gabbros of phase 10 are therefore not necessarily strictly contemporaneous.

The volcanic episode resulting in the emplacement of intrusive phase 2, is believed to have fed the densely porphyritic lavas interbedded with the Jokulfell hyaloclastite and possibly the feldsparphyric hyaloclastites in Efstafell and Graenafell (upper part of Hyaloclastite Unit II). Due to some glaciation (marked by a tillite) prior to the extrusion of Rhyolite Unit II, and then extensive Pleistocene glacial erosion down to sea-level, some uncertainties exist regarding the interrelations and thicknesses of Hyaloclastite Units I and II and the intervening Basalt Lava Unit II in the centre of the volcano. Estimating from the thickness of the stratigraphic units in the flank areas (e.g. Table 2.1), the emplacement depth of the early gabbros (which intrude the top of Lava Unit I and the base of Hyaloclastite Unit I) may have been in the range 300-800 m below the former surface.

Annels and Newman also concluded that the gabbros were emplaced at shallow depth. Annels considered that the Hauksheidi mass was an extrusive complex fed by the Valagil gabbro (in the Svinafell area) and that the upper feldsparphyric lava sub-unit in Lava Unit 1 may also have been fed from the same source. The Hauksheidi mass, however, intrudes the overlying Hyaloclastite Unit I and Annels' interpretation of the Hauksheidi mass is therefore not accepted. However, Annels and Newman's general conclusion that all of these gabbros were emplaced at depths of less than 1 km is confirmed by the present study.

Intrusive Phase 3: This phase consists of feldsparphyric dykes. The phenocrysts are bytownite, with rarer augite in a doleritic matrix. This dyke suite is regarded as slightly younger than the Geitafell gabbro, and is apparently related to the same intrusive episode. These dykes may therefore be feeders to the porphyritic rocks within Hyaloclastite Unit II. Only a few members are found to belong to intrusive phase 3, all of which are shown in fig. 3.2. The north-east quadrant of a radial dyke system is shown in fig. 3.2. This dyke system appears to radiate from a centre in the Svinafell area and has been tilted with the lava pile through some 20-30 degrees. The tilting is reflected in the stereographic projection, where the majority of the dyke-poles cluster in the 60-70° region of the NW quadrant, indicating a 60-70° dip towards the SE quadrant.

Intrusive Phase 4: Phase 4 consists of acid veins, net-veining the Geitafell gabbro, and sparse acid sheets found in the sheet-swarm along the gabbro. The acid veins cross-cut the pegmatite veins in the gabbro and brecciate the gabbro near the southern end. Two episodes of acid veining occurred; the second is sparsely represented, but is observed to postdate intrusive phase 5. Most of the other gabbros are veined by acid rocks; the acid rocks belong respectively to intrusive phases 4 and 11.

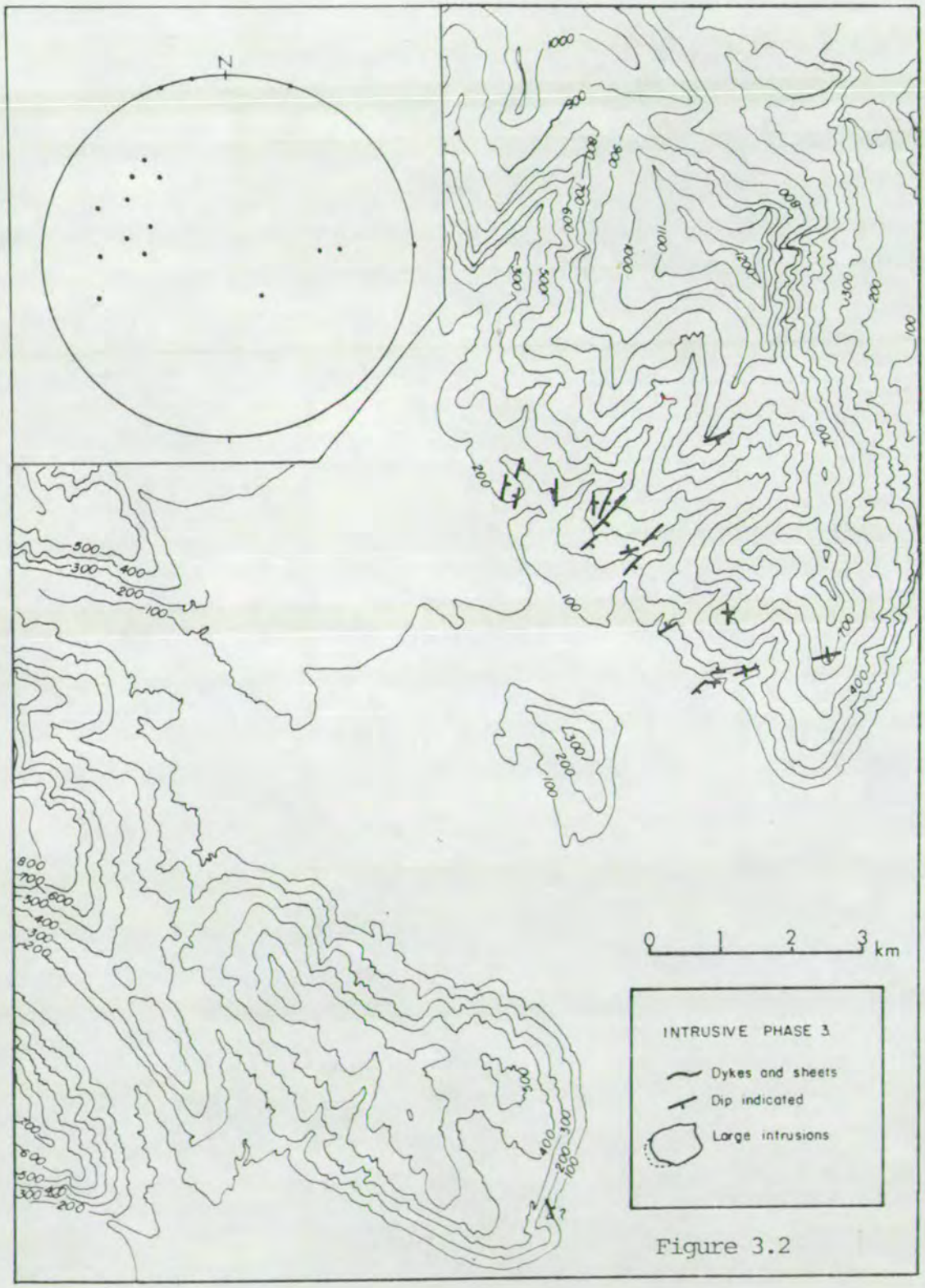
N
0 1 2 3 km
INTRUSIVE PHASE 3
Dykes and sheets
Dip indicated
Large intrusions

Figure 3.2

Intrusive Phase 5: Phase 5 consists of a doleritic cone-sheet swarm. Typically, the sheets are 0.5-0.7 m thick, but range up to 1.5 m. The dolerite has subophitic texture with grain-size of 0.5-1.0 mm. Dispersed poikilocrysts of augite (4-5 mm) enclosing feldspars are not uncommon. The matrix feldspars are labradorite zoned to andesine, accompanied by augite, ilmenite and magnetite. Sometimes this intrusive phase is also sparsely feldsparphyric showing bytownite phenocrysts (ca. 5 mm).

The dolerite sheet swarm is characteristically greyish green and thus differs from all other intrusive phases except phase 7. Commonly it shows gabbro xenoliths of varying size (fig. 3.3). The sheets have undergone greenschist alteration with actinolite and sphene replacing augite and ilmenite. Where the sheets have been most intensively altered, e.g. in Kraksgil, some sheets show peculiar spherulitic weathering surfaces (fig. 3.4). These appear related to uneven amounts of alteration product - the more intensely altered matrix surrounding less-altered spherical cores. A similar alteration pattern is common in a dolerite dyke swarm in the Cyprus ophiolite (Desmet et al., 1979).

The field relations and distribution of intrusive phase 5 are shown in fig. 3.5. The sheet-swarm is widely distributed in the volcano, extending beyond the later caldera fault (compare with Map 1). The concentric pattern of this intrusive phase is displayed in fig. 3.5, and further emphasized in the stereographic projection showing the low-angle cone-sheet nature of the sheet-swarm. Field evidence clearly shows phase 5 to have been injected into fairly flat lying strata, which subsequently became tilted. The later tilting to the NW resulted in increased dips of the sheets in the SE area and decreased dips of sheets in the NW half of the volcano. Low-angle sheets

Figure 3.3. Intrusive phase 5. A typical member of the doleritic sheet swarm, showing a gabbro xenolith.

Figure 3.4. A highly altered member of intrusive phase 5 in Kraksgil showing spherulitic weathering surface. The length of the hammer is 33 cm.

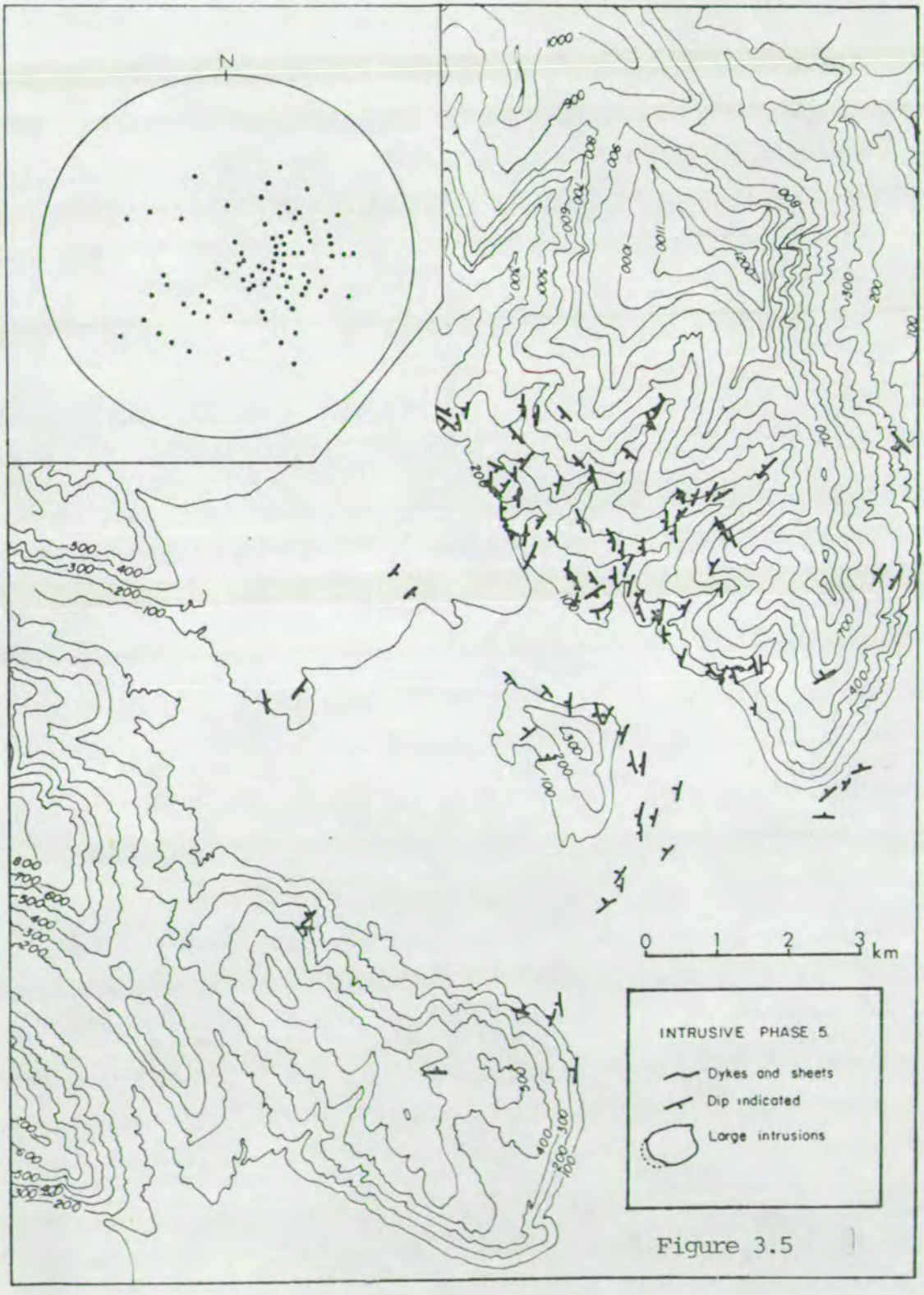
N
0 1 2 3 km
INTRUSIVE PHASE 5
Dykes and sheets
Dip indicated
Large intrusions

Figure 3.5

in the NW-half of the volcano may therefore show inverted dips towards the NW. Sheets dipping towards south to west, or towards north to east would show skewed dip directions towards the west and the north respectively. Some sheets in the Efstafell area apparently show inverted dip, and evidence is clearly found for increased dip in the SE-half of the volcano (e.g. at the caldera fault). The dip of the extrusives, however, is highly variable (10-55° NW), having been tilted both during a caldera event and a flexural event. The sinuous habit of many dykes and sheets, in particular in the hyaloclastites, further complicates meaningful strike/dip relationships. A correction for post-injectional tilting, which would require a detailed structural analysis in each area within the volcano, is therefore not attempted. Therefore, all pole directions and the spatial variance in strike/dip relations of the intrusive phases represent apparent strike-dip relations. The general tendency, however, of the sheets in the Efstafellsnes-Efstafell area, to show northerly strike and dips towards west, while the lavas dip some 20-40°NW, is explained by skewed strike-dip relationships. The pre-tilt strike of the sheets appears to have been roughly northwest with dips to the southwest. The effect of this rough correlation is to move the focal point of the cone-sheet swarm of phase 5 towards the middle of the volcano, towards the Svinafell area. The postulated centres of the radial dyke swarm (intrusive phase 3) and the dolerite cone-sheet swarm (phase 5), therefore coincide.

Using similar reasoning, the second cone-sheet system (phase 6) has a similar centre. The distribution of the third sheet swarm (phase 8), however, appears to have its focal point further to the north and the fourth concentric sheet swarm (part of phase 10) has a focal point in the Vidbordsfjall gabbros.

To define a focus (source depth) for intrusive phase 5, a detailed structural analysis would also be required. A rough estimate, however, is attempted below. There is an observed tendency for inclined sheets in the lava pile furthest away from the assumed centre, to take advantage of the interfaces between lava flows for some distance before continuing upwards at lower angles. Without correcting for this behaviour or post-intrusive tilting, a projection of sheets at the 100 m altitude level showing dips of 40° at 2 km distance from the focal point, 20° at 3 km, and 10° at 5 km, suggests the focus below the focal point to be at 1.7 km, 1.1 km and 0.9 km depth respectively. Therefore, it seems reasonable to assume the source region of intrusive phase 5 is at some 1.5 km depth below the present surface.

The depth to the Geitafell gabbro from the original surface is regarded to have been less than 1 km. The source region of intrusive phase 5 during its emplacement thus appears to have been at some 2.5 km depth.

Intrusive Phase 6: A highly feldsparphyric dolerite sheet-swarm constitutes intrusive phase 6. The feldspar phenocrysts (ca. 5 mm) are bytownite zoned to labradorite, and the dolerite matrix is slightly finer grained than in phase 5, ranging downwards in grain size to basaltic. Sheets of phase 6 are commonly thicker than those of phase 5, typically 0.7-1.0 m. Cross-cutting relation between phases 5 and 6 are common, and phase 6 is chilled against phase 5. The time lapse, however, between the two phases was probably of short duration. There may be a progression, with time, from the dolerite and the sparsely feldsparphyric dolerite (phase 5) to the highly feldsparphyric dolerite (phase 6), possibly indicating magma evolution from a single source. Phase 6 shows much the same degree of alteration as phase 5.

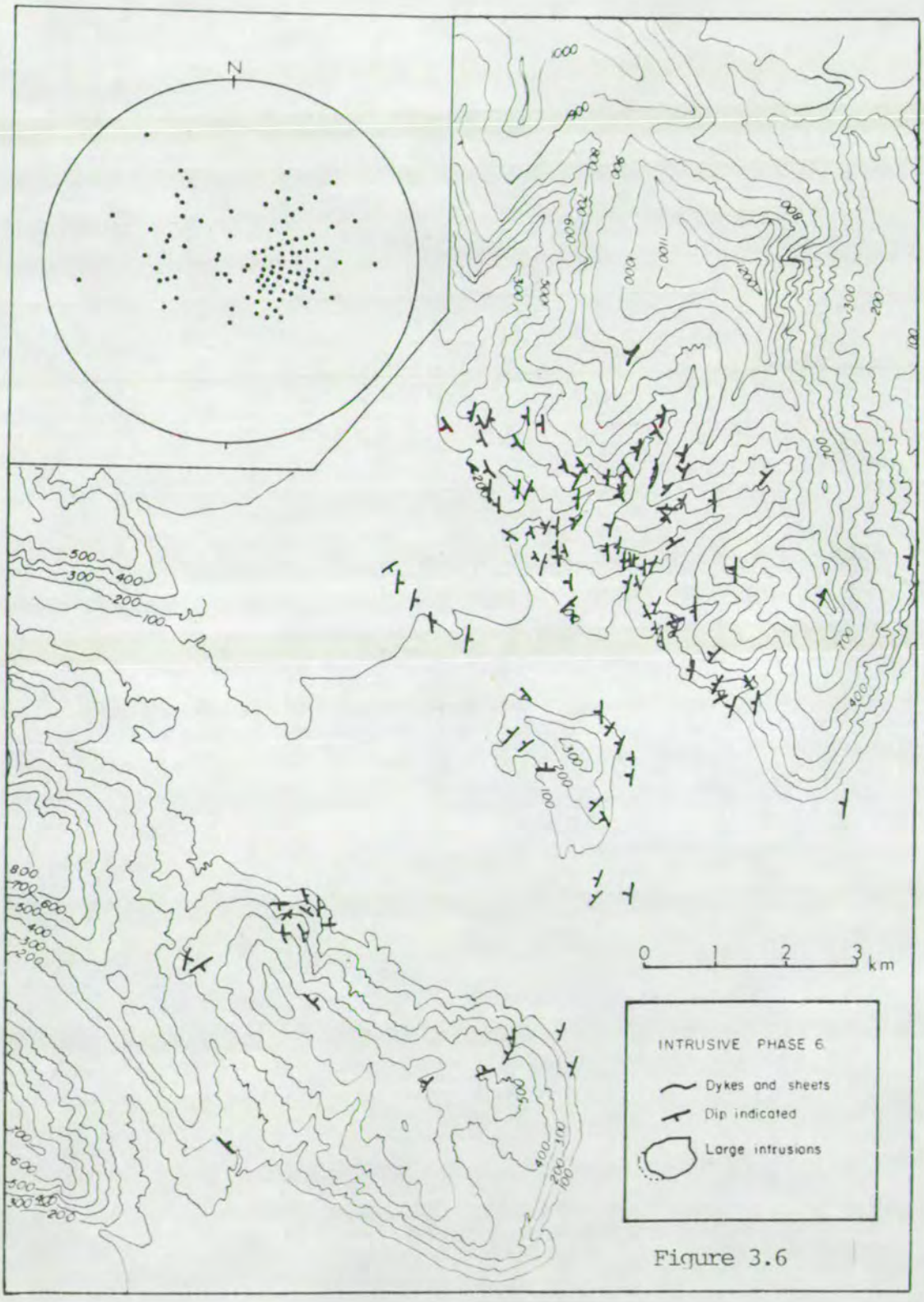
N
0 1 2 3 km
INTRUSIVE PHASE 6
Dykes and sheets
Dip indicated
Large intrusions

Figure 3.6

The field relations of phase 6 are shown in fig. 3.6, which shows a cone-sheet system almost identical to that of phase 5. The apparent focus of phase 6 coincides with those of phases 3 and 5.

Intrusive Phase 7: A dolerite dyke swarm constitutes intrusive phase 7. The dolerite is sometimes feldsparphyric. Thickness is commonly >1.0 m. Intrusive phase 7 has a similar grain size to phase 5.

Relatively few members of phase 7 are found in the field and their field relations are shown in fig. 3.7. Figure 3.8 shows a typical member of phase 7 cross-cutting phase 5.

Intrusive Phase 8: A fine-grained basaltic sheet swarm constitutes phase 8. The sheets vary from 0.3-1.0 m thick and are most abundant in the Efstafellsnes-Efstafell area. Field relations of phase 8 are shown in fig. 3.10 which suggests that the geometric centre (focus) lies further to the north than those for phases 3, 5 and 6. Members of this sheet swarm are commonly sinuous and show complex intrusion brecciation within the hyaloclastites (fig. 3.9).

Intrusive Phase 9: Phase 9 is petrographically identical to phase 8. The dykes, however, are normally thicker (0.7-1.0 m) than the sheets.

The field relations are shown in fig. 3.11. Like the other dyke-swarms, the strike is normally towards the NE and dips are some 60-90° to the SE. A sinuous habit for members of phase 9 is common, and frequently the dykes take advantage of earlier joints or contact planes. This tendency can obscure the field relations, particularly in the hyaloclastites, and distinction between phases 8 and 9 may be difficult. The general relationship, however, between the two phases is still evident. There is also some evidence that intrusive phase 9 may, to some extent, overlap the porphyritic phase 10. Almost ideal exposures, however, where most of the intrusive phases are present,

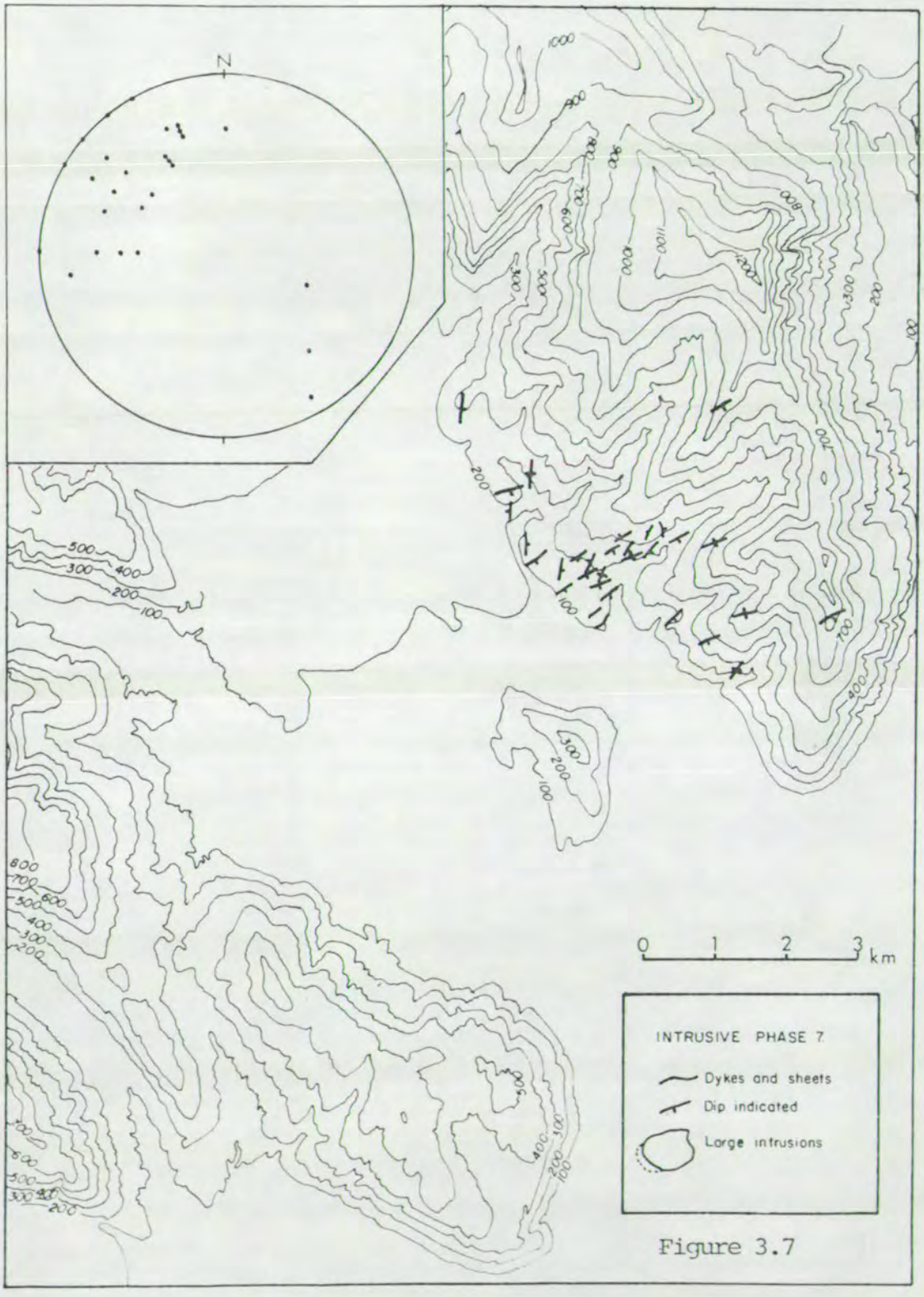
N
0 1 2 3 km
INTRUSIVE PHASE 7
Dykes and sheets
Dip indicated
Large intrusions

Figure 3.7

Figure 3.8. An inclined sheet belonging to intrusive phase 5 (lower right) cross-cut by a high-angle sheet (a dyke) of intrusive phase 7 (left margin of photo). The two sheets have almost identical matrices.

Figure 3.9. Irregular intrusive pattern of a phase 8 basaltic sheet in the hyaloclastite in Oldutangi. The dark blue sheet (upper left) has brecciated into the hyaloclastite (green). Note the alteration patterns - the disconnected and irregular white mineralveins (upper left) and the pale green marginal alteration of the angular basalt fragments. Clear striation marked by the regressing Hoffellsjokull glacier are seen in the clastic rock.

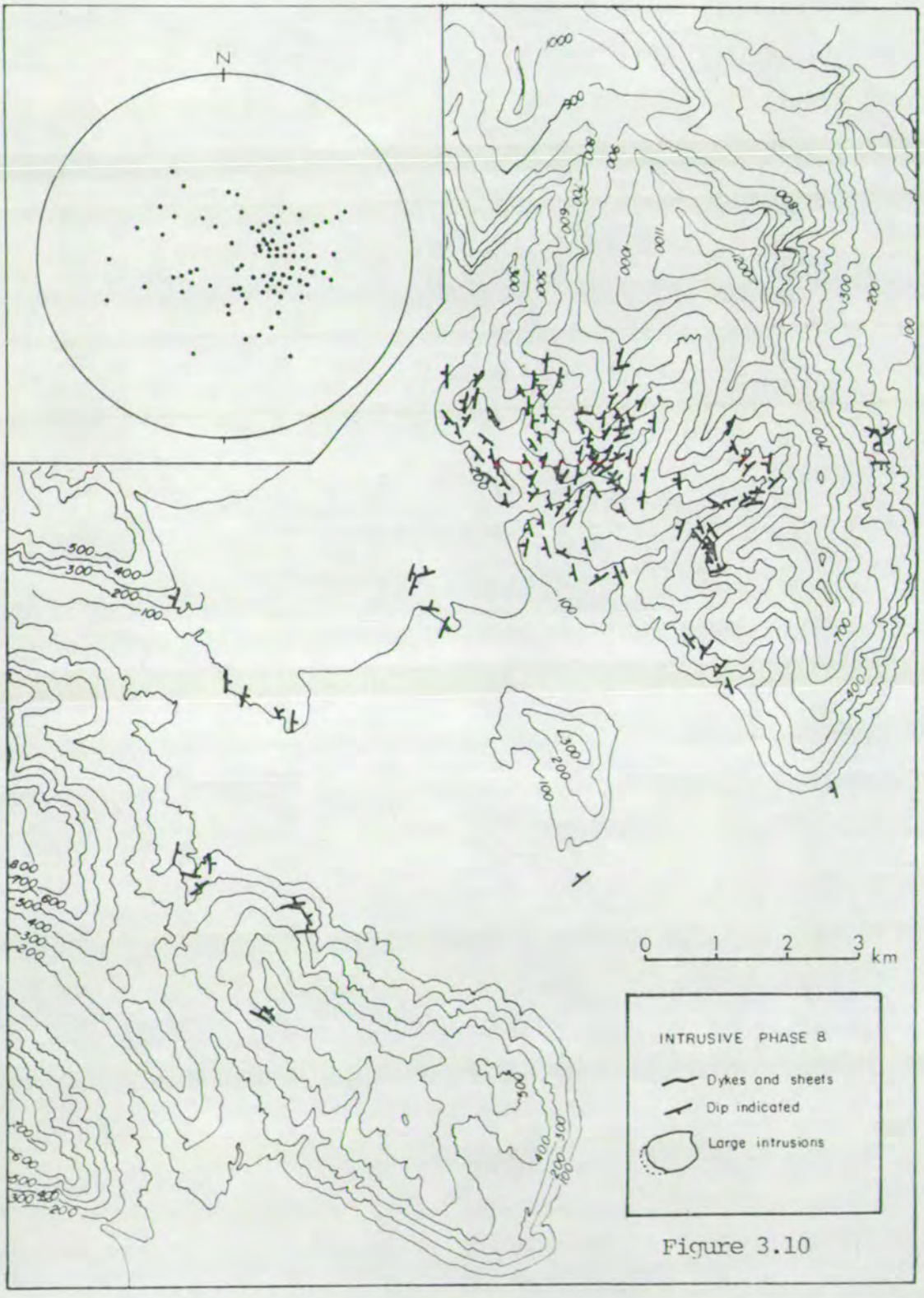
N
0 1 2 3 km
INTRUSIVE PHASE 8
Dykes and sheets
Dip indicated
Large intrusions

Figure 3.10

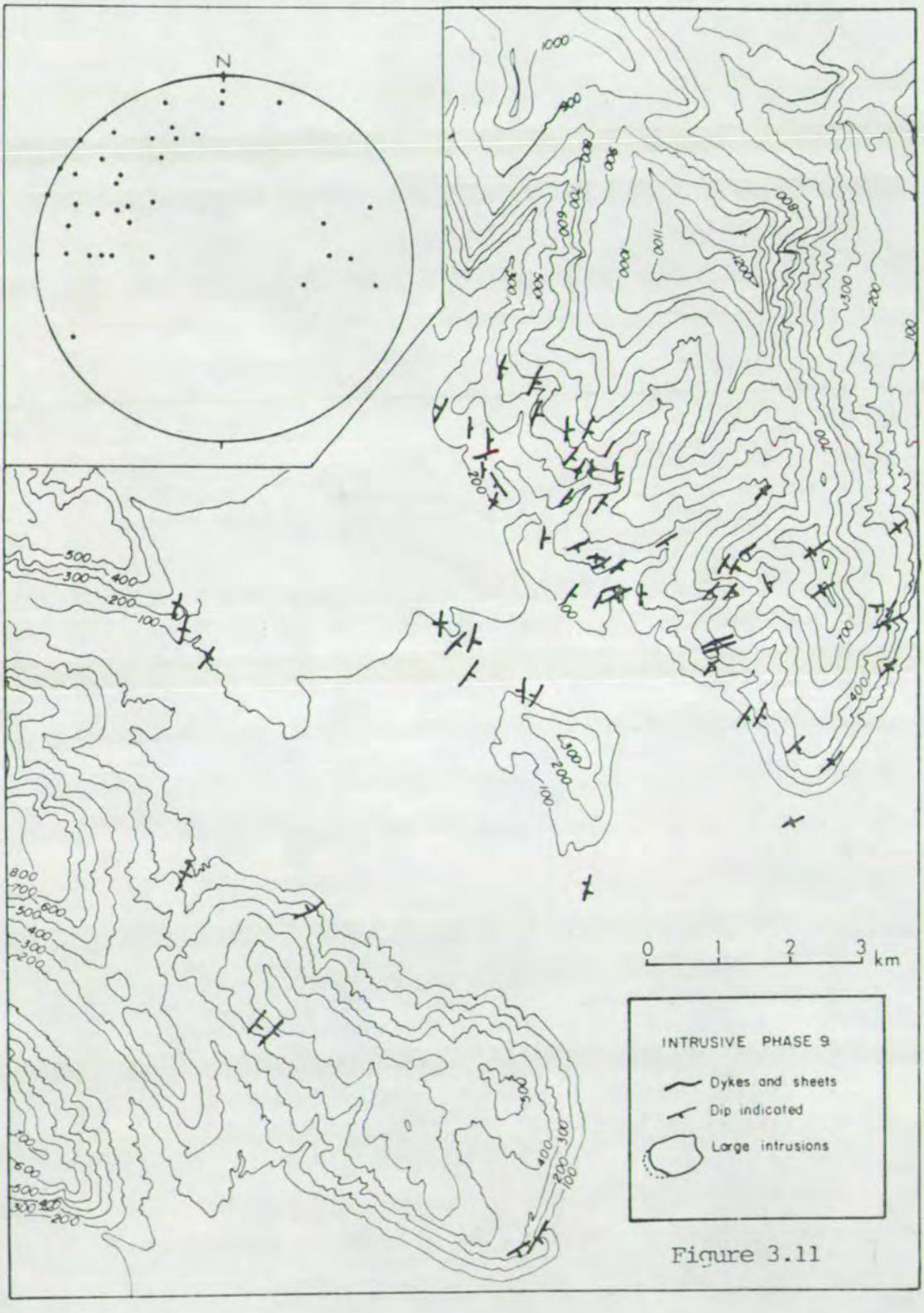
N
0 1 2 3 km
INTRUSIVE PHASE 9
Dykes and sheets
Dip indicated
Large intrusions

Figure 3.11

are required to evaluate such uncertainties. The scarcity of data from intrusive phases 3 and 7 reflect these difficulties, while some members mapped as phase 8 may actually belong to phase 9 and vice versa. It is clear that some time overlap occurs between phases 9, 10, 11 and 12. Such evidence indicates that further separation of the intrusive complex is possible. Further classification, however, is not attempted, but time overlap between phases is indicated.

Intrusive Phase 10: A highly feldspar porphyritic dyke- and sheet-swarm comprises intrusive phase 10, along with apparently contemporaneous gabbro intrusions in Vidbordsfjall (units B and D and possibly A), Kraksgil and Litla Dima. The gabbros have been discussed above, with intrusive phase 2.

The dykes and sheets of phase 10 range from doleritic to basaltic, containing phenocrysts which are typically <2 cm (see fig. 3.12) zoned from anorthite cores to labradorite rims. The size of the phenocrysts often readily indicates intrusive phase 10 in the field. A downward gradation, however, in phenocryst size exists.

Intrusive phase 10 evidently combines a cone-sheet swarm (fig. 3.13) a porphyritic dyke swarm and gabbros. Cross-cutting relationships exist between members of phase 10, in particular in the Vidbordsfjall area. The time overlap indicates magma pulses of similar type, the number of which are unknown. All data is shown together in fig. 3.14 for intrusive phase 10. A local cone-sheet swarm apparently surrounds the gabbro intrusions in Vidbordsfjall, while elsewhere the dykes have a north-easterly strike. A deviation from this general trend in the northeastern half of the volcano, mainly occurs along the caldera fault.

Intrusive phases 10 and 11 are believed to have accompanied the caldera event. Phase 10 is regarded as overlapping the caldera event,

Figure 3.12. A typical member of intrusive phase 10 dykes, showing large anorthite-bytownite phenocrysts (equal or less than 2 cm). The hammer head measures 17.5 cm. The rock is extensively hydrothermally altered - the phenocrysts, for instance, are extensively replaced by prehnite-laumontite-epidote--albite-K.feldspar, and the greenish colour of the matrix is due to extensive replacement of glass and pyroxene by chlorite.

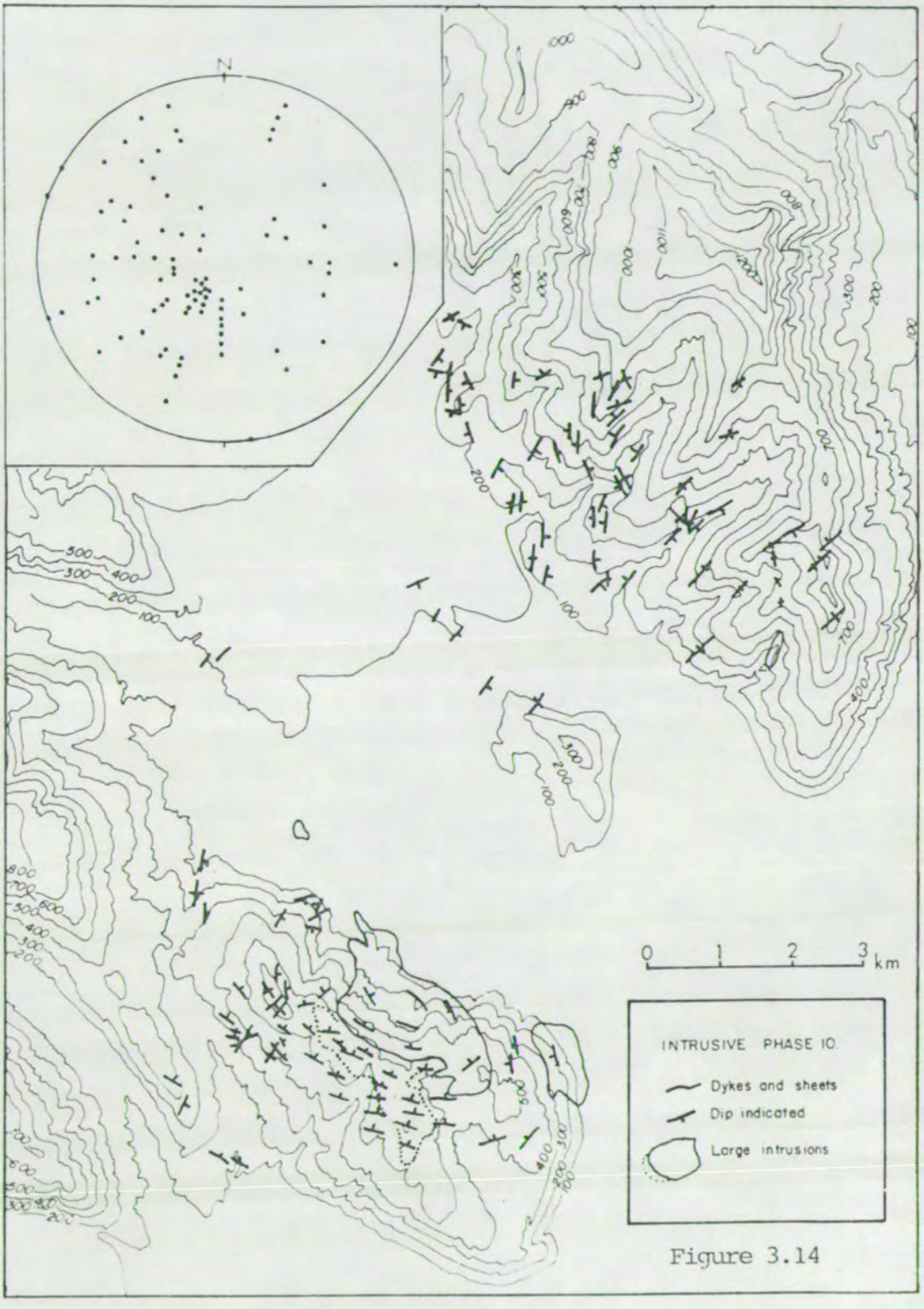
N
0 1 2 3 km
INTRUSIVE PHASE 10
Dykes and sheets
Dip indicated
Large intrusions

Figure 3.14

and phase 10 also overlaps phase 11. Phase 10, in fact, seems to have been injected over a considerable length of time, extending towards the time of phase 12. A highly unusual feature is observed in the felsitic intrusion (phase 11) between Vidbordsfjall and Graenafell. The felsitic intrusion is cut by two differently striking sheets of phase 10. One of these is intruded by a brown dolerite intrusion of phase 12, chilled against the interior of phase 10; it occupies the axial zone of the phase 10 sheet for several metres in the exposure before breaking out through one of the margins. This composite nature of phase 12 inside phase 10, which shows asymmetric chilled margins, may be purely accidental - or it may possibly be a reflection of (a) similar source region, (b) similar stress field, and/or (c) similar age relating the members of the two intrusive phases. The overlap of phase 10 to phase 11, however, is the only clear implication derived from this interesting field phenomenon.

The gabbro intrusion in Vidbordsfjall (like unit B) is partly olivine-bearing (and olivine-normative according to Newman), and some dykes belonging to phase 10 show both feldspar and pyroxene phenocrysts. Newman (1967) described some dykes in the Vidbordsfjall complex as having both modal and normative olivine. These apparently rare dykes are included with phase 10. Densely porphyritic thick lavas at the base of Lava Unit III, immediately above the rhyolite lava (of phase 11) in Geitafell, and above the hyaloclastite in Efstafell (Grjotarbotn), were probably fed by intrusive phase 10. This appears to be the case for the thick lava (12-18 m) in Geitafell which shows the characteristic weathering of an olivine tholeiite and contains phenocrysts of feldspar, pyroxene and olivine.

Intrusive Phase 11: Large felsitic intrusions, and rhyolite or pitchstone dykes and veins constitute phase 11 whose distribution is shown

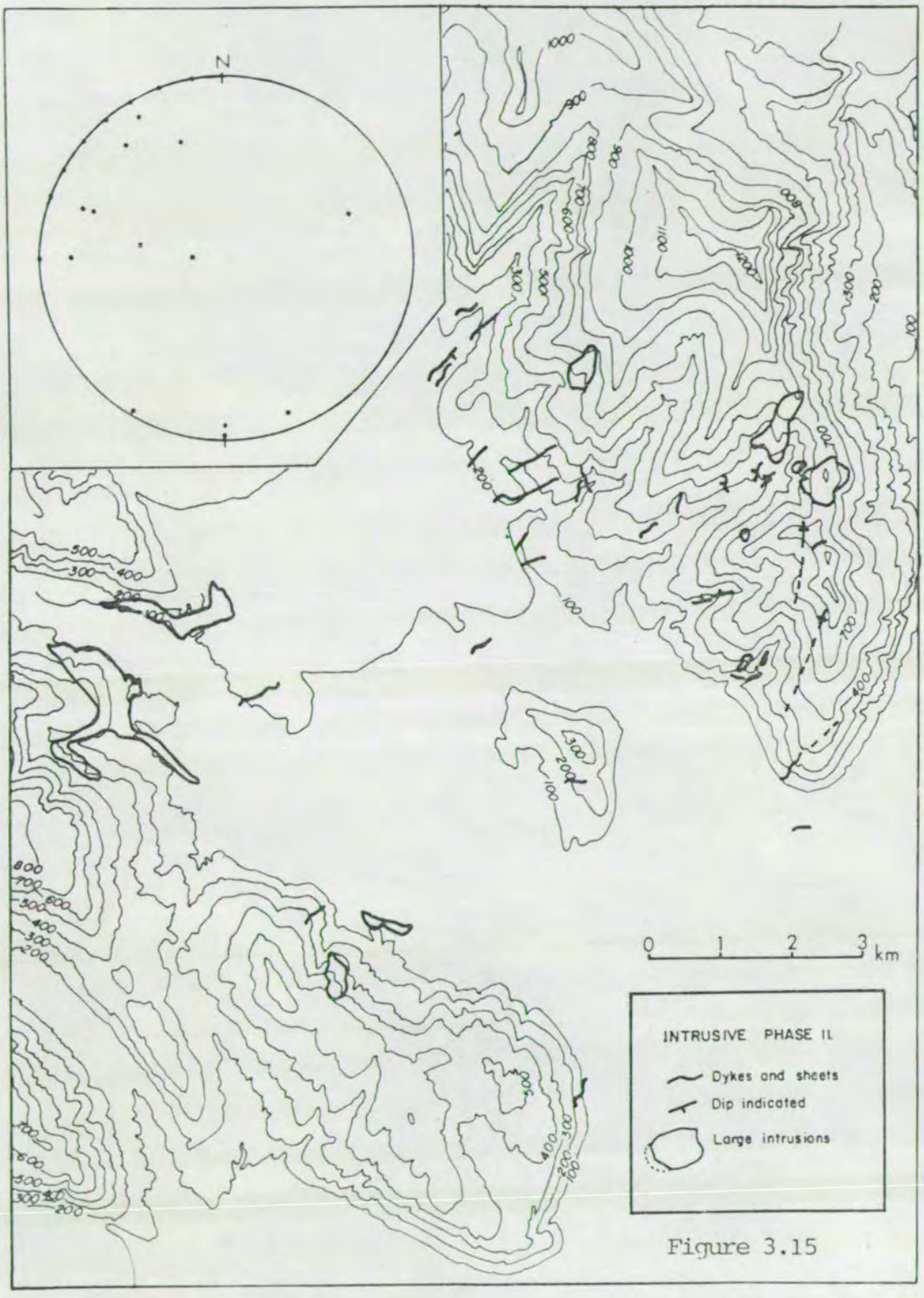
N
0 1 2 3 km
INTRUSIVE PHASE II
Dykes and sheets
Dip indicated
Large intrusions

Figure 3.15

in fig. 3.15. The larger intrusions are located close to, but on either side of the caldera fault. The acid dykes are commonly 1-2 m thick and range from porphyritic to non-porphyritic, and normally show chilled margins. Occasionally, however, the whole dyke is pitchstone and in one case a felsitic rhyolite surrounds a pitchstone middle. Occasional composite dykes are also found with basaltic margins and acid centres.

Rhyolite Unit II (see Map 1) was probably fed by intrusive phase 11. The rhyolite lava near Gjanupsvatn is buried by some eight brown-weathered coarse-grained basalt lavas (80 m thick unit) which are correlated with intrusive phase 12. Acid tuffs and thin acid lavas above the brown lavas, however, are included with Rhyolite Unit II, and may have been supplied by the same general acid intrusive phase (11). This correlation therefore assumes that phase 11 overlaps phase 12 in time to some extent. No direct evidence of phase 12 being cross-cut by phase 11 is found inside the volcano, while the reverse is common.

A close association is seen between intrusive phases 10 and 11. Phase 11 net-veins some of the gabbros of phase 10, for instance in Kraksgil and gabbro unit B in Vidbordsfjall. In the Kraksgil and Litla Dima gabbros, gabbro is seen to grade into subordinate diorite and granophyre. Narrow (several cm) felsitic veins of phase 11 also cross-cut country rocks in Kraksgil in an uncommon zig-zag habit. Annels (1967) described a composite dyke from Kraksgil, having basaltic margins including gabbro xenoliths and rhyolitic centre. The intimate association of acid and basic rock belonging to phase 11 and the time-overlap of phase 10 is therefore clear.

Intrusive Phase 12: Thick dolerite dykes constitute intrusive phase 12. The thickness varies from ca. 0.5-6.0 m, but most of the dykes are close to 2 m across. Unlike the other intrusive phases, the dykes

Figure 3.16. The green host rock is hyaloclastite of Unit II cross-cut by intrusive phase 8 sheet (dark in the foregound), intrusive phase 10 dyke (the thick porphyritic dyke to the left - the same dyke is shown in figure 3.12), intrusive phase 11 (the light brown rock to the right near the ice marginal lake Gjanupsvatn) and intrusive phase 12 dyke, which is the brown dyke in the upper left corner.

are commonly columnar jointed. The dykes are relatively fresh, but develop characteristic brown weathering surfaces. They are commonly vesicular and are easily distinguishable from all other intrusive phases. Annels (1967) called them the 'brown dolerite dykes'. Intrusive phase 12 clearly postdates the high-grade alteration in the volcano, but the dykes are cross-cut by sulphide and zeolite veins.

A typical member of this dyke family can be seen in fig. 3.16 (which also shows members of intrusive phases 8, 10 and 11). The overall field-relations are shown in fig. 3.17. In the stereographic pole projection in fig. 3.17, a distinction is made between dykes occurring northwest (marked with dots), and southeast (circles), of a NE-SW line through the middle of the volcano. This line extends from the northern end of the Vidbordsfjall gabbro across the middle of the Geitafell gabbro. The lavas northwest of this line are tilted some 20-50° to the northwest, while those southeast of this line generally dip from 10-20°. The dykes northwest of the line clearly show shallower dips of some 50-70° southeastwards, while the dykes southeast of the line normally dip southeastwards from 70° to 90°. Two interpretations are possible: (i) that intrusive phase 12 is tilted by the flexural event, or (ii) that these dykes were injected during the flexural event along inclined normal faults in the middle of the flexure zone. Both possibilities are regarded as equally likely. Intrusive phase 12 is believed to have accumulated during the flexural event as described below.

Several lava flows occurring immediately above the rhyolite lava (related to phase 11) near Gjanupsvatn, forming the base of Basalt Lava Unit III, petrographically closely resemble the phase 12 dykes. The brown lavas were probably fed by intrusive phase 12, apparently during the flexural event. These brown-weathered lavas are tilted some 12-15°, and bank against still more steeply dipping older strata.

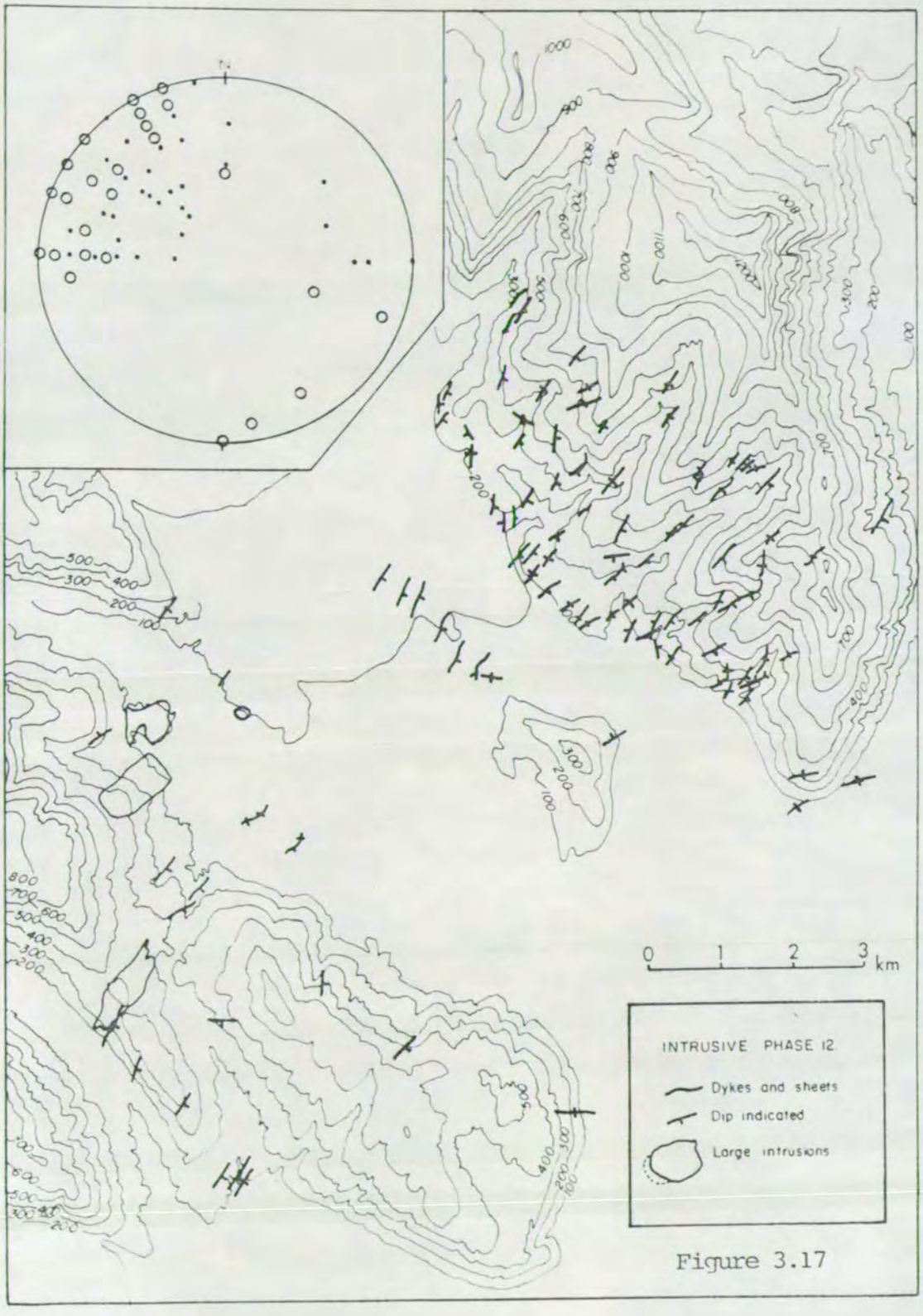
N
0 1 2 3 km
INTRUSIVE PHASE 12
Dykes and sheets
Dip indicated
Large intrusions

Figure 3.17

Some 200-300 m above the brown lavas a 5° structural unconformity occurs and the overlying lavas only dip some $5-6^{\circ}$ NW. In Efstafell the unconformity is of the order of 20° where the upper part of Lava Unit III buries the steeply flexed Hyaloclastite Unit II (figs. 3.25, 2.3 and 2.4). Since both the brown lavas and their supposed feeder dykes themselves show flexing (but less than the preceeding rhyolite etc.) it is inferred that this eruptive episode occurred while the flexing event was still taking place.

Extensional tectonic features which accompanied the emplacement of intrusive phase 12 are neatly displayed. Sometimes the dykes are seen to be arranged in sinistral 'en echelon' fashion (fig. 3.18). The dykes were presumably attending fractures which were either open during the entrance of the dykes or widened during the dykes' emplacement.

The characteristically thicker dykes of phase 12, their en echelon arrangement and the typical presence of vesicles, are features contrasting with other intrusive phases at the same erosional levels. These features and the apparent time relations between intrusive phase 12 and the flexural event are used to model the volcanological evolution of the region. It is suggested that rapid regional extension occurred at the time of emplacement of intrusive phase 12 resulting in flexuring. Intrusive phase 12 occurs most abundantly in the northwestern half of the volcano (the 'brown dolerite dykes' of Annels, 1967) within the steepest dipping strata, as recognized by Annels and confirmed in the present study. Annels further showed the brown dolerite dykes to be arranged as en echelon dyke swarms. These have a sinistral disposition coinciding with the en echelon pattern of the southern part of the flexure zone (Torfason, 1979).

The a) intrusive phase 12 of the Geitafell volcano, b) brown coarse-grained lavas at the base of Basalt Lava Unit III, and

Figure 3.18. Intrusive phase 12 dykes in Geitafellsgil. The columnar jointed dyke narrows to the end. Another dyke of the same intrusive phase is seen to the left on the photo. The distance between the dykes is some 20 m and the two dykes are arranged en echelon (see sketch map below).

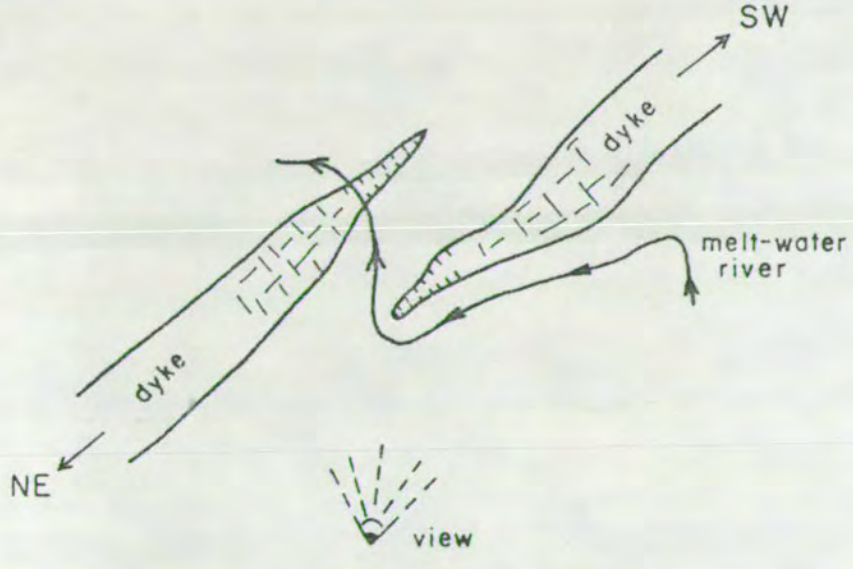

c) flexural event, are believed to be essentially contemporaneous. The last affects older strata in the north and younger strata to the west, and is therefore younger in the western region (Torfason, 1979). The time relations presented in this thesis for the flexural event and intrusive phase 12 of the Geitafell volcano gain some support from recent radiometric age data. Rhyolite Unit II (correlated with intrusive phase 11) is dated at 5.93 ± 0.18 m.y., while phase 12 shows an age of 5.74 ± 0.30 m.y. (K. Albertsson, in prep., pers. comm.; N.B. figures are provisional).

Injection Intensity: Annels (1967) mapped the intensity of the intrusions. The 20% 'intrusion contour' shows a crude eliptical shape, extending SW from the southern end of Jokulfell to the NE-side of Graenafell, along which it runs around the Vidbordsfjall gabbro complex, NE-wards into Geitafellsgil and NW-wards across Geitafell and Efstafell into Gjanupsvatn. 30%, 50% and 75% intensity contours occur within this crude ellipse. This general picture has been confirmed, and shows that intrusive intensity is greatest in the middle of the volcano, around the gabbros and in the northwestern half of the volcano, at the upper stratigraphic levels in Hyaloclastite Units I and II and Basalt Lava Unit II. Illustrations showing varying degrees of intrusive intensity are presented in figs. 3.19, 3.20 and 3.21. While alteration of the volcanic rocks is treated in later chapters, it is worth noting that the extent of alteration is only partly related to intrusive intensity.

Discussion

Two competing models for the formation of cone-sheets, radial dykes and ring-dykes exist. The classical model of Anderson (1936) assumes both radial dykes and cone-sheets to have formed as a result of upward pressure of magma, with cone-sheets occupying hydraulic

Figure 3.19. 95-98% intrusive intensity in the sheet swarm in Geitafellsgil, surrounding the Geitafell gabbro. Most of the inclined sheets belong to intrusive phases 5 and 6, while intrusive phases 3, 4, 7, 8, 9 and 12 are also found. The sheet swarm is extensively fractured and locally faulted.

Figure 3.20. 50-75% intrusive intensity in Efstafellsnes.

Figure 3.21. 25-30% intrusive intensity in Hyaloclastite Unit I in Efstafell. The intrusive intesity drastically diminish in the overlying Hyaloclastite Unit II in Efstafell. The greenish colour is typical for chloritized extensively altered hyaloclastite.

tensile fractures formed during the upward push and swelling of the magma chamber, while ring-dykes occupy shear fractures resulting from subsidence of the magma. This model has been modified by several authors (e.g. Robson and Barr, 1964, and Durrance, 1967) who reverse the order of fracture formation resulting from subsidence and swelling, and suggest that cone-sheets occupy shear fractures, while ring-dykes occupy tension fractures. A critical review is presented by Phillips (1974) who concluded that radial dykes occupy simple hydraulic tension fractures formed periodically during the upwelling of magma, ring-dykes form in shear fractures produced when the cover to the magma body subsides, as explained by Anderson, and suggested that cone-sheets occupy shear fractures formed as a result of dynamic stresses arising from the rapid expansion of magma undergoing retrograde boiling.

Walker (1975a, b) proposed a different model, where the relative densities of magmas and crust are regarded as playing a major role in the localisation of igneous intrusions. A basic concept of Walker's model is that volcanic complexes experience an early event with an acid diapir rising to a high level, at the base of which basaltic magma is located as a result of density differences. He then postulated that the emplacement of cone-sheets is governed by a tendency of rising magma to move in the direction of maximum 'excess hydrostatic pressure', i.e. the amount by which the hydrostatic pressure in the magma exceeds the lithostatic pressure. He further suggests that the curvature of surfaces of equal excess hydrostatic pressure near a high level diapir of low density acid magma, results in the diversion of uprising magma (acid and basic) to form cone-sheets instead of dykes. A late stage in the development of an intrusive centre involves escape of successive batches of acid magma from the diapir, resulting in the

subsidence of the central area and consequent ring-dyke emplacement. Nonetheless, in applying this model to the thesis area there is obviously a lack of evidence for an early uprising of an acid diapir resulting in updoming. An early event, however, in the history of the Geitafell volcano, was the formation of Rhyolite Unit I, evidently related to an early uprising of acid magma in some form, but considerably predating intrusive phases 2-6. The possible presence of an acid body near the surface (below the present erosion level) may have had some effect on the emplacement of the Geitafell cone-sheets (phases 5 and 6) in accordance with Walker's model.

The evidence from the Geitafell volcano shows that the early intrusive phases (2-6) may have been accompanied by major uplift of at least 100 m near the flanks, presumably increasing inwards (section 3.3.3). The episode of uplift may have been initiated with emplacement of massive basaltic magma intrusion into the centre of the volcano where they crystallized as gabbro (phase 2). In direct continuation the intrusive mode changed and an apparent radial dyke-swarm (phase 3) was emplaced, succeeded by two major phases of cone-sheet injection (phases 5 and 6). The stress-field situation during the formation of phases 7-9 is unclear, and the centre of the third cone-sheet swarm (phase 8) appears to have migrated northwards from the earlier situation. The late gabbros (part of phase 10) were associated in time and place with the caldera fault. Their emplacement may have occurred during subsidence in a stress-field similar to that producing the ring-dyke formations in the British Tertiary volcanic centres. In a broad sense, the sequence of events in the Geitafell volcano resembles the general sequence in the British Tertiary volcanoes as summarized by Walker (1975a).

The present study does not provide any evidence to support either model of cone-sheet formation as presented in the earlier paragraphs.

Regular basic cone-sheet swarms, however, in the Icelandic volcanoes do not appear to be common, but have, for instance, been described from three central volcanoes, the Setberg central volcano in west Iceland (Sigurdsson, 1966), the Vididalur-Vatnsdalur central volcano in northwest Iceland (Annells, 1968) and from the Geitafell volcano (Annels, 1967; Newman, 1967; and this study). In other studied volcanic centres in Iceland basic inclined sheets do not form as regular cone-sheet swarms (Walker, 1963, 1974, 1975b; Gibson et al., 1966; Blake, 1964; Hald et al., 1971; Fridleifsson, I. B., 1973).

Presumably, the difference can be explained by the relation of magma upwelling to spreading rate. Slower spreading rate and greater magma upwelling both favour formation of a regular cone-sheet system.

3.3 Structure

Two major structural features within the Geitafell volcano are (a) the caldera fault, and (b) the flexure zone. The time relation between the formation of these structures and the volcanological and hydrothermal evolution are of major concern in the present study. Other structural features include fault and fracture patterns. Representative strike/dip data for the strata and the major faults are shown on Map 1.

3.3.1 Strike/dip Relations of the Stratigraphic Units

Some 200 strike/dip measurements were gathered from the volcano, while only representative strike/dip relations are shown on Map 1. Strike/dip relationships within the caldera are often obscure, in particular within lavas interbedded in the hyaloclastites, as in Efstafellsnes. Variations in strike and dip suggest the prevalence of block faulting, but field-relations are commonly obscured by vigorous intrusive activity.

The area can be separated into two parts, NW and SE of a line through the middle of the volcano, from the northern end of the Vidbordsfjall gabbro into Geitafell. The dip of the strata NW of this line are characteristically high (20-50° NW-wards), while the strata SE of the line dip less than 20° except at the caldera fault where a marked turn in strike occurs and dips of 45-50° are common.

Moving upwards from the base of Lava Unit I (strike 40E, dip 8-10° NW) strike/dip changes to 50E, 10-12°, and further to 90E, 10° N (see Map 1). This deflection is taken to indicate the original 'constructional surface' suggesting a topographical rise over the summit area of the volcano.

The significance of the caldera and the flexural event are dealt with in sections 3.3.4 and 3.3.5.

3.3.2 Fractures and Joints

In the geological sciences two sets of fracture terminology have evolved; while one set is mainly used by field geologists, the other is mainly used by experimentalists. As pointed out by Secor (1965), no general agreement on the precise meaning of terms exists. In field-studies the term 'joint' has been used for fractures that have little or no offset or movement parallel to the plane of the fractures, while the term 'fault' is used for fractures which do show such offset (e.g. Billings, 1954; Price, 1966). In experimental studies the terms 'extension fractures' (formed normal to the least principal stress) and 'shear fractures' (inclined to the direction of principal stress and often forming conjugate sets of joints) have been used (e.g. Griggs and Handin, 1960).

For the sake of simplicity, the terms joints, fractures and cracks are used synonymously in the present study, to indicate fractures showing little or no displacement. While simple dilation joints are commonest, conjugate joint sets are also quite common, sometimes

indicating minor shear movement. It has been useful in the field to separate 'primary joints' from 'secondary joints'. The former being related to shrinkage or flow of lavas and intrusives and the latter to subsequent movements of the strata. Primary joints are normally filled by precipitates from the earliest mineralizing fluids, while the sequence of succeeding joints become mineralized by later fluids. The joint widths vary greatly, from less than 1 mm to more than 1 m. They may be termed micro-joints (hardly visible), minor joints (on millimetre scale), major joints (cm-scale) and master joints (0.2-2.0 m).

The joints are oriented in all directions. While the orientation of minor joints is commonly highly variable (both primary and secondary joints), major and master joints (secondary) commonly show two preferred orientations, (a) striking NE-SW, and (b) parallel to the caldera fault.

Major and master joints commonly occur in zones ranging from widths of several tenths of cm to several m. Alteration in terms of amount of secondary product is normally intense in such fracture zones. One or more faults is commonly encountered within such fracture zones.

All joints and faults filled with minerals are termed mineral-veins or vein systems. Mineral-veins formed over a wide time span and the study of their cross-cutting relations and nature is of major concern in this project, being fundamental for the evaluation of the hydrothermal history.

Extensive fracturing and faulting evidently greatly affected the permeability of the system, and characterises the type of hydrothermal system studied. A rough measure of joint intensity reflects the importance of fracturing processes to a percolating fluid system. A count of the number of visible mineral veins (minor and major joints)

in the Geitafell gabbro (phase 2) showed on average (six measurements) some 26 veins/m^2, measured in horizontal and two perpendicular vertical planes. This roughly indicates that unfractured gabbro blocks larger than 10 cm across are unlikely to exist.

Lavas and sheets in the sheet-swarm adjacent to the Geitafell gabbro show increased vein intensity. The lava shows 44 veins/m^2, but is fractured into fragments not larger than 2 cm across, suggesting some 100 joints/m^2. In this case some of the joints may be mineralised early micro-joints, while others may be related to recent frost shattering. Counting of visible mineral veins in this situation therefore reflects the minimum number of joints. Intrusive phase 5 showed some 50 veins/m^2 and intrusive phase 6 showed 26 veins/m^2.

Lavas in Kraksgil near the caldera fault showed some 55 veins/m^2, while a lava in Hoffellsdal outside the caldera only showed some 22 veins/m^2, of which 12 veins are related to the most recent vein system involving calcite and zeolite. Elsewhere in the volcano mineral vein intensity ranges between these two values.

This crude analysis, where nothing is taken into account but the number of mineral veins reflects the importance of fracture permeability of the hydrothermal system. It is through study of the mineralized fractures (veins) that a chronology of the hydrothermal events can be established.

3.3.3 Faults

Most of the faults, apart from the caldera faults and one reverse fault, are antithetic normal faults, striking NE-SW. Due to lack of marker horizons in the strata, vigorous intrusive activity and fracturing, and/or to inadequate exposures, the size and direction of throw can only rarely be measured. The two largest measured antithetic normal faults have a throw of some 30 and 60 m respectively. Many faults,

however, are seen to involve only minor displacement (several cm to several m). The main faults with throw directions and sizes indicated (where known) are shown on Map 1. The faults are of various ages, the earlier often obscured by later intrusives, while the most prominent antithetic normal faults appear related to the flexural event. Graben structures are rarely positively identified within the volcano, although minor grabens (subsidence of some 10-20 m) are found in Lava Unit III, postdating the flexure.

One reverse fault is found in the Geitafell-Efstafell mountains, striking N-S and NW-SE. The fault is indicated on Map 1 and in fig. 3.22. The fault dips steeply SW (towards the central area) and shows some 100 m displacement of Hyaloclastite Unit I, while only some 50 m displacement of Hyaloclastite Unit II is seen. Part of Hyaloclastite Unit II is regarded to have formed contemporaneously with the early gabbro intrusion (phase 2) in the central area. An early uplift of the central region is therefore suggested to explain this unusual fault. The uplift is some 100 m at the fault and is inferred to increase inwards within the volcano. The steeply NE-dipping hornfelses at the Geitafell gabbro contact may also be regarded as some evidence for uplift of the central region.

3.3.4 The Caldera Fault

The caldera fault is shown on Map 1 and in fig. 3.23. The fault is clearly seen in Hoffellsfjall, crossing through Tungufell and Midfell and can be traced through Geitafell and Efstafell into the Gjanupsvatn area. The fault scar, however, is more obscure in the northwestern part of the area where it crosses the hyaloclastites and it has been inferred from prominent curved fractures and faults (as in the Gjanupsvatn area).

In the southwestern half of the volcano the fault is obscured by the gabbro complex in Vidbordsfjall and unexposed in the hyaloclastites

Figure 3.22. The reverse fault is seen to the left in the photo (marked by the snow patch). The green rock is Hyaloclastite Unit I, overlain by Basalt Lava Unit II, both clearly faulted. The light brown rock is a felsite intrusion (of phase 11, inside Lava Unit II) and an acid lava of Rhyolite Unit II overlain by Basalt Lava Unit III in Grasgiljatindur. A thin bed of Hyaloclastite Unit II including a tillite bed intervenes Lava Unit II and Rhyolite Unit II.

Figure 3.23. The caldera fault in Tungufell. The ravine in the foreground is Midfellsgil. Hornafjordur bay and the Vidbordsfjall are visible in the background.

in the northern part of the area and its trace has also had to be inferred rather generally. Several strike/dip measurements near the inferred fault-line in Vidbordsfjall suggest steeply inward-dipping strata, and to the west, the fault is drawn where the sheet-swarm is sharply terminated (see fig. 3.13).

In the northeastern part of the volcano which has been studied in most detail two faults subparallel to the caldera fault are seen inside the caldera (Map 1). These faults may suggest that the caldera subsidence occurred in a step-like fashion in the NW part of the volcano.

The total subsidence is estimated at some 500 m in the central area, diminishing to ca. 200 m towards the fault. The lavas in Tungufell and Midfell have steep inward dips of some 45-50° near the fault but dips diminish to 15-20° inside the caldera.

Annels (1967) clearly did not recognize this significant collapse structure. However, he related the prominent fault in Tungufell and the steeply dipping lavas to updoming caused by the contemporaneous wedge-shaped gabbro body in Kraksgil. Evidently, some lava-updoming by the Kraksgil gabbro is possible. However, the gabbro strikes obliquely to the caldera fault and steeply dipping lavas occur on both sides of it (Map 1). Therefore the possibility of updoming is regarded as a subsidiary cause of the steep tilting, which is chiefly related to the regional collapse structure.

As seen on Map 1, the reverse fault in Geitafell extends into Midfell where it appears to join the caldera fault. It is possible that the fault in Midfell-Tungufell and Hoffellsfjall first acted as a reverse fault and subsequently as a caldera fault. This, however, remains speculative.

The caldera subsidence occurred fairly late in the volcano's evolution and is regarded as contemporaneous with intrusive phases 10 and

11. Only intrusive phases 10 and 12 are seen to enter and cross the caldera fault.

3.3.5 The Flexure Zone

The regional flexure zone in SE and E-Iceland has been referred to above (Chapter 1.2). The flexure has been defined as the zone where lavas dip in excess of 10° (Walker, 1964) and has been shown to have a sinistral en echelon arrangement in SE-Iceland, changing to a dextral pattern in E-Iceland (Torfason, 1979, see fig. 1.4). The flexure zone crosses lava isochrons, occurring within the youngest rocks furthest to the SW. Torfason suggested that the flexure zone in SE-Iceland was diachronous; 2.5-3.0 m.y. in Lonsoraefi (NE of the Geitafell volcano) and 1.5-2.5 m.y. in Kalfafellsdalur (some 25-30 km to the west of the thesis area). These dates, however, are in conflict with data from the thesis area.

Dips of the strata within the Geitafell volcano are close to, or in excess of, 10°, and Geitafell lies approximately on strike with the general flexure zone, and accordingly the volcano clearly lies within the flexure zone. As said earlier, the flexure is particularly marked in the NW-half of the volcano (figs. 3.24 and 3.25 and Map 1). Lavas in the SE-half of the volcano have been shown to have gained high dips as a result of the earlier caldera subsidence, while lavas of the SE- and E-flanks dip some 10-12°. The unconformably overlying lavas in Grasgiljatindur (of Lava Unit III, fig. 3.25 and Map 1) dip some 6-8° and clearly postdate the flexure. Tilting of lavas in the SE-half of the volcano, due to the flexural event, may therefore be as little as 5°.

Evidence for the new chronology, that the flexure only slightly postdates the volcano, is discussed in more detail elsewhere in Chapters 2, 3, 5 and 8, but is summarized below:

Figure 3.24. Steeply dipping lavas in Flarfjall. A view from Vidbordsfjall to the west. The glacier west of Flarfjall is Flaajokull.

Figure 3.25. Steeply dipping lavas in Hyaloclastite Unit II unconformably overlain by the Lava Unit III in Efstafell. The felsitic intrusion in Efstafell is seen to the right. View to the east from Storihnaus (near Gjanupsvatn).

1. Construction of the volcano throughout the formation of Hyaloclastite Unit II (section 2.2 and 3.3.1).
2. Uplift of the volcano during the accumulation of intrusive phases 2-6 and possibly longer (section 3.3.3).
3. Caldera subsidence occurred contemporaneously with intrusive phases 10 and 11 (section 3.2 and 3.3.4).
4. All intrusive phases suffered post-injectional tilting; this is particularly clearly displayed in the middle of the flexure zone (section 3.2).
5. Intrusive phase 12 occurred during the flexural event in a strongly dilational stress-field, resulting in sinistral en echelon fractures occupied by intrusive phase 12 (section 3.2).
6. The lower lavas of Lava Unit III are regarded as having been extruded from intrusive phase 12 (section 2.2 and 3.2).
7. New radiometric age data suggest a close time relationship between intrusive phase 11 and 12 (section 2.2, 2.3 and 3.2).
8. Intrusive phase 12 occurred at the end of high-grade hydrothermal activity in the volcano, and extensive sulphide-mineralization occurred within the NW-half of the volcano during its emplacement (section 3.3, chapters 5 and 8).
9. The lower lavas of Lava Unit III banked against the flexure, during its formation and are themselves slightly flexed (ca. 5°). The unconformable upper lavas of Lava Unit III buried the volcano and the flexure zone (section 2.2 and 3.2).
10. Stratigraphically discordant zeolite zones are superimposed on Lava Unit III, the flexure zone and the volcano (section 2.2 and chapter 8).

The flexural event in the Geitafell volcano is believed to have occurred between 5-6 m.y. ago, as deduced from the present knowledge

of the age span (Torfason, 4.85 m.y.; Albertsson and this study, 5.74-5.93 m.y.). The flexure slightly postdates the caldera event in the Geitafell volcano, and is accordingly regarded as having been formed within an active spreading zone (i.e. this part of it).

No general agreement concerning the timing or mechanism of formation of the flexure exists (Torfason, 1979, cf. Chapter 1.1). Rocks younger than 5 m.y. overlap the N- and E-Iceland flexures, which form a syncline along the northern Iceland axial rift-zone (Saemundsson, 1979). The suggestion that the flexure in the Geitafell area has an age of 5-6 m.y. may possibly indicate that the syncline extended as far south as to the Hornafjordur area.

Assuming spreading, the Geitafell volcano formed at the western margins of the Vatnajokull area (Grimsvotn-Kverkfjoll region, fig. 1.1) at the junction between three volcanic zones. This area has been referred to as a 'hot spot' overlying a mantle plume (Schilling, 1973; Sigvaldason, 1974). Walker (1975c) assumed that the eastern Iceland volcanic zone was active during the formation of the east Iceland lavas, and suggested that the locus of maximum spreading moved southwards in time. That the eastern Iceland volcanic zone was continuously active during the formation of the east Iceland lavas (i.e. that the lava pile was formed without major breaks from ca. 13 m.y. to the present) has been shown to be the case (Ross and Mussett, 1976; McDougall et al., 1976; Watkins and Walker, 1977). Ward (1971) and Saemundsson (1974, 1979) assumed that the axial rift-zones have shifted from west to east throughout the evolution of Iceland (Saemundsson, 1979). At present, the northern part of the eastern Iceland volcanic zone extends from the south Iceland seismic zone (of transform character) to join the northern Iceland axial rift-zone in the Kverkfjoll area, the junction being coupled to an E-W transverse zone (also possibly of transform character). In view of these complexities, it is probably far

too early to try to answer the question 'why was the flexure formed?'.

The present data shows that late in the evolution of the Geitafell volcano, an episode of major uplift occurred, coupled with gabbro intrusion (phase 2), an apparently radial dyke-swarm, and two cone sheet-swarms (phases 3, 5 and 6). The explanation may lie either in an excess of eruptive activity at a time of normal spreading rate, or relatively constant volcanic activity at a time of low spreading rate. The two possibilities cannot be resolved on the basis of present data, as the area may have been located above a 'hot spot' where volcanic productivity is highest at present (Jakobsson, 1972). Subsequently, however, caldera subsidence occurred contemporaneously with intrusive phases 10 and 11 and a little later still, flexuring of the strata began and proceeded slowly. At this phase the structure became characterized by marked dilational tectonic features, and unusually thick dykes (phase 12) were formed. The thickness of these dykes and their abundance in the middle of the flexure zone may indicate that the volcanic activity was much the same as in earlier periods, while the spreading rate was faster during the formation of the part of the flexure studied.

It is therefore concluded that relatively fast spreading occurred during the formation of the flexure. As seen at present, there is no obvious reason why the flexure in north and east Iceland (south to the thesis area) could not have been formed during the same major episode. Increased activity on the eastern volcanic zone, as related to a shift in the locus of spreading from the western to the eastern volcanic zone approximately 4 m.y. ago (Ward, 1971; Saemundsson, 1974) seems a feasible explanation for the flexure formation. The shift may have been preceeded by deep-seated faulting resulting in subsidence of the eastern volcanic zone associated with intrusive activity and with

extrusions which gradually buried the synclinal structure resulting from the flexing.

3.4 Summary

Chapter 3 is summarized in Table 3.1. Time relations between the main stratigraphic units, intrusive phases and the major structural events are shown. The time relation with the main hydrothermal alteration patterns inside the volcano is roughly indicated.

STRATIGRAPHIC UNITS	INTRUSIVE PHASES		STRUCTURAL EVENTS	HYDROTHERMAL ALTERATION
UPPER PART OF BASALT LAVA UNIT III				zeolite facies
LOWER PART OF BASALT LAVA UNIT III	DYKES	(12)	FLEXURING	sulphides
RHYOLITE UNIT II	ACID INTRUSIVES	(11)		calcite-quartz
	SHEETS GABBROS DYKES	(10)	CALDERA SUBSIDENCE	intermediate facies hornfels
	DYKES	(9)		greenschist facies
	CONE SHEETS	(8)		
	DYKES	(7)		hornfels
	CONE SHEETS	(6)		
	CONE SHEETS	(5)	UPLIFT	
	ACID PHASE	(4)		
	RADIAL DYKES	(3)		
HYALOCLASTITE	GABBROS	(2)		
UNIT II	INTRUSIVE PHASE	(1)		Cold ground-water percolation

TABLE 3.1.

CHAPTER 4.

HYDROTHERMAL ALTERATION AND METAMORPHISM : INTRODUCTION AND GENERAL FEATURES

4.1 Classification.

Nomenclature in hydrothermal geology has developed somewhat separately in different parts of the world. Increased attention on geothermal energy resources has in recent years called for some basic definitions in geothermal terminology.

Ellis and Mahon (1977), for instance, use the term geothermal energy to refer to potentially useful energy stored as hot water or steam in favourable geological situations within the top few kilometers of the earth's crust. It is contained in a geothermal area or a geothermal field with finite boundaries and in a particular rock-hydrological situation (geothermal system). They classified the various geothermal systems into two major types: cyclic- and storage systems. In cyclic systems, the hot water is meteoric water which has passed through a cycle of deep descent, heating and rising. In storage systems, the water is stored in the rocks for geologically long periods and heated in situ, either as a fluid within the formation, or as water of hydration in minerals (Ellis and Mahon, 1977, p. 1 and 32).

All present-day Icelandic geothermal fields represent cyclic hydrothermal systems and fall within subgroup (a) below. Ellis and Mahon (1977, p. 32-33) divided cyclic systems into three broad subgroups:

(a) High-temperature systems associated with recent volcanism.

(b) High-temperature systems in nonvolcanic zones of Cenozoic tectonic activity.

(c) Warm water systems in near-normal heat flow zones (water rarely attains boiling temperatures in this subgroup).

Armstead (1978) has somewhat different approach and classifies all the earth's surface into three broad groups:

(1) Non-Thermal Areas, having geothermal gradients from about 10-40°C/km.

(2) Semi-Thermal Areas; thermal gradients from 40-70°C/km, and

(3) Hyper-Thermal Areas, having thermal gradients many times greater than found in non-thermal areas.

He makes a distinction between a "thermal area" and a "thermal field" based on the presence of impermeable or permeable rock formations. A thermal field is defined as an exploitable part of a thermal area (semi- or hyper-thermal), where the presence of permeable rock formations below ground allows the containment of a working fluid, without which the area could not be exploited. Armstead classifies thermal fields into three types as follows:

(1) Semi-Thermal Fields, capable of producing hot water at temperatures up to 100°C from depths of 1 or 2 km.

(2) Hyper-Thermal Wet Fields, producing pressurized water at temperatures exceeding 100°C, so that when the fluid is brought to the surface and its pressure is reduced, a fraction is flashed into steam while the greater part remains as boiled water.

(3) Hyper-Thermal Dry Fields, producing dry saturated, or slightly superheated steam at pressures above atmospheric.

Hyper-thermal wet and dry fields are sometimes referred to as "water dominated" and "steam dominated" fields respectively (Armstead, 1978, p. 39-40).

In Iceland two types of geothermal systems are distinguished (Bodvarsson, 1961):

1) Low-temperature areas, where temperatures at the base of circulation are below 150°C, and

2) High-temperature areas, with subsurface temperature above 200°C at a relatively shallow depth.

While the high-temperature areas are consistently located within the neovolcanic zones, the low-temperature areas are typical of the flanks of the neovolcanic zones in Plio-Pleistocene and Tertiary volcanics (e.g. Palmason et al.,1979). The geothermal gradient in Iceland, measured outside known thermal fields, ranges from 37°C/km to 165°C/km, increasing towards the neovolcanic zones. Thus, the low- and high- temperature areas are located within regions of low- and high geothermal gradients respectively (Palmason et al.,1979). However, no single temperature gradient or heat flow can characterize the partly convective systems concerned (e.g. White, 1973).

The three classification schemes presented above all refer to present day situation and there is little discrepancy between them. If, for instance, one were to apply Armstead's classification to the Icelandic situation, virtually the whole island would be composed of semi- and hyper-thermal areas, in accordance with the geothermal gradients in each region. In general, without any major modification the Icelandic low- and high-temperature areas could then be placed within Armstead's scheme of semi- and hyper-thermal fields respectively.

These schemes are not appropriate, however, for classifying an area of fossil hydrothermal activity. Such an area may in fact have passed through all of Armstead's classes of areas and fields and they obviously can not be classified using Armstead's (1978) utilization potentials. To use the description of geothermal areas (and geothermal and hydrothermal systems) given by Ellis and Mahon (1977) with the prefix fossil seems adequate for areas of former hydrothermal activity. Indication of the scale (local or regional) of fossil geothermal areas and specification of their geological situation (such as at constructive or convergent plate margins, in tectonic or volcanic zones etc.) is useful.

The fossil geothermal area located within the Geitafell central volcano was once located within an axial rift zone and bears much resemblance to present-day active geothermal fields in Iceland. Comparison with the present-day geothermal fields is therefore useful and aids understanding of the fossil area, whilst study of the fossil area also gives information of relevance to the deeper parts of present-day fields.

The most recent descriptions of Icelandic hydrothermal systems (Palmason et al., 1979, Fridleifsson, I.B., 1979, Kristmannsdottir and Tomasson, 1978) show that fundamental differences exist between high- and low-temperature areas. The high-temperature areas are thought to be fed by fairly localized groundwater systems which withdraw heat from local heat sources within central volcanoes. By contrast, the low-temperature areas are fed by regional ground -water systems and withdraw heat from a large volume of warm country-rocks. These features result in differences in rock alteration; high-temperature areas show alteration ranging from zeolite facies to greenschist facies, while the low-temperature areas only show zeolite facies alteration. Overprinting of the latter situation on the former occurs.

Improved knowledge of hydrothermal systems and the need for simulation of hydrothermal processes coherent with increased exploitation of geothermal energy, has in recent years urged the need for rigid scientific treatment of geothermal processes, and called for classification of geothermal systems based on processes and definition of parameters which describe the respective processes. In a recent paper on the physical aspects of hydrothermal systems, Stefansson and Bjornsson (1982) review the literature on geothermal systems and present a parametric approach to the description of hydrothermal systems as follows:

Descriptive parameters:

Temperature

Pressure (equally valid are density and enthalpy or density and internal energy)

Liquid saturation

Concentration of chemical components

Properties of rock and fluid:

Thermal (heat capacity, thermal conductivity, latent heat)

Hydraulic (porosity, permeability, fluid viscosity)

Chemical

Boundary conditions

Transfer of mass and energy (input and output of the system)

Internal conditions

Distribution of descriptive parameters

Distribution of properties of rock and fluid

Structural discontinuities

Processes

Conduction

Convection

Boiling and condensation

Laminar and/or turbulent flow

Water-rock interactions

By using three descriptive parameters, pressure, temperature, and fluid saturation, Stefansson and Bjornsson recognized four main classes of physical states of hydrothermal systems: liquid saturated, boiling, vapour saturated and supercritical. They further noted that during the lifetime of hydrothermal systems physical conditions change, and both gradual and transient changes are visualized. For further details

the interested reader is referred to Stefansson and Bjornsson (1982) and references therein. The main purpose, however, of parametric evaluation is to describe the hydrothermal system under consideration and enhance the understanding of the phenomena in general.

Inevitably, when dealing with an extinct hydrothermal system, direct parametric definition or evaluation of the formerly active system is greatly hampered for obvious reasons. However, a recognition of the fundamental characteristics of a geothermal system in a volcanic complex is of importance to the present study and is therefore dealt with in the next section - viewed mainly from a geological standpoint and with respect to the thesis area.

4.2 Hydrothermal System in a Volcanic Complex

The state of any hydrothermal system through time is dependent upon the interactions of different lithologies, moving fluids, transfer and availabilities of heat and tectonics within the systems, and the ways in which these parameters interact with one another. This section deals with the nature of these parameters, a schematic overview of which is presented in figure 4.1.

a) Origin and nature of hydrothermal fluids.

Hydrothermal fluids were defined by White (1957 a,b, 1974) to include: juvenile-, magmatic-, meteoric-, connate, metamorphic-, and oceanic waters. Juvenile water was defined as "new" water from mantle-derived magma, while magmatic water was defined as water derived from magma which might have incorporated other generic types of water.

Studies of stable hydrogen and oxygen isotopes in Icelandic geothermal areas (Arnason, 1976) have shown the hydrothermal fluids to be dominantly of meteoric origin, a noticeable exception being the hydrothermal systems of the Reykjanes Peninsula, the landward extension of the Reykjanes Ridge, where the hydrothermal fluid is a brine of partly oceanic origin (Bjornsson et al., 1970, 1972, Arnorsson et al., 1975, Olafsson and Riley, 1978). Increased salinity of geothermal fluids has a profound effect on the solvent action of the fluids and leads to much higher metallic concentration of ocean-related geothermal systems as compared to systems fed by meteoric water (Seyfried and Bischoff, 1977; Bischoff and Seyfried, 1978). A recent experimental study by the above authors on seawater-rock interaction, implies that the removal of Mg from the seawater generates acidity which maintains heavy metals in solution. This result gave them reason to suggest

Figure 4.1

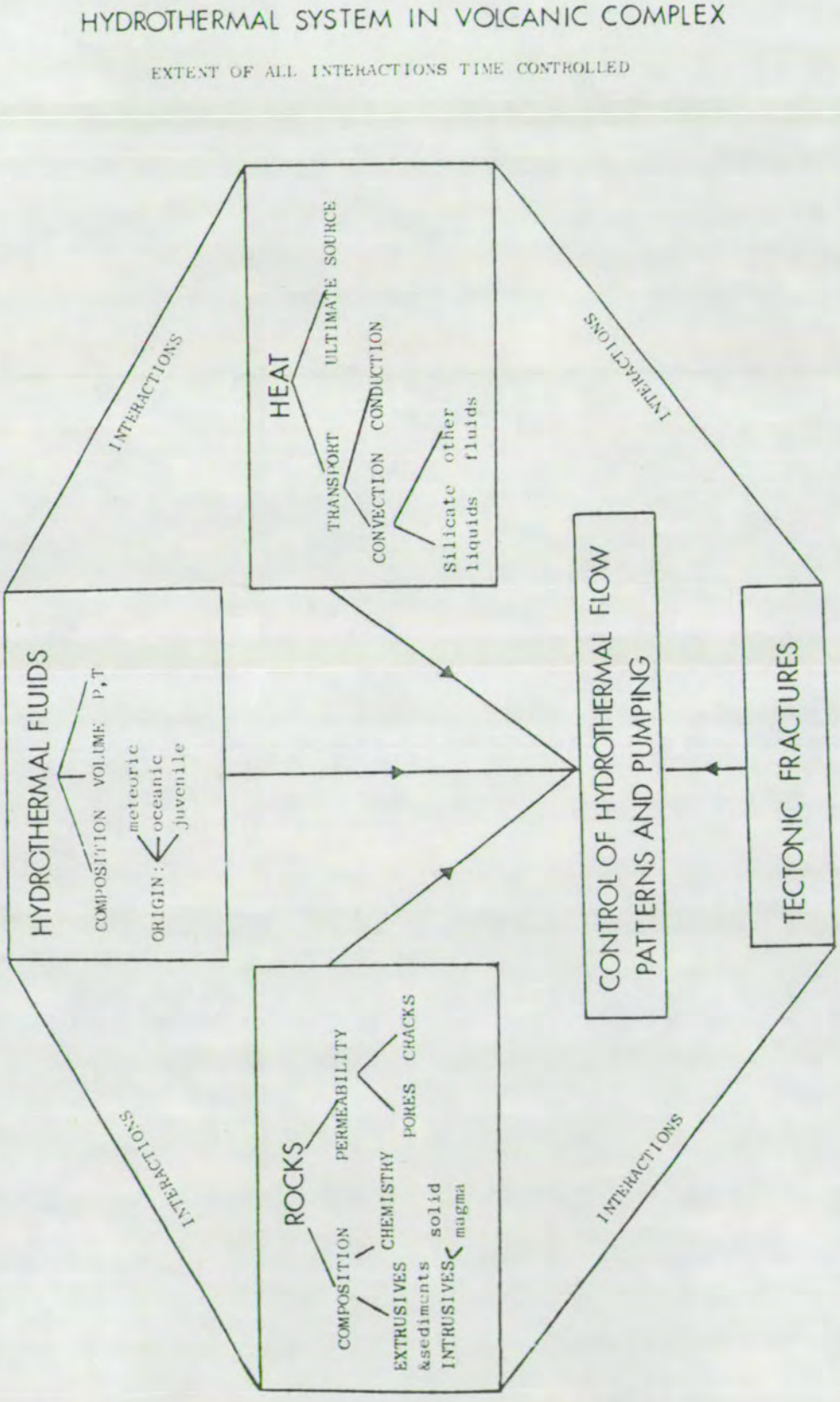
HYDROTHERMAL SYSTEM IN VOLCANIC COMPLEX
EXTENT OF ALL INTERACTIONS TIME CONTROLLED
HYDROTHERMAL FLUIDS
COMPOSITION VOLUME P,T
ORIGIN: meteoric oceanic juvenile
HEAT
ULTIMATE SOURCE
TRANSPORT
CONVECTION CONDUCTION
Silicate other liquids fluids
ROCKS
COMPOSITION
EXTRUSIVES &sedimants
INTRUSIVES solid magma
CHEMISTRY
PERMEABILITY
PORES CRACKS
CONTROL OF HYDROTHERMAL FLOW PATTERNS AND PUMPING
TECTONIC FRACTURES
INTERACTIONS
INTERACTIONS
INTERACTIONS
INTERACTIONS

that seafloor heavy-metal deposits could originate from (a) seawater - basalt interaction at moderate temperature (300°C) and high effective water/rock ratio, or (b) seawater - basalt interaction at relatively high temperatures (ca 400°C) and low (e.g. less than 10) water/rock ratio (Seyfried and Bischoff 1981). Ore deposits in fossil hydrothermal systems may be strongly indicative of oceanic-related origin of the hydrothermal fluids, while the effects of isotopic exchange between meteoric water and igneous rocks in fossil convective systems other than ore deposits are becoming widely recognized (e.g. Taylor, 1974, 1977, Forester and Taylor, 1976, review by White and Guffianti, 1979).

A detailed evaluation of the differences between Icelandic meteoric- and oceanic fed hydrothermal systems with respect to potential ore deposition has not been undertaken. Borehole logging from both types of areas, reveals a similar mineralogy with respect to sulphide precipitates (which, however, have not been studied in detail cf. Tomasson pers. comm.), but a noticeable difference is the common presence of anhydrite in the brine fluid system while anhydrite is virtually absent from the metoric-fed systems. In the fossil system in Geitafell, sulphide precipitates are common, mainly at upper stratigraphic level. The disseminated sulphide occurrences are chiefly composed of pyrite, but subordinate chalcopyrite is also present. These sulphide deposits are not useful in discriminating between the possible fluid origins, but the absence of anhydrite from the mineral assemblages in the fossil system is noteworthy in Geitafell.

In the Icelandic high-temperature hydrothermal and fossil systems, massive sulphide deposits are not known. However, disseminated sulphides (mainly pyrite) are quite common. The acidity of the thermal fluids fed by meteoric water is normally in the range pH 7-9, while the seawater mixed systems at Reykjanes have pH values 4.5-7 (Arnorsson et al., 1978,

Olafsson and Riley 1978). Metallic concentration in the Reykjanes system is considerably higher than average seawater (Olafsson and Riley, 1978). In the Krafla geothermal reservoir in NE-Iceland, fed by meteoric water, the thermal fluids are normally of low metallic content. High metallic concentration (mainly Fe), however, has been measured in some wells. It is considered that this concentration is resulted by very low pH values (down to ca 2) of the fluid due to transient flow of volcanic gases (CO_2, SO_2, Cl_2) related to volcanic activity associated with the presently active rifting episode which initiated in December 1975 (Arnorsson, 1981, Armannsson et al., 1981). These extremely low pH values recorded were short lived phenomena, but apart from the ultimate effects on the fluid chemistry, juvenile/ magmatic contribution to the thermal fluids is in evidence. Since 1975 a profound overall increase in the gas concentration of some well-yields and fumaroles is recorded from the Krafla hydrothermal field - the increase is regarded to be related to a pulsating inflow of volcanic gases from a magma chamber at 3-7 km depth. The volcanic gases are modified by interactions with the overlying hydrothermal system and reach the surface in the form of CO_2 (ca. 98.8%) and H_2S (ca. 1.2%) (Armannsson et al., 1981).

In the case of the fossil hydrothermal system in Geitafell, most of the fluid bulk is likely to be of meteoric- or oceanic origin, or a mixture of both. Some juvenile/magmatic contribution is likely, while connate and metamorphic waters are probably of negligible significance.

Palaeoclimatological and palaeogeographical evidence coupled with the nature of mineral deposits, however, suggests that the fluid was dominantly of meteoric origin. The formation of hyaloclastites within the volcanic pile is believed to be connected with glaciation. the glaciation is believed to have occurred in high ground areas above

a productive axial rift zone, located at divergent plate margins. Assuming drift, projection of the field area to its palaeoposition suggests its former site to have been at the present-day high-ground area near the middle of Iceland (see fig. 1.1, chapters 1 and 2). Compared to present-day situations, the area's palaeoposition virtually rules out infilteration of seawater as a possible fluid source to the fossil hydrothermal system. As mentioned earlier, seawater infiltration occurs into the hydrothermal systems in Reykjanes, the landward extension of the Reykjanes Ridge. Apart from the different fluid chemistry, an important possible contrast between topographically high- and low-lying situations lies in the height of the ground - water table within the rock pile. In the case of low-lying volcanic complexes, the ground-water table would lie fairly high within the volcanic rocks, and hydrothermal mineral alteration and deposition might be expected to begin relatively early in the lifespan of such a system. Conversely, in the case of topographically higher volcanic complexes, the ground-water table would normally stand much lower in the volcanic pile and alteration near the surface might be a fairly late stage feature. Such a situation is documented by mineralogical evidence from the Geitafell Volcano as presented later.

b) Heat source and distribution.

The thermal aspect of a hydrothermal system involves:

1) a heat source, and

2) the nature of heat transport into and through the system by i) conduction, and ii) convection.

The ultimate heat source is simply taken to be hot material (solid or molten) at depth. The manner in which this heat is moved upwards and then distributed throughout the geothermal system determines the type of hydrothermal system established. In the Icelandic

volcanic complexes, high volcanic productivity and high-temperature geothermal systems are contemporaneous phenomena (chapter 1). Therefore, the establishment and the extent of the latter additionally depends on the availability of water within the complexes, at some time during the active lifetime of the volcanic complexes.

Heat conduction proceeds through all material from the source to the surface. In general, due to low thermal conductivity of rocks, the process of heat conduction is sluggish, but will, however, gradually build up and maintain, for relatively long time, a thermal anomaly near the earth's surface above the heat source. The overall pattern of thermal conduction will be affected locally by variations in rock-conductivity. Heat is also transported from a source by the motion of (i) silicate liquids, and (ii) other fluids. Inevitably, such heat convection is a faster transporting process than heat conduction, as it involves mass transfer of the heated substance itself from one place to another. Magma transfer, more or less directly linked to the ultimate heat source, is the most effective and fastest heat transfer of all. In the type of hydrothermal system studied, magma is transferred into and through a percolating hydrous fluid system. Once a hot igneous body becomes solid, it obviously ceases to convect heat itself. Convection may still continue to be connected with it as a consequence of the release of incorporated (juvenile) fluids or as a consequence of promoting motion of external hydrothermal fluids. Such fluids may circulate within (e.g. via shrinkage joints) as well as without the igneous body. Once convection in a hydrous fluid is started, the lower density warm fluid rises from the heat source region while colder fluid sinks towards it and a buoyancy driven convection cell is established.

In hydrothermal systems, two chief types of convection processes are recognized. One is commonly referred to as "an ordinary buoyancy

driven convection" and concerns a single phase fluid convection in porous media. The other applies to a convection process in a mixture of two fluid phases (e.g. liquid water and steam). The two types of convection processes have quite different flow characteristics and the dimensions of the established convection cells are thought to be quite different (e.g. Schubert and Strauss, 1977). The real geometry of ordinary buoyancy-driven convection cells has never been demonstrated in detail in natural hydrothermal systems. One reason that single-phase buoyancy convection is rarely observed in high-temperature systems may be that these are dominated by two phase convection (Stefansson and Bjornsson, 1982).

In the Geitafell central volcano twelve intrusive phases have been mapped (chapter 3). Each phase includes several tens to hundreds of intrusive members (dykes and sheets), all of which act as sub-sources of heat accumulating within the fluid environment. Therefore, numerous local and temporarily independent convection cells may have been established.

c) Rock permeability and fluid flow.

(i) General considerations.

The extent and pathways of movement of hydrothermal fluids attract much attention in geothermal fields. In the case of a fossil field much evidence of fluid movement and distribution is documented in the extent of hydrothermal mineral alteration and deposition now revealed by erosion.

Fluid flow (in the sense of body motion of the fluid and not including diffusion through the fluid) may be of two types:

1) interstitial or porosity flow,

2) fracture flow.

Permeability is a measure of the ease with which fluids pass

through a porous medium and therefore strictly relates to (1) above. However, partly because of the obvious importance to flow of even the smallest fractures, it is common in practice to include flow via fractures as well as porosity when referring to rock permeabilities. Clearly measurements of permeability must take into account temperature and the viscosity of the fluid involved, as well as the nature of the permeated material. In comparing rocks it is therefore standard practise to examine permeabilities under standard condition with the same fluid (e.g. water) and perhaps to isolate the rock controlling factors under the heading "specific permeability" (Dullien, 1979), which is defined as:

$$k = (Q/A)\ n\ (dp/ds)^{-1}$$

where Q is the volume of fluid which passes in unit time through an area A in the direction s of the pressure gradient dp/ds, and n is the dynamic viscosity of the fluid. A permeability of one Darcy (D) corresponds to a flow of 1 $cm^3\ s^{-1}\ cm^{-2}$ for a pressure gradient 1 bar cm^{-1} at T ≈ 20°C and is the unit of permeability most commonly used by geologists.

Typical values of permeability and porosity of volcanic rocks have been given by Davis and De Wiest (1966). In general, the porosity of volcanic rocks ranges from less than 1% in dense rocks to more than 85% in pumice. Typical values for dense rocks (plutons, dykes, denser lavas) range from 1-10%, while the porosity of vesicular lavas is in the range 10-50%. The permeability of volcanic rocks is considered to be in range 0-1000 D by Davis and De Wiest (1966). As noted, the permeability, however, is also a function of fractures. Toulmin III and Clark (1967) considered the contribution from fractures to the permeability of a dense rock having 1% porosity and permeability of 10^{-5} D. A fracture 1 micron wide was calculated to have a permeability of 3×10^{-3} D, and a 1 mm wide fracture to

have a permeability of approximately 3000 D. The contribution of fractures to permeability, and thereby fluid transport, is clearly of importance. Some recent authors have thus chosen to include fractures as an intimate part of the rock porosity when analysing fluid transport processes in dense plutonic rocks (Norton and Knapp, 1977). From analytical data, the above authors recognised three types of porosity: flow porosity (ϕ_F), diffusion porosity (ϕ_D) and residual porosity (ϕ_R), which together compose the total porosity of the rock. The flow porosity of fractured rocks is the portion of the rock which constitutes the permeability; diffusion porosity represents those pores through which the dominant mode of transport is by diffusion through an aqueous phase (earlier used by Garrels et al., 1949) and the residual porosity represents pores not connected to ϕ_F or ϕ_D (Norton and Knapp, 1977). Their treatise of porosity is quite explanatory and may be useful for numerical analyses of fluid transport in dense rocks, while problems evidently arise for analytical application to rocks which have suffered several fracturing events in time and perhaps permeation of several fluids with quite different permeation properties - unless the fracture intensity in time and the fluid nature are first evaluated.

The overall fracture intensity was considered in chapter 3, and extensive fracturing was shown to have occurred in the Geitafell volcano. The visual differences in porosity and permeability of the various volcanic rocks may be useful in separating alteration events. For example, at places where the intensity of mineral alteration is high and overprinting of alteration events intense, the least permeable rocks may show the clearest evidence of overprinting. Conversely, at places where alteration intensity is low, the spatial extent of a particular event may only be detected in rocks of high permeability.

(ii) Porespace and fluid pressure.

A continuous size gradient in rock porespace exists. The porespace is simply classified into micropores (invisible under the microscope), mesopores (less than 1 mm) and macropores (1 mm - 10 cm). As micropores progressively become restricted a transition presumably takes place from a transport of material by an actual fluid flow through the rock to a transport of species by diffusion through a fluid, along grain boundaries and through crystal lattices. Mineral transformation rates, however, strictly related to diffusion are regarded as sluggish even on time scales of 10^8 and 10^9 years (e.g. Fyfe et al.,1978, p. 114). In view of the short lifetime of the Geitafell hydrothermal system (2-3 x 10^5 years, chapter 2) the importance of diffusion to the hydrothermal alteration is regarded as negligible and not considered further.

The meso- and macropores (vesicles) are of particular interest in a study of hydrothermal evolution. Most often several layers of different minerals are seen, forming a time sequence within the vesicles. It is apparent that the preserved mineral species have formed from fluids varying in temperature and/or composition. The temperature range alone is in the order of couple of hundred degrees or more. Reactions, however, between low-temperature minerals and high-temperature fluids often took place. Evidence for growth generations of some minerals (e.g. garnets) have also been found and may possibly relate to fluid pulses of essentially the same type. Most commonly, however, if the mineral layers are unaltered, the transition between the layers is sharp - as if the vesicles had been drained and refilled by different mineralizing fluids several times (e.g. fig. 4.16). The rate of such possible drainage and inflow process is unknown, but an important and close correlation is found to exist in Geitafell between the mineral infillings to the fractures, to form the vein

systems, and to the pores (or vesicles) to form the amygdales, which may support the idea that such a drainage-inflow process took place. A link between two fluid flowage groups, (a) porosity- and (b) fracture controlled, is preserved by the mineral deposits and the combined information from the two sources thus provides some qualitative information on the palaeo-permeability. This important comment is discussed in later chapters while some general discussion on fluid pressures, fluid flow and possible transient events follows.

In the recent book "Fluids In The Earth's Crust", Fyfe et al., (1978, pp. 232-238) emphasize that fluid pressure in the crust can be higher than the theoretical "hydraulic head" (= hydrostatic pressure) at some stage in the history of sedimentary and metamorphic sequences, and that it may approach the lithostatic pressure. They state: "It is indeed fortunate that the evidence points to this unequivocal conclusion, for as we have already emphasized, the entire logic of facies classification in metamorphic rocks hinges on the relationship $P_{H_2O} = P_{rock}$" (op. cit. p. 237). The most common pressures, however, of geothermal reservoirs appear to be closer to hydrostatic values. This requires that liquid water is the dominant fluid phase throughout the hydrothermal system, which is the case in the known majority of hydrothermal systems (i.e. the water dominated systems or hot water systems) but not in the "vapour- or steam dominated" systems, where the pressure throughout the reservoir is governed by the total vapour pressure of the reservoir fluid (White et al., 1971, Truesdell and White, 1973). The only known potential geothermal reservoirs in which the fluid pressure is close to the lithostatic are the so-called "geopressurized reservoirs". These are special cases of deep seated (3-7 km) sedimentary aquifers isolated by impervious and low-conductivity shales above and below them (Rybach, 1981), and thus out of the scope of the present discussion.

To give an idea of the pressure range in liquid dominated hydrothermal systems, which is usually close to hydrostatic values, use may be made of the common pressure equation:

$$P = \int_0^z \rho \cdot g \cdot dz$$

(p: pressure of rock or water, ρ: density, g: gravitational acceleration and z: depth). The density values of volcanic rocks lie somewhere between 2.5-3.0 g/cm^3 which would give a lithostatic pressure, for instance at 2 km depth, of 500-600 bars. The density of pure water ranges from 1.0-0.35 g/cm^3 from 5°C - 374°C. Due to the geothermal gradients within the crust the density variation of water needs to be accounted for, e.g. with the aid of T-ρ tables. For this general discussion, however, a hypothetical water column at 5°C, would exert a water pressure close to 200 bars at 2 km depth. A static water column with thermal gradient of say 100°C/km would exert a pressure close to 190 bars at 2 km depth. If the thermal gradient was 200°C/km the pressure would be close to 160 bars at the same depth, and a water column everywhere following the Clapeyron boiling curve would exert a pressure of some 140 bars at 2 km depth.

While we now may have a rough idea of the numerical pressure values involved in a liquid dominated hydrothermal system, the hydrostatic values are evidently modified by convection within the fluid, frictional resistance to fluid flow and other factors. The Clapeyron boiling curve, or saturation curve, governs the maximum fluid temperature at a given pressure in most hydrothermal systems at upper crustal levels, or up to the critical point (T: 374.15°C, P: 221.2 bars for pure water), above which no hydrous liquid phase exists and the hydrothermal fluid is said to be at supercritical conditions. In a hydrothermal system where the temperature follows the boiling curve for water at all depths the critical point can be reached at approximately

3.5 km depth. Dissolved gases in a hydrothermal fluid, however, will allow boiling to be initiated at lower temperatures for a given pressure, while dissolved solids have the reverse effect. With increased salinity of a hydrothermal fluid, for instance, the pressure and the temperature of the critical point increase (Sourirajan and Kennedy, 1962) and $T_{boiling}$ at a given pressure is higher in saline water than pure (Haas, 1971).

The effect of gas concentration upon boiling can be considerable. Data on CO_2 concentration for instance, in Icelandic hydrothermal waters, show the concentration and the partial pressure of CO_2 (P_{CO_2}) to rise sharply with temperature. In the 200-300°C range the P_{CO_2} increases from 10^{-1} bars to tens of bars near 300°C (Arnorsson and Svavarsson, 1980, Arnorsson et al.,1982). When the sum of the partial pressures of CO_2 and steam exceeds the ambient fluid pressure boiling occurs. The chief effect of any gaseous phase in a hydrothermal fluid is thus to lower its boiling conditions. Despite the low values and the narrow range of fluid pressures in hydrothermal systems, the fluid pressure is an important parameter as it together with temperature controls boiling.

Upon boiling the hydrothermal fluid separates into two phases, steam and a liquid phase. Gases and the more volatile components concentrate in the vapour phase (steam) while the non-volatile components become concentrated in the liquid phase (e.g. Fournier, 1981). This may have a profound effect upon the hydrothermal mineralogy, depending on the chemical composition of the hydrothermal fluid. Provided the chemical composition allows, supersaturation with respect to some mineral species may take place in the liquid phase and result in episodic mineral precipitation. Common examples of mineral precipitates in Icelandic geothermal wells, deposited from flashed (boiled) geothermal waters are carbonates (mainly calcite), silica and several iron-bearing minerals (Arnorsson, 1981).

The steam and the liquid phase of a boiling hydrothermal fluid must either depart or coexist, depending on the geological situation. The convection patterns of the fluid system would further change as the transporting properties of a two-phase mixture are quite different from those of either phase, where the two phases may impede the flow of each other (e.g. Stefansson and Bjornsson, 1982, and references therein). Whether a two-phase flow affects the mineralogy directly is not obvious but seems possible. The difference in surface tension of liquid water and steam may be of importance to the sequence of mineral deposition. Due to higher surface tension of liquid water over steam, liquid water favours small pores and the narrower channels while steam favours the wider channels (White et al.,1971). This might result in earlier mineral deposition in vesicles and the narrower fractures than in the wider fractures - but can neither be supported nor disregarded by the present data.

The P-T conditions of most known high-temperature hydrothermal systems are found to follow the Clapeyron equilibrium as said above. Therefore, the maximum temperatures at each depth in the fluid system are determined by the boiling curve which approaches the boiling curve for pure water. Upper constraints are thus exerted on the P-T field of most hydrothermal minerals. These conditions, however, relate to somewhat "balanced" or long-term aspects of the geothermal reservoirs. Temporary deviation from such a balanced situation may still occur, e.g. accompanying a magmatic injection into the hydrothermal system. A superheated steam layer would presumably separate a hot igneous body at shallow depth from a reservoir fluid at some stage during the cooling history of the intrusive rock. The P-T conditions of a superheated or supercritical fluid are unrelated to hydrostatic values (the Clapeyron equilibrium) and can therefore cover the range from the boiling point value up to magmatic temperatures and lithostatic pressures. Secondary hydrothermal minerals deposited from superheated or

supercritical fluids might therefore be found within and in the vicinity of shallow level intrusive bodies, which clearly expands the possible P-T fields of hydrothermal mineral deposits.

d) Tectonic interactions

In the type of volcanic complex considered, the overall pattern of the tectonics relates to divergent movement of crustal plates, and is accompanied by inflow of magmas to all crustal levels. The general characteristics of the dilation tectonics involved are open fissures and graben at the surface and normal faults at depths. During the life-span of a typical Icelandic volcanic complex there are series of relatively short magmatic-tectonic active episodes between longer dormant periods (e.g. Bjornsson et al., 1977). It is evident that considerable interactions between tectonic and magmatic forces occur during active episodes, with the actions of both having reciprocal effects upon the other on a whole range of scales. While tectonic activity, in general, allows release of fluid pressure, magmatic activity tends to increase the fluid pressure of the system. High fluid pressure may build up in a fluid neighbouring magma and hydraulic fracturing may result. Any sort of fracturing processes will result in fluid flowage and directly affect the overall permeability of the system. Subsequent to magmatic-tectonic episodes the fluid system would tend to stabilize. Slower convection- and conduction processes would dominate the system during such dormant periods.

The effects of tectonic activity on a fluid system resulting in transient fluid transport have been described recently (Scholz et al., 1973, Sibson et al., 1975, Fyfe et al., 1978). The process is called seismic-, tectonic- or fault-pumping, and its effect is to cause intermittent fluid transport and possible episodic mineralization (Sibson et al., 1975, Fyfe et al., 1978). Sibson et al. (op.cit.) considered the mechanism of tectonic pumping based on a dilatancy/fluid "diffusion"

Figure 4.2

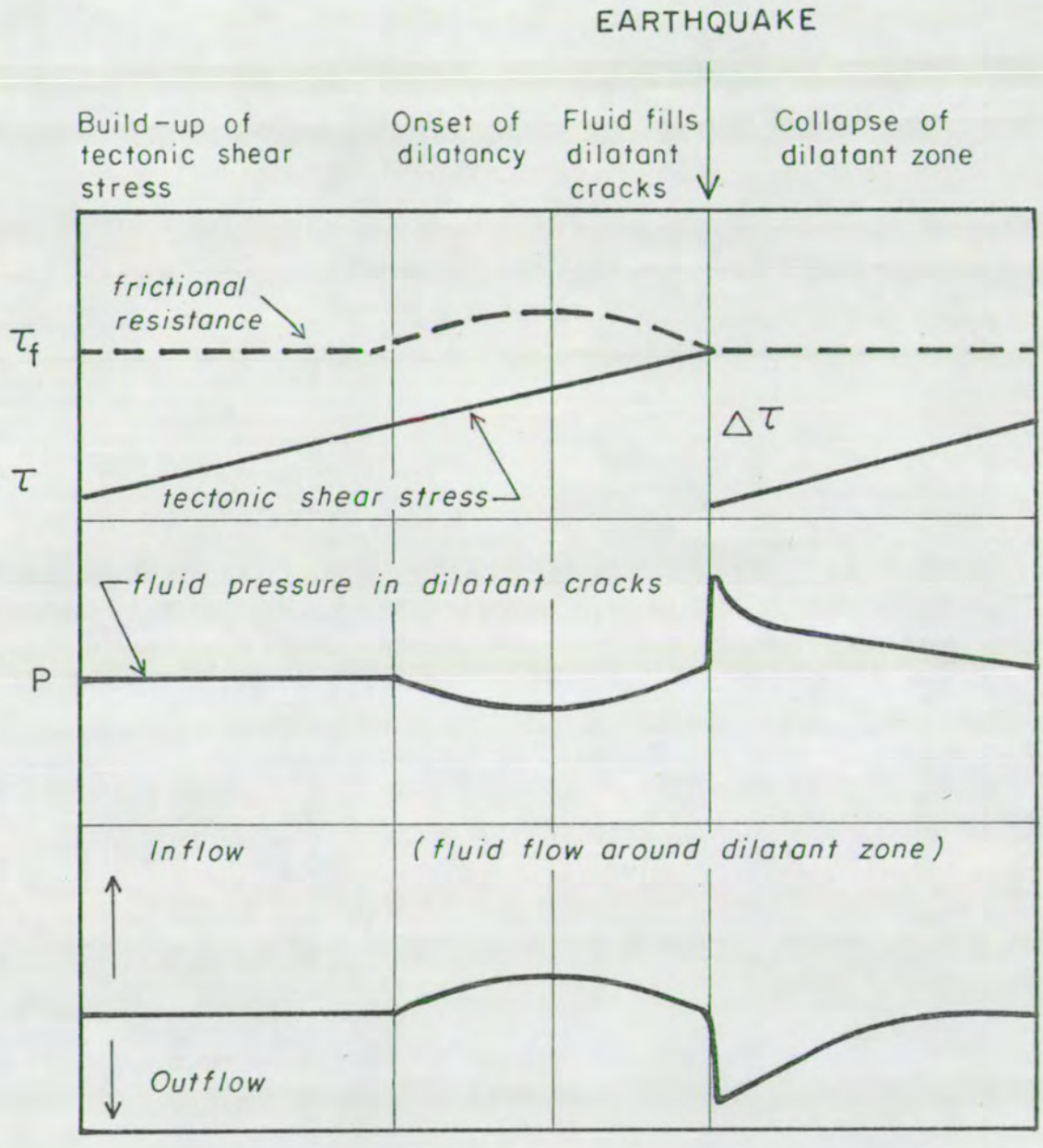

Synoptic diagram of the teconic pumping process
(from Sibson et al. 1975) see text for explanation

model (figure 4.2). In a simple form, the model supposes that prior to seismic shear failure along an existing fault, the region for some considerable distance around the focus of a subsequent earthquake dilates in response to rising tectonic shear stress (τ) by opening of extension fractures normal to the least principal compressive stress (σ_3). The developed fracture porosity causes the fluid pressure (p) in the dilatant zone to decrease, inducing a slow inward migration of fluid from the surrounding crust. At the onset of dilatancy, the drop in fluid pressure causes a rise in the frictional resistance to shear along the fault ($\tau_f = \mu\sigma_n - p$), (where μ is the coefficient of static friction and σ_n is the normal stress across the fault). As the migrating fluid fills the cracks, fluid pressure rises again and frictional resistance decreases. Seismic failure eventually occurs when the rising shear stress equals the frictional resistance. The rapid partial relief of shear stress which accompanies faulting allows the cracks within the dilatant zone to relax and the fluid they contain must be expelled rapidly in the direction of easiest pressure relief (Sibson et al., 1975). According to an empirically derived relationship, the precursory dilatant periods for earthquakes of magnitude M1, M2, M3, M4 and M5 are ca 0.08, 0.5, 3, 19 and 120 days respectively ($\log t = 0.8M - 1.92$; t: days, M: magnitude) (Whitcomb et al., 1973).

Tectonic pumping clearly provides a mechanism for relatively fast partial draining of vesicles, which subsequently can be infilled by new fluids as pore-fluid pressure builds up anew. Depending on the physical condition of the fluid, tectonic pumping might further induce boiling and thereby the flow patterns might change due to the phase separation, which might additionally result in supersaturation of the liquid phase with respect to some mineral species and intermittent mineral deposition might occur, either within the rock pores or the fractures or both.

Having now glimpsed through some of the fundamental characteristics of a hydrothermal system, several compelling questions arise. Is it possible, for instance, to detect a mere fraction of the complex interactions bound to occur in a hydrothermal system through a study of the hydrothermal mineralogy? A prerequisite to a solution of this question is to establish a time sequence for the extrusive rocks in relation to possible tectonic and magmatic events, to which the hydrothermal mineralogy need to be added. The establishment of such a time sequence was dealt with in chapters 2 and 3 (summarized in tables 2.1 and 3.1), while the latter will be dealt with in the remainder of this thesis.

4.3 Hydrothermal Alteration and Metamorphism - General Features.

In Iceland, hydrothermal alteration in extinct volcanic complexes has hitherto received but minor attention. Most studies, however, of the fossil volcanic centres, describe propylitized cores of the volcanoes, characterised by intense alteration with chlorite-epidote as a typical assemblage, abundant quartz and calcite deposits and, sometimes, a note is made on the occurrence of most of the minerals described in later sections. An outer aureole, characterised by calcite and laumontite, has commonly been described as surrounding the propylitic cores. One of the more detailed studies of a propylitized area is that of Annels (1967) from the present field area. He mapped four mineral zones from the propylitic area, the outer boundaries of which are based on disappearance of index minerals. An outer calcite zone, and progressively inwards, a narrow chlorite zone, surrounding a large epidote core-zone, including andradite aureoles around some of the gabbros. Annels did not, however, sort out in detail the hydrothermal history in connection to structural and intrusive events, which is the scope of the present study. Consequently, both the zonal boundaries and their implication take a new form.

In general, three types of alteration and metamorphic processes are observed:

(i) Contact metamorphism,

(ii) Hydrothermal alteration,

(iii) Deposition of minerals in veins and vesicles.

The history and interrelationship of these three processes is dealt with in the remainder of this thesis. As an introduction to the detailed description of each characteristic sub-area within the volcano, a general discussion of the principles involved is presented first.

4.3.1 Intrusive/host rocks - Reciprocal Interactions

Study of the effect of intrusives on the host rocks and of the host rocks on the intrusives can yield information about the hydrothermal history in two main ways:

(i) Direct effects of intrusives on host rocks. Narrow aureoles of contact metamorphic hornfelses are seen around some of the larger gabbro intrusions. Sometimes the hornfelses are found to be surrounded by outer contact aureoles which show some diagnostic mineral assemblages apparently related to thermal effects from the neighbouring gabbro. Occasionally, also, metamorphic aureoles are seen adjacent to the margins of some dykes, in which case some earlier secondary minerals are metamorphosed. In both cases the nature of the metamorphosed material can yield information about the extent of alteration before the time of the intrusions.

(ii) Effects of host rocks on the intrusives. Information from this source is of two kinds, physical and chemical:

a) The nature of the host rock may determine the mode of emplacement of the intrusions. The tendency of dykes to brecciate within hyaloclastites is a common example already discussed in chapter 3. It is not as yet clear, however, whether hydrous pore-fluid in the hyaloclastites plays an important role in such brecciation, as not all intrusions brecciate, instead showing irregular pillow formation, while others cross unaffected by the host. Presumably, a relatively fast heat transfer would be effected by brecciation. However, no separate alteration events have been identified in brecciated intrusives and this possibility can not be confirmed and is not dealt with further.

b) The state of the intrusive body can be used to infer the presence or absence of fluids in the host.

(i) The absence of early alteration distinguishable from the host rock alteration seems to point to either a dry magma, a dry host rock or both.

(ii) An early distinct alteration in the intrusive body can be taken to imply the converse: wet magma, wet host rock or both.

However, the general absence of primary hydrous minerals within all the intrusive phases, and the general absence of early alteration features in sheets and dykes outside the "propylitic core", and their common presence in some intrusive phases inside the core of the volcano, seems to point unequivocally to early interactions between hydrous fluids from the host rocks and primarily dry magmas, rather than the other two alternatives in case (ii) above.

It is not known, however, at which stage such hydrous fluid was incorporated in the intrusives- at the magmatic-stage in situ or at some depth, or after solidification in situ -, and the possibility of an immiscible juvenile fluid would complicate the situation. The importance of "incorporated fluids" implies a continuity of heat convection from the magma to the hydrothermal system as said in section 4.2. The effect of such early "internal" fluids is to give rise to an early diagnostic mineral alteration. Four characteristic types are described below.

Some of the gabbros have suffered initial alteration which may be described as an "alteration flux". Such fluid or alteration fluxes chiefly acted along crystal boundaries and early shrinkage joints, and were operative throughout the intrusive body in some cases, while only within the margins of the gabbros in other cases. This feature is in marked contrast to subsequent hydrothermal alteration within the gabbros, which is mainly restricted to vein-wall rock alteration. The alteration fluxes have caused actinolite and sphene to replace

pyroxene and ilmenite respectively, and possibly the pseudomorphing of the rare olivine and orthopyroxene by talc, "green fibrous amphibole", chlorite, and magnetite or hematite.

In the case of dykes and sheets there are three types of initial alteration. In some cases intrusives at high altitude show higher-grade mineral assemblages than are found in the surrounding host, for example the replacement of pyroxene by actinolite within the intrusive while chlorite replacement is seen in the host rock or by chlorite in the intrusion while smectites were formed in the host. In other cases sulphides (pyrite, chalcopyrite) were formed in disconnected vesicle-bands or veins, most often parallel and close to the margins of the dykes or sheets. In the third case, a vesicular dyke (from phase 12) shows a siderite-calcite-pyrite-iron rich smectite assemblage in vesicles and matrix, which is not formed in the surrounding host.

In general, the presence of distinct early alteration features within the intrusives implies the corresponding presence of a fluid system in the host and may give a rough indication of the fluid composition- in particular the relative activities of CO_2 and sulphur. The presence of high-grade assemblages in outer- or high-level intrusives causes local anomalies to appear in the index mineral boundary pattern.

Finally, as successive intrusives are emplaced their cross cutting relationships helps to clarify the hydrothermal evolution of the volcano.

4.3.2 Dating of Mineral Veins and Alteration Effects

The cross cutting relationships of mineral veins and intrusive igneous rocks provide means by which "hydrothermal events" resulting in vein formation can be dated on a relative timescale. The mineral

assemblages in veins and wall rocks may also be compared with the overall alteration in a host rock and the relation between interstitial fluids and mineral vein systems established.

While the hydrothermal evolutionary model is based primarily on the cross-cutting relationships of the mineral veins and the intrusives, other sources of information include:

a) mineral infilling sequences in vesicles,

b) mineral reactions between primary and early secondary minerals and later generations of fluids, and

c) comparisons of the overall extent of alteration in intrusives of varying ages and their host rocks.

4.3.3 Mineral Infilling Sequences in Vesicles

The following general observations may be made:

(i) A correlation exists between an infilling sequence and vesicle size. Small vesicles are commonly filled by the material which forms either a sedimentary layer at the bottom of, or a band at the walls of larger ones. For example, fine-grained "clays" often fill the smallest vesicles, sometimes showing two or three colour bands. In slightly larger vesicles, concentric smectites and chlorite layers may fill the remaining void in the vesicles, while in the largest vesicles subsequent infillings of e.g. calcite, quartz, epidote, andradite, zeolites commonly occur. There are exceptions to this, for example where the earliest infilling material (fine-grained clayish material) fill larger vesicles, while smaller adjacent vesicles have not suffered the early "clay" infilling etc. The general correlation, however, between infilling sequences and size-grading vesicles still holds (compare figures 6.1 - 6.4).

(ii) A correlation exists at any locality between minerals in

vein systems and minerals filling vesicles. Small vesicles are often filled by the same material as early mineral veins, whilst the sequence of vein fillings is repeated by layers in larger vesicles. Sometimes, late mineral veins are seen to cut entirely through early filled small vesicles but only through one or more mineral layers in larger ones. A late mineral vein may show continuity with the final infilling episode in the middle of a vesicle (for example see figures 6.4 and 6.8).

(iii) Reactions of early infilling minerals to later fluids are common. Limonite reacting with later fluids to yield andradite, or chlorite reacting with fluid to yield actinolite are common examples of processes inferred from partial replacement textures (compare figures 6.10 - 6.12, 6.5 - 6.7).

Mineral infilling sequence clearly provide valuable information on the hydrothermal alteration history and could be of great value in predicting prevailing condition in active hydrothermal systems.

4.3.4 Mineral Reactions

Seven types of reactions can be inferred from replacement textures and pseudomorphs. These are hydration, oxidation, carbonation, sulphidization, solid-solid reactions, dehydration and decarbonation. Examples of hydration and carbonation are involved where pyroxene and plagioclase break down to actinolite, epidote, chlorite, prehnite, zeolites and calcite; oxidation where magnetite changes to hematite and replacement of iron oxides and hydroxides by pyrite involves sulphidization. Solid-solid reactions are encountered where plagioclase (An 90 - 50) change to albite and K-feldspars. Dehydration has occurred where chlorite has reacted with fluid to yield actinolite and water, which may possibly be caused by fluctuating CO_2/H_2O ratios, and decarbonation

seems to have occurred although the evidence is somewhat obscure. "The resorption appearance" of anhedral calcite in the interstitial matrix may be an example.

The f_{H_2O}, f_{CO_2}, f_{O_2} and f_{S_2} have apparently fluctuated with time and the sequence of pulses may be established from the vein systems. The most obvious reactions are listed below, while the chemical components involved in some of these reactions will be dealt with in the next chapter.

FELDSPARS to oligoclase, albite, adularia, quartz, calcite prehnite, epidote, wairakite, laumontite, stilbite, heulandite, scolecite, thomsonite, chlorite, celadonite, apatite, sphene.

PYROXENES to actinolite, chlorite, epidote, calcite, apatite, sphene.

OLIVINE to iddingsite, actinolite, chlorite, calcite, talc, hematite.

ORTHOPYROXENE to talc.

ILMENITE to sphene, hematite, TiO_2 (rutile?, anatase?, brookite?, leucoxene?), pyrite, chalcopyrite.

MAGNETITE to hematite (limonite, goethite), pyrite, chalcopyrite.

ACTINOLITE to chlorite, calcite.

CHLORITE to actinolite, epidote, andradite.

WAIRAKITE to laumontite, heulandite, (prehnite?).

CALCITE to aragonite?

LIMONITE to hematite, magnetite, andradite, ferrosalite.

HEMATITE to andradite, ferrosalite, actinolite, epidote.

SMECTITE to chlorite.

PYRITE to goethite.

Some clays are quite common in association with many of the reaction products listed above, but the clay type is only occasionally distinguishable with the electron-microprobe or the microscope.

4.3.5. Mineral Abbreviations.

The following mineral abbreviations will be used throughout the remainder of this thesis, where appropriate, unless otherwise clearly specified.

ab : albite
act : actinolite
amph : amphibole
and : andradite (in chapters 9 and 10)
ap : apatite
cc : calcite,(aragonite)
cha : chabazite
chl : chlorite
clay : unspecified clay-like alteration product
cpy : chalcopyrite
ep : epidote
fs : ferrosalite (chapter 7), hd_{ss} in chapters 9-12
fsp : feldspar
gt : garnet, most often andradite - (grossular possible)
gr : grossular - where known
hd_{ss} : hedenbergite solid solution
heu : heulandite
hm : hematite
id : (ferro)iddingsite
ilm : ilmenite
K.fsp : potassiumfeldspar - most commonly adularia, apparently
lau : laumontite
lim : limonite,(goethite)
mt : magnetite
mo : mordenite
ol : olivine
opx : orthopyroxene
ore : ore minerals (unspecified, oxides and/or sulphides)
pr : prehnite
px : pyroxene, usually augite
py : pyrite
qtz : quartz
sco : scolecite
sm : smectite
sp : sphene
stb : stilbite
su : sulphide, unspecified
tho : thomsonite
TiO_2 : (leucoxene,anatase,brookite,rutile) - phase unidentified.
wai : wairakite
wo : wollastonite (chapters 10-11)

4.4 Mineral Zones - Introduction.

Four mineral zones are presented in map II. For convenience in discussion these zones are tentatively referred to as representing an up-grade sequence in the following order :

(1) Chlorite zone (chl)

(2) Epidote zone (chl,ep)

(3) Andradite zone (chl,ep,gt)

(4) Actinolite zone (chl,ep,gt,act).

These mineral zones reflect the distribution of four index minerals within the host rock, mineral veins and amygdales, resulted from an active high-temperature hydrothermal system. Within the actinolite zone all the four index minerals (chl,ep,gt,act) occur, three of them within the andradite zone (chl,ep,gt), two in the epidote zone (chl,ep) and only chlorite (chl) in the chlorite zone. The chlorite zone thereby envelopes the high-temperature hydrothermal system and mark the onset of green alteration within the rocks. It will be shown that these zones do not represent any one time event, but rather they represent a composite picture of the formation of the index minerals over most of the high-temperature hydrothermal history. Information from active high-temperature hydrothermal fields in Iceland (Chapter 11) suggests that fluid temperatures from within the chlorite zone through the epidote zone ranged between ca. 200-300°C during the index mineral formation, and within the andradite- and actinolite zones fluid temperature above ca. 300°C were reached. Irrespective, however, of the actual physical and chemical conditions involved in the formation of the index minerals, their occurrence shows a relatively simple distribution, which is roughly concentric around the centre of the volcano, while the boundary patterns of the zones clearly relate to strati-

graphic depth, structure (caldera fault), rock types and the distribution of major intrusions.

Not shown on map II is the presence of high-grade mineral assemblages in outer- and high-level intrusions (e.g. phase 5) which causes local anomalies in the index mineral zonal patterns. Such anomalies, however, are referred to in the text.

Sulphide mineralization (pyrite, chalcopyrite) is particularly common at upper stratigraphic levels within the caldera. In order to draw attention to this, a sulphide zone is shown superimposed on map II. The sulphides, however, also occur at lower stratigraphic levels, though less abundantly.

In order to draw attention to the geological and mineralogical relationships a simplified map of the mineral zones in the NE-half of the volcano is shown in figure 4.3, and simplified profiles are shown in figure 4.4 and figure 4.5. The location of the profiles is shown in figure 4.3, while the data for all the figures come from map I and II. In addition, the studied mineral vein localities are shown in these figures as are the location of traverses described in chapter 6.

Figures 4.3-4.5 provide a simple field-key to the descriptions of the hydrothermal alteration in the NE-part of the volcano - sequentially including: (i) the vein systems and their time-relation to the intrusive rocks (chapter 5); (ii) the amygdale infilling sequences (chapter 6); (iii) the contact metamorphic hornfelses and skarn mineral formation (chapter 7). A comparison with other parts of the volcano is the subject of chapter 8, while descriptions of the overall host - rock alteration is combined with a summary in chapter 8.3. This seems necessary as important evidence concerning the processes of host-rock alteration is discussed in the preceeding chapters.

Figure 4.3

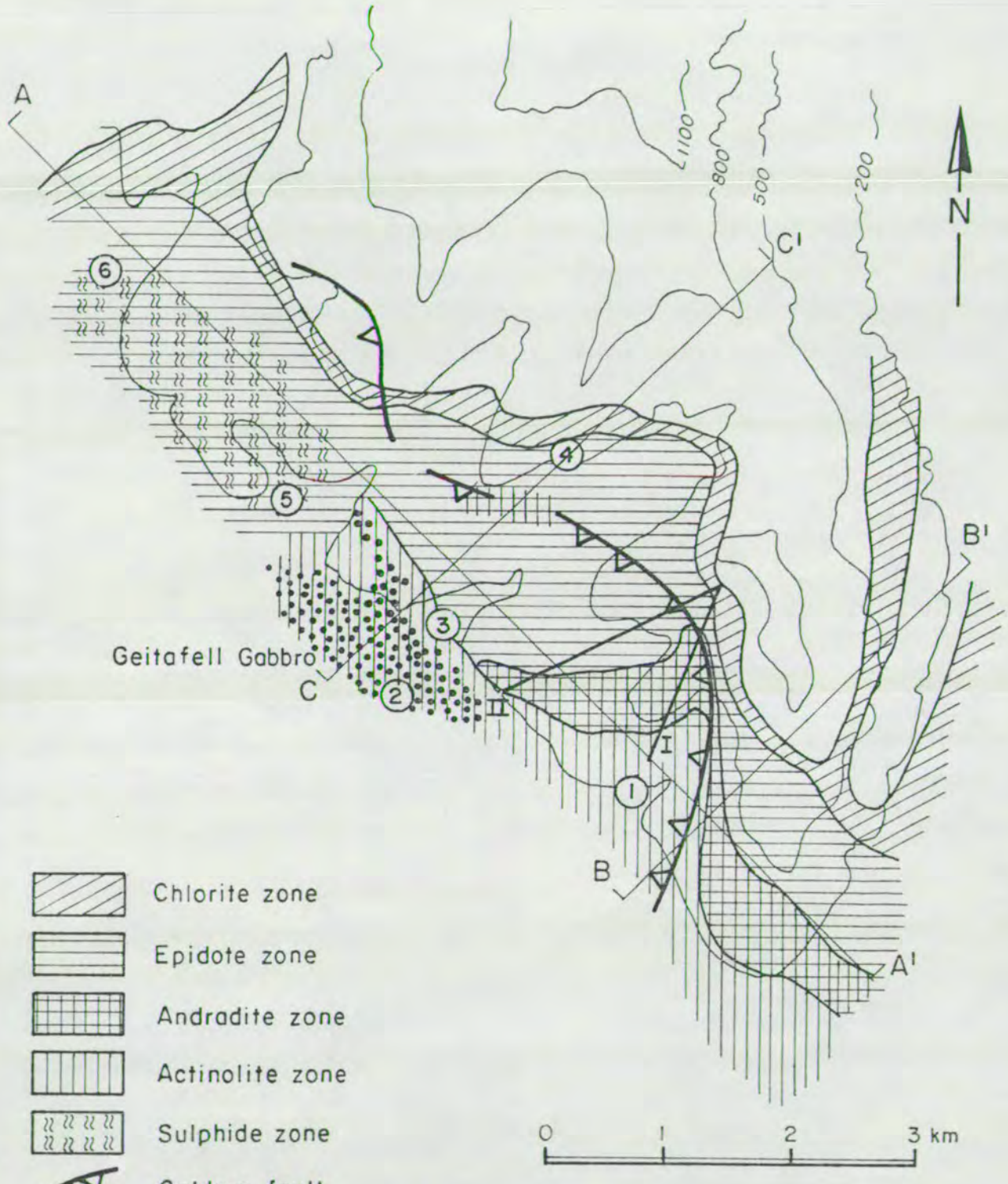

Chlorite zone

Epidote zone

Andradite zone

Actinolite zone

Sulphide zone

Caldera fault

B B' Location of profiles in figure 4.4 and 4.5

① — ⑥ Approximate location of vein-study localites 1–6

II I Approximate location of traverses described in chapter 6

traverse I: Tungufell, traverse II: Miðfell

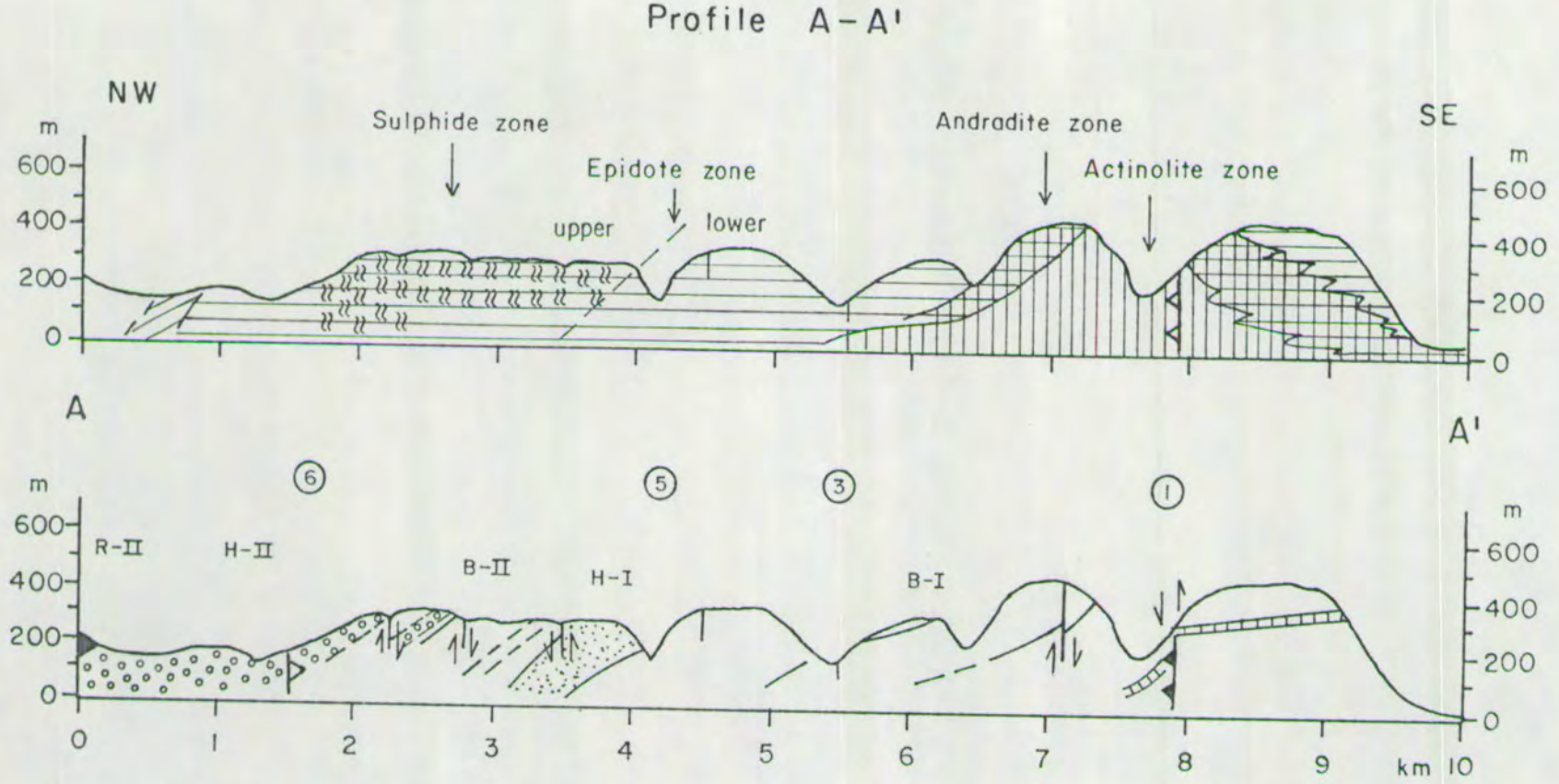

Legend : see figure 4.3 and below:

R-II and R-I : Rhyolite Units II and I, H-II and H-I : Hyaloclastite Units II and I, B-II and B-I : Basalt lava Units II and I

Figure 4.4

Profiles B-B' and C-C'

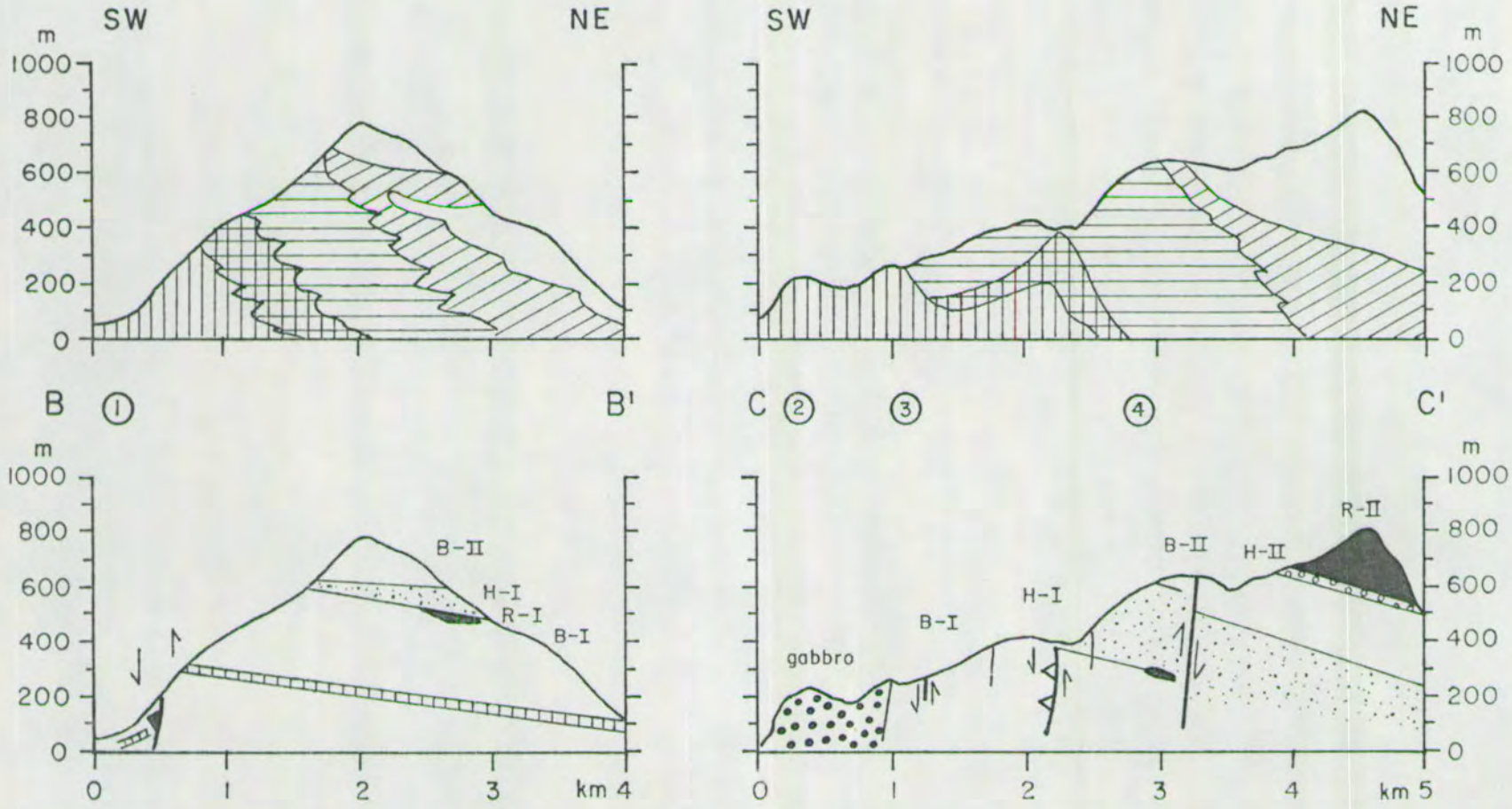

Legend: see figure 4.3 and 4.4.

Figure 4.5

CHAPTER 5

MINERAL VEINS

In this chapter vein relations from within the mineral zones are described in a sequence from the actinolite zone up- and outwards. The term "vein system" is used to indicate a group of veins within each area which were formed during the same time period. The vein systems and the apparent vein-wall-rock alteration zones are described, including the time-relation of vein systems to the intrusive rocks, and, where appropriate, the intrusive rock alteration.

The suites of mineral veins were studied at several well exposed localities in the NE-half of the volcano. The approximate position of these localities within the mineral zones and their relationship to the lithology and structure of the volcano is shown in figures 4.4 and 4.5, where the study localities are indicated by the numbers 1-6 (circled). The location of the fig. 4.4 and 4.5 profiles are shown in fig. 4.3. The detailed studies of vein relations at localities 1-6 form the basis of generalisations concerning vein relations elsewhere in the field area. A summary of the data is presented below in sequence from localities 1-6. Essentially this sequence is in order of decreasing depth below the palaeo-surface of the volcano from approximately 2 km down to ca. 200-400 m below the former surface. The following descriptions refer to vein relations within the actinolite zone (loc. 1 and 2) through the boundary of the actinolite-epidote zone (loc. 3) and upwards and outwards through the epidote zone

(loc. 4, 5 and 6). Time relations of the vein suites to the intrusive phases are presented where appropriate.

Close to locality 1, which is within the caldera but close to the fault, alteration reaches the highest grade of greenschist facies, where some of the denser basalt lavas are found to be completely converted to the greenschist facies assemblage; actinolite-albite-epidote-sphene. Characteristically, however, within each zone, the hydrothermal alteration of the lavas is incomplete (with the exception of the contact metamorphosed hornfelses). Rocks of higher porosity (i.e. scoria and hyaloclastites), however, are commonly found to be completely replaced by secondary mineral assemblages in all mineral zones. The detail vein-studies were usually performed within lavas or the oldest intrusive rocks at the sites.

5.1 Vein System within the Actinolite Zone.

(i) Locality 1 in Kráksgil

In the Kráksgil river bed unweathered lava exposures were ideal for detailed vein studies (locality 1). One such exposure is shown in figures 5.1 , 5.3 and 5.4 and reference to these figures is made in the list of the mineral veins below.

1-a) Iron-oxide (-hydroxide ?) veins are the earliest at locality 1. They have dark appearance in the field and are relatively rare. The veins are fragmented and apparent strike/slip movements have taken place (see sketch in figure 5.2a). In thin-section the veins are seen to have been altered to a hematite mineraloid intermixed with quartz and epidote.

1-b) Clay or mud-veins. While rare in the actinolite zone such veins are fairly common elsewhere (e.g. in Hoffellsfjall), but their occurrence is of interest in relation to vesicle infilling sequences (see

later). The material in these veins is fine grained and commonly clay-like, and appears to have been derived from minute particles suspended in the percolating ground-waters, which were deposited in fractures and vesicles before the hydrothermal system became active. The fine-grained material is common in lava vesicles everywhere within the volcano, within which it often forms a sediment (often layered) on the vesicle floors. Such layered deposits in vesicles were used as tilt indicators by Walker (1974) who termed them mud deposits. Commonly within the actinolite zone only relict textures of the layered deposits are preserved within the vesicles, as the fine-grained material has altered to various hydrothermal minerals (see later). Due to subsequent hydrothermal alteration it may therefore be difficult in the field to distinguish vein system 1-b from the next vein system which also contains some clay-like material.

2-a) Jasper veins. These are relatively rare within the actinolite zone, but where present they usually occur in one or two discrete fractures within the exposures. At locality 1 the nearly vertical jasper veins strike eastwards. The vein-thickness ranges from less than 1 cm up to ca. 5 cm. This width-range has been observed along the length of the same fracture. In thin-sections the veins appear altered and show the assemblage: hm-qtz-ep-clay material.

2-b) Quartz-veins. These occur in a polygonal fracture set, the fracture hade deviating slightly from the vertical at locality 1 (see figures 5.1 and 5.3, vein marked III). Quartz veins ca. 1 mm thick belonging to this system are also found in near horizontal planes - apparently controlled by flow-banding interfaces in some of the lavas. The spacing of these veins is quite variable between exposures (compare figures 5.1 and 5.3 against figure 5.4). Sometimes, epidote

FIGURE 5.1. Vein relations at study locality 1 in Kráksgil. The host rock is a relatively dense basalt lava. In the field the veins were marked in apparent chronological sequence: I, II, III and IV. However, in thin-section, cross-cutting relations showed veins II and IV to belong to the same system (3-a in text). Deep-blue wall-rock alteration is associated with the white veins (III in the photo = system 2-b in text), while pale-green wall-rock alteration is associated with the yellow veins (system 3-a in text). For further explanation see sketches in figure 5.2 a,b,c, and the text.

and more rarely ep-gt occur in the middle of the quartz veins, but cross-cutting relations are usually clear, showing epidote to be younger (see figures 5.2a and 4.8). Commonly the quartz in system 2-b shows pseudopolygonal cleavage and optical flash figures. These features are presumed to be a secondary effect related to the evolution of the hydrothermal system.

Wall-rock alteration is associated with vein system 2-b (dark-bluish in figure 5.1 and 5.3, along the quartz veins marked III). The wall-rock mineral assemblage is ab-chl-ore with minor calcite, and characteristically it is free of epidote unlike the alteration zones associated with 3-a vein system wall-rocks.

2-c) Chlorite veins. These are not found at locality 1 but are common within the actinolite zone on both sides of Kráksgil, in Tungufell and Hoffellsfjall and are apparently older than veins of system 3.

3-a) Epidote (ep), gt, act, cc, qtz, pr, wai, lau, stb, heu veins. Like vein system 2-b, system 3-a occurs in a polygonal fracture set, with the fracture hade deviating slightly from the vertical. The thickness of the veins varies from less than 1 mm up to 1 cm, but most commonly the thickness range is from 0.5 - 3.0 mm. As was observed for system 2-b, the spacing of these veins is variable. The vein-mineral assemblages of system 3-a are also quite variable. Summarized from thin-section data from a number of veins indicate the following minerals or mineral assemblages: ep, ep-qtz, ep-qtz-cc, ep-gt-act-($\pm$ cc $\pm$ qtz), ep-ab, ep-qtz-cc-stb, ep-gt-lau-heu, ep-gt-stb-heu, ep-gt-cc-pr-wai. Epidote is clearly common to all the mineral assemblages.

The variation in the mineral assemblages may indicate that several generations of mineralizing fluids took part in the growth of vein system 3-a. Evidence for this comes from the multiple veins which commonly show subparallel but irregular mineral layers. Often, the qtz-cc-z assemblage occurs in the middle and may show cross-cutting relation to earlier deposits of epidote-bearing assemblages (compare the former assemblage to vein system 4-a). In other cases, cross-cutting relations are either not observed or poorly developed. This is particularly true for the common ep-qtz-cc assemblage, while some doubts are raised concerning the zeolites - as their emplacement texture most often shows evidence of a somewhat later origin for the zeolites. A simplified sketch of a typical multiple vein thin-section is shown in figure 5.2 b. The emplacement texture of the mineral layers - involving poorly developed cross-cutting relationships between the layers (excluding the zeolite vein), and the different grain size of the epidote crystals within the layers - may suggest that the mineral layers were deposited during quite separate (?) episodes. The variation of the mineral assemblages between the three layers (ep, ep-cc, ep-cc-qtz) may indicate that the fluid chemistry was somewhat variable during each episode. An alternative explanation is that slight physical changes in the fluid system might produce a similar emplacement texture. While neither possibility can be excluded, the emplacement texture and the overall variation of the mineral assemblages of system 3-a probably indicates that several generations of fluids took part in constructing vein system 3-a.

A marked wall-rock alteration is usually associated with the system 3-a veins (see figures 5.1 and 5.3, veins marked II and IV). The wall-rock alteration is characterized by extensive epidote replacement of the rocks producing a fine-grained assemblage of ep-act-ab-

Figure 5.2

SIMPLIFIED SKETCHES FROM THIN-SECTIONS

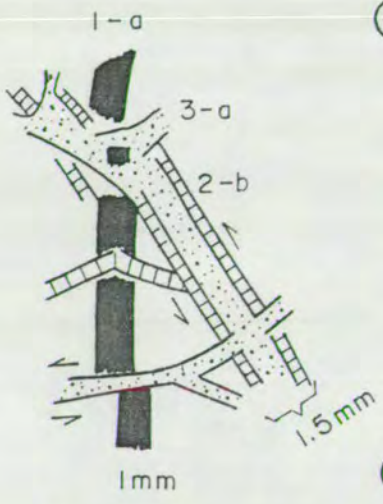

ⓐ from sample 7926

Vein systems 1-a, 2-b, 3-a
showing clear evidence of time relation

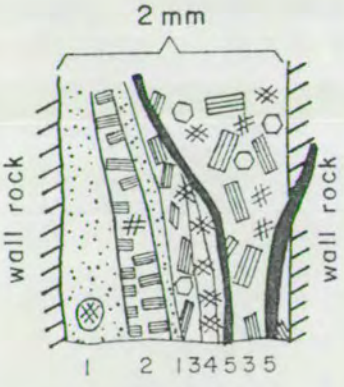

ⓑ from sample 7929

Multiple vein of system 3-a
Apparent time sequence:
1: fine-grained epidote
2: ep-cc
3: ep-cc-qtz (coarse-grained)
4: cc
5: stilbite

ⓒ from sample 7928

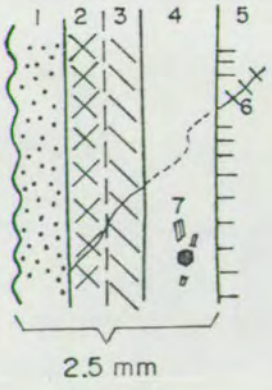

① Ep-gt-act-cc vein of system 3-a
② ab-act-ep wall rock
③ ab-chl-ep wall rock
④ Quartz vein of system 2-a
⑤ ab-chl wall rock
⑥ Ep-microvein (ab-chl-ep wall rock)
⑦ Ep-gt formed within the quartz vein in vein-centre cavity, but appears related to ① and ⑥

sp-qtz-cc-(chl-su). As can be seen in figures 5.1 and 5.3, the width of the pale green alteration zones is highly variable, and in other cases the pale green alteration cannot be related to visible mineral veins. This latter alteration is not readily explained but may partly relate to variability in rock porosity. A specific example is shown in figure 5.3 (centre of the photo) where the faulted white vein III (system 2-b) is crossed by the subparallel yellow brown vein IV (system 3-a). The wall-rock alteration zones related to vein IV are asymmetric in width. In a thin-section (see figure 5.2 c) it is seen that the epidote replacement alongside vein 3-a, diminishes towards the neighbouring quartz wall and is not seen on the other side of the quartz vein. This may partly relate to decreased porosity in and next to the quartz vein. In the micro-vein region (fig. 5.2 c), however, the permeability was apparently not reduced and the epidote mineralizing fluid appears to have passed through and caused some rock alteration at the outer side of the quartz vein.

While this interpretation seems possible, the situation is complicated by the two different wall-rock zones associated with the two veins. The wall-rock zone at the right-hand side of the quartz vein (5 in fig. 5.2 c) shows chlorite-albite as the dominant constituent of the wall-rock assemblage (chl-ab-ore(primary?-su)-cc-sp?) whereas on the left-hand wall of the quartz vein (3 in fig. 5.2 c) chl-ab-ep-(+ rest) is developed which is gradually replaced by amph-ep-ab (2 in fig. 5.2 c) next to the ep-act-gt-cc vein. In the fine-grained rock matrix away from the veins, primary pyroxene and feldspar occur together with chl-ab-ore. Therefore, the asymmetric wall-rock zones may be controlled by the different compositions of the mineral assemblages on either side of the epidote-bearing vein. Despite the lack of mineralogical details, this example indicates how the rock alteration proceeded with time. Apparently, chl-ab was formed within the rock at the time of vein system

2-b (quartz), while ep-act-ab was formed contemporaneous to vein system 3-a.

With reference to the visible wall-rock alteration zones in figure 5.3, it appears that the most prominent wall-rock zone (palest green) was produced by the last vein system (vein V in photo, system 4-a in text). However, it is seen in this section that a mineral assemblage belonging to system 3-a occurs at the wall of vein V. In other words there is a multiple vein involving two systems suggesting that the wall-rock alteration relates to system 3-a rather than to system 4-a. This conclusion gains some support from the observation that vein V runs clear of the pale green zone as shown in Fig. 5.3 (left centre, just above compass). However, the pale green alteration only becomes prominent where the two veins combine which, in turn, may suggest that the wall-rock alteration was related to the vein-fluids of both systems. In a thin-section the wall-rock assemblage is seen to include ep-ab-amph-chl-ore, i.e. to be probably related to system 3-a. No visible effect from vein V, (which includes stb and cc), is seen in the thin-section although some wall-rock alteration may still exist but not have been noted since the small grain-size of the rock hampers detailed study. Referring still to figure 5.3, one can see that some of the white veins (system 2-b) pass imperceptibly into the wall-rock zone discussed, suggesting that the palest-green zone may also be related to vein system 2-b. The situation just described demonstrates how difficult it can be to be precise about which part of the wall-rock mineral assemblage belongs to each vein system. The example, however, does throw some light

Figure 5.3. Vein relationships at locality 1 in Kraksgil. The faulted vein III in the photo belongs to system 2-b (see sketch below), veins II and IV to system 3-a and vein V to system 4-a. Note the wall-rock alteration - asymmetric along vein III (see sketch) and the palest-green alongside vein V. See text for explanation.

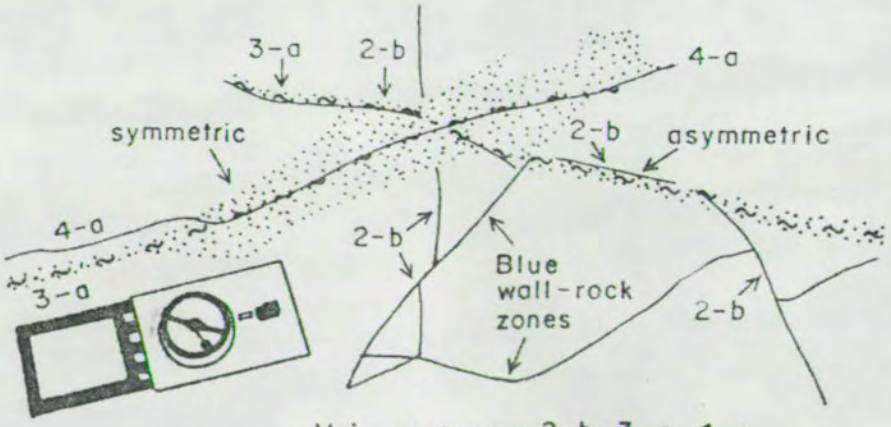

Vein systems: 2-b, 3-a, 4-a.

Wall-rock zones to 3-a stippled.

on the hydrothermal alteration of the rocks of high porosity (e.g. scoria), within which a complex overprinting of alteration events has resulted in complex mineral assemblages. In such rocks, almost the whole range of hydrothermal minerals present in the field may be visible in a single thin section.

A third example is taken from a somewhat simpler situation within study locality 1 (see fig. 5.4). Here it is easily seen in the field that the yellow vein (2-3 mm wide) belongs to system 3-a. The vein cuts into a large lava cavity (diameter ca. 150 mm). The width of the visible wall-rock zone alongside the narrow vein is ca. 3-4 mm on each side, while the wall-rock zone around the cavity is some 40 mm wide. The fluid/rock ratio may be the chief variable leading to the different widths of the wall-rock zones. In the two cases, the rock-fluid interface per square unit at the walls is equal, while the fluid volume was evidently much greater within the cavity - if it is assumed that the cavity was filled with fluid. Assuming further, that fresh supplies of the reactive fluid were fed towards the solid/fluid interface by circulation within the fluid, it is tempting to relate the different widths of the wall-rock zones to the fluid/rock ratio. However, a number of assumptions are already implicit, namely:

1) the vein-fluid was not actually flowing through the system. If so, this could obviously have changed the volumetric relationships,
2) the initial fluid composition was identical in both the vein and the cavity. This need not have been the case if some fluid existed within the cavity, which - in turn - could already have caused some wall-rock alteration,
3) the wall-rock porosity was identical in both cases, which would not have been the case had the cavity wall been

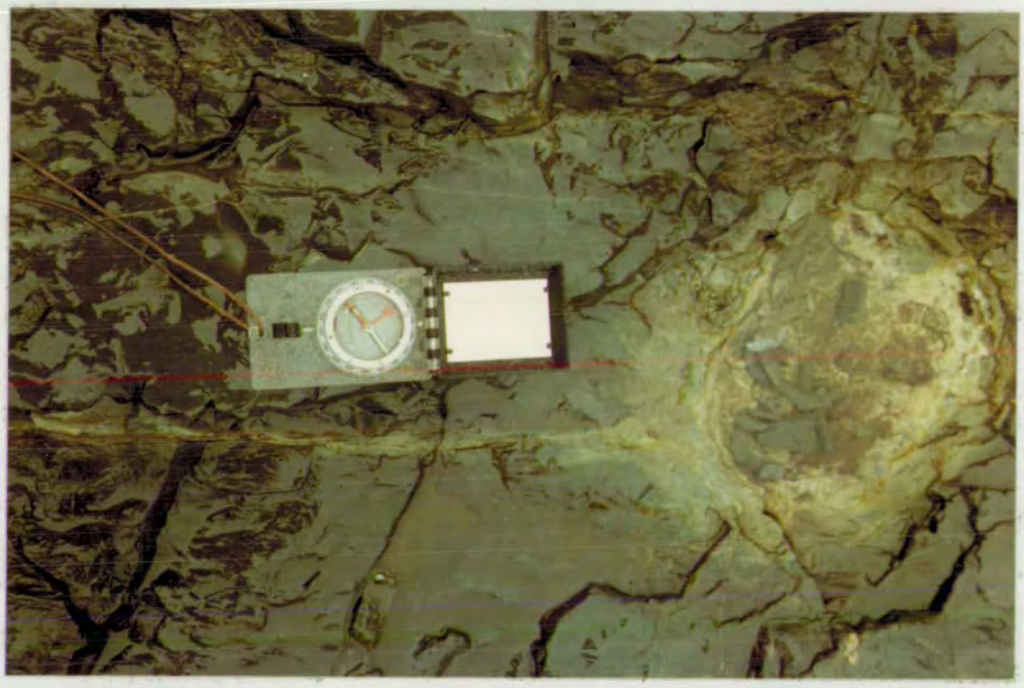

Figure 5.4. Further vein relationships at locality 1 in Kraksgil. The yellow vein belongs to system 3-a. The vein cuts into a lava cavity (diameter ca. 150 mm). Note the different widths of the wall-rock alteration, and the different spacing of veins compared to fig. 5.1 and 5.3 See text for discussion.

coated by some mineral layers. In the present situation, a mud sediment (composed of turbid quartz at present) occurs on the cavity floor, and presumably the cavity wall was already coated with a qtz-chl-(cc?) assemblage (see chapter 6 on the vesicle infilling sequences).

Since the third, and probably the second, assumption cannot be valid, it is evident that simple volumetric considerations are inadequate to explain alteration features which may appear simple in the field. In the previous discussion of the wall-rock zones seen in figures 5.1 and 5.3 it appears, that the mineral assemblages are related to three or more alteration events. The same appears to apply to the vesicle-wall rocks, as the vesicles become infilled by minerals in a sequence similar to that seen in the vein systems. The implications from this are discussed further in chapter 6 on the vesicle infilling sequences. At present - the discussion of wall-rock alteration is concluded with the observations that in the field wide veins reveal wider wall-rock alteration zones than narrow veins of the same system. The extent of wall-rock alteration, however, appears to vary between the vein systems. Secondly, alteration halos surrounding some of the lava vesicles are commonly observed within the actinolite zone. Often veins of system 3-a cut these vesicles - revealing a similar relationship to that seen macroscopically in fig. 5.4 (see also chapter 6).

3-b) Ab-ep-wai veins, found in Tungufell, and laumontite veins found in Hoffellsfjall appear to be contemporaneous with vein system 3-a, but direct evidence is lacking.

4-a) Qtz, cc, stb, heu veins. At locality 1, the most prominent of these veins strike E-W and are near vertical. Often, veins of this system are found to be monomineralic, but normally some

combination of the four minerals listed constitute the vein-mineral assemblages. As already noted, mineral types of this system are the same as those in the later generations of system 3-a. This may broadly indicate a progressive evolution of the fluid system from vein system 3-a to 4-a. However, in particular, the variation of the vein-mineral assemblages of system 4-a, may indicate that several fluid generations were involved in vein system 4-a.

Wall-rock alteration is seen associated with veins of this system. Extensive replacement by some of the vein minerals are seen in the wall-rock zones - the most common replacement mineral being calcite. While the wall-rock assemblage appears to vary depending on the extent of earlier rock alteration these wall-rock zones have not been studied in detail.

4-b) Scolecite veins, are apparently contemporaneous with system 4-a, but are rarely found within the actinolite zone except in Hoffellsfjall. In a case study (sample 1 30/6 '77) a scolecite vein crosses a feldsparphyric lava. Phenocrysts cut by the vein may be completely pseudomorphed by scolecite while vein-free phenocrysts are unchanged. The wall-rock alteration in the fine-grained rock matrix (fsp-px-ore) is similar with respect to the feldspar, but on the whole not as prominent, as the pyroxene and the ore appear unaffected by the scolecite-mineralizing fluid.

Chronology of veins and intrusive phases.

Intrusive phase 3, 5, 6, 7, 8, 9, 10, 11 and 12 are all present within or near Kráksgil in the actinolite zone, while phases 3, 5, 6, (8 or 9), 11 and 12 were recognized nearby study locality 1. Based mainly on field work, and to a lesser extent on petrography, it appears that all the intrusive phases except 12, are cross-cut by some

variant of system 3-a veins. The critical mineral in order for a vein to be assigned to system 3-a is epidote - which is easily recognized in the field. Vein system 2-b and the older systems, pre-date intrusive phase 5, while the time-relation between vein system 2-b and intrusive phase 3 are unknown. Intrusive phase 12 is only cross-cut by vein system 4-a.

In the simplest interpretation, these field relations might indicate that the formation of vein system 3-a post-dated intrusive phases 3 - 11 but pre-dated phase 12. However, multiple veins of system 3-a are common, and as already suggested, it appears that vein-fluid generations were responsible for system 3-a. This may suggest that a part of the veins in system 3-a were formed during progressive intrusive activity although the intrinsic details are lacking.

The field- and time-relations from elsewhere in the volcano clarify the overall time-relation of events at low levels within the actinolite zone. In the contact aureole to the Geitafell gabbro, exposed some 1.7 - 2.0 km NW of locality 1 and some 400 m higher in the strata, changes in the vein mineral assemblage similar to those recorded between vein systems 2-b and 3-a occurred, evidently pene-contemporaneous with the gabbro emplacement. A general steepening of the geothermal gradient in the volcano probably accompanied the gabbro emplacement and the change in vein-mineral deposition from system 2-b to 3-a at locality 1 may well date back to the Geitafell gabbro event.

Intrusive phase 5: the cone-sheets emplaced immediately post-gabbro intrusion reveal an interesting alteration feature inside the epidote- and the actinolite zones. A characteristic secondary mineral assemblage formed within the sheets <u>outside</u> the actinolite zone is <u>actinolite</u>-sphene-albite-epidote. The actinolite formation within the epidote-zone is restricted to members of intrusive phases 5 and 6.

Since the mineralogical composition of the basaltic sheets is similar to other basaltic rocks (lavas and intrusives) it seems feasible to relate the restricted actinolite occurrence to an early interaction of water and hot intrusive rock (i.e. during and shortly after the sheets emplacement). Most likely, similar behaviour occurred within the actinolite zone - and may support the idea that vein system 3-a dated back to the gabbro event, as the cone-sheets were emplaced shortly after the gabbro in Geitafell.

Within the actinolite zone sheets of intrusive phase 5 are substantially more altered than those at higher levels. Occasionally, rather peculiar alteration texture is observed in some of the sheets - which in the field appear to be fragmental (see figure 3.4). This field appearance is due to the combined effect of alteration and weathering, whereby the harder cores (see fig. 3.4) are composed of relatively unaltered rock, while the softer intervening zones are composed of extensively altered rock (act-ab-sp-ep and other minerals). A similar alteration texture is observed in one of the major intrusive "phases" in the sheeted-dyke complex in the Troodos ophiolite but has not been explained (Desmet, Rocci and Lapierre, pers. comm.). In the Icelandic example, it appears that a long time-component (i.e. from phase 5 through 11) was involved in the formation of the alteration texture.

A composite gabbro-diorite-granophyric felsite intrusion in Kráksgil belongs to intrusive phases 10 and 11. The gabbro pyroxene is extensively replaced by actinolite and chlorite, while epidote and secondary feldspar are common replacement after primary feldspar. The greenschist facies assemblage ep-act-ab-sp was clearly formed within the gabbro of phase 10 and epidote-bearing veins are found within boulders of the gabbro.

A large felsite intrusion emplaced close to the Kráksgil gabbro, together with a strongly transgressive system of felsite veins, away from the gabbro belong to intrusive phase 11. Epidote veins at and within the felsites are grouped with vein-system 3-a.

The only intrusive rocks in Kráksgil not cut by vein system 3-a are intrusive phase 12 dykes and some acid dykes of phase 11, which are only cross-cut by veins of system 4-a. Apparently the phase 12 dykes in Kráksgil are more altered than their close relatives elsewhere, being extensively replaced by calcite and zeolites. Heulandite is common within the dyke-vesicles which are sometimes cut by calcite veins.

(ii) Vein-study locality 2 and the Geitafell gabbro alteration.

The Geitafell gabbro is composed of feldspars (bytownite and more frequently labradorite, commonly zoned to andesine), augite ($Wo_{44}En_{43}Fs_{13}$ commonly zoned to $Wo_{42}En_{40}Fs_{18}$), magnetite and ilmenite. The relative proportion of these minerals varies slightly but no distinctive zonation has been observed. Occurring in subordinate amounts are olivine (always pseudomorphed) and hypersthene ($Wo_{3.5}En_{67}Fs_{29.5}$) (usually pseudomorphed). Apatite is an accessory mineral. The gabbro matrix is generally 'massive', but occasionally minute vesicles occur filled with chlorite and amphibole. The vesicles, however, are rare and not discussed further. The gabbro matrix is normally extensively fractured with irregular cracks traversing the primary minerals and more regular joints filled by secondary minerals and constituting mineral veins. The development of secondary from the primary minerals is listed in chapter 4.3.4, from data gathered from all rocks within the volcano. Within the gabbro the following secondary minerals are found: act, sp, chl, tc, cc, qtz, ep, pr, oligoclase, ab, K.fsp, lau, stb, sco, tho, id, hm, TiO_2, py, cpy, ap, clay, sm.

The gabbro appears remarkably unaltered since the extent of the secondary mineral development is small. However, the extent of alteration varies and quite altered gabbros can be adjacent to prominent mineral veins. Actinolite and sphene are found in most thin-sections, marginally replacing augite and ilmenite respectively. The chl-hm-cc-act-id-tc-qtz assemblage, in whole or in part, is fairly commonly found replacing olivine or hypersthene. Chlorite, calcite and albite are also fairly common, but these and the other secondary minerals appear more or less confined to vein wall-rock alteration zones.

For time relation purposes, three early igneous veins are listed together with the hydrothermal veins below:

1) Pegmatite veins of feldspar and pyroxene (possibly contemporaneous to intrusive phase 3) occur at the SW-margin of the gabbro. They seem to have formed a little later than the main gabbro and trend northwards, parallel to the elongation of the gabbro. They are 5-10 cm across and are either vertical or show steep dips to the east.

2) Felsite veins (intrusive phase 4) have sharp but unchilled contacts with the gabbro and sometimes follow the same joint planes as vein system 1 (occurring in the middle of the pegmatite veins). However, cross-cutting relationships are frequently seen showing the felsite veins to be somewhat younger. They trend northwards at study locality 1 (SW-margin of the gabbro), and are either vertical or show steep eastward dips. Their thickness is from 0.5-10 cm. Two generations of felsite veins appear to be present, although the latter is rarely found. The later generation has been found within the gabbro-host cross-cutting intrusive phase 5, which may be of importance to the overall chronology of events, since intrusive phase 5 is regarded as contemporaneous with vein system 4. The two generations of felsite veins are both confined to the gabbro and its aureole. However, there is a lack of data concerning the extent and distribution of the later generation of felsite veins and none have been found to cross-cut actinolite veins despite careful search. Therefore, the later generation of felsite is presently grouped within vein system 2.

Wall-rock alteration alongside the felsite veins appears to be insignificant. Within the felsite, however, secondary amphiboles replace pyroxenes, and actinolite veins (system 3) are sometimes found at the margins of the felsite veins. Albite and K.feldspar are both found within the felsite, and sometimes the gabbro plagioclase shows a narrow zone of oligoclase, albite (and K.feldspar) next to the felsite veins. This apparent wall-rock effect is taken into consideration in table 5.1.

3) Actinolite veins including sphene, minor chlorite, minor andesine and chalcopyrite, trend northwards and are either vertical or show a considerable dip to the west (up to 45°). Their thickness is usually 1 mm or less. Sometimes they follow the margins of the felsite veins, but cross-cutting relations demonstrate that the actinolite veins are younger. The veins are chiefly composed of actinolite ; second in abundance is sphene. Chlorite is commonly intermixed with actinolite although it is not clear whether the chlorite belongs to the initial mineral assemblage or is related to later overprinting by hydrothermal events (see vein systems 5 and 6). Chalcopyrite has been found at the vein walls but shows an irregular distribution, and andesine is sporadically found within the veins. The andesine, however, may represent xenocrysts spalled from the (gabbroic) vein walls.

A marked wall-rock alteration is associated with the actinolite veins (see figure 5.5). The pyroxene next to the veins is either partly or completely replaced by actinolite, and ilmenite is partly replaced by sphene. The feldspars, however, appear to have remained unaffected by the actinolite-vein fluid and microprobe analysis showed no change in composition from a core of a feldspar grain towards an actinolite vein wall. Irregular microveins (less than 0.1 mm) containing actinolite (or chlorite) are common in the gabbro. Often such veins emanate from the main actinolite veins (see figure 5.5). The same wall-rock effect is seen associated with the micro-veins just as with the main veins. Elsewhere in the gabbro (i.e. away from the vein contacts) the pyroxene may be unaltered or marginally replaced by actinolite. Therefore, a fluid system possibly synchronous with the actinolite vein-fluid seems to have percolated the gabbro via fractures and crystal boundaries. The extent of the actinolitization within the gabbro matrix is in marked contrast to the development of other secondary minerals which is more restricted to the wall-rock alteration zones

Figure 5.5

VEIN SYSTEM 3 IN THE GEITAFELL GABBRO

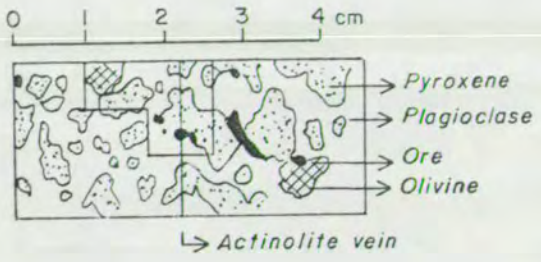

ⓐ Sketch of a thin section (sample 213) Scale: 1:1

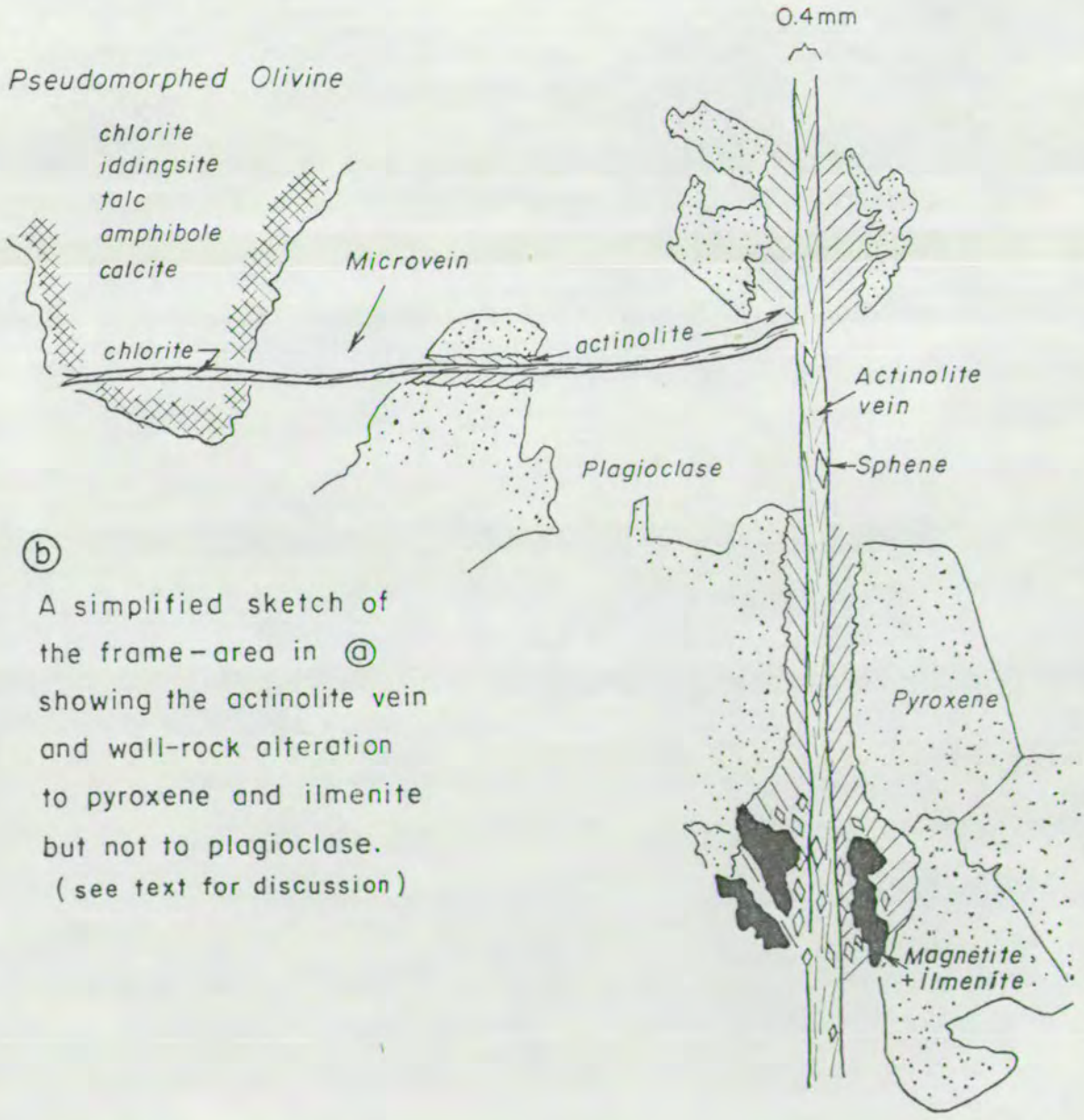

ⓑ A simplified sketch of the frame-area in ⓐ showing the actinolite vein and wall-rock alteration to pyroxene and ilmenite but not to plagioclase. (see text for discussion)

associated with later vein systems. An exception to this may be the development of chlorite in olivine, hypersthene and micro-joints.

The hydrothermal alteration of olivine and hypersthene in the gabbro may relate to the time of vein system 3 formation. In figure 5.5 a pseudomorphed olivine cut by an "actinolite" micro-vein is shown. Inside the olivine the micro-vein contains chlorite; while it is not clear whether this chlorite is of primary or secondary origin with respect to the dominantly actinolite mineralizing vein fluid. The olivine is completely pseudomorphed by chl-id-amph-tc-cc. In table 5.1 the olivine and hypersthene alteration is tentatively regarded as synchronous with vein system 3.

4) Basaltic veins. These are several cm in thickness, trend northwards and appear to cut veins of system 3. Their former glassy margins show the mineral assemblage: chl-K.fsp-cc. These veins are thought to be related to intrusive phases 5 and/or 6.

5) Ep $\pm$ chl veins. These trend northwards and are usually less than 1 mm across. Ep, ab, K.fsp are detected replacing wall-rock feldspar.

6) A group of closely related veins. Several generations of vein fluids appear to have formed this vein system, and multiple veins are common. The following three sub-systems are distinguished:

6-a) Ep-clay veins, trending eastwards, less or equal to 1 mm across.

6-b) Ep, chl, qtz, cc, pr, lau, py veins. The mineral assemblage in individual veins may include all or part of the minerals above. The veins trend eastwards and their thickness is variable, usually less than 1 cm. Multiple veins of this system are common. Apparently these veins fill dilation joints, and episodic dilation seem to have occurred in some cases, e.g. where vein system 7 transects multiple veins of system 6-b.

6-c) Cc, qtz, z, clay veins, trending between E and NE, these have thicknesses variable from 1 cm up to 100 cm aggregate-thickness in zones of closely spaced veins.

Wall-rock alteration is associated with vein system 6. In the field this alteration is not as distinctive as at vein study locality 1 (e.g. in fig. 5.1 and 5.3). Replacement of pyroxene by chlorite related to vein system 6 is not as prominent as is the actinolitization accompanying vein system 3. Thus, pyroxene-breakdown seems to have diminished by the time of vein system 6. The actinolite, however, is partly replaced by chl-cc apparently associated with vein system 6. The extent of this replacement appears to increase towards veins of system 6. In addition, apatite is sometimes found inside the partly replaced actinolite. Magnetite is commonly replaced by pyrite (or py-hm) in the wall-rock zones of vein system 6 and both sp and TiO_2 (mineral-phase unidentified) are found replacing ilmenite. The most extensive wall-rock alteration, however, related to vein system 6 concerns the feldspars which are replaced by some or all of the following minerals: ep, cc, qtz, pr, lau, clay, ap, ab, K.fsp, oligoclase.

The extent of wall-rock alteration varies but is commonly extensive near wide or closely spaced veins. For example, where narrow veins are filled by epidote, the wall-rock feldspars are incompletely replaced by ep-ab-K.fsp. In contrast alongside wide or closely spaced veins of calcite, the wall-rock feldspars are commonly replaced by calcite, ± subordinate ep, qtz. In the third and perhaps an extreme case, severely altered gabbros are seen as complex wall-rock zones to several veins. As an example, in one thin-section of an extensively altered gabbro from a gabbro-dyke stemming from the main gabbro in Geitafell towards the north, all the primary minerals are partly or completely pseudomorphed by minerals belonging to all the hydrothermal

vein systems together with ab, K.fsp, TiO_2, sp, ap, hm, cpy. In the latter two cases it is rather difficult to outline a detailed sequence for the breakdown of the primary minerals as the primary minerals breakdown seems to relate to a sequence of events connected with vein systems 3, 5 and also with the fluids constructing vein system 6. Therefore, at present, only the overall hydrothermal alteration sequence of the gabbro alteration can be listed (see end of the section).

Vein system 6 was deposited within the gabbro during the emplacement of intrusive phases 7-12. Intrusive phases 9-12 have similar trends (between E and WE) to vein system 6. Most members of these intrusive phases contain parallel to sub-parallel mineral veins which are some variants of system 6. However, epidote, prehnite and chlorite are absent from veins in intrusive phase 12 which allows for the distinction of sub-system 6-c to be established.

7) Zeolite veins (stb-sco-tho), trending eastwards, thickness from less than a mm to 1-2 cm. In a sample from study locality 2, stilbite lines the vein walls with thomsonite and scolecite in the centre. Feldspar in the wall-rock zone is partly replaced by stilbite.

In order to summarize the sequence of secondary mineral development both in veins and wall-rock zones in the gabbro, the more diagnostic and abundant secondary minerals are underlined in the table below:

1) Extensive development of actinolite and sphene, with minor development of ab, K.fsp, ep, chl, qtz, cc. Associated with vein system 3 and 5.

2) Extensive formation of epidote, chlorite, albite, K.feldspar, quartz, calcite, possibly with minor development of sp, act. Associated with hydrothermal vein systems 5 and earlier generations of 6.

3) Extensive formation of calcite, quartz, prehnite, albite,

K.feldspar, laumontite, with minor development of ep, chl, sp, stb, ap, TiO_2. Associated with later generations of vein system 6.

4) Formation of stilbite, scolecite, and thomsonite, and some qtz, cc. Associated with vein system 7.

In order to make comparison to other vein study localities, a simpler table 5.1 is presented showing the time-relationships between mineral veins and the intrusive phases and the apparent periods of secondary mineral development. Similar tables are presented later for the other areas.

TABLE 5.1 DEVELOPMENT OF SECONDARY MINERALS IN THE GEITAFELL GABBRO

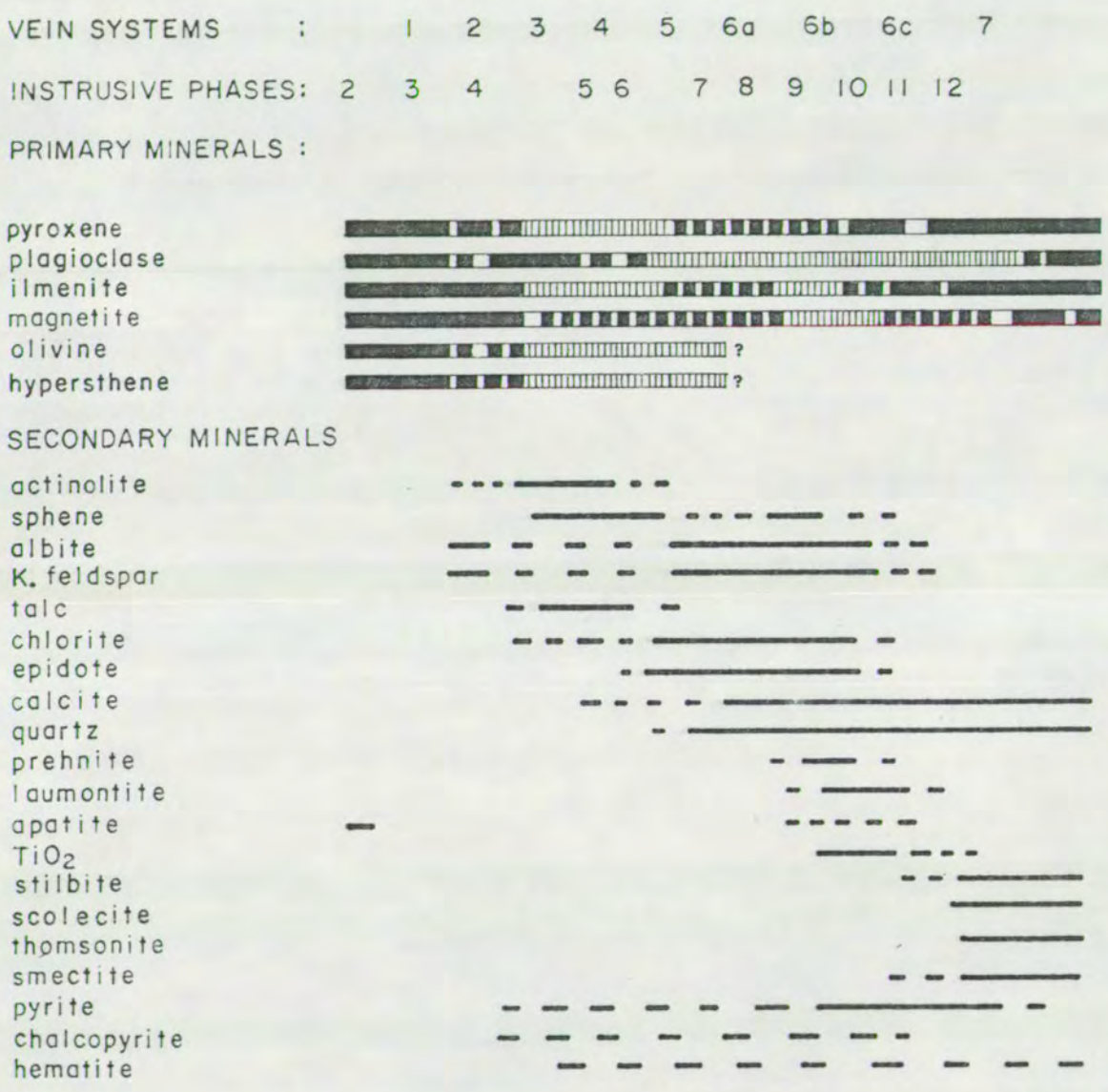

LEGEND:

PRIMARY MINERALS:
- apparently stable
- unstable, limited breakdown
- unstable, extensive breakdown

SECONDARY MINERALS:
- growing
- in slow or uncertain growth

(iii) Vein-study locality 3: sheet-swarm at the Geitafell gabbro contact.

Vein-study locality 3 is at the outer fringe of the Geitafell gabbro contact aureole, within a dense sheet-swarm (ca. 95% of the rocks are intrusives). Data from the vein suites were collected from the sparse intervening lavas and the intrusive rocks. Although intrusive phases 3-12 are all found within the sheet swarm, it is composed chiefly of low-angle sheets of intrusive phases 5 and 6.

Within the aureole, actinolite partly replaces pyroxene in the lava matrices and was deposited in lava vesicles. The pyroxene in intrusive phases 5 and 6 is also partly replaced by actinolite, while the amphibole has not been found within the vein mineral assemblages. As can be seen in figure 4.3 the contact aureole of the gabbro is narrow (ca. 100-200 m) as it lies within the boundary of the actinolite zone.

The aureole includes (poorly-exposed) hornfels and hydrothermally altered lavas and intrusives. The overprinting by hydrothermal events is extensive in the contact aureole and the hydrothermal alteration has proceeded in a similar fashion to that already described for the gabbros adjacent to veins. Hydrothermal effects related to pore-fluid flow, however, add to the complexity of the lava alteration. As the relation between the two fluid flow systems (porosity and fracture controlled) is not obvious, the overall alteration in the contact aureole is described later (chapter 7 and 8.3). The following descriptions of the vein systems relate to the vein-intrusive relationships, and only the most obvious wall-rock effects alongside the veins are noted.

1-a) Dark clay-like veins with clear quartz in the middle.

These are restricted to the lavas (see also below). In thin-section

the dark clay-like material shows light brown to dark gray colour bands. Microprobe analyses show the composition of these fine grained materials to be irregular, with SiO_2 constituting some 69-87% of the total (89-100%), TiO_2 (2-9%), Al_2O_3 (3-4,5%), FeO (0,5-7%), MgO (0-3,5%), CaO (2-8,4%), K_2O (0,2-3,1%) and Na_2O (0-0,9%). These veins may be contemporaneous with vein system 1-b (mud veins) at locality 1 and possibly also vein system 2-a (jasper veins). A "clay-like" sediment at the bottom of vesicles has a similar composition to the vein materials above (see chapter 6). The composition of the clay-like material shows it to be turbid silica, possibly related to later hydrothermal alteration. The turbid silica deposit at the vein margins changes sharply to clear quartz in the vein centres, which suggests a progressive evolution of the fluid system yielding the deposits. The quartz in vein system 1 above may be synchronous with vein system 2-b (quartz veins) at study locality 1. Dark clay-like material including minor chalcopyrite and pyrite, is also found in a shear joint in intrusive phase 3. The relation between the shear joints deposits to vein system 1-a is unclear.

1-b) Opaque disconnected bands found in lavas, apparently at flow banding interfaces. These bands (or irregular veins) contain hematite and some pyrite. The formation of these veins may relate to the formation of limonite deposits in vesicles (chapter 6), and vein system 1-a at study locality 1, all probably due to cold groundwater percolation. The chronology between systems 1-a and 1-b at locality 3 is not clear but both are cut by vein system 2.

2) Ep, wai, (chl, cc, cpy) veins. These veins are commonly narrow (ca. 0,1 mm) and show variable strike/dip relations. At least two generations of veins exist within this system, the earlier containing epidote alone and the later ep-chl-cc. Occasionally, veins

containing ep-wai are found and grouped within system 2, while their time-relationship to the two variants above is not clear. However, these veins are clearly younger than intrusive phase 5. No wall-rock alteration associated with this vein system has been seen in the field. However, minor replacement of feldspar phenocryst by epidote next to a narrow epidote vein (less than 0,05 mm) cross-cutting intrusive phase 3 suggests that some wall-rock alteration was associated with this vein system.

3) Pr-cc-lau-stb veins. These are somewhat thicker than veins of system 2, up to 1-2 mm and are younger than intrusive phase 7. In one of the samples, pr-cc lines the walls, while the assemblage lau-stb-cc-pr fills the vein centres.

Wall-rock alteration was studied in intrusive phase 6. In a sample free of veins, the matrix and phenocryst fsp are relatively fresh but partly replaced by ab, while chl, act replace some of the augite. In a sample including a system 3 vein, the fsp at the vein-wall is completely replaced by pr-cc-stb-qtz, and the px is almost completely replaced by chl-ep-cc-qtz-act.

4) cc, qtz, z, chl, sm veins. These are the most prominent veins at study locality 3 and much thicker (up to 20 cm) than veins of the older systems, with calcite as the chief mineral. Vein zones, more than 1 m across, are occasionally found. The veins commonly run parallel to the intrusive dykes and are found to cross-cut intrusive phase 12.

At least three generations of veins compose vein system 4. Insufficient evidence, however, was found to give clear distinction of formation times, but smectites are definitely associated with the later veins (e.g. those cutting intrusive phase 12), while chlorite is associated with the earlier veins in this system. Joint-width

seems to be a factor determining mineral assemblages ; narrow branches from main joints may, for instance, show monomineralic deposits, while the main vein shows the whole assemblage. The texture of some of the wide veins further suggests that some of the veins may be multiple, though this has not been studied in detail.

The following assemblages have been found in veins classified as system 4: cc, cc-chl, cc-chl-qtz, qtz, qtz-cc, cc-sm, cc-z, cc-z-sm-(±qtz), z (one or more types). Only stilbite and heulandite have been analysed from vein system 4, while other zeolite types may be present.

Wall-rock alteration associated with vein system 4 is prominent. Examples are discussed from intrusive phases 5, 9 and 12. Intrusive phase 5 contains small augite phenocrysts (ca. 3 mm) ($Wo_{39}En_{48}Fs_{13}$) in a medium-grained (ca. 1/2 mm) doleritic matrix composed of augite ($Wo_{40}En_{42}Fs_{18}$), feldspar (zoned from An_{53} to An_{40}), magnetite and ilmenite. In samples free of veins, the px is seen to be partly replaced by act, chl ; and the fsp is partly replaced by qtz, ab, K.fsp, wai, stb, analcime. Mt is marginally replaced by hm, and ilm is partly replaced by sp. In a sample including vein of system 4 (here cc-z-clay) the opaque minerals are found to be only partly replaced by hm, sp, while the px is almost completely replaced by chl-brownish clay and the fsp likewise replaced by qtz-cc-clay . Accessory minerals in the altered rock are py, cpy, ap.

A sample containing a narrow vein of cc-chl in intrusive phase 9 was collected close to a thick vein of system 4. The fine-grained rock matrix is almost completely replaced by cc-chl-cp-clay, but some primary fsp is still preserved. Large py grains are dispersed in the secondary mineral assemblage. No wall-rock effect is seen associated

with the narrow vein, while the rock alteration appears to be related to a wall-rock effect from the main vein.

Two samples from a dyke of intrusive phase 12 were collected at study locality 3. One is from the centre of the dyke, and is free of mineral veins, and the other is from the dyke margin and includes vein of system 4. The sample from the dyke centre contains abundant amygdales in a coarse doleritic matrix composed of labradorite zoned to andesine, augite ($Wo_{41}En_{41}Fs_{18}$), slightly oxidized ore (mt, ilm) and altered glass. The original glass is replaced by brown to green smectite (iron-saponite), siderite and pyrite. The vesicles are filled by siderite-cc-sm-py. The formation of siderite is apparently restricted to this dyke phase. The sample from the margin of the dyke shows a finer-grained rock and a vein containing cc-qtz-stb-sm. The wall-rock is entirely replaced by sm-cc ; the smectite composition is close to that of montmorillonite, both in the vein and the wall-rock.

The three examples described above show that the intrusive rock alteration was related to both pervading pore-fluids and vein-fluids. The extent of rock alteration related to each fluid and the extent of overprinting of all the hydrothermal events is variable between the samples and is seemingly related to the former fluid distribution within the rocks. This distribution depended on the permeability (combination of joint- and pore distribution) which evidently changed with time (formation of new joints and mineral-infilling of pores). In addition the intrusive rocks appear to have a distinctive type of alteration associated with them judging from the secondary mineral assemblages which are restricted to some of the intrusive phases (e.g. intrusive phase 5 outside the actinolite zone and phase 12 described above). All this variation makes it difficult to be precise

as to which part of the secondary mineral assemblages observed in the vein-wall rock zones strictly relates to the neighbouring veins. At present, however, it is clear that if wall-rock alteration does accompany the veins, a part of the wall-rock mineral assemblages contains some or all of the mineral types which occur in the veins.

5.2 Vein Systems within the Epidote Zone.

The extent of the epidote zone in the north-western half of the volcano is shown in figures 4.3, 4.4 and 4.5. The epidote zone is divided into upper- and lower sub-zones. The division line is shown in figure 4.4 indicating that the lower sub-zone is stratiform, existing within and below Hyaloclastite Unit I. The lower sub-zone is characterized by the common occurrence of epidote as a part of the rock replacement-, vesicle- and vein mineral assemblages. In the upper sub-zone, however, the occurrence of epidote is more or less confined to mineral veins and vein-wall rock zones, and epidotization of the rocks is only prominent in the vicinity of some major faults and fractures. Thus, fracture-bounded "blocks" of rocks, free of epidote, exist within the upper part of the epidote zone. The distribution of epidote at the outer margin of the epidote zone (zone of undefined width towards the boundary of the chlorite zone) is similar to that in the upper sub-zone, being more or less confined to the vicinity of fractures and faults.

In figures 4.3, 4.4 and 4.5 the location of vein-study localities 4, 5 and 6 are shown. Locality 4 is in Geitafell at high altitude at the boundary between the lower and upper sub-zones and near the outer flank of the epidote zone. Locality 5 is in Efstafellsgil close to the boundary between the lower and the upper sub-zones at low altitude, and locality 6 is furthest to the north-west, at the highest stratigraphic level of all the study localities. Locality 6 is in the vicinity of the inferred caldera fault, close to which there is a local increase in epidote abundance.

While study localities 4 and 5 are from the boundary between the upper and lower sub-zones, vein relations in the lower part were

studied in the field and appear to be similar to those at study locality 3. Further items worth mentioning include (a) early jasper veins in the lower part of the epidote zone, which may be contemporaneous with vein system 1-a at loc. 3, (b) wairakite veins, apparently correlating with system 2 (at loc.3) in the lower part of the zone, and (c) a marked wall-rock effect related to the wairakite veins which was visible in the field. Two samples of wairakite-bearing veins are described below.

A sample (092) from intrusive phase 5 cross-cut by several wairakite veins was collected at some 400 m altitude on Geitafell. The veins in the sample are 0.1-0.3 mm wide, while pale grey wall-rock alteration zones are 1.5-2.5 mm wide at each side of the veins. The doleritic sheet itself is extensively altered; the feldspar is more or less replaced by secondary fsp, qtz, z, the interstitial glass is converted to chl which also partly replaces the px and the ore minerals (mt, ilm) appear somewhat oxidized (hm) and sp marginally replaces the ilm. In the vein wall-rock zone the rock alteration is identical in all respects except that the primary fsp is completely replaced by wai-ab. In thin-section the wall-rock zones are far less distinctive than in hand-specimen.

An interesting sample for comparison (sample 038) was collected in Midfellsgil (the next ravine south-east of Geitafellsgil), much closer to the boundary to the actinolite zone. Wall-rock effect was not noted in the field, but the wairakite-bearing vein (1 mm) includes albite (somewhat hydrated ?) growing perpendicular to the vein-wall, an inner layer of albite growing parallel to the wall with a central infilling of ep-wai-cc. The centre infilling is clearly associated with vein system 3-a at loc. 1 and system 2 at loc. 3.

In section the wall-rock zone is not very distinctive, although the feldspar is replaced by ab-cc-ep. The calcite replacement is clearly related to a vein wall-rock effect.

The data from study locality 3 and the lower part of the epidote zone clearly indicate that the two vein systems at locality 3 (systems 2 and 3) are separable in the epidote zone. The two vein systems are comparable in type to vein system 3-a at locality 1. Vein system 3-a, however, was not successively sub-divided by direct cross-cutting evidence, while several generations of mineralizing vein fluids are believed to have produced the system. The assemblage ep-pr-wai-gt-cc does exist in veins of system 3-a in the actinolite zone, while part of the assemblage, namely ep-wai, is a part of system 2 in the epidote zone and the prehnite is a part of the assemblages of system 3. The difference between the vein systems at different altitudes may thus be real, and could possibly give some information to the evolution of the fluid system as a function of (a) depth and (b) time. While such possible implications are discussed later in this chapter, the nature and chronology of veins at still higher levels within the volcano are discussed in the ensuing section.

(i) Vein-study locality 4 in Geitafell.

A summary of vein relationships from above 500 m altitude up to ca. 800 m altitude in Geitafell is shown at locality 4 in figure 4.3 and 4.5. The main difference from the relationships at lower levels within the epidote zone is that vein systems 2 and 3 which were separable at loc. 3 are indistinguishable at loc. 4.

1) Jasper veins compose vein system 1 at locality 4. The vein

thicknesses are usually close to 1 cm. The jasper veins post-date intrusive phase 1 but pre-date intrusive phase 5.

Two samples of intrusive phase 1 were collected at high altitude on Geitafell (sample 101 from 800 m and sample 108 from 650 m). Both include veins of (1) jasper of system 1 above, (2a) ep-pr-qtz, and (2b) qtz-cc of system 2 below. The jasper is cross-cut by (2 a,b) while the age relation between (2a) and (2b) is deduced from the vein texture, where (2b) appears to be younger. Direct cross-cutting evidence, however, is lacking and (2a) and (2b) are thus regarded as representing two vein fluid generations within vein system 2 below. The multiple veins are cross-cut by (3) calcite-bearing veins (cc--aragonite-qtz-sm-z). Wall-rock alteration is associated with the multiple veins and appears to be related to (2) above. In the fine--grained wall-rock, epidote replacement of the feldspar and the glass is more intense than elsewhere in the rock.

2) Ep, pr, chl, cc veins. Several generations of vein fluids appear to have generated this vein system. Epidote is common to the mineral assemblages in the earlier generation(s) of veins, which are younger than intrusive phase 5, but older than intrusive phase 10 in this area. Intrusive phase 10 is cross-cut by the later generation(s) of veins of this system (i.e. pr-chl and chl veins).

Due to weathering of the hyaloclastites and the lack of adequate exposures the vein relations in this area were not discerned. The overall vein pattern could, however, still be studied in the various rock types in the field, and several "key-specimens" were collected from intrusive rocks showing cross-cutting veins. Sample 061, from intrusive phase 6, was collected at some 600 m altitude in Geitafell and contains two prehnite-bearing veins. The earlier vein pr-ep-chl-

-wai-su is 0.5 mm wide and appears to be cross-cut by the later prehnite vein (pr-dark clay -chl-su)which is of similar thickness. These veins are rather irregular and the cross-cutting relation is poorly developed. Therefore, it is preferred to regard the two veins as belonging to the same system and apply the term vein-fluid generations to explain the apparent age relation. Vein wall-rock alteration is not obvious in either case, while the rock itself is quite altered. The densely feldspar-phyric dolerite has a matrix composed of fsp-px-ore-altered glass. It is quite vesicular with amygdales of chl-pr-cc or chl-cc. The interstitial glass is chiefly replaced by chl but to some extent by ep. The fsp is extensively albitized and sphene marginally replaces the ore, while the px appears unaltered. The adjacent host rock contains the same secondary mineral assemblage as does the intrusive rock.

A common feature of the inclined sheets of phases 5 and 6 at high altitude levels in Geitafell (i.e. in the hyaloclastite and above) is their irregular strike/dip relationship. The sheets commonly approach the vertical with increasing height. Typically also, the high-level sheets are quite vesicular, and commonly they are auto-brecciated within the hyaloclastite. When compared to the sheets at lower levels it is clear that vesiculation increased as the palaeosurface was approached. Another typical feature of the high-level sheets in Geitafell, particularly of phase 5, is that they are extensively actinolitized, with the pyroxene more or less replaced by amphibole. This local actinolite occurrence within the sheets seems to indicate that early interaction took place between hot intrusives (at sub-solidus temperatures) and a colder host-rock fluid. A sample (100) showing this feature was collected from the upper- and outer margin of the epidote zone between 700-800 m altitude, and includes

5 sub-parallel veins. The doleritic rock is extensively altered where the augite is more or less replaced by actinolite and to a smaller extent by chlorite. The fsp is partly replaced by ab, K.fsp, ep, pr, cc, z, and both chl and ep are found in micro-cracks within the feldspar grains. The ore minerals are partly replaced by hm, sp, su. The numerous vesicles are filled by chl, ep. While it seems possible that a primary amphibole was formed in the matrix, the overall replacement texture of actinolite after pyroxene is taken to indicate that the amphibole is dominantly of hydrothermal origin. Most of the alteration appears unrelated to, and older than, the mineral veins in the sample. Two of the five sub-parallel veins seen in thin-section are filled by prehnite, one by zeolites and the remaining two are open micro-joints partly infilled by calcite. Their apparent time relationship is: (a) The prehnite veins may belong to system 2. The vein mineral assemblage is pr-ep-chl. These veins are 0.1 mm wide and a wall-rock alteration is not prominent. Some of the wall-rock feldspars, however, are partly replaced by prehnite. (b) The zeolite vein may belong to system 3 below. The vein is 1-2 mm wide and chiefly consists of heulandite. One to two mm wide wall-rock zones are attached to each wall. in which the feldspar is extensively replaced by some low birefringent zeolite (not identified - possibly chabazite or analcime). Within the heulandite vein an open micro--joint is seen, its walls partly being coated by calcite. The two open micro-joints elsewhere in the sample are similarly partly infilled by calcite. The apparently later formation of calcite suggests that fluid generations also constructed vein system 3 below.

As said earlier, vein system 2 is younger than intrusive phase 5, while only the later generation(s) of system 2 cross-cuts through in-

trusive phase 10 in this area. Green narrow chlorite veins (which sometimes include prehnite) cross-cutting phase 10 constitute the later generation of system 2. Of similar age may be the pr-clay-chl--su vein in sample 061, mentioned earlier. Intrusive phase 12, however, is only cross-cut by vein system 3 below.

3) cc, qtz, heu, stb, mo, sm veins. These veins are commonly thicker (1-10 mm) than veins of earlier vein systems. As shown by some of the examples above, several generations of mineralizing vein--fluids may have constructed system 3. Wall-rock alteration is found attached to sampled veins of this system. It is chiefly the wall-rock feldspar which is replaced by some of the minerals which compose the vein mineral assemblage. Smectite, replacing glass, is also found in these wall-rock alteration zones.

(ii) Vein-study localities 5 and 6.

The position of localities 5 and 6 is shown in figures 4.3 and 4.4. Two mineral zones coincide in this area as indicated in the figures. This two-fold zonation calls for some field descriptions which may clarify the situation.

The upper part of the epidote zone extends from Efstafellsgil (study loc. 5) some 2 km to the northwest to the Gjanupsvatn (ice-marginal lake) area (loc. 6). The epidote occurrence in this zone is more or less restricted to veins and vein-wall rock zones, and wairakite appears to be absent from the rock replacement-, vesicle- and vein mineral assemblages. The stratigraphic relationships in the area are not too clear, partly due to the widespread occurrence of hyaloclastites. Local constructional unconformities, for instance, are found at some of the hyaloclastite contacts with the lavas, which

in addition to poor exposures due to frost shattering, or coverage by moraine and vegetation, make mapping difficult. The more resistant intrusive rocks are abundant in this area, and constitute from 25% to 80% of the exposed rocks (chapter 3). Commonly the intrusive rocks in the area are quite vesicular, and often the dykes and sheets are seen to have auto-brecciated in the hyaloclastite. Unless the exposures are adequate, this makes a clear distinction between the host rocks and the intrusive rocks difficult. The field relations are further complicated, (a) the caldera subsidence and (b) flexuring of the rock pile, which resulted in two sets of major faults and fractures (map I) additional to the faults and fractures parallel to the inclined sheets (3 phases) and the dykes (7 phases).

Overprinted in this are complex alteration patterns. Apparently, several generations of calcite, quartz, prehnite and sulphide deposits have occurred, and - in general - widespread occurrence of calcite and sulphides characterizes the hydrothermal alteration in the area. The sulphides, which chiefly comprise pyrite ($\pm$ cpy) are commonly found in wall-rock alteration zones along major faults and in vein wall-rock zones parallel to the margins of some of the dykes of phase 12. The sulphide-bearing rocks are also found in near-circular outcrops (1-6 m^2) which do not show relation to any particular structural feature. The rocks which are extensively replaced by sulphides are easily distinguishable in the field due to rusty-brown weathering surface of the pyrite (which alters to limonite or goethite), an example of which is shown in figure 5.6 . The near-circular sulphide-bearing outcrops may represent conduits to former hot-springs at the palaeosurface, while evidently all the vein suites may have taken part in feeding such hot-springs. The mineralogy of one of the circular sulphide outcrops is described later. As noted above, extensive

Figure 5.6 . Rusty sulphide zones along faults which possibly formed during the flexural event. The Svinafell area is at the far side of the glacier and Vidbordfjall is in the background.

Figure 5.7. Quartz-calcite-prehnite vein zone related to vein system 4 from near Gjanupsvatn. The veins may have formed in connection to the caldera event.

Figure 5.8 . Platy quartz and calcite associated with vein system 4 from near Gjanupsvatn - possibly related to the caldera event.

carbonation characterizes the upper part of the epidote zone. Thick calcite veins (0.5-1.5 m) are sometimes found and vein-zones (closely spaced veins) are common, in particular close to the inferred caldera fault near vein-study locality 6, examples of which are shown in figures 5.7 and 5.8.

Evaluation of the vein relations in this area is difficult. The localized occurrence of some of the veins (e.g. in brecciated zones, fig. 5.7), the great variation in vein thicknesses, the irregular and disconnected habit of veins to the hyaloclastite (e.g. fig. 3.9), and the tendency for sulphides to occur in altered wall-rocks along some faults and fractures but not as discrete or massive veins, all tend to obscure the field relations. The situation was dealt with by noting the apparent relationships in the field and collecting representative samples. The overall conclusion was that several episodes of calcite, quartz and sulphide deposition took place.

Vein-study locality 5. Apart from vein systems 1 and 6 below, the following veins were observed and sampled from intrusive phase 3 in Efstafellsgil.

1) Jasper veins which appear to be the earliest veins in the area and are only found in the host rocks. The jasper (amorphous silica containing ferric iron) is altered to qtz-hm-ep-(-chl-cc-py).

2) Felsite veins (igneous). These veins are confined to a dyke of intrusive phase 3 in this area - the dyke being closely related in time to the Geitafell gabbro event (phase 2). The felsite veins are ca. 2 mm wide and strike northwards (sample 7941 A). No wall-rock effect associated with the vein was found in the host of feldspar- and pyroxene-phyric dolerite (or fine-grained gabbro). The dolerite, however, shows hydrothermal alteration in which the px is partly replaced by act, chl, ep; the fsp by ab, K.fsp, pr, cc, ep,

and the ore by sp, TiO_2, su.

3) Ep, qtz, chl, cc veins, ca. 1 mm wide and strike N-S. Wall-rock effects are not visible in the sample (7944).

4) Pr, qtz, cc veins, including ep, chl in subordinate amount. These veins are 1-2 mm wide and show polygonal strike relations. Inside poorly-defined wall-rock alteration zones, the fsp is more extensively replaced by pr, cc than elsewhere in the sample (7941 A and B).

5) Calcite and dark clay veins. The clay type is un-identified. In the samples already referred to these veins are narrow (0.1 mm) and show an eastward strike. No wall-rock effect is visible in the sample.

6) Qtz-stb-heu veins. These veins parallel intrusive phase 12 which cross-cuts phase 3 at the study site. Intrusive phase 12 is not cut by the earlier veins.

In the surrounding area ep-bearing veins (system 2) cross-cut intrusive phases 3, 5 and 7. Judging from the ep-act replacement inside intrusive phase 3 which appears unrelated to the ep-veins, and the strike of the veins (N-S) parallel to the felsite veins, it seems likely that epidote formed in veins just after the intrusive event (phase 3) and continued to be formed until intrusive phases 5 and 7 had been emplaced. Vein system 6 evidently post-dates intrusive phase 12.

The time of formation of the near-circular outcrops of sulphidized rocks relative to the vein systems is not clear, but they may date back to vein system 3. Samples (024 and 025) from one such outcrop, show a relict igneous texture completely replaced by secondary minerals. The secondary assemblage (analysed) includes ep-chl-py-

-cpy-cc-qtz-ab-sp-TiO_2-clay. Pyrite is the chief sulphide (± cpy). The ep-bearing assemblage may be time-related to vein system 3.

At another locality in Efstafellsgil, a sulphidized alteration zone transecting a dyke-like apophysis of the Geitafell gabbro (phase 2) is cut by lau-cc vein. Nowhere in the volcano have lau-veins been found to cross-cut intrusive phase 12 suggesting that some of the sulphidization pre-dated the intrusive phase 12. Rusty sulphide zones, however, are also found at the margins of some of the phase 12 dykes in the upper part of the epidote zone, and py-heu-cha veins cross-cut phase 12 dykes. The sulphides may thus have formed continuously (intermittently ?) in the rocks of this area throughout the intrusive history of the volcano.

Vein-study locality 6 is situated near Gjanupsvatn. Part of the exposures studied is shown in figures 3.16, 5.7 and 5.8. The depth from the palaeosurface to this locality is estimated to have been in the range 200-400 m. The host rock is hyaloclastite (Unit II).

1) Jasper veins, up to 5 cm thick are the earliest veins found. These veins are clearly faulted and cross-cut by system 5 below.

2) Pyrite "veins". These are narrow zones consisting of extensively pyritized rock in an assemblage with quartz and some chlorite. The pyritized zones are clearly cross-cut by system 4 below (sample 7971).

3) Ep-pr-chl veins, including, in subordinate amount, py, cc, qtz. Variable strike relationships are observed (polygonal system). These veins are younger than intrusive phase 10, which is extensively altered in this area (see figures 3.12 and 3.16). The fsp in phase

10 dykes is extensively replaced by ep-pr, the ep-replacement being somewhat anomalous (see discussion below).

4) Pr-qtz-cc-clay veins. The clay type is unidentified. This system has polygonal strike-relations, but prominent wide vein zones strike NE (e.g. figure 5.7). Veins of this system, observed in vertical exposures, contain quartz with a platy habit ("desert roses", figure 5.8) with calcite and prehnite. In one sample (7971) the vein (2 cm) cross-cuts system 2 above, and is chiefly composed of pr-qtz. A 2 mm wide wall-rock alteration zone is seen in the thin section. The wall-rock is completely replaced by pr-cc-chl-py. Beyond the wall-rock zone the rock is also completely replaced by secondary minerals, now by pr-qtz-chl-py-TiO_2.

5) Calcite veins, striking between NE and E. The vein thicknesses vary from few mm up to 1.5 m. The vein system appears to be somewhat younger than system 4 above, but may partly pre-date intrusive phase 12, while thin calcite veins are found within the dykes of phase 12.

A progressive change in the vein assemblages from system 3 to 4 and 5 is evident, with abundance of calcite increasing with time (both relatively and volumetrically). These vein systems may all be associated to the caldera collapse - as is the case for intrusive phase 10 (chapter 3). The replacement of the fsp by ep in the intrusive phase 10 dykes is unusual in the NE-half of the volcano. At lower stratigraphic levels (e.g. phase 10 dykes cross-cutting the Geitafell gabbro and the dykes in Geitafell (loc. 4) the characteristic rock replacement assemblage is chl-pr, while ep is absent from both the rock replacement - and vein assemblages. The local abundance of epidote within and near intrusive phase 10 at study locality

6 may relate to an early interaction between hot intrusives (phase 10) and fluids in the host rocks. Such early interactions have been discussed above, while the evidence concerning their former existence is circumstantial and deduced from the apparently higher-grade mineral assemblages within the intrusive rocks - and in this case also in the adjacent host rock area.

The wide veins and the brecciated vein zones of systems 4 and 5 appear to occupy caldera-related faults. Some of these faults show prominent curvature (see map I) and dip some 60-70° towards the southeast, and are truncated by the later flexural event. The implication from the prominent alteration effects observed along the length of the caldera fault from Kraksgil in the southeast to the Gjanupsvatn area in the north is summarized and discussed in chapter 8.3.

The mineral deposits in veins believed to post-date the caldera event in the upper part of the volcano include sulphides formed at NE-SW striking faults related to the flexural event, and along some members of intrusive phase 12, and zeolites (heu, stb, sco, tho, cha, analcime) in veins and amygdales. The zeolites are either found in monomineralic deposits or in some polymineralic assemblages ($\pm$ qtz, cc, py). The zeolite formation is thus clearly superimposed upon the higher-grade hydrothermal alteration of the volcano.

In the field, wall-rock alteration zones are clearly seen alongside some of the late zeolite veins. An example of a zeolite-bearing vein cross-cutting brown hyaloclastite at some 400-500 m altitude in Efstafell was found within the upper part of the epidote zone near its outer margin to the east. The pale-brown hyaloclastite consists of glassy and partly glassy basalt fragments. The glass is partly replaced by brown smectite while feldspar microliths in the hyalocrys-

talline fragments are unaltered. Pale-green wall-rock zones (few cm wide) accompany 2 cm wide heu-cc vein. The altered glass in the wall-rock zones consists of sm-heu-cc assemblage. A noteworthy observation concerns intrusive sheet of phase 5 found nearby. The vesicular doleritic sheet appears more altered than the hyaloclastite host. The dolerite is partly replaced by chl (after px) lau, ab, K.fsp (after fsp) and sp (after ilm), while the adjacent brown hyaloclastite is partly replaced by smectite (after glass). The higher-grade secondary mineral assemblage in the intrusive sheet may relate to an early interaction between hot intrusive rock and colder host-rock fluid.

5.3 MINERAL VEINS - SUMMARY.

The mineral veins have been grouped into several vein systems each of which comprises a group of veins within areas which apparently were formed contemporaneously. Cryptic variation in vein mineral assemblages between veins of the same vein systems is found to exist. This feature, together with the texture of some of the multiple veins studied, indicating that the vein minerals were deposited during several episodes, is taken to indicate that several generations of mineralizing fluids were involved in the genesis of many of the vein systems.

The overall time relationship of the veins to the volcanological evolution was established from cross-cutting relationships between vein systems and the intrusive phases. A simplified summary of these relationships at various levels within the volcano is shown below, while a more detailed evaluation is made in the summary of chapter 8.

Locality	Mineral Zone	Vein Systems:
6	ep-upper	1 2 3 4 5
5	ep-u/1	1 2 3 4 5 6
4	ep-u/1/o	1 2 3
3	ep-act	1a,b 1a 2 3 4
2	act-u	2 3 5 6a,6b 6c, 7
1	act-l	1a,b,2a 2b 3a,and 3b 4a,b
	INTRUSIVE PHASES :	2,3,4,5,6,7, 8,9,10,11,12

Explanation: The first column stands for the vein-study localities, the second for the position within the mineral zones (epidote (ep)- and actinolite (act) zones , and u: upper, l: lower, o: outer).

The later generations of vein systems 5 (loc. 6), 3 (loc. 4), 4 (loc. 3) and 4 (loc. 1) post-date intrusive phase 12, while the construction of the vein systems appear to have initiated at some point in time in relation to the intrusive phases as indicated. Prior to the gabbro intrusion in Geitafell (phase 2), limonite and "mud" were deposited in fractures. As time passed the geothermal gradient rose and turbid silica (jasper) and then quartz form the mineral veins. In direct continuation of the gabbro intrusion a sharp change in vein mineral deposition occurred which varied with depth. At the deepest stratigraphic level (loc. 1) the characteristic vein mineral assemblage is ep-gt-act-(+others), at intermediate level ep-chl-wai-pr-(+others), and at the uppermost level chl-qtz-pr-(+others). Local thermal effects are detected in relation to some of the intrusive rocks (e.g. the contact metamorphosed hornfels at the gabbro contact (see later) and by the local anomalies in the index-mineral zonal patterns). A high-temperature hydrothermal system was established in continuation of the gabbro intrusion and lasted until intrusive phase 10 was accomplished. The hydrothermal system evolved with time and calcite-bearing veins characterize the later vein systems at all levels. The last veins are always zeolite-bearing, postdating the youngest intrusive phase at all depths. The youngest intrusive phase bears a typical low-temperature secondary mineral assemblage (smectite and zeolites) indicating that the thermal gradient had subsided prior to its intrusion and a low-temperature hydrothermal system was already established.

Wall-rock alteration zones are found alongside all vein systems except the first. In the wall-rock zones the primary minerals or glasses are altered to some of the minerals found in the veins and

usually to some minerals foreign to vein assemblages. The most common of such foreign minerals are chlorite replacing glass and pyroxene (and the rare olivine), albite and K.feldspar replacing the primary feldspar. Chlorite is also a common vein mineral while albite and K.feldspar are rarely found as a part of the vein assemblages. All three, however (and particularly chlorite) are found in amygdales.

To avoid too many repetitions,the details of the high-temperature hydrothermal system are postponed to the summary section of chapter 8.

CHAPTER 6

VESICLE MINERAL INFILLING SEQUENCES

In chapter 4.3.3. general observations were made on the mineral infillings of vesicles. These were that:

(i) A correlation exists between an infilling sequence and vesicle size.

(ii) A correlation exists at any locality between minerals in vein systems and those in vesicles.

(iii) Reactions of early infilling material with later fluids were common.

The amygdales reflect the porosity-controlled fluid and its spatial variation at any time. Relevant data can be obtained by studies of (i) and (iii) above. The interrelation of the porosity- and the fracture-controlled fluids can be investigated through (ii) above.

The vesicle mineral infilling sequences are briefly described below along traverses I and II (see fig. 4.3). For clarity the simpler sequences are presented first (section 6.1), taken in up-grade order from the chlorite zone, through the epidote- and the andradite zones into the actinolite zone. This gives way to descriptions of more complex situations (section 6.2), and finally the overall infilling sequences from all the mineral zones are summarized (section 6.3).

6.1 Simple Sequences.

The vesicles under discussion range from mesopores (< 1 mm diameter) to macropores (1-100 mm diameter). The correlation between vesicle size and infilling sequence is broadly generalized, as the infilling materials are unevenly distributed throughout the rocks. This is particularly true for the earliest infilling material, which is horizontally layered "mud" and layered limonite growing randomly into some vesicles in a botryoidal habit.

The layered "mud" is extremely fine-grained sediment on vesicle floors, chiefly composed of SiO_2 (see discussion of the clay-like vein system 1-b (loc.1), and chemical analysis of the "clay" vein system 1-a (loc. 3)). The mud layers were deposited horizontally on vesicle floors and subsequently tilted in accordance with tectonic disturbances. Since there is no indication of depositional tilt between the layers, the muds were formed before tilting of the lava pile.

The limonite ($Fe_2O_3(OH)_x$) is an isotropic mineraloid which grows in a botryoidal habit into amygdales. Commonly the limonite botryoids are found at the vesicle roof or walls rather than on the floors.

The layered mud and the limonite are only present in some vesicles, but show a regional distribution as they are found both within and outside the propylitic core of the volcano. From their regional distribution the mud and limonite are considered to be unrelated to the hydrothermal system and were probably formed from suspended particles and dissolved ferric iron respectively in percolating (cold) ground waters. Their formation within the propylitic core of the volcano may well extend from the time of the host lava (and hyaloclastite) eruption until the hydrothermal system became established (possibly 7-8 x 10^5 years).

The uneven distribution of the layered muds and limonite within the amygdales is exemplified in figures 6.1, 6.2 and 6.4. It is not known which of these two materials was first to become deposited. The opaque ore dispersed throughout the mud in fig. 6.2 may indicate contemporaneous formation while the opaque layer at the floor of the amygdale in fig. 6.4 may suggest the limonite was earlier. The intrinsic time-relationship between the two, however, is not regarded as of importance to the evolution of the hydrothermal system. In the

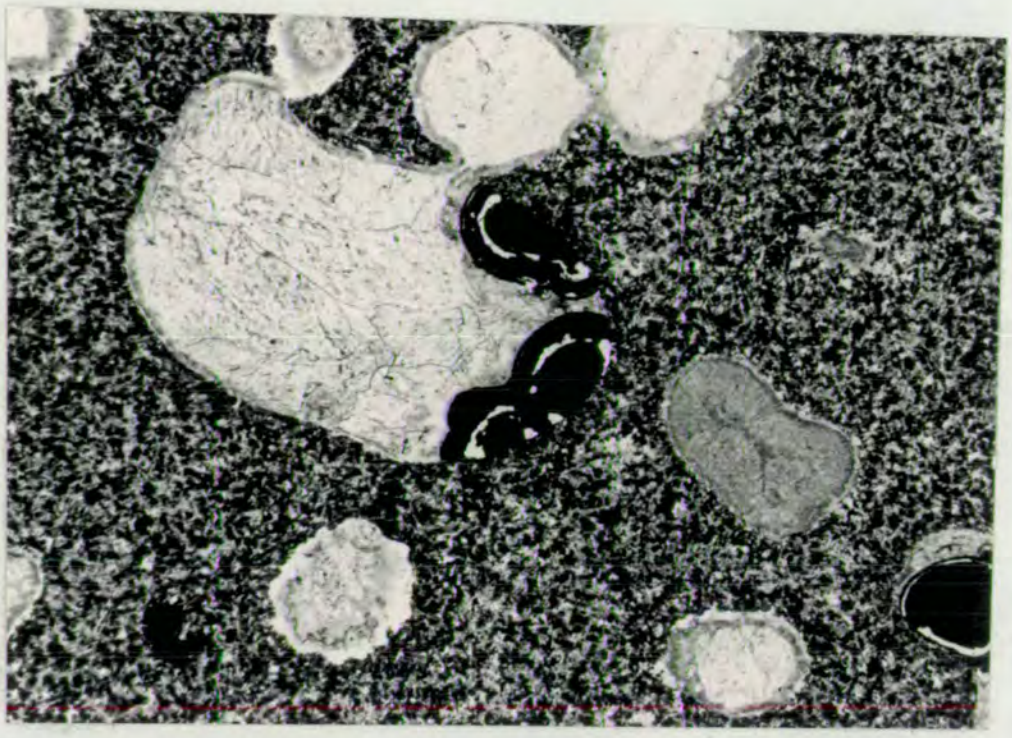

Figure 6.1. Midfell, 750 m, sample 074 A, from the chlorite zone. The largest vesicle is ca. 4 mm long. The limonite botryoids (black) are layered (white concentric bands inside the limonite are voids). Chlorite (grey in photo) forms a layer at or near the walls of most of the vesicles and fills one of them. The centres of the other vesicles are either filled by calcite or void space.

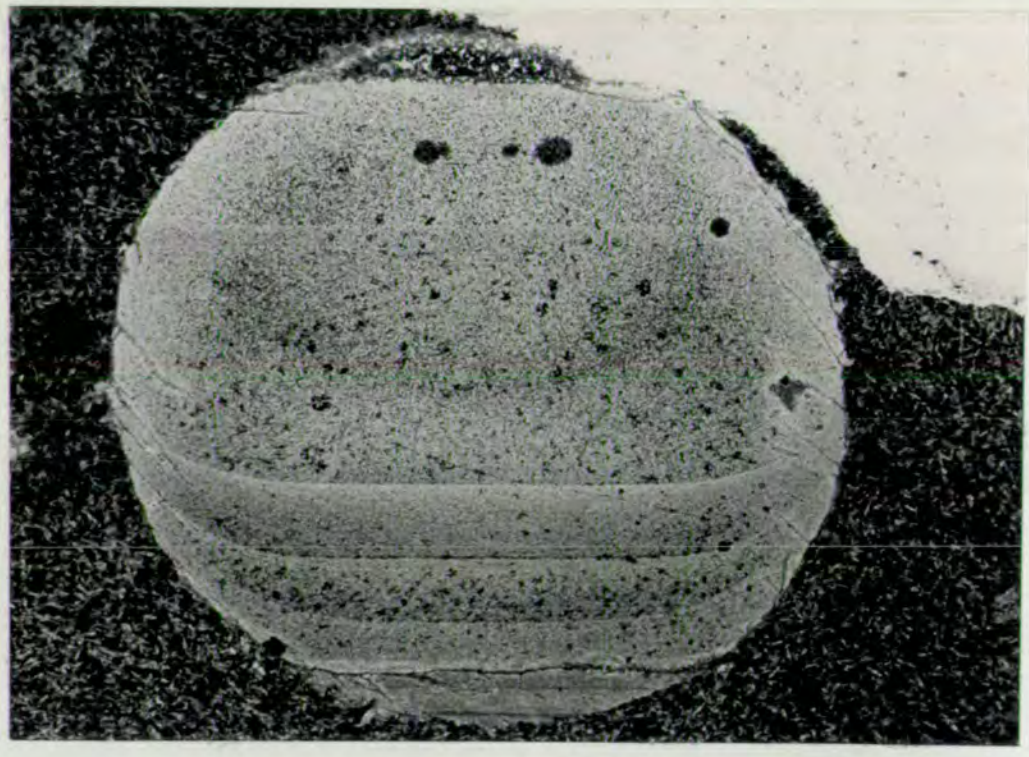

Figure 6.2. Tungufell, sample 085, from the andradite-zone. The vesicle diameter is ca. 4 mm. Layered sediment ("mud" deposit) may completely fill some vesicles.

following discussion, the mud and the limonite will thus be regarded as contemporaneous.

Traverse I is shown in fig. 4.3. This extends from Midfell outside the caldera in the chlorite zone, across the fault and the epidote zone into the andradite- and actinolite zones in Tungufell. Figs. 6.1 - 6.12 show representative vesicle infillings along this traverse. The variation of amygdales within a sample is exemplified in figs. 6.2, 6.5 and 6.6 which are all from the same sample. Basically, however, these figures (6.1 - 6.12) show the mineralogical changes in vesicle infillings in an up-grade order from the chlorite- to the actinolite zone. Since the layered mud and limonite are randomly distributed within the rocks, two sets of examples are shown for completeness, one including the layered mud (fig. 6.3 - 6.7) and the other including limonite (fig. 6.1, 6.8 - 6.12).

Figs. 6.3 and 6.4 show amygdales in lavas at the boundary between the chlorite- and the epidote zone. The figures show three amygdales from the same thin-section exemplifying the correlation of vesicle sizes with mineral infillings (along (i) above) and the correlation of vein- and vesicle mineral infillings (along (ii) above). The infilling sequence essentially involved 5 or 6 principal infilling episodes in the order (1) layered mud was deposited on the vesicle floor, (2) deposition of quartz around the vesicle walls, (3) a brown "chlorite" (or smectite) layer, (4) green chlorite and (5) a centre infilling of calcite (fig. 6.3). The amygdale on the left in fig. 6.4 is smaller (ca. 1x2 mm) than the amygdale in fig. 6.3 (ca. 3x4 mm) and is almost filled by (1) mud layers. At the very top a quartz layer (2) followed by (3) a brown phyllosilicate layer fill the remaining void of the vesicle. This correlation of vesicle size with mineral infillings is found everywhere within the volcano; the larger

the vesicles the more numerous are the infilling layers. The mineralogy/size correlation, however, is only broadly true as some vesicles have been bypassed by the early infillings. This is well seen in fig. 6.4 , where the small (< 1x1 mm) amygdale to the right is not filled by mud but shows mineral layers of (2), (3) and (4) above. In addition, subsequent to slight faulting, instead of the centre being filled by (5) calcite as in fig. 6.3 , (6) quartz-epidote is found in the small amygdale in fig. 6.4 . An interesting feature is that the fault plane itself is occupied by quartz and epidote, and thus there is continuity between the vein minerals and the infilling of the vesicle centre. This type of evidence is commonly encountered while the sample in fig. 6.4 demonstrates that the infilling layers are of different age, since the formation of layers (2), (3) and (4) prior to the faulting is evident.

A similar feature is seen in fig. 6.5 which shows a sample in the andradite zone. The vesicle suffered slight faulting subsequent to infilling episode (4)(the chl layer). The faulting and/or an apparent incipient alteration of the phyllosilicate layers caused the chlorite at the vesicle roof to subside into the vesicle, giving rise to the complex texture in the amygdale centre. Similar complex infillings are commonly observed in the more porous rocks (e.g. scoria), in which the minerals may form assemblages related to several infilling episodes. A common assemblage from the actinolite zone is ep-cc-gt-qtz-stb, where the gt, ep are embedded in qtz-cc-stb assemblage. The existence of such a mineral assemblage, can now be partly explained by the interactions of earthquakes, gravity, fluid movements and mineral-fluid reactions which may cause replacement/displacement of earlier formed infilling minerals. A general observation suggests that the evidence for infilling sequences is best preserved in the

Figure 6.5 . Tungufell, 450 m, sample 085 (the same as in fig. 6.2 and fig. 6.6), from the andradite-zone. The apparent infilling sequence is :

(1) layered sediment at the floor, followed by
(2) and early generation of quartz which lines the vesicle wall, followed by
(3) brown "chlorite" (altered), and then
(4) green chlorite and finally a centre infilling of
(5) epidote-andradite-quartz-calcite (and chlorite).

The vesicle was slightly faulted subsequent to infilling (4), and the chlorite band at the vesicle roof seems to have collapsed into the vesicle. Here, gravity is partly responsible for the texture of the central infillings, while an earthquake (related to the fault) and/or an incipient reaction between the brown "chlorite" and the later andradite-yielding fluid may have caused the chlorite-roof to subside into the vesicle (see figure 6.6 from the same sample for comparison).

lava vesicles, where the meso- and macropores are not interconnected. For clarity the examples described are thus more or less restricted to the lava vesicles.

Figs. 6.3 and 6.4 show the infilling sequences common near the boundary of the chlorite- and the epidote zone. Within the epidote zone and the higher grade zones, the brown phyllosilicate layer, however, is not found. The amygdale in fig. 6.6 from the andratite zone shows essentially the same texture as that in fig. 6.3 , with mud at the base followed by a quartz layer and an apparently altered phyllosilicate layer with calcite occupying the middle. Instead of the brown phyllosilicate layer, an irregular dark outer layer of andradite garnet occurs and on the inside of the green chlorite layer, a layer of andradite is also seen. The brown phyllosilicate layer may thus have been replaced by andradite, and possibly the green layer shows incipient alteration. The garnets on the inside of the chlorite contain inclusions of calcite, which then may indicate that the central calcite had been deposited prior to the garnet, or that the two were formed contemporaneously. The overall implication from the study is that the calcite centre was related to an earlier depositional episode than the garnet.

Two other important features can be viewed in fig. 6.6 . Looking at the adjacent amygdales in fig. 6.6 no garnets are found to exist within them. This is not an uncommon observation, particularly close to the boundaries of the mineral zones, but may relate to uneven distribution of the mineralizing fluids. The presence of garnet in the centre amygdale in fig. 6.6 , might,for instance, relate to a mineral vein outside the field of view. The third dimension of course needs to be considered when viewing the distribution in a two dimen-

Figure 6.6 . The apparent infilling sequence is (first to last):

(1) Layered sediment on the vesicle floor,

(2) a turbid quartz layer

(3) a dark layer of andradite garnet (possibly replacing a brown "chlorite"),

(4) altered chlorite layer (note the colour change from green to brown and compare to the typical green chlorite in the adjacent vesicles),

(5) subhedral light brown andradite sitting on the inside wall of the altered chlorite layer. Calcite inclusions are seen in the garnet.

(6) Centre-infilling of calcite.

The andradite garnets of (3) and (5) may have been the last to be formed in the vesicle (see text for discussion).

Figure 6.7 . Moving up-grade into the actinolite zone some of the amygdales show textures similar to those in fig. 6.6 . Layered sediment was deposited on the vesicle floor, and the centre--infilling is calcite with an outer layer of brown andradite. Instead of the chlorite layer a layer of green fibrous actinolite surrounds the garnet layer in an assemblage of act-gt-ep-qtz-cc, and instead of the turbid quartz layer in fig. 6.6 the outer fringe of the amygdale shows an assemblage of qtz-ep-cc (see text for discussion).

Figure 6.6. Tungufell, 450 m, sample 085 (the same as in fig. 6.2 and fig. 6.5). The vesicle in the centre of the photo is 2.5 mm long. See text on opposite page for explanation.

Figure 6.7. Tungufell, 400 m, sample 080 from inside the actinolite-zone. The vesicle is 4 mm long. See text on opposite page for explanation.

sional field. The other important feature seen in fig. 6.6 concerns the interconnection of the macropores. The vesicles in the centre and on the left were apparently disconnected after infilling episode (2)(the quartz layer). An alternative explanation of the different infilling of the centre amygdale might postulate that the centre vesicle was connected to a still larger vesicle outside the field of view, and that the difference related to variable fluid distribution.

Fig. 6.7 shows a typical amygdale from the actinolite zone. The amygdale texture is quite similar to that in figures 6.3 and 6.6 , with mud deposit at the base, a calcite core and an outer layer of andradite (similar to figure 6.6). However, instead of outer layers of phyllosilicates ((4) and (3)) and quartz (2), a layer of act-ep-qtz-cc is found. The act is more abundant near the centre where the chl layer is sited in the other examples (figures 6.3 and 6.6). It thus appears that early phyllosilicate layers might have been replaced by gt, act. The apparent transition from chl to act is commonly found near the border of the actinolite zone where both are still present, while the example in figure 6.7 shows a situation where no chl is left.

The layered mud deposit is principally composed of quartz (see earlier discussions), which may either have segregated from a silica rich sediment upon alteration, or been impregnated into poorly consolidated sediment in relation to infilling episode (2) above. Well within the actinolite zone (in Kraksgil), however, other minerals completely replace the mud, preserving only a relict texture of the sediment. Garnet, epidote and prehnite have been found in such situations.

The other infilling sequence followed in an up-grade order along traverse I, includes the early limonite in amygdales. Fig. 6.1 shows typical limonite inside the chlorite zone, with concentric shells of limonite with void space between. Such concentric shells are commonly observed and suggest that the limonite was deposited during more than one episode. While void 'shells' are common within, and beyond the chlorite zone, the concentric shells are always filled by some minerals in the epidote - and higher grade zones.

It has already been mentioned that the formation of limonite and mud may have extended from the time of the extrusive rock emplacement until the hydrothermal system became active. Therefore, it might be expected to find larger limonite botryoids and possibly more numerous concentric layers in limonites at deep stratigraphic levels as compared to shallower levels. In fact, this may be so, as large botryoids, with radii up to 2 mm are commonly found at low levels (e.g. in Kraksgil, fig. 6.11 and 6.12, and Midfellsgil, fig. 6.15 and 6.16), in contrast to the much smaller botryoids at higher stratigraphic levels, with radii much less than 1 mm (fig. 6.1, 6.8 - 6.10). However, alteration may have had some tendency to increase the apparent radii of the (now partly or completely pseudomorphed) botryoids inside the andradite and actinolite zones.

Fig. 6.8 shows the time-relationships of the infilling materials, where the limonite was the first and subsequently cross-cut by a microscopic dilational fault, revealing slight shear movement (possibly an evidence for dilatancy (see chapter 4.2 d), occupied first by chlorite and then calcite. Moving towards the chlorite-epidote zone boundary (fig. 6.9) the concentric layers are infilled by quartz and calcite but not by the phyllosilicate. Moving further

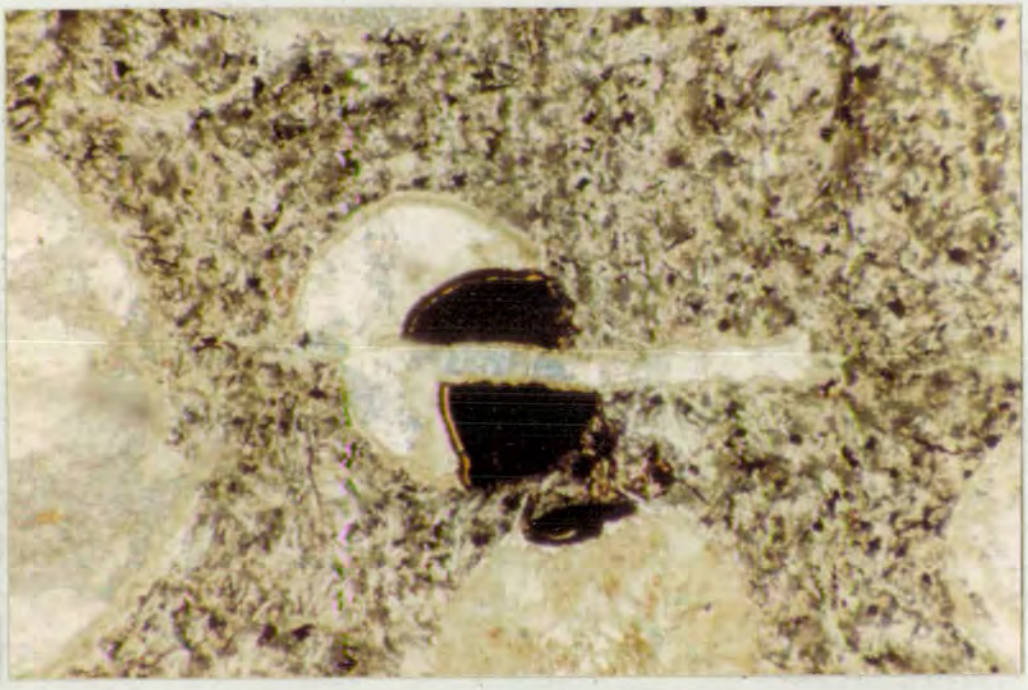

Figure 6.8 . Midfell, 750m, sample 074 A, from the chlorite--zone outside the caldera fault. The vesicle diameter is ca. 0.5 mm. The limonite (1) botryoid has been slightly faulted and minor extension has occurred perpendicular to the fault. Subsequently (2) a chlorite layer was deposited at the vesicle- and the fault walls, followed by (3) central infilling by calcite.

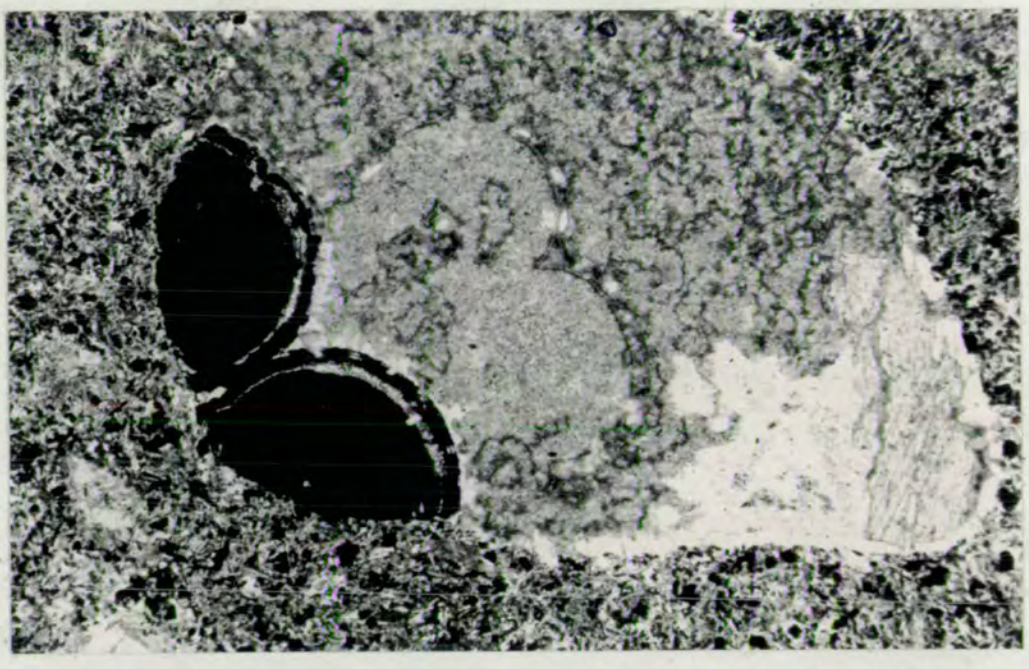

Figure 6.9. Midfell, 650 m, sample 076 A, from outside the caldera fault at the boundary between the epidote- and the chlorite-zone. The limonite appears slightly altered while the formerly void concentric layers are mainly occupied by calcite and quartz in the limonite. Chlorite (upper part, grey) and calcite (lower part, right) fill the vesicle which has 1.7 mm diameter. (See text for discussion).

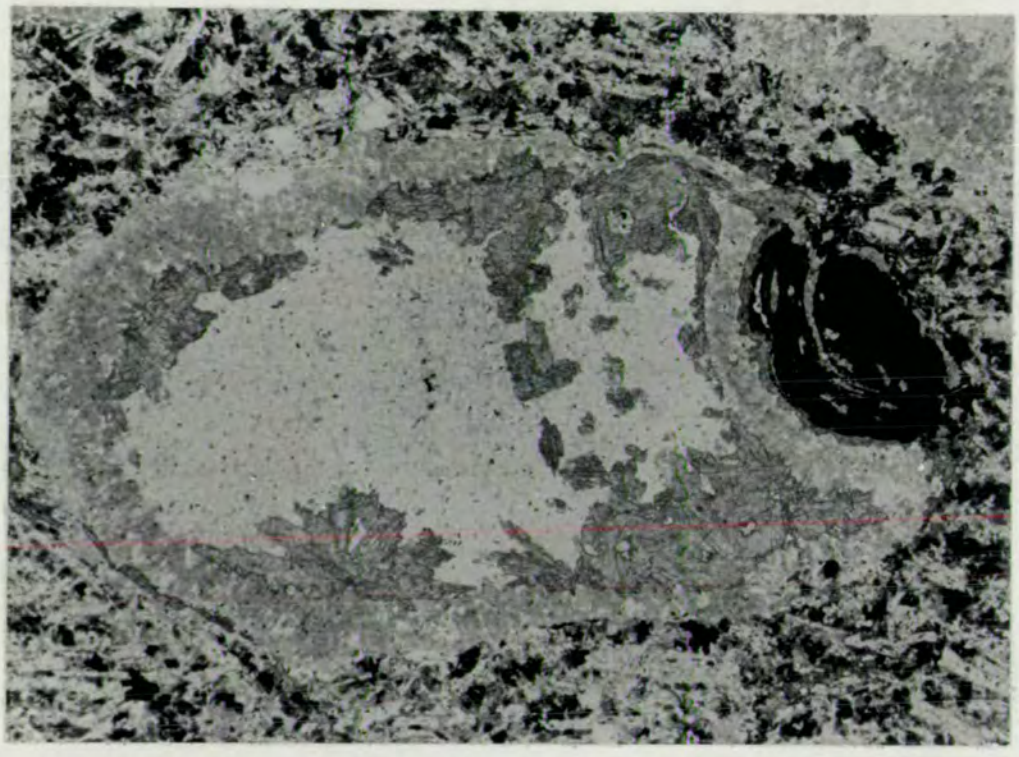

Figure 6.10. Midfell, 700 m, sample 072, inside the caldera in the epidote zone. The first mineral to be deposited in the 3 mm vesicle was botryoidal limonite, followed by a layer of chlorite (pale grey in the photo) lining the vesicle wall. Subsequently an epidote layer (dark grey and core infilling of calcite (mostly lost in preparation of the thin-section). Epidote also occurs on the outside wall of the limonite and fills the concentric layer in it. The presence of epidote next to the limonite may indicate that Fe^{+3} in the limonite participated in the formation of the epidote but not in the chlorite which chiefly contains Fe^{+2}.

up-grade (fig. 6.10) into the epidote zone, it appears that epidote was formed after the chlorite. The epidote seems to have penetrated the outer chlorite layer to recoat the limonite botryoid and fill its concentric voids.

Inside the andradite- and the actinolite zone the limonite botryoids are usually pseudomorphed by epidote, andradite and actinolite. Fig. 6.11 shows a pseudomorphed botryoid in which large andradite crystals (ca. 0.5 mm), containing numerous iron-oxide inclusions, replaces the limonite. Fig. 6.12 shows a relict botryoidal texture next to a vesicle wall composed of gt-act-ep-cc-qtz. It thus seems that the limonite was (partly) dissolved by hydrothermal fluids in the higher-grade mineral zones; Fe^{+3} entered the hydrothermal solutions to subsequently be deposited in epidote and andradite. However, both these minerals were also deposited elsewhere, where limonite was absent.

It is of interest to note the amygdale limonite inside the epidote zone just above the andradite zone along traverse II (see fig. 4.3). As one passes from the chlorite zone into the epidote zone (across the caldera fault) at high altitude on Midfell, amygdale limonite is present as shown in figs. 6.1, 6.8, 6.9, 6.10. Descending within the epidote zone to ca. 500 m, the former limonite botryoids may appear as in figs. 6.13 and 6.14. Two amygdales in the same thin-section (sample 069) are shown in these figures (see also the fig. captions). Elsewhere in the section the amygdales are filled by chlorite and/or calcite. From the infilling sequence at higher levels the chlorite seems to have been formed earlier than the calcite, while the latter occurs both on the inside and the outside of the chlorite layers, and is also found replacing feldspars in the

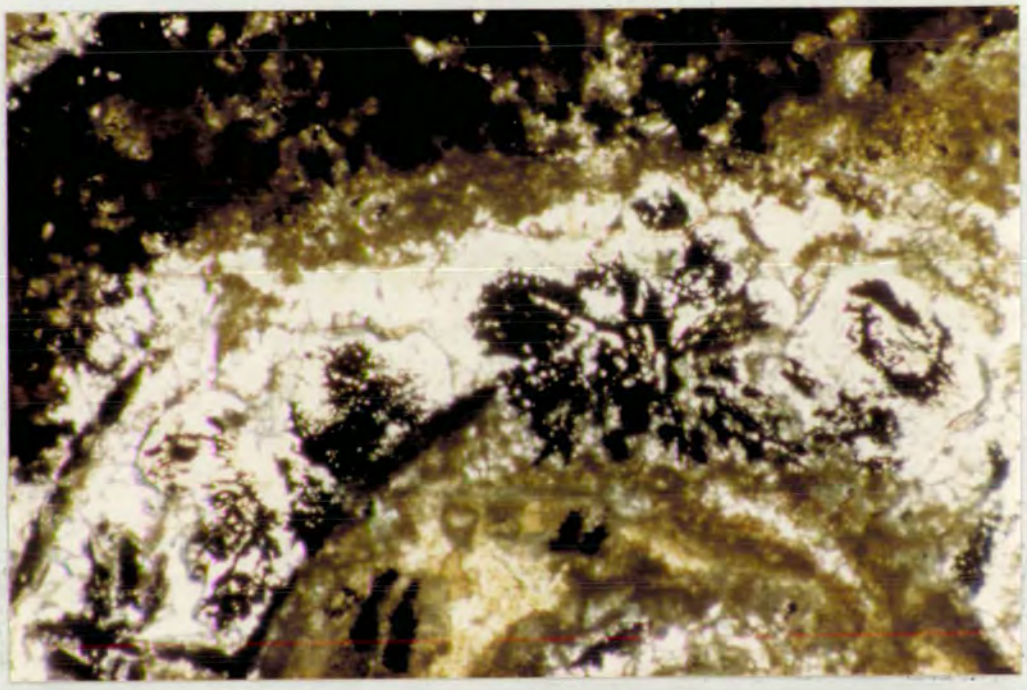

Figure 6.11. Sample 053, from 250 m in Kraksgil inside the actinolite-zone close to the caldera wall, showing the inside of a pseudomorphed limonite botryoid. Concentric layer of 'colourless'andradite crystals (containing hematite inclusions). The 'colourless'garnets are 0,5 mm in diameter. The remainder of the limonite (yellow-opaque) is pseudomorphed by gt-act-ep--chl-qtz-hm. Pr-K.fsp, mo are also present within the amygdale..

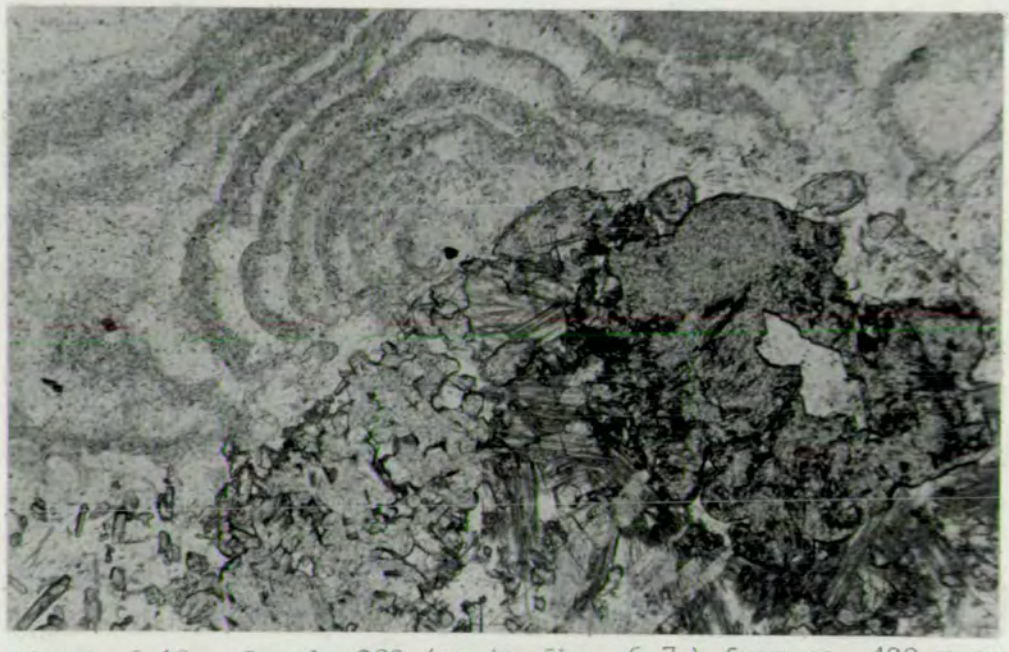

Figure 6.12. Sample 080 (as in fig. 6.7) from ca. 400 m on Tungufell. Pseudomorphed botryoidal limonite (?). The concentric dark layers in the upper half are isotropic and possibly composed of microcrystalline garnets (not analysed) embedded in quartz. Large andradite crystals (0.5 mm diameter) occur inside the botryoid (lower right) along with fibrous actinolite, euhedral epidote (light grey) and calcite (white).

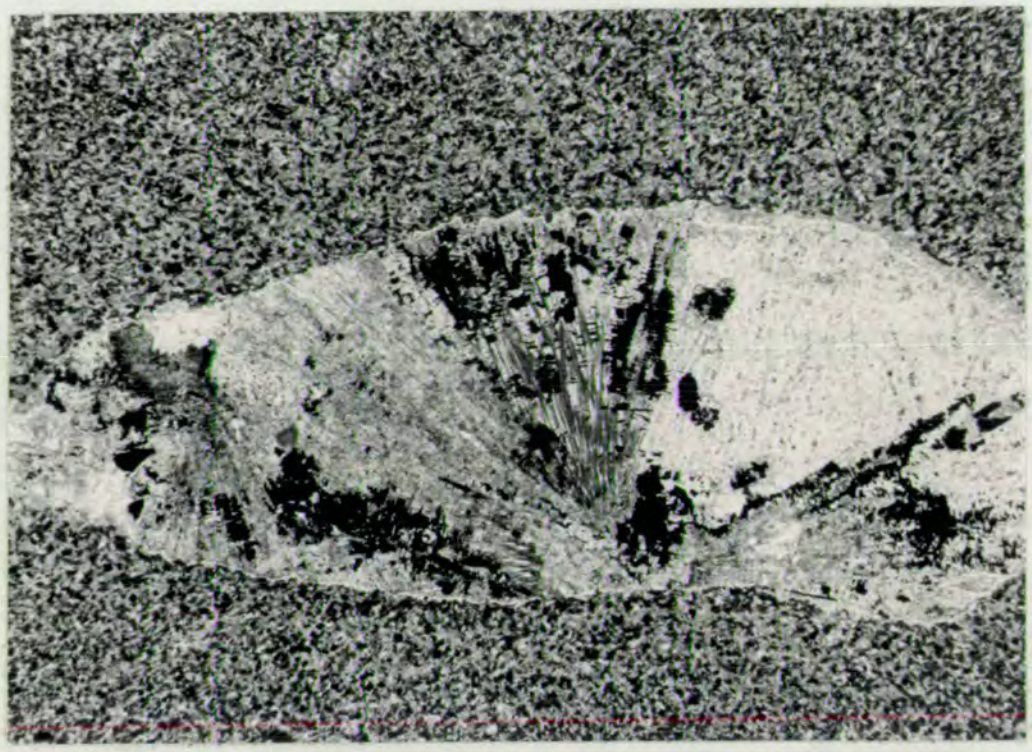

Figure 6.13. Sample 069, from ca. 500 m on Midfell, from the lower part of the epidote zone. The vesicle is 4 mm long and is filled by hematite (black) and calcite (grey). The radiating distribution of hematite from two cores at the wall (upper left and centre middle) suggests that the hematite formed at the expense of limonite botryoids.

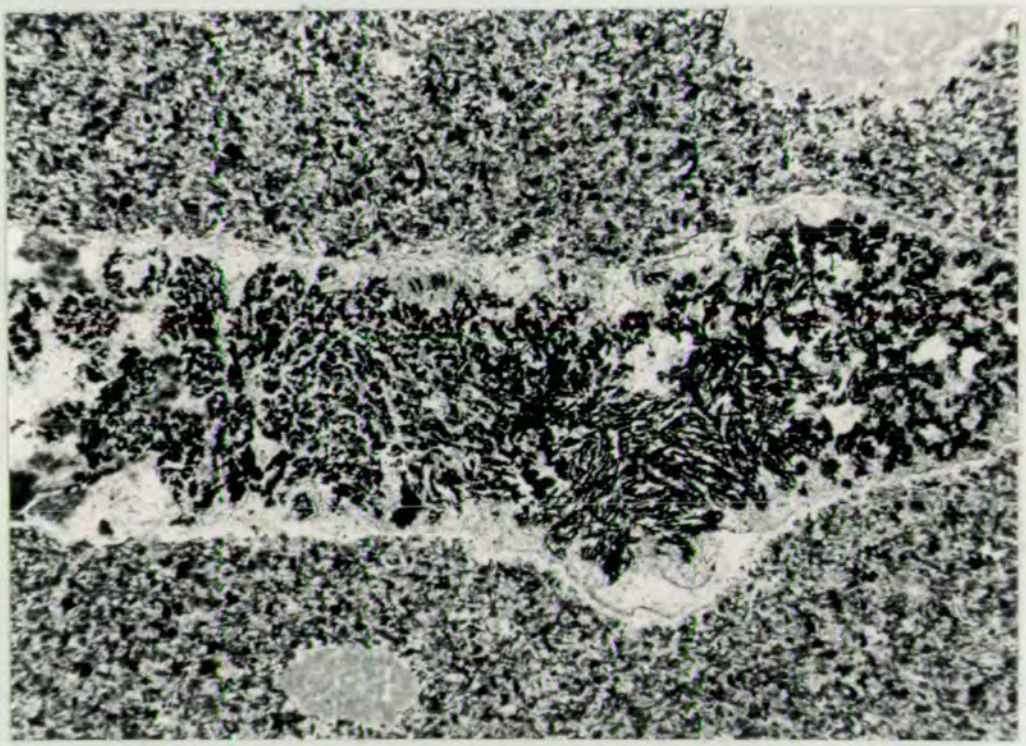

Figure 6.14. Sample 069 (as in fig. 6.13). The vesicle is ca. 3 mm long, and contains dendritic hematite embedded in calcite. No evidence for a possible connection of hematite to limonite is seen in this photo (see text for discussion).

surrounding rocks as 'calcite halos' around the amygdales. Epidote is found in one amygdale of the sample on the inside of a chlorite layer, and in some amygdales, partly pseudomorphed limonite occurs, showing the typical botryoidal habit. Within other amygdales, however, the iron-oxide seems to have been redistributed. In fig. 6.13 the iron-oxide (black) seems to be radiating from two cores which might have been the centre of former limonite botryoids, while in fig. 6.14 the dentritic iron-oxide (possibly hematite) shows no textural connection to a limonite botryoid. While several explanations are possible, it seems likely that a highly active fluid may have dissolved the limonite and retained the iron enriched solution within the vesicle, perhaps as a result of rapid deposition of calcite. From the relative lack of epidote in the sample the calcite deposition could have occurred after the chlorite deposition or soon after the beginning of the high-temperature hydrothermal system (and the gabbro intrusion in Geitafell; intrusive phase 2). A boiling zone (see section 4.2, chapters 7 and 11) may have resulted in rapid and extensive calcite deposition, and possibly this sample provides evidence for such boiling, which is tentatively proposed. It is clear that at higher levels (c.f. fig. 6.3) calcite was deposited after chlorite and did not form replacement halos around the amygdales, while at deeper stratigraphic levels, and at greater distances from the gabbro in Geitafell, calcite similarly appears to have post-dated the chlorite (e.g. fig. 6.6 and 6.7). The amygdale texture in figs. 6.13 and 6.14 may thus be a remnant of a self-sealing process around the gabbro. Whatever the true explanation, it is evident from the textures in the examples shown, that an early calcite depositional episode post-dated the chlorite-infilling episode, and affected the

still earlier amygdale limonite as the early gabbro intrusion is approached.

Descending further downwards towards the Geitafell gabbro, into the outer margin of the contact aureole, textures like those in figs. 6.15 and 6.16 are encountered. These show pseudomorphed botryoidal limonite in an amygdale from a lava sample ca. 200 m away from the Geitafell gabbro. A wide quartz layer, dating from infilling episode (2) in fig. 6.3 , seals of the limonite from the amygdale centre which is filled by qtz-chl-ep-pr-wai, and both andradite and grossular have been found in lava vesicles in the surrounding rocks. The quartz layer apparently prohibited direct contact between the limonite and fluid, while the limonite seems to have reacted to form hematite -magnetite assemblages in a dendritic pattern within the quartz layer. The contact aureole is described below (chapter 7). However, a similar sequence is common in the aureole with early fluid-limonite reaction producing a)hematite and b)magnetite (see later). To conclude, limonite alteration within the hydrothermal system seems to depend on the environment in which alteration occurs. The variation is systematic within the mineral zones. That this is also true for other early infilling material is exemplified by figs. 6.1 to 6,16.

6.2 Complex sequences.

So far the progressive changes along traverses I and II have been described. For clarity, the discussion has been somewhat restricted to amygdale textures in unconnected vesicles of intermediate size (less than 1 cm) although similar textures are also found in the interconnected and larger amygdales. Commonly, however, the textures of the larger amygdales are more complex than in the examples already shown, because of re-solution and/or alteration of the early infilling minerals. The key to the amygdale textures in the larger and the

Figure 6.15. Sample 033, at ca. 100 m on Midfell from the andradite-actinolite-zone boundary shows a large pseudomorphed limonite botryoid embedded in quartz. The limonite appears to have been sealed off from later ep-gt yielding fluid by a thick quartz layer. The quartz layer grew as large euhedral prisms towards the vesicle centre (right side of the photo). The terminations of the quartz prisms,however, are anhedral towards the infilling of wairakite-prehnite in the centre (upper right) as if they had been dissolved by the central fluid. Field of view ca.5x7 mm.

Figure 6.16. The same vesicle as in fig. 6.15, showing dendritic hematite-magnetite in quartz formed at the expense of limonite botryoid. The field of view is ca. 1x1.5 mm.

interconnected vesicles thus emerges from the more regular textures preserved in the smaller amygdales which allows determination of amygdale mineral infilling sequences from all the index mineral zones, (see end of this chapter). Textures in several examples of the interconnected and larger group of amygdales will, however, be discussed:

Fig. 6.17 shows an amygdale in a scoriaceous sample collected from the actinolite zone close to the caldera fault on Tungufell. The scoria is completely altered and most of the interconnected vesicles are filled by partly distorted mud layers-ep-chl-qtz-cc. Some of the amygdales are also filled by albite-adularia assemblage (fig. 6.17), which is rare in amygdales and is only found within the actinolite zone. The overall distribution of the ab-K.fsp. as a part of the amygdale assemblages is not clear, but it is most commonly observed in samples from near the caldera fault on Tungufell and in Kraksgil.

Albite-adularia mineral deposits have not been described from active hydrothermal fields in Iceland although adularia-precipitate was recently found by the author in well KJ-17 in the Krafla geothermal field. K.fsp, however, has been detected in samples from the active areas, by use of electron-microprobe (Kristmannsdóttir, pers. comm.). Adularia is a common part of the hydrothermal assemblages in active geothermal fields elsewhere in the world (Browne, 1978). Browne (1970, 1978) showed a positive correlation between the nature of feldspars in aquifer rocks and the measured well-permeability in the Broadlands Geothermal Field, New Zealand: In order of increasing permeability the following sequence was observed: andesine, albite, albite-adularia, adularia. The common occurrence

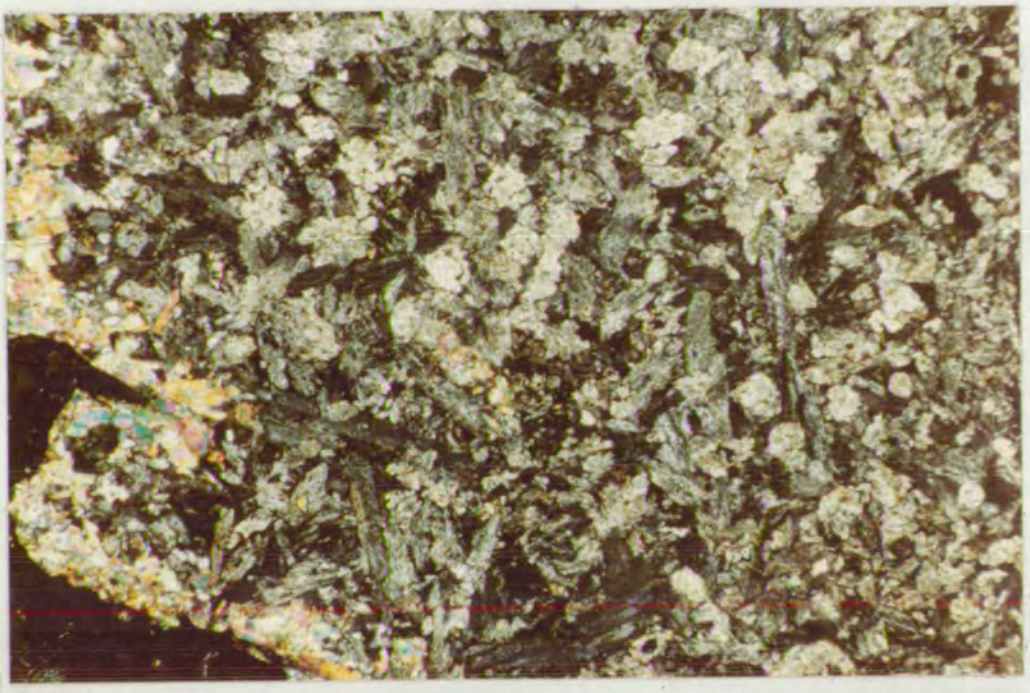

Figure 6.17. Sample 089, from ca. 700 m on Tungufell, near the caldera fault. An assemblage of albite-adularia-epidote forms most of the field while epidote-quartz occurs near the margin of the vesicle. The lath-shaped turbid albites are somewhat hydrated and altered to zeolites. The monoclinic adularia shows pseudo--orthorhombic habit, where the (010) face is narrow or absent in the subhedral crystals cut normal to c-axis (typical for adularia). Field of view: ca. 5x3 mm.

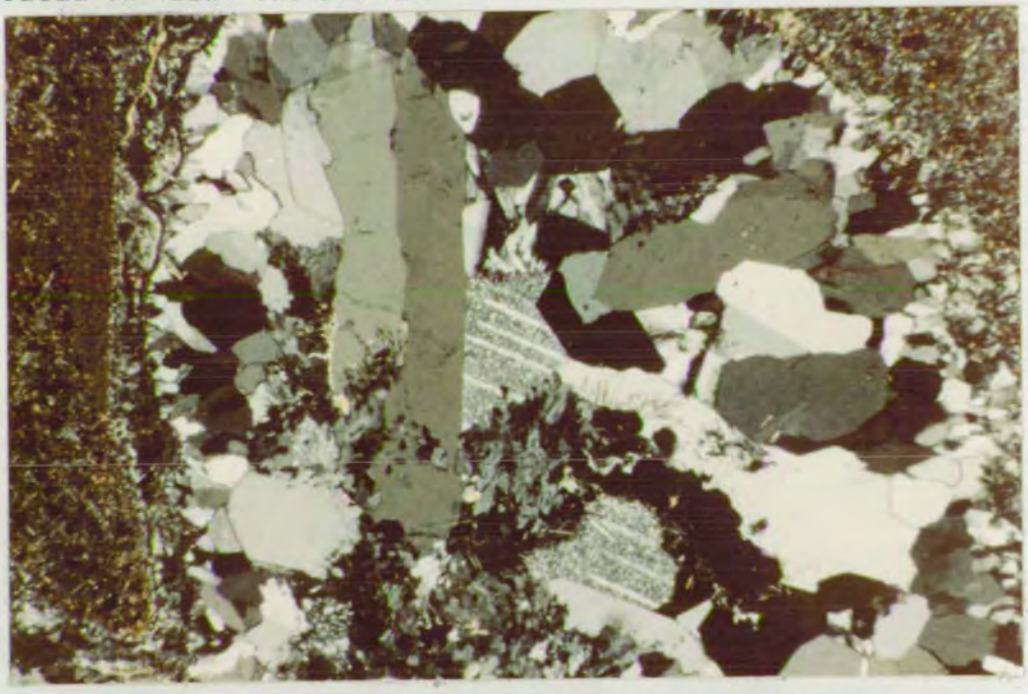

Figure 6.18. Sample 080, from ca. 400 m on Tungufell. Andradite and epidote (& actinolite ?) inclusions occur in quartz. Calcite and a zeolite (natrolite?) are seen in between quartz in the middle and albite-adularia in the lower middle. Note the irregular twin--plane in quartz. A mud layer is seen at the vesicle wall (left) indicating the former orientation of the lava (i.e. rotated 90° clockwise to position shown). The vesicle cross-section from left to right is ca. 4 mm.

of albite and adularia in the feldspar replacement assemblages in the Geitafell palaeo-geothermal area (section 8.3) and the local abundance of adularia as a part of the vesicle assemblages near the highly permeable caldera fault in rocks showing interconnected pore space, may therefore partly reflect the palaeo-permeability, and is taken to imply, along with other evidence, that large quantities of fluid passed the caldera fault region.

Fig. 6.18 shows a part of a relatively large lava amygdale (ca. 2 cm), containing ab-K.fsp-wai assemblage which fills the centre part of the vesicle. A part of the same amygdale is also shown in fig. 6.12, showing an apparently pseudomorphed limonite at the vesicle wall. These two figures should be compared to fig. 6.7 which shows a smaller amygdale in the same thin-section. The centre infillings are clearly different possibly because of variation in vesicle size in accordance with the observed correlation (i) (see beginning of this chapter). Additionally, it may also relate to different fluid/rock ratios and the effective permeability at the time of deposition, as well as the possibility of variable fluid chemistry.

Elsewhere inside the actinolite zone, the centre infillings more commonly show assemblages of ep-cc-qtz-gt- (± wai, pr, stb, amph, ab, K.fsp). The early chlorite infilling layers are found everywhere within the actinolite zone, but become scarcer in amygdales closer to the centre of the zone in Kraksgil. The chlorites show a range in birefringence and colour-variation from light brown to deep green. Small vesicles filled by chlorite commonly show the low birefringent variety (dark-grey), while the larger amygdales, additionally containing ep, gt and other centre infilling minerals, more commonly show chlorites of higher birefringence and of more brownish colour. How-

ever, no systematic chemical variation has yet been found between the chlorite varieties. In general, the chlorite within the actinolite zone appears to be at various stages of alteration following the trends outlined in figs. 6.3 , 6.5 , 6.6 and 6.7.

With respect to vesicle wall-rock alteration the overall tendency appears to be, that the extent of replacement by secondary minerals seems to increase towards the vesicles, while the type of the primary mineral replacement mineralogy is essentially the same everywhere within the rock matrices. Sometimes the vesicle walls within the actinolite zone lose sharpness because of replacement of the primary minerals, and two chief types of secondary mineral halos around the amygdales are found. Both have already been mentioned - the epidote halos which are exemplified on a macroscopic scale in figure 5.4, and the calcite halos (figs. 6.13 and 6.14). In both cases the primary feldspars are completely replaced by the respective mineral type, while the other primary minerals are more commonly only partly replaced by some secondary mineral. Alteration halos are discussed further in chapter 7.

Within the andradite zone, the vesicle infilling sequences are similar to those in the actinolite zone. The andradite zone, in fact, represents an area enclosing the actinolite zone defined by the apparent lack of actinolite in the host rocks and its amygdales and the presence of andradite. Garnet, however, occurs in both zones and is mainly red-brown andradite. The only sample (scoria; 1 11/7'77) additionally containing grossular was collected in Midfellsgil (at the end of traverse II in fig. 4.3) from the outer fringe of the Geitafell gabbro contact aureole. This grossular is colourless. The sample is completely altered and composed otherwise of ep-cc-

-TiO_2-hm-($\pm$ qtz,chl,py,gt). The amygdales are of various sizes, most commonly composed of : ep-grossular-cc-($\pm$qtz), ep-cc, or ep alone. Less commonly the amygdales contain (i) chl spotted with ep, and possibly gt (this assemblage being restricted to the smallest amygdales), while some of the larger include (ii) a chl-rim, spotted with ep, and an inner layer of andradite with ep-cc centre. The andradites are only found in this situation (as in fig. 6.6) suggesting that the presence of andradite hinges on the earlier presence of chlorite in the vesicles. The grossular-bearing amygdales, however, are typically chl-free. The grossular contains inclusions of iron-oxide and pyrite. The two garnet types do clearly not form an assemblage in the strict sense as they occur in separate amygdales. Several garnet analyses are provided in table 3, appendix 1, and plotted in figure 10.2. A mean of 6 grossular analyses gives the formula : $Ca_3(Al_{1.81}Fe_{0.19}Cr_{0.01})Si_{2.99}O_{12}$. The rare presence of grossular in an Icelandic hydrothermal area (which in this case may relate to the gabbro contact aureole) is discussed further in chapters 7 and 10.

Within the epidote zone the early vesicle infillings are similar to those in the underlying mineral zones. Chlorite still appears to precede epidote (e.g. fig. 6.19), while in other instances the two minerals may also have been deposited simultaneously. In figure 6.19 the vein-related epidote fills the centre of the amygdale and penetrates the earlier formed chl-layer at several places to become deposited next to the vesicle wall through ca. 180° as if the precipitating fluid had dissolved the chl from the wall-rock contact. Nonetheless the chl-ep assemblage appears otherwise compatible in the sample. Similar amygdale textures are also found in the underlying

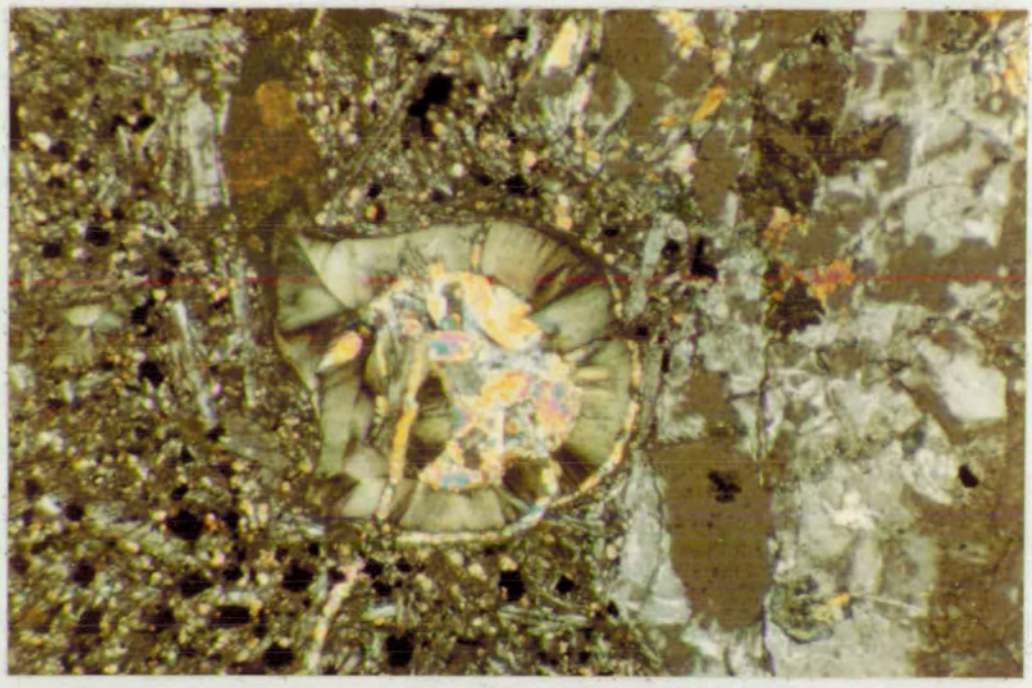

Figure 6.19. Sample 11 25/8'77, at ca. 300 m in Geitafellsgil, within the epidote zone. The vesicle is ca. 0.6 mm across. Crossed nicols. The epidote is clearly later than the chlorite, while lack of reaction features suggests that the two minerals were compatible. Note also the partial replacement of the feldspar phenocryst on the right by ep-ab-qtz (? $\pm$ K.fsp, z).

mineral zones and imply that care must be taken in interpreting infilling sequences from the textures. The simplest method is evidently to study a number of amygdales in any area to deduce the overall infilling sequence. The next two figures serve as an example.

Figs. 6.20 and 6.21 show the same vesicular basaltic tuff under uncrossed and crossed nicols respectively. The light-green microcrystalline chlorite shows a range in birefringence from almost nil upwards, and can be compared with chlorites in the earlier figures. Within the largest amygdale (upper right) the chl-ep-qtz forms an assemblage; the three minerals may have formed contemporaneously (as suggested by the infilling sequences listed below). In the surrounding smaller vesicles (which appear disconnected in the photos but need not be in three dimensions), chl occupies the amygdales with or without a complete or partial outer layer of ep-qtz. Within the upper size range of amygdales in the sample eq-qtz composes an additional central filling. The overall texture might imply that an early infilling of ep-qtz preceeded a chl depositional episode, followed by later deposition of ep-qtz-(chl). However, the overall implication from the neighbouring rocks and the epidote zone in general suggests, that an early chlorite depositional episode preceded a period when ep-qtz-chl-(and other minerals) were deposited, (as is postulated in the listed time sequences below). The outer ep-qtz layer in the two figures may thus be related to the later depositional period by a similar fashion to that demonstrated in figure 6.19. The general sequence, however, does not exclude relatively short depositional episodes within the longer depositional periods. The evidence for such episodes, however, is often obscured within the amygdales by variation in the infilling mineral emplacement mode as

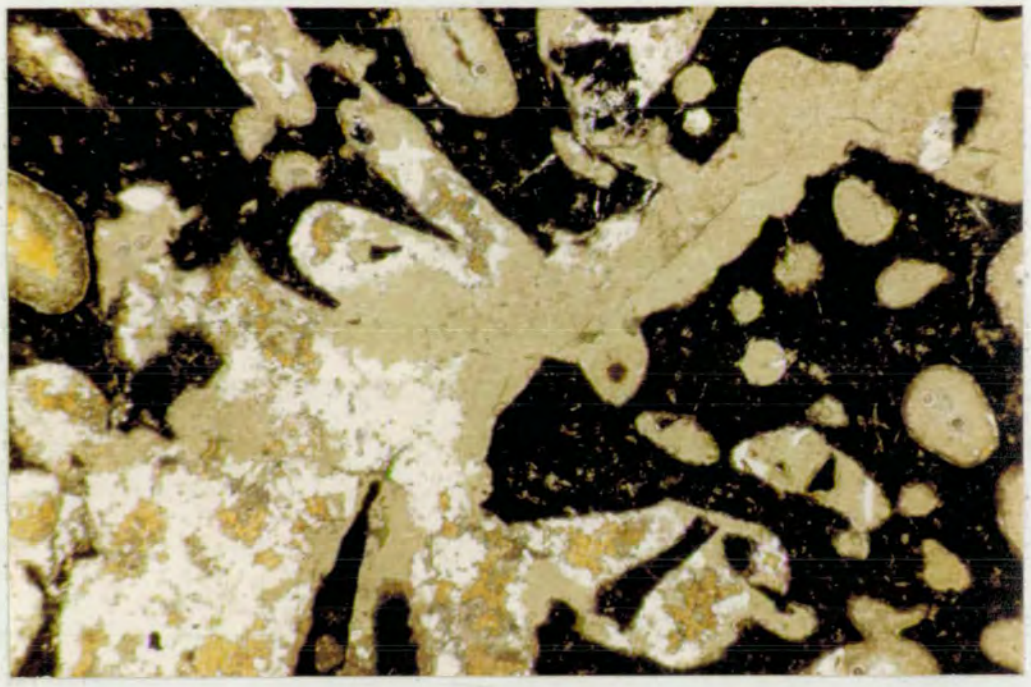

Figure 6.20. Sample 221 at ca. 340 m in Geitafellsgil, close to the caldera fault showing a vesicular basaltic tuff. Note the light-green microcrystalline chlorite. Field of view: 4x3 mm.

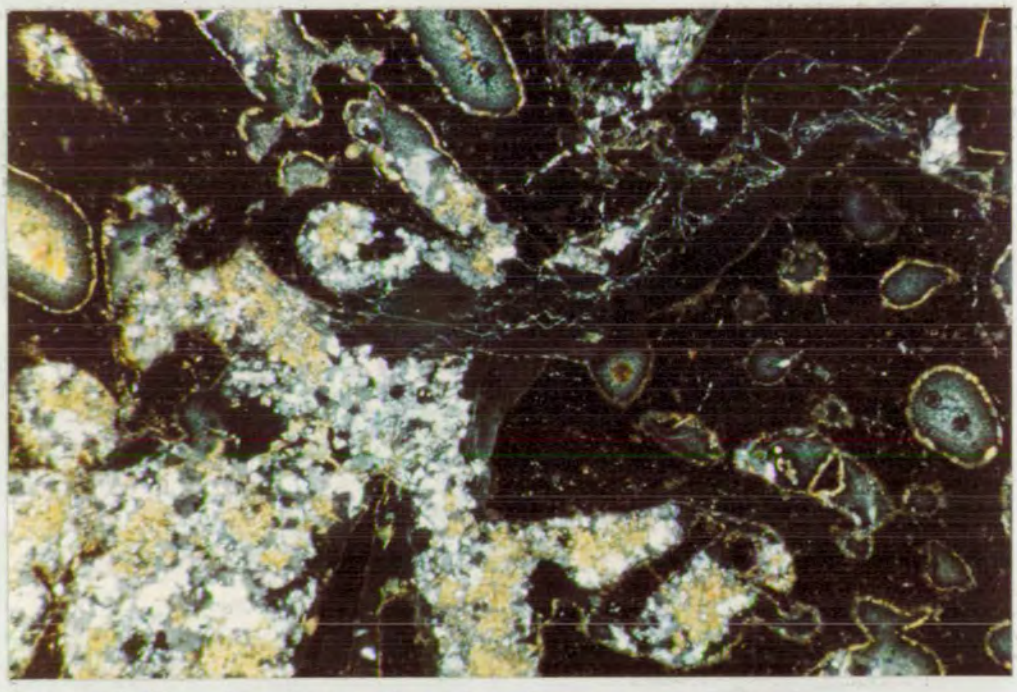

Figure 6.21. As above viewed under crossed nicols. Note the range in chlorite birefringence by comparing with chlorites in other figures. (See text for discussion on the apparent infilling sequence.).

has been demonstrated above. Within the vein systems such depositional episodes are indicated by the apparent existence of vein fluid generations within most of the vein systems (e.g. within vein system 3-a at study locality 1). This general discussion of principles is of some importance when it comes to interpretation of amygdale textures where relationships are undefinable. One example is shown below.

Figs. 6.22 and 6.23 show an amygdale in a basalt fragment from hyaloclastite in Geitafellsgil. The sample was collected from the andradite zone enclosed by the epidote zone at the caldera rim (see figs. 4.3 and 4.5 along profile C-C'). The extent of the garnet distribution within the amygdales in this zone is limited. Only minute garnets (figs. 6.22, 6.23) occur within pseudomorphs after limonite. The time of formation of the garnet with respect to the other amygdale minerals is unknown. Taking a traverse from the botryoid in the lower left of the figures towards the amygdale centre, and assuming a simple infilling, the sequence : (i) cc (ii) hm, partly replaced by py (iii) cc-gt (iv) hm-cc (v) chl (vi) cc (vii) chl (viii) cc (ix) ep, could be countered. However, from study of the limonite alteration (figs. 6.8 - 6.12) at lower levels within the volcano, and the common habit of early infilling layers to be resorbed and/or altered by later fluids, the apparent infilling sequence in the amygdale in figs. 6.22 and 6.23 seems to be : (i) lim (ii) chl (iii) cc (iv) ep (or cc-ep, cc-gt). The association of garnet and the caldera fault, and the extensive hydrothermal alteration close to the caldera fault elsewhere, suggests that the formation of garnet in the epidote zone took place at the time of caldera collapse. It could be related to ascent of high-temperature fluids along the

caldera-fault. Supporting evidence comes from the locally extensive development of ab-K.fsp (ep,gt,act) in amygdales at lower levels and the locally extensive ep-pr occurrence close to the caldera fault at the highest stratigraphic level within the hydrothermal system.

Zeolites play a major role in amygdale assemblages within the epidote zone, particularly within the larger amygdales. Sometimes evidence suggesting reactions between early-formed zeolites and later fluids to form other zeolites is observed. For example : A large amygdale (ca. 3 cm across, sample 010) contains an assemblage of (euhedral)wai-ep-pr-qtz-cc occurring next to the vesicle wall, including an irregular chl-layer. Traversing inward from the vesicle wall, the wairakite becomes partly pseudomorphed by anhedral laumontite in an assemblage containing ep-pr-qtz-cc, followed by a layer of (sub- to anhedral) laumontite-(euhedral)heulandite, and then by a central infilling of (euhedral) heulandite-chabazite. The apparent reaction sequence is wairakite hydrating first to laumontite and then, further (with addition of SiO_2) to heulandite (cf. Coombs et al., 1959).

It should be noted, (i) that wairakite is absent from the upper part of the epidote zone, and (ii) that the common presence of pyrite ($\pm$ cpy) within the amygdales in all zones can not be related to any particular infilling episode from the amygdale textures, but can be interpretated from the vein systems within the upper part of the epidote zone.

6.3 SUMMARY

The amygdale infilling sequences from the four mineral zones are summarized in table 6.1 and discussed below.

TABLE 6.1

Amygdale filling sequence within the actinolite zone :

1a	limonite	I-1a		R-4
1b	mud deposit	I-1b		R-4
2abc	jasper, chalcedony,qtz	I-2abc		R-4
3a	smectite?	I-3a		R-3b,4
3b	chl	I-3b	P-3b	R-4
4	ep,gt,act.qtz,cc,(pr,chl?)	I-4	P-4	
5	ab,K.fsp (caldera rim)	I-5		
6	wai (analcime?)	I-6		R-7
7	lau,qtz,cc	I-7	P-7	R-8
8	heu,stb,sco,mo,cc	I-8	P-8	
9	cha	I-9		

Within the andradite zone the infilling sequence from 1-3 is the same :

4	ep,gt,qtz,cc	I-4	P-4	
5	pr,wai	I-5		R-6
6	lau,qtz,cc	I-6	P-6	R-7
7	heu,stb,(other z?)	I-7	P-7	
8	cha	I-8		

Within the lower part of the epidote zone the infilling sequence from 1-3 is essentially the same :

4a	ep,chl,qtz,cc,pr	I-4a		
4b	wai	I-4b		R-5
5	lau,cc,qtz	I-5	P-5	R-6
6	heu,stb,sco,cc,qtz	I-6	P-6	
7	cha	I-7		

In the upper part of the epidote zone the infilling sequence from 1-3 is still the same; in the latter part both epidote and prehnite have restricted occurrence and wairakite is absent :

4	chl,qtz,cc,su,ep	I-4
5	ep,pr,qtz,cc,(caldera rim)	I-5
6	pr,lau,qtz,cc(")	I-6
7	cc,qtz,py,lau	I-7
8	stb,heu,sco,py	I-8

Finally, in the chlorite zone the infilling sequence from 1-2 is the same :

3	smectite	I-3
4	chl	I-4
5	cc,qtz,sm,lau?	I-5
6	stb,heu,sco,tho,cha	I-6

Explanation: The successive infilling episodes are numbered consecutively 1, 2, 3,..... ; small letters in alphabetical order indicate uncertain but apparent time relationship, with brackets indicating limited occurrence, and the following abbreviations are used to indicate :

I : minerals deposited directly from introduced fluid (no signs of reactions with earlier solids)

R : mineral(s) behaves as a reactant with introduced fluid.

P : mineral is a product of reaction between mineral and later fluid.

By comparing the infilling sequences in table 6.1, it is clear that most of the observed amygdale minerals occur in the actinolite zone. In the andradite zone, actinolite,albite and adularia do not occur in amygdales, and garnet is lost from amygdales on entering the epidote zone. In the upper part of the epidote zone wairakite also disappears from the amygdale assemblages, and finally, neither epidote nor prehnite are present in the chlorite zone. It can also be seen that the index minerals of the mineral zones all formed during the same infilling period (number 4). A noteworthy difference between the actinolite- and the epidote zone, is that chlorite does not appear to be formed in amygdales in the actinolite zone during infilling episode 4 while at the same time it was clearly formed in the epidote zone.

The reactions between the early infillings and later fluids are variable within the progressive mineral zones. Lim (1a) is unaltered within the chl-zone, only partly replaced by ep,py within the ep-zone downwards, partly pseudomorphed by ep,gt or by mt-hm in the andradite zone, and by ep-act-gt (including mt-hm inclusions) in the act-zone. The mud deposit (1b) is composed of turbid qtz in all zones but within the act-zone ep,gt,pr appear in addition. The jasper (2a) alteration is identical in the ep-, gt- and act-zones, being replaced by hm-qtz-py-clay. The former amorphous chalcedony (2a) is composed of crystalline quartz in all mineral zones. Dissolution of the quartz (P-2b,I-2c) is only found in the act-zone (exemplified in figs. 6.15 and 6.18). Pseudo-twinning of the qtz is only found within the act--zone (fig. 6.18); optical flash-figures in qtz are more commonly observed within the act-zone than elsewhere as is the pseudo-polygonal cleavage of the early qtz.

The early smectite (3a) is only preserved in the chl-zone, but if it was present in the ep- and the higher grade zones, it has altered to chlorite. Finally the chl (3b(4 in the chl-zone)) is unaltered in the chl- and ep-zones, often partly replaced by gt,ep in the gt-zone, and commonly, though not always, pseudomorphed by gt, act,ep in the act-zone.

Well-developed alteration halos, of ep or cc, surrounding amygdales may be found from the ep-gt-zone boundary downwards, but are only poorly developed or absent in the overlying mineral zones.

From the textures and alteration sequences in the amygdales it is demonstrable that the actinolite zone represents the highest grade hydrothermal alteration within the Geitafell volcano. Therefore, in order of increasing grade, the hydrothermal mineral zones are : chlorite-, epidote-, andradite- and actinolite zones. This zonal sequence is indirectly confirmed from data on active hydrothermal systems in Iceland where the development of chlorite, epidote and actinolite can be related to progressive increase in the minimum fluid temperatures (chapter 11).

Comparison with the vein systems (chapter 5) shows that the sequences established for the mineral veins and the amygdales are quite similar, indicating that the porosity- and fracture-controlled fluids were closely related. The overall coherency may not appear surprising, although before this study it was not known whether - or how - the two were related in a fossil Icelandic high-temperature hydrothermal system. The combined data from the two sources,(veins and amygdales) in relation to the intrusive rocks and the structural history, allow evaluation of the evolutionary history of the Geitafell hydrothermal system.

CHAPTER 7

THE CONTACT AUREOLE OF THE GEITAFELL GABBRO

The extent of the narrow gabbro contact aureole to the N and NE is shown by the enveloped actinolite zone in figure 4.3. The contact aureole is loosely divided into an inner- and an outer aureole. The inner aureole envelopes metamorphic hornfelses at the gabbro contact, while the outer aureole comprises intrusive sheets and dykes, and unmetamorphosed lavas containing skarn mineral deposits in amygdales - closer to the gabbro contact - and actinolite-bearing host rocks elsewhere within the aureole. Three types of vesicle halo zones are found within the outer aureole, chlorite-albite halos (or calcite-free halos), epidote-halos and calcite-bearing halos.

7.1 The Inner Aureole - Hornfelses.

Hornfelsed lava produced by contact metamorphism has been found in one exposure at the eastern margin of the Geitafell gabbro (intr. phase 2), while most of the scattered contact exposures are between gabbro and later intrusive rocks (dykes and sheets). The lava hornfelses strike to the NW and dip ca. 60°NE, almost perpendicular to the regional strike of the lavas, indicating the hornfelses have been deformed by the gabbro emplacement. The hornfelses consist of a fine-grained secondary mineral assemblage of augite-andesine (An_{44})-ore. The primary vesicles of intermediate sizes are filled by pyroxene (augite-salite)-andesine (An_{30}) of slightly larger grain-size than those in the hornfels matrix, while the ore minerals are confined to the hornfels matrix and the vesicle wall-zones. The ore mineral grains at the vesicle walls are somewhat larger than the matrix ore. Some of the smallest vesicles contain chlorite alone, which may indicate that the chlorite formed prior to gabbro emplacement and survived the contact metamorphism. The largest vesicles show px-fsp

development around their walls and may additionally contain the assemblage gt-cc-qtz-ep-act-chl (sample 214), a part of which may be related to secondary hydrothermal alteration. Some of the matrix augite in the hornfels is marginally replaced by actinolite; small grains of ab, K.fsp, qtz, chl, cpy also occur within the matrix and may be related to subsequent hydrothermal alteration.

The lava hornfels (sample 215) was extensively analysed by the microprobe. The pyroxene analyses are presented in table 1, appendix 1, while their composition in the pyroxene quadrilateral (Wo-En-Fs) is shown in fig. 7.1. The composition field of the secondary augite embraces that of the matrix augite. The secondary feldspars vary from An_{44} in the hornfels matrix to An_{30} in the amygdales.

The contact metamorphosed lava can be classified as a pyroxene hornfels, and may belong to the pyroxene-hornfels facies or the sanidinite facies of contact metamorphism. The latter was defined by Eskola (1939) to cover mineral assemblages formed at maximum temperatures and minimum pressure of metamorphism, while the basaltic assemblages of the sanidinite facies are essentially the same as those of the pyroxene-hornfels facies (cf. Turner, 1981, p. 286). In the present case the depth from the palaeosurface to the Geitafell gabbro was $\leq$ 1 km (chapter 3), and the hornfelses are cross-cut by unchilled felsite veins (intr.phase 4) which may have been intruded at temperatures between 900-1000°C. The low-pressure/high-temperature regime may thus suggest the lava hornfelses should be placed within the sanidinite facies (see also chapter 10. This may be irrelevant to the present study, however, as in either case any hydrous fluid in the apparent thermal regime would have had to be at supercritical conditions (chapter 4.2), a conclusion of importance to this study.

Figure 7.1

Composition of metamorphic pyroxene from the Geitafell gabbro contact

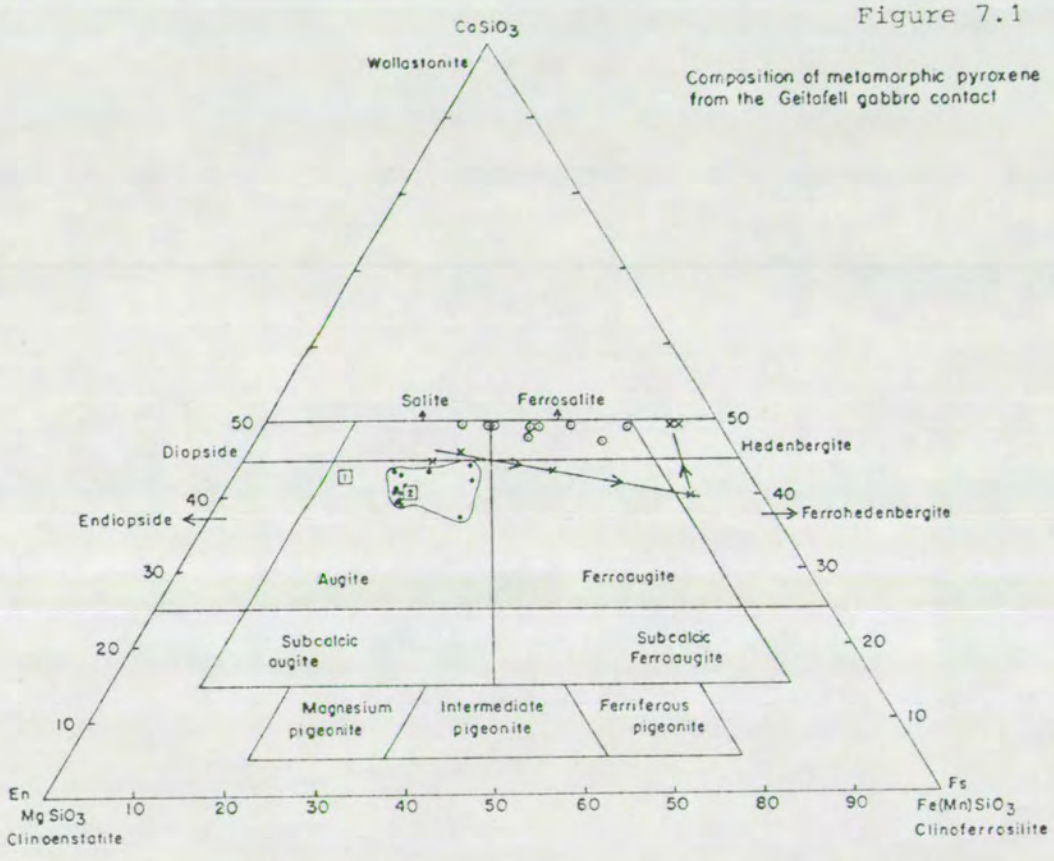

Legend:

- Primary augite, 1: phenocrysts, 2: matrix augite
- Hornfels augite, field enveloped
- Vein mineral pyroxene
- Direction of compositional trend from wall rock zone to vein centre.
- Amygdale pyroxene

Pyroxene nomenclature after Poldervarrt and Hess 1951

The hornfelsing clearly accompanied the gabbro emplacement (intr.phase 2). Secondary alteration in a dyke of intrusive phase 3 (chapter 3) which appears to cross-cut the hornfelses is also studied. The dyke (sample 216) contains bytownite phenocrysts (zoned to labradorite) smaller augite phenocrysts ($Wo_{43}En_{37.8}Fs_{20.6}$) and ore minerals. Actinolite and chlorite occur in subordinate amount as hydrothermal minerals partly replacing augite while albite partly replaces the primary feldspar. The dyke is cut by rather unusual mineral veins occurring as a trail of elongated amygdales connected by narrow channels, striking nearly perpendicular to the dyke walls. Narrow wall-rock zones are found alongside the mineral veins composed of andesine (An_{43-46}) and salitic pyroxene ($Wo_{45-47}En_{30-34}Fs_{21-23}$, see fig. 7.1), whose composition suggests a genetic relation to those of the hornfelses. A brown layer between the wall-rock zone and the vein centre consists of clinopyroxene (ferroaugite/ferrohedenbergite) -gt-act-sp-ap. (The garnet in this layer was too small for analysis). Hedenbergite grows from the brown marginal layer into the vein centre or occurs independently in the vein centre assemblage with qtz-ep and lesser ab-K.fsp-pr-stb. The variation in the pyroxene composition from the rock into the vein centre is thus : augite, salite, ferroaugite, ferrohedenbergite, hedenbergite, the direction of this trend is indicated by arrows in fig. 7.1.

These mineral veins appear to indicate a genetic relation to the thermal metamorphism by the gabbro since they have not been found within any other intrusive rocks within the volcano. Intrusive phase 3 (radial dykes) was introduced shortly after the gabbro event. It therefore seems possible that a gas-rich metamorphic fluid may have penetrated the hot intrusive rock to form the parallel aligned inter-

connected amygdale trails described above. The converse explanation to the "vesicle-vein" formation might be sought to a gas-rich fluid related to the hot intrusive rock itself. However, while amygdale--trails (filled by sulphides) are common within other intrusive dykes, they always strike parallel to the intrusion itself and usually only occur close to the chilled margins. Therefore, if the explanation above is correct it implies a fluid moving within the metamorphic aureole; this was probably a hydrous fluid at supercritical temperatures which may have been responsible for the ferrosalite and andradite precipitated in lava amygdales within the outer contact aureole.

Felsite veins (intr.phase 4) also cross-cut the hornfelses. Within sample 215, the felsite vein consists of zoned feldspar (labradorite-andesine) marginally replaced by ab, K.fsp, and augite phenocrysts nearly completely replaced by act, in a matrix of qtz-ab-K.fsp--px-ilm-hm-act-chl-ap-zircon. No signs of contact metamorphism, wall-rock alteration, or chilled margins exist between the hornfelsed lava (and its amygdales) and the felsite vein.

7.2 The Outer Aureole - Including Skarn Minerals.

Within the outer contact aureole there are several noteworthy differences in the alteration products from those seen in the actinolite zone elsewhere. It is still clear from the amygdale textures in lavas of the aureole, that both botryoidal limonite and mud deposits (related to infilling periods 1-a and 1-b, table 6.1) had been formed prior to the gabbro intrusion. Similarly, there are indications from within the amygdales and veins (loc.3, chapter 5), that the silica minerals (jasper, chalcedony, quartz; infilling period 2, table 6.1) had also been formed prior to the gabbro event. Additionally, there is some circumstancial evidence that both smectite (infilling 3-a) and chlorite (infilling 3-b) might have

formed prior to the gabbro. A few sample descriptions are necessary to show how the infilling sequences of the contact aureole lavas differ from the general infilling sequences provided in table 6.1.

One of the key samples from the contact aureole contains ferrosalite in amygdales. The basaltic lava (sample 134) is composed of phenocrysts of feldspars (bytownite-labradorite) and augite in a matrix of fsp, px, ore. The lava is unmetamorphosed but partly replaced by hydrothermal ab,ep,wai,sco (replacing primary fsp), act,chl (replacing px, and former glass(?)), and sp,hm,py (replacing the primary ore). Three amygdales are present in a polished thin-section, two of which have a diameter less than 5 mm, while the third has a diameter close to 10 mm. One of the smaller amygdales is almost filled by partly pseudomorphed limonite botryoids, and contains an assemblage of mt-hm-fs-wai, with ep occurring at the vesicle wall. The other of the smaller amygdales shows pseudo-botryoidal zones at the vesicle wall (pseudomorphed limonite) containing fs-gt-ep, with a centre of gt-(clear)wai-fs. The andradite is full of inclusions; two species of which were successfully analysed as calcite and salite. Most of the inclusions appear to be salite which appears to contain an abnormally high MnO content (5.1 %, see appendix 1). The largest amygdale contains qtz-(turbid)wai-gt. Numerous px inclusions appear embedded in the gt-grains, and some of the latter show marked anisotropism. Some of the andradite may also be replacing earlier pyroxene.

The absence of calcite in the three amygdales is noteworthy as is its presence as inclusions in the andradite. The pyroxene shows a marked compositional variation across the ferrosalite field (see fig. 7.1), while the only analysis of the pyroxene inclusion in the andradite plots within the salite field. The MnO content of the px

inclusion (5.1 %, table 1,appendix 1) is abnormally high in comparison with the nine ferrosalite analyses shown in fig. 7.1, which on average contain 0.64 % MnO (standard deviation of 0.23 %). The manganese enrichment may indicate that a reaction took place between the pyroxene and garnet in which the pyroxene provided a sink for manganese. The amygdale assemblages above show a remarkable resemblance to typical gangue minerals in skarn deposits, and are compared and discussed further in chapter 10.

From the evidence cited so far (chapter 6) and the apparent sequence in sample 134 the amygdale infilling sequence is : lim, fs, gt-ep, wai, qtz. The lim may additionally have altered to mt-hm. The presence of the px inclusions in the andradites and the pseudomorphing of px by anisotropic gt suggests a later, or prolonged formation of the andradite.

Two types of garnets may be present in the contact aureole, though only found in one sample (1 11/7'77) containing both andradite and grossular, which was described above (p. 207). The two garnets may be related to contact metasomatic effects in the gabbro aureole, although no direct field-evidence can be provided. It is only the spatial location of the sample (from the outer fringe of the aureole) which may point to a relationship between the two garnet types and the contact aureole, but evidently the locality requires further study.

Three types of halos surrounding the lava amygdales occur in the lavas of the outer aureole: (i) chl-ab halos (or cc-free halos), (ii) ep-halos and (iii) cc-bearing halos. The latter two have already been discussed from within the actinolite and epidote zones (chapter 6). The chl-ab halos (cc-free) show an interesting feature with respect

to elemental mobility during vesicle wall-rock alteration. These halos are well developed in one of the lava samples (014) from the contact aureole.

Sample 014 is an aphyric fine-grained vesicular basalt. The primary mineral composition may have been labradorite, augite, magnetite, ilmenite and glass(?). The lava suffered extensive hydrothermal alteration which resulted in the complete loss of glass (?) and primary fsp, and partial loss of px and ore. In general the fsp is replaced by ab (+cc,ep), the px and glass(?) by chl (+cc,ep) and the ore minerals by hm(?),sp, py. The lava further appears to have experienced an extensive (patchy) cc-ep overprinting, so that cc-free halos surround the lava amygdales and cc-free patches exist within the lava matrix.

The lava amygdales have a diameter range from <1 mm to ca. 5 mm and compose ca. 12 % of the thin-section area. The smaller amygdales are filled by chl-ore(mt or hm and py), while the larger amygdales additionally contain strained qtz, ep, cc. One vein of ep-cc clearly cross-cuts an amygdale which was earlier infilled by chl-ore assemblage. The vein related ep-cc deposit appears to have impregnated the earlier formed chl without causing any visible alteration of the chl.

Calcite-free amygdale wall-rock zones typically surround the amygdales (e.g. vesicle diameter ca. 2 mm, width of halo zone ca. 1 mm). The wall-rock zones are composed exclusively of chlorite-albite. The cc-free patches within the lava matrix appear to be composed of chl-ab-ore-sp, while the extensively carbonized matrix elsewhere additionally contains partly altered px, cc, ep.

The chl-ab halos (cc-free) suggest that an early alteration event resulted in the complete replacement of the primary minerals

by chl-ab. Part of the Fe from the ore minerals and the px, and Mg from the px may have been used in the formation of the chl, additionally requiring Al from the primary fsp and Si from either fsp or px, while the primary fsp was replaced by ab. Excess Ca must have been removed by the reactive fluid from the reaction zones and carried away by the fluid. Part of the mobilized Fe may have been used to the formation of the vesicle ore, while the remaining elements (e.g. Ti) must have been carried away by the fluid. Therefore, the cc-free halos may simply be due to the total lack of Ca to form calcite (and ep). Within the cc-free patches in the lava matrix, primary fsp and px had already been replaced by chl-ab prior to the cc-ep overprinting event, while in the extensively carbonized parts of the lava matrix both primary fsp and px were available reactants.

The apparent simplicity of the case example above may be used to explain the epidote- and calcite halos found within the contact aureole, and elsewhere, in relation to the porosity and permeability. In the example above the essential mechanism for the primary mineral alteration is passage of reactive fluid through the rock. The extent of the fluid-rock reaction evidently related to the porosity/permeability as the rock became completely altered in the vesicle wall--rock zones but only partly altered elsewhere in the rock. Therefore, the development of epidote- and calcite vesicle halos elsewhere may relate to the presence of reactants in areas of high porosity/permeability.

A further feature of interest in the contact aureole (sample 013) are the poorly-developed cc-free halos around some amygdales, in contrast to cc-bearing halos around others. Within one of these cc-bearing halos, the primary ore-cubes are absent, while irregularly elong-

ated 'strings' of opaque minerals are present, being an order of magnitude larger than the primary ore grains in the surrounding rock. These secondary opaque strings (hm?) are only found within this halo zone and may be due to solution of the primary ore and redeposition as secondary ore which was later enveloped by calcite. The halo is thus composed of chl-ab-ore-cc with the presence of cc being possibly related to the former presence of primary px and/or fsp in the halo which later reacted with the cc-precipitating fluid.

To conclude this discussion on secondary mineral halos surrounding lava amygdales, the reader is referred back to figs. 6.13 and 6.14. The lava sample (069) depicted was collected some 300 m above and laterally ca. 1 km to the east of the Geitafell gabbro and contains cc-bearing halos around the amygdales. Within the latter early limonite botryoids appear to have been mobilized and redeposited as mt or hm together with cc. It was suggested (p. 200) that the phenomenon provided evidence for a hydrothermal boiling zone (or a self-sealing zone). The relationship between the time of the metamorphism caused by the gabbro, and the amygdale textures in- and outside the contact aureole is obviously important and the conclusions are summarized below.

7.3 Summary.

Within and beyond the gabbro aureole the amygdale-filling sequence had extended into infilling episode 3 before the intrusion of the gabbro. After the intrusion a narrow zone of hornfels was formed around the gabbro and a metamorphic fluid-flow was established which gave rise to salitic, ferroaugitic, ferrohedenbergitic, hedenbergitic pyroxenes and (apparently) garnet within the inner aureole. The (hydrous) fluid involved may be assumed to have been at supercritical temperatures. Towards the outer aureole the deposition of skarn

pyroxene in amygdales is likely to have been contemporaneous with a prolonged deposition of andraditic garnet. Calcite inclusions in the garnet may be evidence for the former presence of CO_2-containing fluids in this environment, although calcite was not deposited within the contact lavas at this time. Still further out ep-act-chl-qtz--ore was deposited in some lavas, while elsewhere passage of highly reactive fluid appears to have resulted in deposition of chl-ore in amygdales and replacement of rock matrix by ab-chl to an extent controlled by the porosity and permeability. During this event both Ca and Fe were driven out from the host rocks into the hydrothermal fluid. At the outer fringe of the contact aureole amygdale limonite was contemporaneously metamorphosed to magnetite-hematite in isolated situations (figs. 6.15, 6.16).

Outside the contact aureole extensive deposition of calcite took place above and around the gabbro (figs. 6.13, 6.14). With time, however, the altered rocks in the contact aureole subsequently became extensively overprinted by calcite-epidote and other hydrothermal alteration products.

The extensive calcite deposition at high levels within the volcano indicates the former existence of a self-sealing process (and/or a boiling zone) above and around the gabbro heat-source. A boiling of the hydrothermal fluid, however, would be expected to have commenced in the gabbro contact aureole and to have progressively moved upwards and outwards with time until, with cooling, it ceased. The different times of calcite formation within the volcano may thus provide evidence for the likely sequence of events discussed above.

The most important conclusion,however, is that there is an overall consistency of alteration processes at all levels in the volcano available for study, indicating that a high-temperature hydrothermal system was established in the wake of the emplacement of a large, high-level heat source, namely the gabbros of intrusive phase 2.

CHAPTER 8

COMPARISON AND SUMMARY OF ALTERATION PROCESSES

8.1 The Central and the South-Western Half of the Volcano.

Hydrothermal processes affecting the central (Svinafell) area and that forming the south-western half of the volcano (Vidbordsfjall, Graenafell and Jokulfell) have only been given a broad reconnaissance study. However, a crude mirror image of the index-mineral zonal patterns in the NE-half of the volcano is observed for the SW-half (map II), while the topography clearly controls the pattern of the mapped mineral zones. The mineral zones in the SW-area are much as shown in the maps by Annels (1967) and Newman (1967), although the actinolite and sulphide zones are new (map II).

A few important points relating to the chronology of the hydrothermal and metamorphic events are discussed below. Most have emerged from the study of the gabbro complex in Vidbordsfjall which comprises several generations of gabbro injections which, on the basis of cross-cutting relationships, are grouped within intrusive phases 2 and 10 (chapter 3). The earliest gabbro on Vidbordsfjall (unit C) is cross-cut by vein systems similar to those in the Geitafell gabbro; earlier veins include act,sp,ep, and qtz,cc,z compose the later veins. The remaining three gabbro units (A,B, and D) of intrusive phase 10 on Vidbordsfjall show different alteration patterns, where early actinolite-bearing veins only occur at the margins of the gabbros (units B and D). This implies that an early hydrous fluid did not permeate

all the gabbro bodies following their emplacement, as was the case for gabbro unit C in Vidbordsfjall and other gabbros belonging to intrusive phase 2. The central portion of the late gabbros includes vein mineral deposits mainly of cc, qtz, pr, z. The extent of hydrothermal overprinting with respect to the types of mineral veins is thus less within the central portion of the late gabbros than in the older gabbros. The difference between the early and late gabbros with respect to actinolite is indicated by the actinolite zone (map II). The finer details of the zonal patterns, however, still require further study.

In a broad sense the alteration differences between the younger and older gabbros relates to evolution of the hydrothermal system within the volcano. A physical control by the volumes of the gabbros with respect to the surrounding fluid-containing country rocks might also have played some part in the alteration pattern. The whole Vidbordsfjall gabbro complex covers an area of ca 3.5 x 2.0 km, including narrow screens of altered host rocks between the gabbro units (see fig. 3.1), while the earlier gabbros of intrusive phase 2 are elongated bodies covering areas of ca 2.0 x 0.5 km (Geitafell, Valagil and unit C in Vidbordsfjall). The small gabbro bodies of phase 10, however, like those of Kraksgil and Litla Dima appear hydrothermally altered throughout in a fashion similar to that of the early gabbros and the marginal facies of the late gabbros. This may imply that the volume of the gabbro bodies was a factor governing the extent of early fluid percolation via shrinkage joints, e.g. through variation in joint patterns from margins to centres. Because of lack of data this cannot be verified, although the volumetric relation between host-rock fluid and the size of an intrusive body are likely

to have been important. Nevertheless, the late gabbros were injected into an evolved hydrothermal system within which the CO_2-content of the fluid increased with time. The overall tectonics were also different ; uplift of the volcano accompanied intrusion of the early gabbros, while the late gabbros accompanied the caldera formation. Different paths of fluid movement might thus play a role in the alteration differences, since they were also affected by the flexuring of the volcano which created prominent dilational fractures and occurred shortly after emplacement of the late gabbro.

Contact metamorphic hornfelses (a few tens of metres wide) occur at the east side of gabbro unit B. While these are very similar to the Geitafell gabbro hornfelses, a noteworthy difference concerns the presence of contact metamorphosed members of intrusive sheets of phases 5 and 6 within the exposure, clearly demonstrating the time relations between the gabbros and the hydrothermal events. A "thermal boost" to the hydrothermal system must have been provided by the late gabbros to maintain the high-temperature hydrothermal system. This heating event is possibly manifested within the host-rock amygdales by the formation of a second generation of andradite as described below.

The early amygdale filling sequence, studied in samples from the Vidbordsfjall-Graenafell area, is identical to that in the NE-half of the volcano (chapter 6) and thus does not need description. The secondary alteration of the early infillings in the two areas is also similar. The contact aureole around the Vidbordsfjall complex, shows similarities to that of the Geitafell gabbro, e.g. showing development of the ferrosalite within the amygdales. A noteworthy difference, however, is found in sample 9 23/8'77 from the host-rocks

between gabbro units C (phase 2) and D (phase 10)(see fig. 3.1). The sample shows the same range in amygdale sizes and a combination of amygdale textures as already described from the Geitafell aureole but the largest vesicles also contain turbid assemblages of fs-gt--K.fsp-ep-act-chl-stb close to the vesicle walls and clear central fillings of gt-ep-cc-stb-heu. The andradite in the centre is entirely free of inclusions and often grows around earlier andradite grains which contain numerous inclusions of (?)pyroxene and (?) other minerals. The presence of two andradite generations has only been found within this sample and may suggest that two fluid pulses of similar type; related to the two separate gabbro units respectively, permeated the host-rock.

The shape of the mineral zones in the Vidbordsfjall aureole (map II) is also worth comment: To the south and SE the mineral zones extend farthest away from the gabbro at low altitudes while higher (above 400-500 m) the mineral zones lie close to the gabbro contact. Furthermore towards the NW into Graenafell, the chlorite zone disappears due to the steep NW dip (ca 20°) of Hyaloclastite Unit II in Graenafell and the height. A similar topographic effect on the shape of the mineral zones in addition to the regional dips is also seen in the NE-half of the volcano. The mineral zones are therefore dome-shaped within the volcano and the highest-grade zones reach their highest levels at the contacts of the major intrusions.

The sulphide zone inside the caldera (see NW-sector of Map II), extends across the NW-half of the volcano, overprinting both the chlorite- and epidote zones. While the formation of the sulphides at the upper stratigraphic levels within the volcano may have extended through the lifetime of the high-temperature hydrothermal system (section 5.2),

the presence of pyrite-zeolite veins in intrusive phase 12 dykes and faults related to the flexure zone (chapter 3) appears to cast light on the chronology of the structural events; (i) the caldera subsidence and (ii) the flexuring. Outside the caldera but within the flexure zone, sulphide mineralization is not prominent in phase 12 dykes. Inside the caldera, however, both the variation with depth in the low--grade hydrothermal alteration of phase 12 dykes and their pyrite, zeolite, calcite vein systems (chapter 5) clearly indicate that the high-temperature hydrothermal system had cooled substantially prior to intrusive phase 12, while the hydrothermal system of the Geitafell volcano was not extinct. The extent of the sulphide occurrence within the NW-sector of the caldera and the distinctive partial relation of sulphidization to phase 12 dykes is clear; further evidence regarding timing of the flexure zone was discussed in section 3.3.5.

8.2 The Flank Areas of the Volcano.

Outside the chlorite zone in the flank areas (map II), the rock replacement minerals include : smectites, limonite (or iron-oxides), celadonite, iddingsite, calcite, quartz and zeolites (see discussion below). The amygdale infillings include : mud deposits, limonite, jasper, opal, chalcedony, quartz, calcite, smectite, celadonite and the zeolites : stilbite, heulandite, mordenite, scolecite, mesolite, thomsonite, chabazite and analcime. Most of these minerals are also found in veins.

The early vesicle filling sequence in the flank areas is similar to that in the caldera (table 6.1) up to infilling period 3a . The subsequent mineral deposits in vesicles and veins are characterized by quartz and calcite deposits, the formation of which may have

lasted throughout the lifetime of the volcano's high-temperature hydrothermal system. During this time silica deposits (opal and jasper) and smectites may also have been formed, in particular at the upper stratigraphic levels and close to the active hydrothermal system. It is probable, though unknown, that zeolites formed within the flank areas during this period. Nevertheless, it is clear that the zeolite deposits in general were superimposed on the earlier--formed amygdale deposits in the flank areas.

The zonal pattern of zeolite deposits in active high- and low--temperature geothermal fields in Iceland and their regional distribution on eroded strata was discussed in chapter 1 (pp. 7-9). The regional zeolite zonal boundaries are considered as indicative of palaeo-isothermal surfaces, the zeolite zones being with increasing depth : 1) chabazite-thomsonite, 2) analcime, 3) mesolite-scolecite and 4) laumontite (see chapter 1 and fig. 1.2). Two zeolite zones were mapped by Annels (1967), a lower analcime zone, characterized by analcime and chabazite amygdales, and an overlying chabazite-thomsonite zone, containing chabazite, thomsonite and sometimes opaline silica amygdales. Both zones occur within Basalt Lava Unit III in the Grasgiljatindur-Gjanupstindur area (see map I and II), and Annels' map is accepted as substantially correct although the analcime zone may extend further downwards into Hyaloclastite Unit II. Annels did not group the underlying zeolite occurrences with Walker's (1960) mesolite-scolecite zone. However, the type of zeolites listed above and their general late origin do justify inclusion of these occurrences within the mesolite-scolecite zone; this has been superimposed on the Geitafell hydrothermal system (chapters 5 and 6).

Within the NE-half of the volcano the mesolite-scolecite zone there-

fore extends from within Hyaloclastite Unit II in Efstafell downwards through the volcano.

Within the SW-half of the volcano the mesolite-scolecite zone is also superimposed on the volcano, and extends further upwards into Basalt Lava Unit III in the Vidbordsdalur area in the NW (see map I or II). The stratigraphically discordant zeolite zones appear to relate to regional zeolitization and have already been used in chapter 2 (pp 38-39) as evidence for the volcanological/structural chronological sequence (chapter 3, p.91 and table 3.1, p. 95).

In chapter 2 it was shown that only the lowest 100 m of Lava Unit III formed as the final product of the Geitafell volcano. Within these lavas, (e.g. in Austurgja), extensive jasper deposition took place which may be related to near-surface deposition from the underlying hydrothermal system. Inside the caldera, jasper veins were amongst the earliest vein systems (chapter 5). In the flank areas, however, jasper veins are also found along late dykes (phases 10 and 11) and extensive jasper formation is found within Lava Unit II in Hoffellsfjall (flank area). Therefore, the jasper deposits in the central volcanic region may have been formed throughout the lifetime of the Geitafell hydrothermal system.

The jasper deposits in Hoffellsfjall have been excavated for exterior domestic decoration. Thick calcite veins also exist in Hoffellsfjall (flank area) and were mined by local farmers some 40 years ago for use in optical instruments. One of the largest single crystals of iceland-spar ever found (ca. 170 kg) was found in Hoffellsfjall. According to Gísli Arason (curator of a museum in the Hofn village), who took part in the mining operation, large crystals were extracted from a small cave occurring between a lava and a dyke margin. Stalag-

mitic iceland-spar covered by stilbite plates, grew from the cave's roof and floor, while the largest iceland-spar crystals were dispersed on the floor. These mines have long since become covered by screes, although calcite veins up to 1.5 m across (mostly turbid calcite) can still be found on Hoffellsfjall.

While calcite formation in the flank areas may have occurred throughout most of the lifetime of the high-temperature hydrothermal system the most extensive formation appears to be of rather late origin, possibly contemporaneous to the caldera event. Many of the calcite veins in Hoffellsfjall occur along late dykes (e.g. phase 9) striking NE-SW, and calcite veins clearly cross-cut intrusive sheets of phase 5. In Efstafellsnes (study locality 6, section 5.2) thick calcite veins also occur and appear time-related to the caldera event, supporting the hypothesis for (generally) late calcite formation suggested above. Finally, the stilbite deposit on the iceland--spar stalagmites may be correlated with the zeolite formation elsewhere being the latest mineral deposition in the flank areas.

The hydrothermal mineralogy in the flank areas provides information concerning the host-rock alteration described below (8.3). Calcite, quartz and zeolites have sometimes partially replaced their host-rocks in the flank areas. Chiefly it is the volcanic glass which has been replaced but also the feldspar to various extent. Most commonly, however, the host-rock replacement of this type is confined to localized development of the hydrothermal minerals, as in vein wall-rock zones.

The most common replacement minerals in basaltic rocks are those of the smectite group, which chiefly appear to replace glass. This type of host-rock alteration is found everywhere within the host-rock

matrices, and is thus not confined to localized occurrences. A typical occurrence of flank-rock smectite is shown in figure 8.1. Brown to yellow and green smectite fills the amygdale (ca.2 mm across), and brown to green smectite is also seen dispersed within the fine-grained basaltic matrix, apparently or chiefly replacing former basaltic glass. The possibility of early growth of smectites (infilling period 3a, chapter 6) has been discussed in description of the hydrothermal system (see chapters 6 and 7), although all evidence relating to its former presence has been obliterated by subsequent high-temperature alteration. Clearly smectite has replaced volcanic glass in the flank areas in low-grade hydrothermal environments, suggesting that the volcanic glass within the later high-temperature system had already been at least partly transformed to smectite, thus providing a different reactant for later hydrothermal fluids.

Most of the (sparse) olivine in the lavas may similarly have been transformed to iddingsite at an early stage. Within the flank areas some olivine phenocrysts may be found (figure 8.2), partly pseudomorphed by typical iddingsite.

Limonite (or hematite) is a common alteration product within the flank area host-rocks, partly replacing the ore and glass, in both basaltic and acid rocks. Fig. 8.3 shows flow alignment of feldspars in a lithic fragment in acid tuff of Rhyolite Unit II, occurring outside the chlorite zone in Efstafell. The red iron-oxide more or less obscures the fine-grained matrix within a discrete zone parallel to the flow alignment. The limonite (or hematite) also impregnates the andesine phenocrysts along cleavage planes forming thin films (micron widths), showing clearly in the photo as the section is cut oblique to the cleavage planes. The green alteration mineral elsewhere in the rock is celadonite.

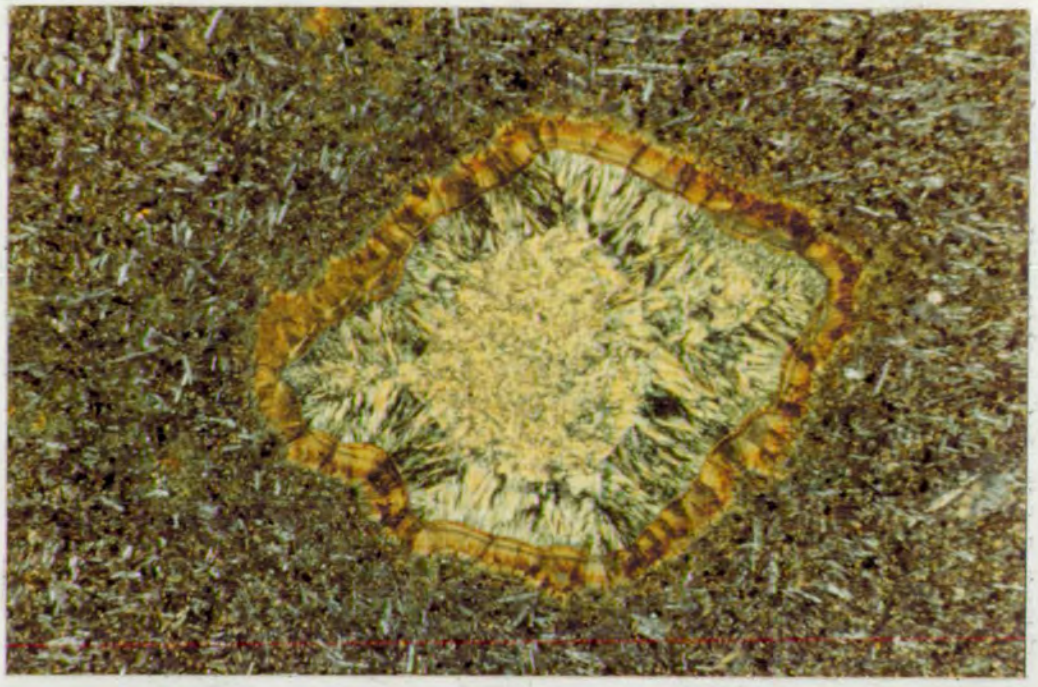

Figure 8.1. A basaltic lava sample (194) from the flank area in Hoffellsfjall. The amygdale (ca. 2 mm across) shows a brown to yellow green smectite. Smectite also replaces basaltic glass within the matrix.

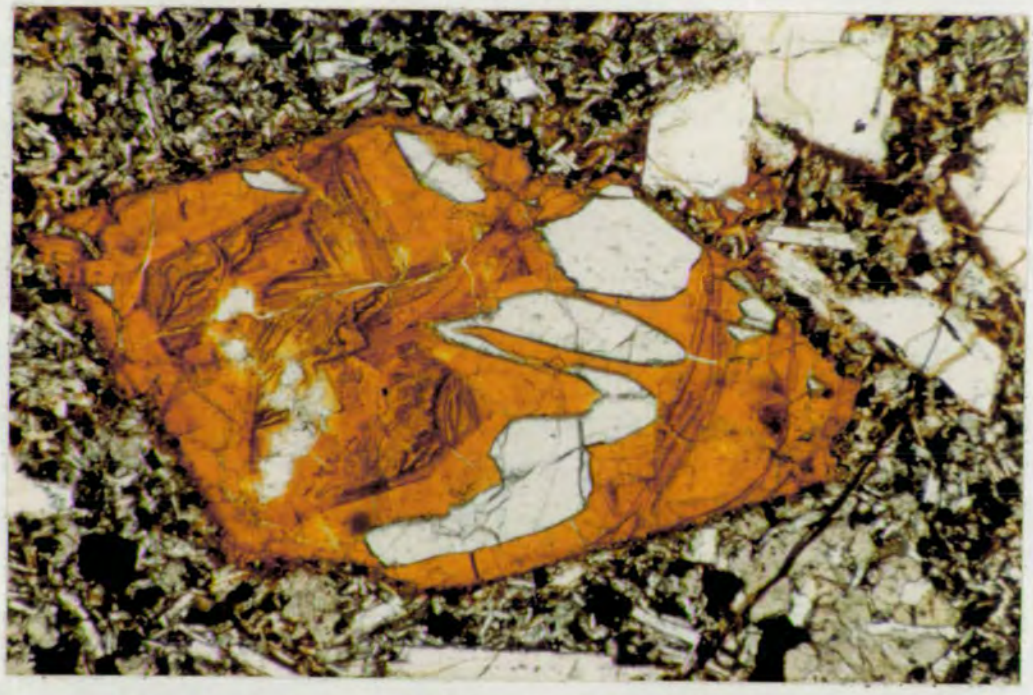

Figure 8.2. Olivine tholeiite lava from the top of Geitafell, outside the chlorite zone (sample 155). The olivine phenocryst (ca. 2 mm long) is partly pseudomorphed by iddingsite.

Figure 8.3. Acid rock from Efstafell (sample 159) showing flow alignment and andesine phenocrysts (the larger is ca 2 mm long).

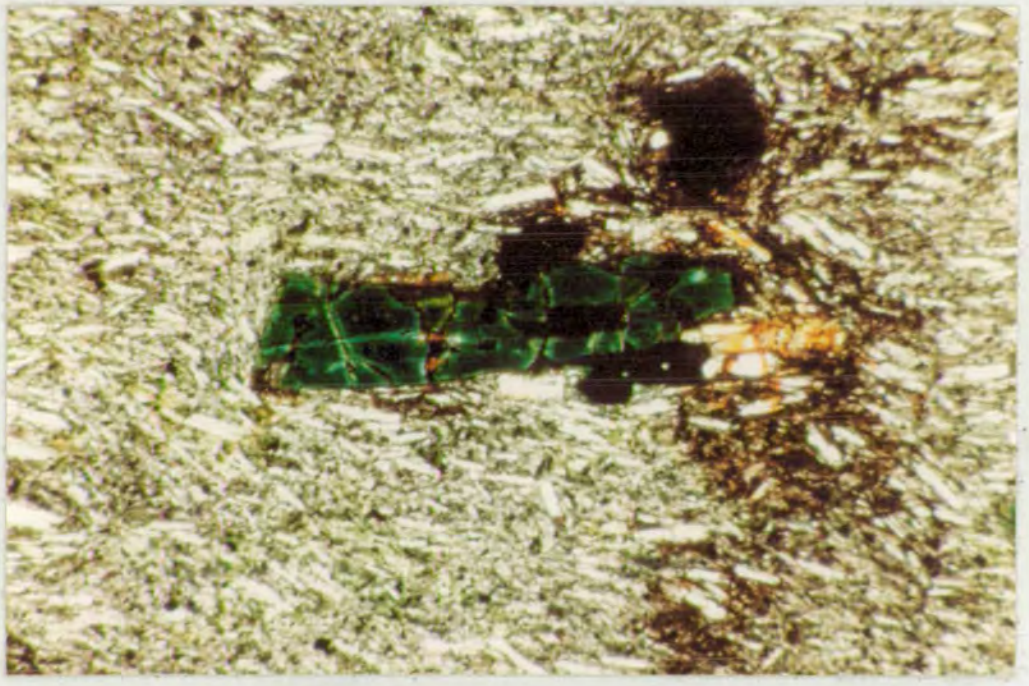

Figure 8.4. Same sample as above. Some of the andesine phenocrysts are completely replaced by deep green celadonite, but also contain the 'iron-oxide' films. The pseudomorphed andesine is 1.2 mm long. Celadonite is also found to replace sparse augite phenocrysts in the sample, and sparse magnetite phenocrysts are also found, marginally replaced by the 'iron oxide'.

Celadonite occurs within the acid rocks. It contains up to 9% K_2O and belongs to the illite family of clay minerals. It is characteristically deep green - one of the finest examples being shown in figure 8.4. Apart from replacing the acid glass it also partly pseudomorphs the andesine and pyroxene phenocrysts. Within the pseudomorphed andesine the 'iron-oxide' films can also be seen. The sparse magnetite phenocrysts of the rock can also be seen marginally replaced by the 'iron-oxide'. The distinctive celadonite formation within the acid rocks presumably relates to the high potassium content of the acid rocks.

In conclusion, the potential host-rock reactants within the extrusive rocks of the Geitafell high-temperature hydrothermal system were : feldspars, pyroxene, magnetite, ilmenite, olivine-iddingsite, limonite-hematite, smectites, volcanic glass, and locally celadonite.

8.3. Host-Rock Alteration and Summary.

In chapter 4.4 it was stated that a description of the host-rock alteration would be combined with a summary in chapter 8.3. In chapters 5-8.2, vein wall-rock alteration zones, amygdale wall halos and intrusive rock alteration within the hydrothermal system, and the flank area host-rock alteration (unrelated to mineral veins) were described. The conclusions from these studies concerning the hydrothermal alteration of the host-rocks are discussed below.

Vein wall-rock alteration zones appear associated with all the mineral vein systems at all stratigraphic levels. However, the extent of these zones varies greatly from non-existent or hardly discernible from the surrounding host-rock replacement mineralogy, to well-developed wall-rock zones of various widths. The wider mineral veins of each vein system usually show better developed and wider wall-rock alteration zones, a feature probably related to high fluid/rock ratio. In general, clearly developed vein wall-rock zones are more commonly found at the deeper stratigraphic levels, particularly within the actinolite zone.

The mineral veins are normally found to relate to their associated wall-rock zones by containing one or more minerals in common. As with the mineral veins the wall-rock zone mineralogy varies with (i) time, and (ii) depth.

All the rock replacing hydrothermal minerals found within the vein wall-rock zones are also found elsewhere within the extrusive rocks. However, the extent of rock replacement by hydrothermal minerals shows a positive correlation with porosity. The former pore fluid and the vein fluids within each mineral zone were closely re-

lated during each depositional time period, as indicated by the filling sequences of the amygdales and veins. This suggests that the hydrothermal fluids flowing through the fractures (later mineral veins) also pervaded the host-rocks, and therefore, a time sequence for the host-rock alteration can be established from the secondary mineralogy of the vein wall-rock zones, and to a lesser extent from the vesicle halos. Such chronology for the primary mineral breakdown and the development of secondary minerals has already been established for the Geitafell gabbro in table 5.1, and could be provided for the denser intrusive rocks from elsewhere within the volcano.

In establishing a detailed history for the hydrothermal alteration of the extrusive rocks, there are problems related to the overall anisotropy of the extrusive rock porosity. The distribution of open fractures during each time period of the hydrothermal system reinforces (locally) the anisotropic nature of the permeability, while the overall effect of open fractures is to reduce the anisotropy related to pore distribution. The fluid permeation anisotropy may temporarily and locally allow different fluids (with respect to mineral precipitates) to exist within the host rocks. The result is visible within the amygdales, since the complete filling sequences are not present in all amygdales of similar size within each sample (e.g. figures 6.4 and 6.6) while the general correlation of amygdale filling sequences to (i) vesicle size and (ii) mineral veins, holds in each area. Similarly the type of rock replacement may have been variable within the rocks, even on a hand-specimen scale. The overall tendency of a hydrothermal system, however, is to force the hydrothermal fluid of each time period through the rock matrices tending towards homogenisation of the rock replacement assemblages. For in-

stance, within the outer parts of the actinolite zone, the chl-ab assemblage is widespread within the lavas, while the act-ab assemblage occurs locally. But closer to the centre of the zone (e.g. in Kraksgil) the act-ab assemblage becomes more widespread while chl progressively disappears from the assemblage. The chl disappearance is rather irregular, apparently as a result of permeability variation which allows for variation in fluid properties (e.g. f_{CO_2}). Both chl and act may thus have been formed simultaneously within the rock, despite the fact that the amygdale textures suggest later formation for the act (e.g. fig. 6.6 and 6.7). The situation is further complicated in the fossil hydrothermal system by the overprinting of subsequent alteration assemblages upon earlier ones within the rock matrices. The result of all this -porosity/permeability variation and overprinting is that the hydrothermal alteration:

1) is commonly incomplete while the extent of rock replacement hinges on the porosity/permeability character, and
2) includes metastable rock replacement mineral assemblages, which may be variable over short distances - related to some or all the hydrothermal events.

Therefore, the only practicable way to relate rock replacement assemblages to time is from the characteristics of the vein wall-rock zones and where present, vesicle halos while the porosity/permeability needs be kept in mind for univariant mineral assemblages, in view of the textural variation observed within amygdales over a scale of a few cm.

Of fundamental importance also is the related matter of the former fluid/rock ratio (sensu lato) as the fluids were moving. The type of host-rock alteration may depend on this relationship as has

been demonstrated by the chl-ab amygdale halos (cc-free) in the contact aureole of the Geitafell gabbro. This example provides insight as to the course of hydrothermal rock alteration. The halos were composed of chl-ab, produced by reaction between hydrothermal fluid and the primary rock constituents. The reaction locally reached completion, driving all available Ca from the primary minerals into the fluid phase. A later hydrothermal fluid pervaded the same rock and reacted with Ca-bearing primary minerals (fsp-px) to precipitate cc and ep. Again, depending upon available reactants, and high fluid/rock ratio (sensu lato), the ep- and cc-bearing halos can be explained, as well as the various vein wall-rock alteration zones, and the extent of subsequent overprinting events on both. The extent of overprinting was demonstrated by the cc-free halos in the contact aureole - a situation also applicable to the vein wall-rock zones in figures 5.3 and 5.2 c. The same general principle is evidently applicable to all the hydrothermally altered rocks. One may conclude that the three factors governing the extent and type of hydrothermal rock alteration were : a) availability of reactants, b) fluid/rock ratio, and c) degree of physico-chemical instability between fluids and rock. To this d) time may be added as a further important parameter.

Except very locally the abundant presence of primary reactants may be assumed. The fluid/rock ratio (sensu lato) was dependent on the porosity and permeability while the degree of physico-chemical instability between fluids and rocks requires further discussion.

In general, from the development of the vein wall-rock alteration zones in relation to the vein systems, it is obvious that the rocks and fluids were at all times in disequilibrium. The consequent degree of instability also varied between the hydrothermal fluids of each

period, and may be envisaged by the extent of secondary mineral formation within the rocks in relation to each fluid system. However, detailed understanding would require a knowledge of the time component involved for each fluid system and similarly a knowledge of the fluid/rock ratio is essential. On the other hand, the type of secondary products related to each fluid system can be determined allowing evaluation of the physico-chemical details. A list of the most obvious mineral reactions is provided in chapter 4.3.4. (p.126). Most of the listed reactions are not isochemical and need removal or addition of various elements and (commonly) addition of H_2O, S and CO_2 by the hydrothermal fluids. Apart from the reaction products providing andradite and ferrosalite (not found as rock replacement product), all the other breakdown products (p.126) existed within the actinolite zone. Within the lower part of the epidote zone, all the reactions involving actinolite can be omitted from the list for the extrusive rock alteration, while actinolite was formed locally within intrusive phases 5 and 6. Sphene as a biproduct of feldspar- and pyroxene reactions with fluids can similarly be omitted, as can (probably) the formation of magnetite from limonite within the rocks. In the upper part of the epidote zone, wairakite may be omitted from the list of feldspar breakdown products. Apatite occurrence within both index mineral zones is restricted, as is that of olivine and its associated breakdown products. Orthopyroxene has only been found within the gabbros. Finally, oligoclase is only occasionally found as a replacement mineral of the primary feldspars. Volcanic glass has been deliberately omitted from the list since its former presence during the evolution is unclear. A low-grade breakdown sequence of volcanic glass, however, was discussed along with the description of

rock alteration in the flank areas. We are therefore left with relatively few abundantly occurring hydrothermal breakdown products within the host-rocks. A simplified time sequence for the formation of the rock replacement minerals is presented and discussed for the remainder of this section. Somewhere in the rocks in each mineral zone the secondary minerals were replacing all the appropriate reactants in accordance with the list of reactions provided on page 126, and the time sequence below. The characteristic rock replacement minerals are underlined.

I. Limonite, and/or hematite, were the first to be formed everywhere within the volcano and can be related to oxidizing environments in cold ground water. As a result of slow rise of the geothermal gradient, their formation was prolonged and succeeded by,

II. Smectite, iron-oxides, iddingsite, celadonite and possibly silica mineraloids and minerals developed upon further rise in the thermal gradient within the later high-temperature hydrothermal system.

III. Chlorite, albite, hematite, sphene, and quartz may have been formed at low levels (vein system 2b at study loc.1), with the assemblage gradually moving upwards to take over from rock replacement assemblages related to II above, prior to the injection of the centre gabbros (intrusive phase 2). Following gabbro emplacement vigorous rejuvenation of the hydrothermal fluid system occurred and

IVa. contact metamorphic hornfelses formed at the gabbro contacts, extensive chlorite-albite rock replacement occurred locally within the contact aureole, with development of actinolite-albite-sphene-

-epidote elsewhere, while ferrosalite-andradite-magnetite grew locally within the lava vesicles.

IVb. Stratigraphically below the gabbro, outside the contact aureole, extensive rock replacement, identical in type to III above, may have continued, but was quickly superimposed by V (below) associated with intrusive phases 5 and 6.

IVc. Above and outside the gabbro aureole, extensive rock replacement by calcite seems to have occurred, possibly related to a boiling zone above the gabbro. CO_2 was probably supplied to the hydrothermal fluid by magmas of intrusive phase 2. Uplift of the volcano accompanied emplacement of the central gabbro. Fluid channels from below were locally provided by the radial dykes of intrusive phase 3. Sulphur may similarly have been fed into the fluid system by the early magmas, leading to ore replacement by pyrite and chalcopyrite, particularly in the neighbourhood of the gabbros.

Clearly a high temperature hydrothermal system was established at high levels within the volcano following emplacement of intrusive phase 2. Additional heat and gas (CO_2,SO_2,Cl ?) was supplied to the hydrothermal system by the cone-sheet systems of intrusive phases 5 and 6.

Va. Within both the epidote and the actinolite zones early interaction took place between the hot intrusives (phases 5 and 6) and the surrounding fluid system within the host rocks. This caused extensive actinolite-sphene replacement of augite and ilmenite respectively within the intrusive rocks, and perhaps less extensive albite-adularia replacement of the feldspar, which however, is not discernible from subsequent alteration of the feldspar.

Vb. Within the actinolite zone extensive rock replacement by actinolite-sphene-albite-adularia-epidote-hematite?-magnetite? began, and eventually completely replaced some of the denser basaltic lavas in the centre of the zone (e.g. in Kraksgil), and also rocks of higher porosity. At other places within the actinolite zone rock replacement by chlorite rather than actinolite may have persisted.

Vc. Within the lower-part of the epidote zone extensive rock replacement by chlorite-albite-adularia-sphene-epidote began, and was maintained throughout the active lifetime of the high-temperature system.

Vd. Within the upper-part of the epidote zone the type of rock replacement was identical to that in the lower part of the zone, except that the epidote formation was somewhat restricted to vein wall-rock alteration zones. Also of somewhat restricted distribution was the replacement of ilmenite by sphene. Locally, however, the ilmenite was replaced by the formation of TiO_2 as fine-grained material (leucoxene, anatase, rutile or brookite?). In addition, rock replacement by calcite,quartz, pyrite and chalcopyrite, and possibly smectite, appears to have been maintained throughout most of the lifetime of the high-temperature hydrothermal system within the upper-part of the epidote zone. Of somewhat later origin additional rock replacement by :

VI. Prehnite, wairakite, quartz, calcite occurred within the actinolite zone and particularly within the lower-part of the epidote zone. The evidence is provided from the type of vein systems cross-cutting intrusive phases 5 and 6.

Once the intrusive rocks had cooled to ambient temperatures, they became hydrothermally altered as other host-rocks, while the alteration of the densest intrusives (e.g. the gabbros) was chiefly related

to vein wall-rock alteration. The high-temperature hydrothermal system was maintained for some 2-3 x 10^5 years, overlapping in time with intrusive phases 7, 8,9 and 10, and part of phase 11 and the caldera collapse. The host-rock replacement mineralogy was similar to Vb-d above and evolved to include VI above. Judging from the development of various mineral veins with one or more minerals in common (e.g. the vein generations of system 3a, study loc. 1), the host rock replacement mineralogy may have changed with time to include only part of the rock replacement assemblages in each area, listed by Vb-c and VI above. Insufficient data, however, on the time sequence of the vein fluid generations within the vein systems does not allow for rigid classification, the recognition of which might still be of importance. For instance, the presence of laumontite as a part of one of the vein generation of system 3a (loc.1, see p. 137) might imply a temporary cooling of the hydrothermal system prior to the caldera event - a possibility which requires further study - while at present the formation of the complex vein system 3a in the actinolite zone overlaps the high-temperature hydrothermal system, suggesting that the low-temperature zeolites of vein system 3a may post-date the high-temperature system (see also chapter 11).

No separate widespread early alteration appears to have accompanied intrusive phases 7, 8 and 9, the intrusive sheets and dykes showing hydrothermal alteration indistinguishable from the host-rock alteration elsewhere. This may relate to lack of data - but at present it is known that the hydrothermal fluid system had evolved considerably from the time of the emplacement of intrusive phases 5 and 6, e.g. where both CO_2 and sulphur had been added to the fluid system. This may have played a part in changing the nature of interaction

between hot intrusive rocks and hydrothermal fluid. Intrusive phases 8 and 9 (fine-grained basaltic sheets and dykes) may also have cooled more rapidly than the much coarser-grained dolerites of phases 5 and 6.

The gabbros of intrusive phase 10 (e.g. in Kraksgil, Litla Dima and the marginal facies of the Vidbordsfjall gabbro complex), however, show early alteration similar to that of the older gabbros and intrusive phases 5 and 6, while actinolite did not develop within the feldspar-phyric dykes of phase 10 in the NE-half of the volcano. Intrusive phase 10 took place at the same time as the caldera and overlapped in time with the emplacement of intrusive phase 11. The effect of these intrusive/structural events is clearly discernible within the rock replacement assemblages as well as in the vein- and vesicle mineral deposits. Within the caldera fault region and the spatially related gabbro intrusives:

VIIa. a thermal boost to the hydrothermal system is indicated by the formation of new metamorphic hornfelses, and the development of ferrosalite and a second generation of andradite in the gabbro contact aureoles, and a :

VIIb. prolonged development of rock replacement mineralogy identical to Vb at low stratigraphic levels continued in the caldera fault region. Along the fault, however, rock replacement of type Vb was particularly intense in the Kraksgil area, possibly as a result of the combined effect of large quantities of fluid ascending in the fault region and intrusion of a wedge shaped gabbro body. Within this area albite-adularia deposits in vesicles (fig. 6.17) are widespread.

VIIc. At higher stratigraphic levels - now in the lower part of the epidote zone and far from the exposed gabbro in Kraksgil - rock replacement by type Vc is intense. Part of this may relate to the caldera event. Locally minute garnets were formed (fig. 6.22, 6.23) giving rise to a localised garnet zone within the epidote zone (see fig. 4.3 and 4.5). This is also probably time-related to the caldera event.

VIId. At still higher stratigraphic levels - now in the upper part of the epidote zone within the fault region - rock alteration by type Vc is locally very extensive (e.g. feldspar replacement by epidote--prehnite within some dykes of intrusive phase 10 and their immediate host-rocks).

Intrusive phases 10 and 11 may have been emplaced during a period extending from the caldera event until the emplacement of intrusive phase 12. This is reflected in the intrusive rock hydrothermal alteration. Some late members of both phases (10 and 11) contain fresh (or slightly devitrified) glassy margins and low-grade hydrothermal alteration suggesting that they post-date the high-temperature hydrothermal system. For instance, a late acid dyke in Kraksgil (greenschist facies lavas) occurs margin to margin with a member of intrusive phase 12. The acid dyke has flow aligned felsitic margins and a pitchstone centre. The dyke is not cross-cut by epidote veins as other earlier felsite (or felsitic) intrusives related to phase 11 in Kraksgil, described below. The overall hydrothermal rock alteration of intrusive phase 12 was described in chapter 5 and chapter 8.1. The two dykes of phase 11 and 12 in Kraksgil thus post-date the high-temperature hydrothermal system, as do some other members grouped within intrusive phases 10 and 11.

The hydrothermal alteration of the acid rocks has so far received but minor attention. Most of the extrusive acid rocks, however, are located outside the caldera, and belong to intrusive phase 11. The distribution of acid intrusions of phase 11 is shown in figure 3.15. One acid lava of Rhyolite Unit I is found within the caldera (map I). A noticeable difference from the hydrothermal alteration of the basic rocks is the lack of chlorite and amphibole in the secondary mineral assemblages although not entirely absent at low levels. Within and below the lower part of the epidote zone, the secondary rock replacement mineralogy in many members of phase 11 and older acid extrusives includes: turbid qtz-ab-clay(illite?), K.fsp, ep, py, cpy, hm, cc ; any former acid glass is always devitrified.

Within the upper levels of the volcano, the absence of epidote is noteworthy, and the characteristic replacement assemblage is <u>calcite-quartz</u>. The acid glass may be unaltered, while hydrothermal clays (celadonite - smectite ?) replace it to various extents elsewhere. The hydrothermal alteration of the acid intrusives of phase 11 at all levels may thus relate to the high-temperature hydrothermal system. However, during the emplacement period of the later members of intrusive phases 10 and 11, the thermal gradients subsided considerably, and a <u>low-temperature</u> fluid system was established within the volcano prior to intrusive phase 12. The timespan from the caldera event to intrusive phase 12 is not known.

The flexuring (chap. 3) of the volcano at much the same time as the caldera collapse thus appears to be correlated with the cooling of the hydrothermal system. The flexuring was accompanied by the development of prominent NE-SW faults and fractures through the vol-

cano which were attended by considerable volumes of hydrothermal fluid both inside and outside the caldera, as seen from the widespread presence of thick, late-stage calcite-bearing veins. The flexuring with its attendant fracturing, may thus have induced considerable cooling of the fluid system. In any case, cooling proceeded downwards with time, as seen from (a) the variation in the hydrothermal alteration associated with intrusive phase 11, with depth and time, and (b) the more extensive calcite and zeolite replacement of intrusive phase 12 dykes at depth.

The time sequence of the hydrothermal mineral deposits in veins and amygdales and rock replacement during the cooling period appears to have proceeded as below :

VIIIa: prehnite-quartz, calcite, laumontite, clay

b: quartz, calcite, laumontite, mordenite, smectite, pyrite, TiO_2.

c: calcite, laumontite, smectite, mordenite, stilbite, heulandite, quartz, pyrite.

Intrusive phase 12 injection,

VIIId: stilbite, heulandite, scolecite, quartz, calcite, smectite, pyrite,

e: stilbite, heulandite, chabazite, scolecite, thomsonite.

The characteristic minerals during each period (a-e) are underlined. From this list and comparison with the listed mineral reactions in section 4.3.4 (p.126), it is clear that chiefly the primary feldspars within the rocks suffered secondary replacement by calcite, quartz, and zeolites. The ore replacement by pyrite and TiO_2(leucoxene?) was locally extensive during periods b-c above, while pyrite was also formed in veins during period d above. Limonite-hematite may have formed within the rocks during VIIIa-e. Pyroxene may have been

replaced by calcite in vein wall-rock zones, while there was little or no pyroxene replacement by smectite, the smectite chiefly being found in mineral veins and as impregnations within vein wall-rocks. Glass in later intrusives, however, was transformed to smectite to various extent during the cooling history. Early zeolites were locally replaced by later zeolites (e.g. wai → lau → heu). Characteristically extensive rock replacement during VIII a-e was confined to vein wall-rock zones. Finally, from the sequence above it is clear that the low-grade zeolites were the last to be formed, superimposed upon all earlier hydrothermal alterations within the volcano.

To summarize the relationships above, table 8.1 is constructed for the actinolite zone and the lower- and upper-part of the epidote zone in the same way as table 5.1 for the Geitafell gabbro (p.158).

Actinolite zone
Epidote zone, lower part
Epidote zone, upper part
Intrusive phases
Vein systems
Vesicle infillings
1 - 3 b 4 (5 & 6 ?) 5 6 7 8 9
1 - 3 b 4 a b 5 6 7
1 - 2 3 a 3 b 4 5 6 7 8
Mud deposit
Silica (opaline / jasper)
Limonite
Iron-oxide hm / [mt]
TiO2 (phase ?)
Pyrite
Chalcopyrite
Smectite
Quartz
Calcite / [siderite]
Chlorite
Sphene
Albite / K. feldspar
Andradite / [grossular]
Actinolite
Epidote
Prehnite
Wairakite / [analcime]
Laumontite
Heulandite / stilbite
Scolecite / mesolite
Mordenite
Thomsonite
Chabazite
Hedenbergite SS
DEVELOPMENT OF SECONDARY MINERALS WITH TIME
Growth in time
Uncertain growth with time
Limited distribution

TABLE 8.1

Review of the study.

The present study of the Geitafell central volcano has established the overall chronology of volcanological, structural and hydrothermal events. A close relation between intrusive episodes and the establishment and maintenance of a high-temperature hydrothermal system has been demonstrated and attempts have been made to explain some of the observed features. The hydrothermal system is now ready for further physico-chemical studies of selected areas, which could be investigated by small-scale mapping and sampling e.g. to sort out the time relation and homogeneity of the vein generations within the vein systems and the associated wall-rock zones. Application of isotopic- and fluid inclusion studies, for instance, might provide useful information on the fluid system. At present, however, the account of the hydrothermal system will be concluded with a description of the mineral chemistry (chapter 9); a classification of the system within the metamorphic facies concept, including a discussion on the thermo-chemical aspects of the hydrothermal mineralogy (chapter 10), and a comparison with active hydrothermal fields (chapter 11).

CHAPTER 9

MINERAL CHEMISTRY

The electron micro-probe was extensively used for mineral identification and to study the mineral chemistry. Both primary and secondary minerals were analysed. An emphasis is laid on the chemistry of the secondary minerals. Where appropriate, however, the composition of the primary feldspars and the pyroxenes, in terms of An-content and WoEnFs composition respectively, have been reported in earlier chapters. The primary ore has similarly been analysed, chiefly though for qualitative information, reavealing the presence of both iron and iron-titanium oxides in most of the samples studied, reported as magnetite and ilmenite respectively.

Most commonly, the analysed primary fsp are labradorite (An 50-70) or bytownite (An 70-90), the latter chiefly occurring as phenocrysts, sometimes with an anorthite (An >90) core (e.g. in I.P. 10 dykes). The fewer analyses of primary fsp in the acid rocks showed the fsp - composition ranging from albite to labradorite (An 5 ≃ 60).

Apart from one analysed hypersthene in the Geitafell gabbro, all the analysed primary pyroxenes of the basaltic rocks are augites, the matrix augites being higher in Fs content (e.g. see fig. 7.1, and table 1, appendix 1, no. 13-14). The analysed px in the acid rocks include both augite and ferroaugite (e.g. in sample 192, see appendix 2).

The primary ore usually shows some degree of alteration, either being partly or wholly oxidized to hematite (or maghematite ?) or replaced by sulphides, sphene or TiO_2 (up to 94% TiO_2 of analytical totals up to 96%). A crude estimate of the oxidation state of the

ore was made by converting FeO to Fe_2O_3, commonly requiring both Fe^{2+} and Fe^{3+} present in the primary Fe-oxides and the skarn ore, while the chemical analyses of the secondary ore elsewhere (limonite, goethite, hematite) allowed all Fe^{2+} to be converted to Fe^{3+} with analytical totals still ranging from ca 80% towards 100%.

Chemical analyses of the hornfels- and the skarn pyroxenes, are shown in tables 1-2, appendix 1, and discussed in chapters 7 and 10. The garnet chemistry is discussed in chapter 10 and representative analyses are shown in table 3, appendix 1.

The mineral chemistry of the other common secondary silicates is reported below.

9.1 The Secondary Mineral Chemistry

PHYLLOSILICATES. The low-grade clay mineral identified as smectite chiefly occurs within the flank rocks of the volcano, but within the former high-T hydrothermal system smectitic clays are encountered in late zeolite-bearing veins (z, cc, qtz, sm), their wallrock zones, and in late dykes (I.P.12). The smectite clays range in colour from dark brown to yellowish green. A typical example of the flank rock smectite was shown in figure 8.1.

Representative chemical analyses of smectites, from the three occurrences discussed above, are shown in table 4, appendix 1 (no 1-6). The smectite chemical composition is quite variable. The silica content, for instance, ranges from 35-50% SiO_2, Al_2O_3 from ca 4% - 18%, FeO from 10-30% and MgO from 2-18%. While only few chemical analyses of smectites are available the smectites fall into two compositional groups: (sm-1) that of iron-saponites (analyses 1-4) and (sm-2) the other of montmorillonites (analysis 5).

The sm-1 group is the more common one, both replacing volcanic

glass and forming amygdales in the flank rocks and the I.P.12 dykes. The sm-2 clays have only been analysed from a late vein in an I.P.12 dyke, forming an assemblage with cc-qtz-stb. Analysis 6 (table 4) is from a saponitic clay found associated with a late vein crossing the Geitafell gabbro. This smectite differs from the others in having much higher MgO-content.

The most common smectites from active hydrothermal fields in Iceland are iron saponites (Kristmannsdóttir, 1976, 1983). Chemical analyses of these smectites are few but comparable to those reported here. Chemical analyses of secondary minerals from extinct hydrothermal areas in Iceland are similarly few, the notable exception being the recently drilled IRDP-hole in eastern Iceland.
The IRDP-hole (1920 m deep) was sunk into Tertiary basaltic strata, á few km away from the Thingmuli central volcano, and covers a stratigraphic section from ca.1-3 km below the original top of the volcanic strata. Smectites are common in the upper 800 m of the IRDP-core. Reported smectite analyses from this drillhole (Mehegan et al., 1982) are iron-saponites, similar to those of group sm-1 from the Geitafell volcano. The IRDP-smectites and the Geitafell iron-saponites all fall within the compositional field "sm-1" shown in the ACF-diagrams in figure 9.3. while analyses of the sm-2 smectites from Geitafell are only available from 1 sample only, the "sm-2" field is also shown in fig. 9.3 to illustrate the mineralogical evolution of the hydrothermal system. The smectite chemistry appears to be inherited from its immediate environment, the sm-1 group typically replacing basaltic volcanic glass, while the sm-2 smectite is found in an assemblage with zeolites (-cc-gtz) and is thus richer in both silica and alumina.

The other low-grade sheet silicate, less abundantly occurring

in Geitafell, is celadonite. Its occurrence appears somewhat restricted to the acid rocks. Chemical analyses of celadonites are available from only two samples, one of which is shown in figs. 8.3. and 8.4. The celadonite from this acid rock (no. 7-8, table 4, appendix 1) is quite low in Al_2O_3-content (≃ 2%) compared with the IRDP-celadonites from amygdales within basaltic lavas, which contain 8-13% Al_2O_3 (Mehegan er al., 1982). The acid rock celadonite (no. 7 and 8) is characteristically deep green, which makes it easily distinguishable in hand specimens or thin sections from the more common brown to yellowish green smectite clays. Analysis 9 in table 4, however, represents a red-brown K-rich clay formed in vesicles and as interstitial matrix clay in a basaltic dyke of I.P.10 from within the flank rocks. In hand-specimens or thin sections this redbrown K-rich clay mineral would be indistinguishable from the smectitic clays. This may imply that the celadonite formation within the flank rocks is more widespread than presently recognized, while the smectitic clays apparently predominate.

MIXED LAYER CLAYS (MLC). In active geothermal fields in Iceland, the up-grade transition from iron-saponites to chlorites, is bridged by a zone of randomly interstratified mixed layer sm/chl clays (Kristmannsdóttir, 1976, 1983). This transition is observed by sequentially XRD-analysed dry, glycolated and heated clay samples. The basal spacings (d 001 in Å) of 14-15 Å in dry samples expands to 15-16 Å upon glycolation and collapses to 12-13 Å after heating at 600°C. This contrasts with the XRD-patterns of the smectites (12-15 Å, ≃17 Å, <10 Å) and the chlorites (14-14.6 Å, 14-14.6 Å, ≃14 Å) (Kristmannsdóttir, 1976).

Accounts on the chemical composition of the MLC from the active fields in Iceland are meagre, while two analyses from drillhole Rn-8 in Reykjanes (Kristmannsdóttir, 1983) are shown in figure 9.1. Reconnaisance XRD-studies of MLC - sm/chl clays, followed by numerous chemical analyses, however, are available from the Del Puerto ophiolite in California (Evarts and Schiffman, 1983). The Del Puerto MLC typically plot within the diabantite field of Hey's (1954) classification diagram, shown in figure 9.1. The mixed layer sm/chl clays from both the Del Puerto ophiolite and the Reykjanes field are typically silica richer (30-35% SiO_2) than the normal chlorites from both localities, and contain significant CaO, K_2O and Na_2O on interlayer sites. This is also (apart from Na_2O) the case for the recognized MLC - sm/chl in Geitafell.

An up-grade transition in the clay mineralogy in Geitafell is observed, particularly within the chlorite zone enveloping the epidote zone (map II). This transition involves a change in colour from brown, or yellowish green, and commonly poorly crystallized clay, to deeper green and typically fibrous chloritic clay (e.g. see figs. 6.3 and 6.4). This up-grade transition in the clay mineralogy was chemically studied by the electron microprobe. Two sets of representative analyses are shown in table 5, appendix 1, no 1-4 and 5-8 respectively, while their compositional variation is shown in figure 9.1. Compared to the MLC chemistry from Kristmannsdóttir (1983) and Evarts and Schiffman (1983), analyses 1-6 in table 5 are from MLC - sm/chl, truely supported by the mineralogical character.

The transition from brown to green MLC (no 1-4, table 5) and from brown MLC (no 5-6) to green chl (no 7-8), both involve a decrease in SiO_2 and Al_2O_3 and an increase in FeO and MgO. Despite existing stoichiometric variation

Figure 9.1

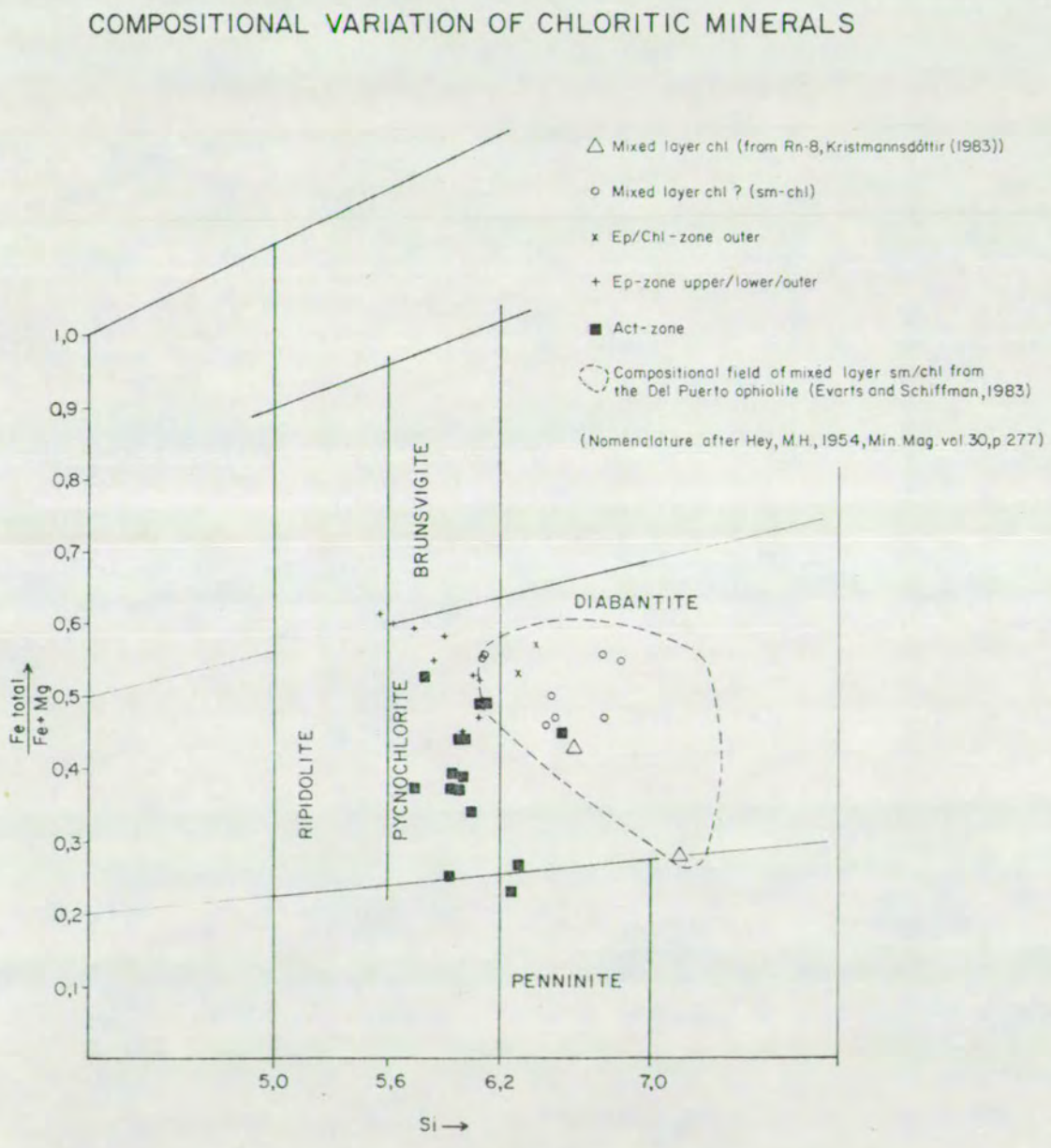
COMPOSITIONAL VARIATION OF CHLORITIC MINERALS
△ Mixed layer chl (from Rn-8, Kristmannsdóttir (1983))
○ Mixed layer chl ? (sm-chl)
x Ep/Chl-zone outer
+ Ep-zone upper/lower/outer
■ Act-zone
Compositional field of mixed layer sm/chl from the Del Puerto ophiolite (Evarts and Schiffman, 1983)
(Nomenclature after Hey, M.H., 1954, Min. Mag. vol. 30, p. 277)
RIPIDOLITE
PYCNOCHLORITE
BRUNSVIGITE
DIABANTITE
PENNINITE
Fe total / Fe+Mg
1,0
0,9
0,8
0,7
0,6
0,5
0,4
0,3
0,2
0,1
5,0
5,6
6,2
7,0
Si →

in both the MLC and the chl, this up-grade chemical trend is systematic on intersample basis.

The minor element (Ca, Mn, K) contents in sm, MLC - sm/chl and chl is also worth mentioning (compare tables 4, 5 and 6, appendix 1). Mn is only detected in some of the smectites but always detected in the MLC and the chl. CaO content in the smectites ranges from 1.5-3.0% CaO, and Ca is always detected in the MLC ($\lesssim$0.7% CaO), while only sometimes in the normal chlorites. Minor amounts of K is similarly detected in both the sm and the MCL - sm/chl but not in the chlorites.

CHLORITES. A further up-grade alteration of the phyllosilicates, now involving a transition from the typical green chl to brown chl within the andradite- and the actinolite zones, was discussed in chapter 6 (see figs. 6.5, 6.6, 6.11). Representative chemical analyses from the up-grade alteration products are shown by analyses 9-12 in table 5 (appendix 1). Again, despite stoichiometric intrasample variation of the chlorite chemistry, a systematic intersample chemical trend appears - different from that above involving the MLC → chl transition - now involving an increase in both Al_2O_3 and MgO but a decrease in FeO at relatively constant SiO_2. Thus, the overall up-grade alteration of the phyllosilicates is towards high-Mg chlorites.

Representative chemical analyses of chlorites from both the epidote- and the actinolite zone are shown in table 6. As seen from figure 9.1 most of the analysed chlorites from the Geitafell volcano are pycnochlorites. In fig. 9.1 a distinction is made between chlorites from the epidote zone and the chlorites from the actinolite zone. This shows clearly that the high-Mg chlorites are restricted

to the actinolite zone, while both high- and low-Mg chlorites coexist within the actinolite zone.

The low-Mg chlorites resembles the IRDP-pycnochlorites, described by Mehegan et al.,1982, Exley, 1982 and Viereck et al.,1982, and analysed chlorite from the Krafla high-T active field (Kristmannsdóttir, 1979). The IRDP-hole, however, only penetrates lower-grade hydrothermally altered rocks than those of the actinolite zone in the Geitafell volcano. Interestingly, relatively high-Mg chlorites are reported as hydrothermal products of sea-water basalt interaction (Humphris and Thompson, 1978). These chlorites, however, showed very little chemical variation (MgO ≃ 20%) irrespective of metamorphic grade (Humphris and Thompson, 1978), which contrasts with the Geitafell chlorites. Those chlorites in Geitafell having MgO ≳ 20% invariably occur within the gabbros and the gabbro contact aureoles.

AMPHIBOLES. Representative microprobe analyses of amphiboles are shown in table 7, appendix 1, while the compositional variation of these and other amphiboles from Geitafell is shown in figure 9.2. A distinction is made in fig. 9.2 between the amphiboles occurring in amygdales and veins and those replacing primary augite in both basaltic and acid rocks. Typically, the amygdale - and vein amphiboles are iron-rich and plot within the ferro-actinolite field in fig. 9.2, while the replacement amphiboles are higher in MgO and rest within the actinolite field. Exceptions from this, however, can be seen in figure 9.2. In addition, one available amphibole analysis from an I.P.5 dyke reveals an actinolitic-hornblende (no 13). All the other available amphibole analyses from the volcano are either of actinolites or ferro-actinolites.

Figure 9.2

COMPOSITIONAL VARIATION OF AMPHIBOLES

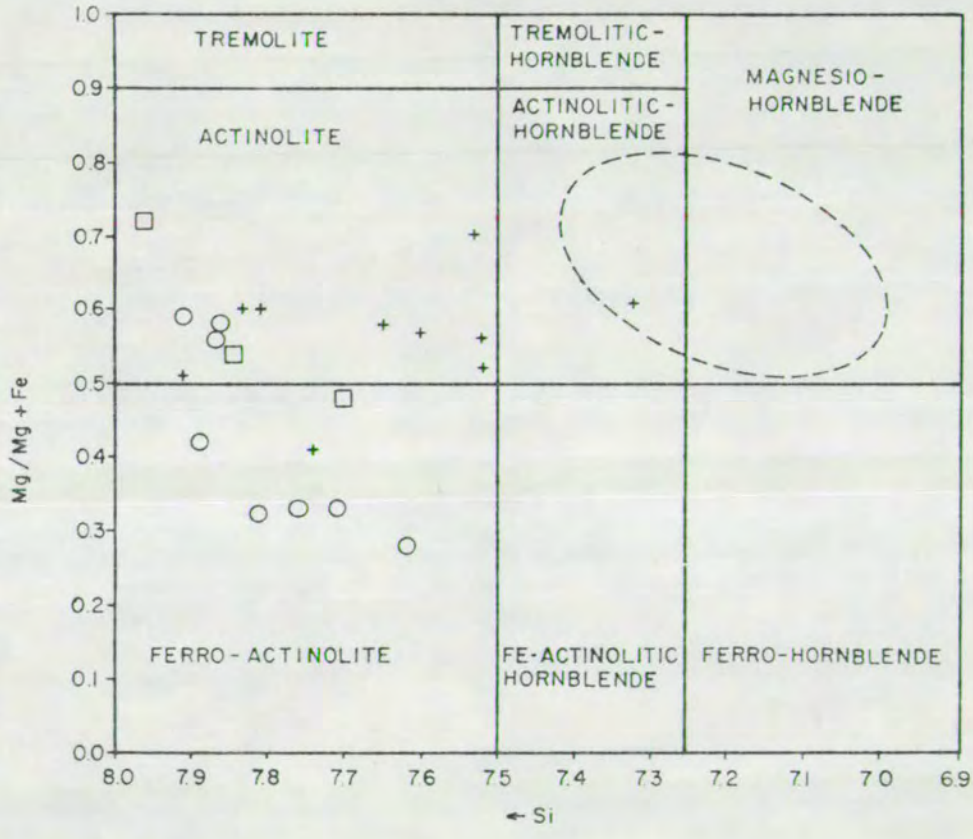

○ Amygdales and veins

\+ Px-replacement in basaltic rocks

□ Px-replacement in acid rocks

◌ Igneous amphiboles at the Del Puerto ophiolite (Evarts and Schiffman, 1983)

(Nomenclature from Leake, 1978, Am. Mineralogist, v 63, pp. 1023-1052. Slightly modified, see Amphiboles, Reviews in Mineralogy, v. 9A, 1981.)

The actinolitic amphiboles from Geitafell are low in Al_2O_3 ($\leq$5.5%, table 7) and comparable to the actinolites from the active Krafla field (Kristmannsdóttir, 1979). Similarly, actinolites described by Humphris and Thompson (1978) from hydrothermal basalt-seawater interactions (e.g. Al_2O_3 3-7%) are comparable to the Geitafell replacement actinolites, as are the secondary actinolites from the Del Puerto ophiolite (Evarts and Schiffman, 1983). Primary late-magmatic (or metamorphic) amphiboles similar to those from the Del Puerto rocks (see the dash-line field in fig. 9.2), however, are lacking at Geitafell, except for one analysed member in an I.P.5 sheet within the I.P.2 contact aureole (no 13, table 7). The lack of late-magmatic amphiboles may support the general conclusion discussed in chapter 4, that the Geitafell intrusive rocks primarly consisted of dry magmas - interacting with meteoric waters to produce an early actinolite - sphene secondary assemblage. The finding, though rare, of an actinolitic-hornblende in an I.P.5 sheet is of interest with respect to the early hot intrusives - water interactions postulated to have occurred in Geitafell. More extensive chemical studies of the I.P.2, 5 and 10, and the contact aureole amphiboles are thus clearly of interest. Still, it is clear that all the other analysed amphiboles, both from the gabbro contact aureoles (no. 1, 2, 3, 5, table 7) and the I.P.2, 4 and 6 intrusive rocks (no. 9-12, 14, table 7), are actinolites.

EPIDOTE. Representative analyses of epidote are provided in table 8, appendix 1. Total iron is reported as Fe^{3+}. The structural formula calculated on basis of 12.5 oxygens gives a mean from 15 analyses:

$Ca_{2.00}(Al,Fe^{3+})_{2.95}Si_{3.04}O_{12}(OH)$, suggesting that most of the iron is Fe^{3+}, as Fe^{2+} substitution for Ca is not required. Mn was detected in 4 of the 15 analyses, Cr in 1 of the 15 analyses.

No correlation between epidote chemistry and stratigraphic position is found to exist. Stoichiometric variation, however, in Fe^{3+}/Al^{3+} ratio exists, as shown by the pistacite component at the base of table 8 (Ps: 100 $Fe^{3+}/Fe^{3+}+Al$). The Ps-component ranges from Ps 19.06-42.81. A mean from 15 analyses gives Ps: 28.8 (s. dev. 6.8).

Notable is the general absence of minor components (Ti, Mn and Mg), which are commonly below detection limits. Ti was detected in 1 of 30 analyses, Mn in 12 of 30, and Mg never. Na and K were not detected in the Geitafell epidotes.

The epidotes from the Geitafell volcano resemble those from the IRDP-drill hole in eastern Iceland. Exley (1982) reports on 447 epidote analyses from 17 samples from the IRDP-hole, where he observed a wide variation in major and minor element contents, both on inter-sample and intrasample basis. The variation in Fe^{3+}/Al^{3+}-ratio in the IRDP-epidotes, however, was found to be larger within individual probe sections than the variation between averaged Fe^{3+}/Al^{3+}-ratios of epidotes in different sections. This being due to strong compositional zoning within the epidote grains (Exley, 1982). The range in Ps-component was 15.43-49.95 in the IRDP-epidotes, or similar to that in the Geitafell-epidotes. Exley's (1982) 16 representative epidote analyses give a mean Ps-value of 30.8 (s. dev. 7.9) wich is slightly higher than the mean Ps-value for the Geitafell epidotes.

The IRDP-epidotes are low in TiO_2 ($\leq$ 0.33%), MgO ($\leq$ 0.10%) and the MnO content ranges from 0.02-0.62% (a mean of 0.07% MnO). Mn, however, showed enrichment towards crystal rims (as did Al) while Ti (and Fe) was higher in the crystal cores (Exley, 1982). The IRDP-epidotes

further range in SrO-content, from below detection limits up to 0.90% SrO, with a mean of 447 analyses being 0.23% SrO. The Geitafell epidotes were not analysed for chemical zoning or Sr-content.

The Icelandic epidotes, on average, have higher Fe^{3+}/Al^{3+}-ratios than the Del Puerto epidotes, which range in Ps-component from 4-36 mole percent with a mean value of ca. Ps_{23} (Evarts and Schiffman, 1983).

PREHNITE. Prehnite is a widespread mineral in both the epidote- and the actinolite zone, deposited in veins and amygdales and replacing feldspar and glass. Representative analyses of prehnites are shown in table 9, appendix 1.

No depth-related chemical variation in prehnites is found to exist, while an apparent variation in the extent of Fe^{3+} substitution for Al^{vi} exists. Total iron is reported as Fe^{3+} as Fe^{2+} substitution for Ca is not required (table 9, appendix 1). The Fe_2O_3-content in amygdale- and vein prehnites appears significantly lower (0-1.90% Fe_2O_3) than the Fe_2O_3-content in prehnites replacing primary feldspar and glass (1.20-3.45% Fe_2O_3 up to 6.04% Fe_2O_3 respectively). This variation appears to be systematic on intersample basis and seems to indicate a local source for Fe^{3+} within the samples. Chemical zoning in individual prehnite grains, however, has also been observed, showing Fe_2O_3 enrichment in the cores of the replacement prehnites. In general, the prehnites within the Geitafell volcano are of later origin than the epidotes, as discussed in earlier chapters. Further studies on the Fe^{3+} substitution for Al^{vi} in prehnites may thus be of interest.

A similar variation in Fe_2O_3 content (0.32-7,45%) was observed

in the IRDP-prehnites in eastern Iceland (Exley, 1982). As with epidote, the amount of Mn, Mg and Ti in the IRDP-prehnites appear slightly higher than in the Geitafell-prehnites. In the IRDP-prehnites, TiO_2, MnO and MgO were always detected but in amounts < 0.07% (Exley, 1982), while in the Geitafell-prehnites, Ti is detected in 3 of 20 analyses, Mn in 4 of 20, and Mg in 1 of 20 analyses. Na and K were not detected in either case.

ZEOLITES. Representative analyses of zeolites are shown in table 10, appendix 1. These include: wairakite (formula: $CaAl_2Si_4O_{12}\cdot 2H_2O$), laumontite ($CaAl_2Si_4O_{12}\cdot 4H_2O$), heulandite ($(Ca\ Na_2)Al_2Si_7O_{18}\cdot 6H_2O$), stilbite ($(Ca\ Na_2\ K_2)Al_2Si_7O_{18}\cdot 7H_2O$), scolecite ($CaAl_2Si_3O_{10}\cdot 10H_2O$), analcime ($NaAlSi_2O_6\cdot H_2O$) and mordenite ($(Na_2\ K_2\ Ca)Al_2Si_{10}O_{24}\cdot 7H_2O$). Despite devolatilization under the microprobe beam, commonly observed, the zeolite analyses are remarkably consistent. As can be seen in table 10, the analysed zeolites from Geitafell are close to ideal composition and usually free from impurities. The analytical totals of wairakite and analcime are usually close to 90%, the laumontite totals close to 85%, the heu-, stb- and sco-totals close to 80%. As can be seen from the structural formulas the zeolites water content increases in the same order. Only two analyses are available of mordenite, both deficient in alkalis. Only few analyses are available from the rare analcime, most of which are from feldspar pseudomorphs.

The wairakite analyses most often show near end-member wairakite (e.g. no. 1-2) and intermediate members between wairakite-analcime are not found. Rarely, though, wairakite pseudomorphs after primary feldspar may contain up to 2.3% Na_2O (Na 0.3 per formula unit).

These wairakites form an assemblage with ab-K.fsp ± other zeolites ± pr ± ep. The fine grain size of the pl-pseudomorphs makes these high-Na wairakite analyses somewhat doubtful, and in any case these wairakite analyses are not consistent in the Na-content from spot to spot.

Analyses 1-6 (table 10) are all from the same amygdale - described in chapter 6 (p. 213), but showing from rim to core: wairakite, laumontite, heulandite + chabazite. The chabazite was not successfully analysed. The laumontites (as in no. 3-4) commonly contain minor K_2O. The same applies to the optically identified heulandites - where analysed, both K_2O and Na_2O are detected. The stilbites, however, are most commonly free of Na_2O and K_2O. The analytical totals of the stilbites are commonly slightly higher than those of the heulandites. Some of the analysed "stilbites" may in fact be epistilbites with 5 H_2O per formula unit instead of 7 H_2O in the common stilbite. Reconnaisance XRD-analyses of the zeolites in Geitafell revealed the presence of both, though most often stilbite. The two are virtually identical optically and thus indistinguishable in thin sections.

The scolecite (no. 9-10, table 10) is much lower in SiO_2 than the other zeolites in Geitafell, and thus unmistakable. The scolecite occurs less abundantly in the Geitafell volcano than the silica-richer zeolites, and, where found, invariably takes part in the last vein system.

SECONDARY FELDSPARS. Albite and adularia (or K.feldspar) are amongst the ubiquitous secondary replacement minerals with in the former high-T hydrothermal system. Most commonly, both take part in the primary feldspar pseudomorphs, but are locally formed in veins and

vesicles. Representative microprobe analyses are shown in table 11, appendix 1.

The analysed K.feldspars are most commonly pure (Or_{100} Ab_{0} An_{0}), while minor Na and Ca are sometimes detected (up to Or_{90} Ab_{7} An_{3}). The analysed albite, however, normally contains some Ca and ranges from Ab_{90-98} An_{10-2}. Rarely, secondary oligoclase was analysed, either from within the gabbros or the contact aureoles, while albite is by far the more common secondary feldspar both there as elsewhere.

The problem of mixed analytical results from the finer grained ab-K.fsp-z assemblages was commonly encountered, both within the primary fsp pseudomorphs and the altered lava matrices. This was solved by careful tracking into the mineral phases studied, in the case of secondary fsp, resulting in near end-member albite or K.feldspar analyses, while intermediate analyses might cover the compositional range of the Ab-Or series. Test-analyses on margins between ab-K.fsp gave similar results. A few microns inwards, either way, "end-member" ab or K.fsp, identical to the analysed crystal-cores, resulted - suggesting that little or no mixing took place between the two phases. The commonly fine-grained K.fsp, forming irregular, anhedral patches within partly pseudomorphed fsp-host, or participating in multimineralic assemblages, are somewhat problematic in microscopic identification, which may have bearing on the discussion below.

Adularia is recorded as a hydrothermal alteration product of feldspars in active high-T hydrothermal systems world-wide (e.g. Browne, 1978), while its presence in the active Icelandic fields appears sporadic (Tómasson and Kristmannsdóttir, 1972). Adularia, however, is found in fsp-pseudomorphs within the active Krafla field

(Kristmannsdóttir , 1978) and in a vein or an amygdale deposit (drill cuttings) recently found by the author. Its presence in some of the active fields is thus clear - irrespective of its abundance. The lack of both drillcores and extensive microchemical studies from the active fields in Iceland, creates difficulties concerning the K.fsp abundance and its distribution within the active fields. A result from the present study on the fossil Geitafell system would evidently suggest that adularia may be more common in the active fields than presently recognized. In support, a result from the IRDP-core in eastern Iceland showed that adularia was the second most common alteration product of plagioclase, increasing in abundance downwards (Viereck et al., 1982).

SPHENE. Representative analyses of secondary sphene are shown in table 11, appendix 1 (no. 7-10). Like the secondary fsp, sphene is an ubiquitous part of the hydrothermal rock replacement assemblages, most commonly observed marginal to the FeTi-oxides. The sphene is also found in fsp-pseudomorphs (no. 8, table 11) and in actinolite veins.

The observed range in Al and Fe (FeO as total iron) substitution for Ti can be seen in table 11. A similar range in Fe-Al-Ti substitution is found in the IRDP-sphene from within the mafic host rocks, while the felsic- and ignimbrite IRDP-sphenes showed higher Al substitution for Ti suggesting a host-rock control on the sphene composition (Viereck et al., 1982).

The abundance of sphene appears to increase with depth within the fossil hydrothermal system. Within the actinolite zone sphene is additionally formed in fsp-pseudomorphs and actinolite veins.

In the upper part of the epidote zone - particularly within highly carbonitized rocks related to the later vein systems - sphene commonly forms an assemblage with some fine-grained TiO_2 mineral.

OTHER MINERALS. The distribution of the most voluminously occurring secondary minerals, calcite and quartz, has been discussed earlier. Their compositional spectra was rarely collected, but showed near pure SiO_2 and Ca. However, the carbonate spectra was frequently looked at in most of the analysed samples, in a search for a second carbonate if suspected. Siderite was found in one sample of an I.P.12 dyke, described earlier, forming an assemblage with calcite and iron saponite (fig. 9.3f).

The sulphides, where present in the polished sections, were studied by the microprobe, after reconnaisance reflected light microscopic study. Commonly only one or two sulphide grains are present in the sections. Only pyrite and chalcopyrite have been found in discrete grains, and both usually contain minor Co and Zn (<0.6 wt%) In one case (sample 090A), a little bravorite may be present, enclosed in cpy, while the analytical result appears mixed from the two ($Fe_{20.2}$ $Co_{11.8}$ $Ni_{13.2}$ $Cu_{13.6}$ $Zn_{0.2}$ $S_{40.1}$; in wt %). In an other case, a discrete tiny ore grain composed of $Cu_{58.2}$ $Zn_{35.1}$ (wt %) was found in a sample (085), additionally containing cpy as the only sulphide present. Otherwise the disseminated sulphides studied only comprised cpy and py, of which the py is by far the more common one. Not uncommonly, the pyrite is marginally replaced by an hydrous iron oxide (e.g. FeO: 75.1% of total: 79%; if Fe_2O_3: 83.6%, total 87.5%). This secondary replacement, at least partly, relates to present-day weathering.

Amongst the less common secondary minerals are talc, replacing the rare olivine and hypersthene in the I.P.2 gabbro, "illitic" clay replacing feldspars, and the secondary apatite. Microprobe analyses of the former two are only available from one sample each, shown in table 12, including two representative analyses of apatite.

9.2 Mineral Paragenesis

The mineralogical evolution of the Geitafell hydrothermal system, summarized in chapter 8.3, can be illustrated briefly by a sequence of ACF diagrams, shown in figure 9.3. While this presentation involves considerable simplification, the principal silicates, characteristic of a given time period can be shown. Tielines are drawn between the common mineral assemblages. A thermal regime is added to each diagram, while the thermo-chemical aspects are discussed in chapter 10 and 11.

Figure 9.3 a shows a primitive situation within the volcano, at ca.1 km depth just prior to the emplacement of the central gabbros (I.P.2). The earliest sm-1 group clays had evolved to the MLC clays and possibly chl upon slow rise in the thermal gradient. Additional mineral phases include lim, hm, opal,chalcedony, quartz.

Figure 9.3 b illustrates the condition within the I.P.2 contact aureole shortly after the gabbro emplacement. A steep thermal gradient existed within the contact aureole. The characteristic skarn mineral assemblage formed is illustrated by the hd_{ss}- and assemblage in fig. 9.3 b. The other silicates shown in the diagram, may have

FIGURE 9.3

MINERAL PARAGENESIS ON ACF - DIAGRAMS

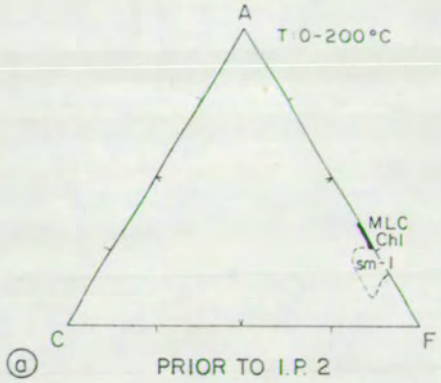

ⓐ PRIOR TO I.P. 2

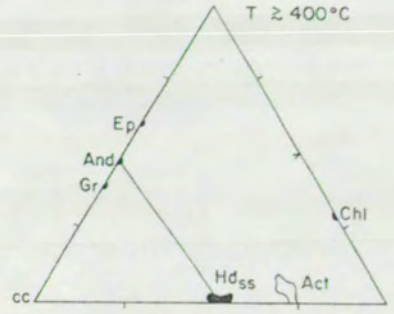

ⓑ I.P. 2 CONTACT AUREOLE

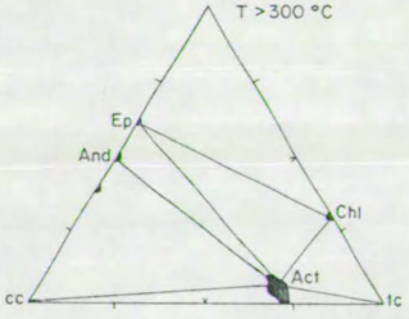

ⓒ ACTINOLITE ZONE

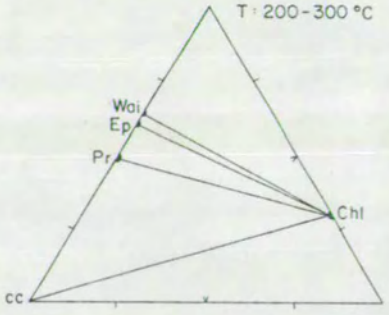

ⓓ EPIDOTE ZONE

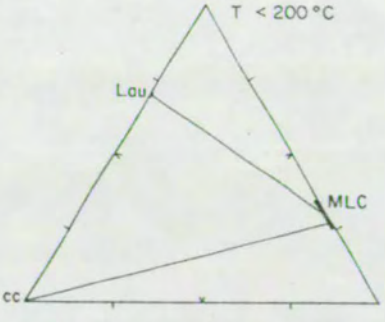

ⓔ COOLING OF HIGH-T SYSTEM

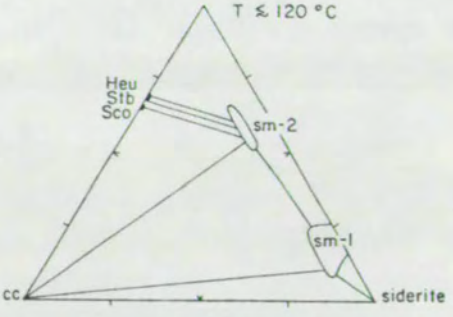

ⓕ ZEOLITIZATION

formed during this time but are generally superimposed. Additional minerals not shown in figures 9.3 b-d include mt, hm, sp, ab, k.fsp, qtz, cpy, py.

Figure 9.3 c and 9.3 d show the principal mineral assemblages formed at two depth levels within the subsequent high-T hydrothermal system. The chief difference between the higher-grade actinolite zone and the epidote zone is shown in figs. 9.3 c-d. Both andradite and actinolite formed hydrothermally within the Actinolite zone, along with epidote and chlorite. Within the lower-T Epidote zone the principal mineral assemblage include ep, chl, pr, wai, cc.

The progressive alteration of the chloritic minerals within the Actinolite zone, discussed in chapter 6, but principally involving the earlier sm and MLC clays and fluids, producing assemblages of and+cc+ act+ep+qtz ± high-Mg chl, are not shown in fig. 9.3 c, as the resulted assemblages relate to timing of mineral growth at variable mole fractions of CO_2 ($^{X}CO_2$) in the fluid phase - e.g. where both andradite and actinolite appear produced from the chloritic minerals (+qtz+cc) at low $^{X}CO_2$ (chapter 10).

Figure 9.3 e illustrates the chief paragenetic mineral assemblage formed during the cooling period. Additional minerals formed during the cooling period include qtz, hm, TiO_2, mo, analcime, py, cpy.

Finally, figure 9.3 f illustrates the characteristic mineral assemblages formed during the zeolitization within the former high-T hydrothermal system. Additional minerals to this diagram include qtz, hm, cha, tho, py.

The temperature indication shown at each diagram in figure 9.3 basically reveals the mineral paragenesis in relation to a simple heating-cooling sequence. The superimposition at the deeper levels

within the fossil high-T system can thus be illustrated by imposing the later diagrams on the former, with a minor addition. A second thermal boost related to I.P.10 (situation 9.3 b) was superimposed upon the actinolite- and the epidote zones (9.3 c-d). Similarly, part of the situation depicted in fig. 9.3 c was temporarily and locally imposed on that shown in fig. 9.3 d, in relation to the I.P.5 emplacement and the caldera event. The presently mapped mineral zone boundaries thus reflect the hydrothermal peak conditions at each site within the volcano. During the active lifetime of the high-T hydrothermal system the shown thermal boundaries necessarily moved in space with time.

CHAPTER 10

PHYSICO-CHEMICAL CONSTRAINTS

10.1 The Facies Concept and its Application to the Field Area.

The facies concept has recently been reviewed by Turner (1981). The term mineral facies was initially proposed by Eskola (1915) to include any association of metamorphic rocks within which there is a constant correlation between mineral- and chemical composition. Subsequently the concept of mineral facies has been considered in two alternative ways: (a) with"mineral facies"referring to mineral assemblages of associated rocks but not to actual metamorphic conditions, and b) "mineral facies" referring to mineral assemblages in thermodynamic equilibrium. Both alternatives have called for the introduction of several new mineral facies, in addition to Eskola's (1939) 8 facies, and numerous subfacies. The usage of subfacies has been criticized (e.g. Lambert, 1965) as having become both "confused" and "cumbersome". Turner (1981) therefore proposed to discontinue attempts to divide facies into minor units of more than local significance, and adopted the definition of mineral facies by Fyfe and Turner (1966), namely:

"a metamorphic facies is a set of metamorphic mineral assemblages associated in space and time, such that there is a constant and therefore predictable relation between mineral composition and chemical composition".

Turner (1981) amplified this definition in several respects, but the main significance of Turner's simplification of the facies concept was to limit the number of mineral facies and to restrict their definition "in terms of mineral assemblages, which are the end product

of what may have been a complex and protracted metamorphic process". "The equilibria represented by the mineral assemblages that define any facies have broad fields of stability (in terms of T and P) in common. Within this broad field are narrower, possibly overlapping fields of stability of constituent subfacies represented by zonal assemblages" (op.cit. p.60,66). Subfacies are thereby either included within the general facies or represent transitional situations between two main facies. Therefore, Turner recognized 11 main facies, shown in figure 10.1 a.

Following Turner, three mineral facies are recognized in the field area, namely sanidinite-, greenschist- and the zeolite facies. The recognition of these three facies allows a grouping of the metamorphic- and hydrothermal minerals within broad T-P stability fields (figure 10.1 b and c) to be made. Temperature estimates and the diagnostic mineral associations in the Geitafell meta-volcanics belonging to these facies, and transitions between them are listed below :

1) Percolation of cold ground-water resulted in mud and limonite deposits, with temperature ca. 4°C upwards. Upon slow rise in the geothermal gradient silica mineraloids, smectite, quartz and then chlorite developed.

2) After early gabbro intrusion (phase 2) and again later (intrusive phase 10), contact metamorphic hornfelses were formed. Due to the shallow emplacement of the gabbros ($\leq$ 1 km, $P_{lith} \leq$ 0.3 kbars) and high temperatures in the metamorphic aureoles, as evidenced by unchilled cross-cutting felsite veins, the hornfelses are regarded as belonging to the sanidinite facies, with the diagnostic mineral assemblage: andesine - augite - ore, produced over a temperature range of ca. 900-800°C (fig. 10.1 b).

Figure 10.1

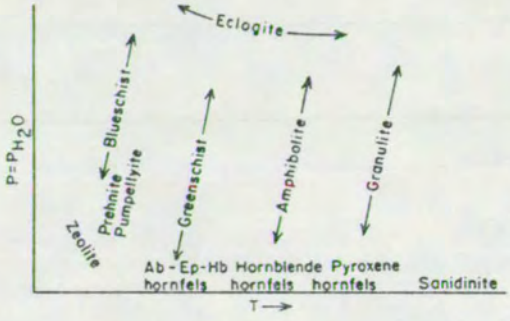

(a) Schematic relation of facies to T and P (P_{H_2O} = P) (Fyfe and Turner, in Turner 1981).

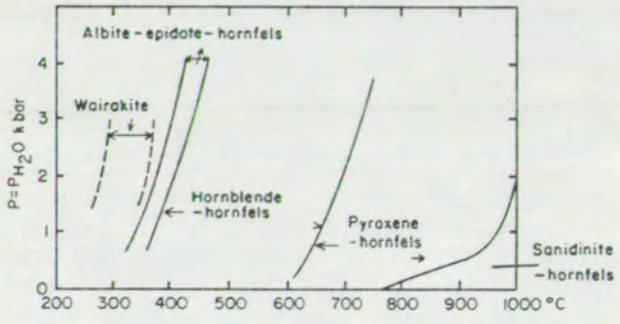

(b) T-P fields of the contact metamorphic facies (simplified from Turner 1981, the stability limits of wairakite from Liou (1971 e (p.399)).

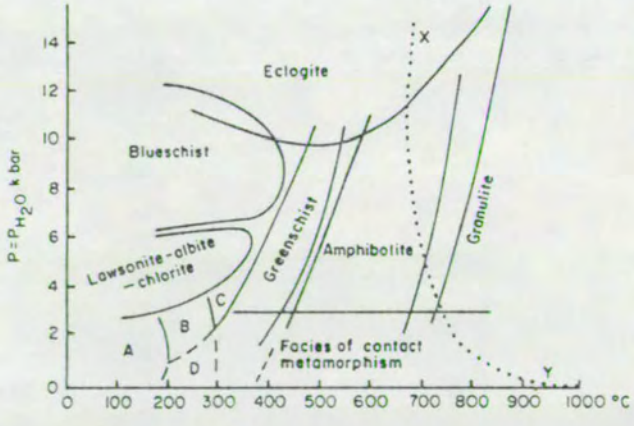

A : zeolite
B : prehnite - pumpellyite
C : pumpellyite - actinolite
D : prehnite - wairakite
X...Y beginning of melting in basalts (excess H_2O)

(c) Tentative scheme of facies of regional metamorphism in relation to P and T, from Turner 1981. The dashed curves are inserted from the present study to show the approximate field of transition (D) between the zeolite - and greenschist facies in the Geitafell hydrothermal system.

3) At lower temperatures, ca. 600-400°C, contact metasomatic skarn deposits developed in vesicles, and were characterized by : hedenbergite$_{ss}$-andradite-magnetite.

4) The diagnostic mineral assemblage of the greenschist facies, formed at temperatures < 400°C, is actinolite-albite-sphene--chlorite-epidote.

5) Transitional between the greenschist- and the zeolite facies is the assemblage : chlorite-epidote-albite-prehnite-wairakite.

6) Finally, at temperatures < 200°C the zeolite facies mineral assemblages were produced. These include: laumontite, stilbite, heulandite, mordenite, scolecite, mesolite, thomsonite, chabazite.

Thus fluids over the temperature range from ca. 0-900°C may have existed within the volcano. Within this broad temperature field other physico-chemical constraints are recognized and discussed below.

10.2 Other Physico-Chemical Constraints.

Using well-developed hornfels textures as a criterion for the recognition of contact metamorphic rocks, it is clear that only those rocks containing augite-andesine amygdales represent true hornfelses. From lithostatic pressure estimates (< 0.5 kbar) and high temperature felsite veins the hornfelses are tentatively regarded as belonging to the sanidinite facies, while the basalt-hornfels mineral assemblage is essentially identical to that of the lower temperature pyroxene--hornfels facies (cf. Turner 1981).

The typical basic assemblage of the hornblende-hornfels facies is marked by almost simultaneous appearance of plagioclase (An 20) and hornblende in place of actinolite (Turner, 1981). However, since

this mineral assemblage does not occur in the contact aureole of the Geitafell gabbro it is not considered further.

The mineral assemblages which form the outermost fringe of contact aureoles appear to belong to the albite-epidote-hornfels facies. A typical basic assemblage is : ab-ep-act-chl (qtz,biotite) (Turner 1981). However, this index mineral assemblage also belongs to the greenschist facies and therefore the lack of hornfels texture warrants the exclusion of ab-ep-hornfels facies from the contact aureole.

The evidence thus implies that the high-temperature metamorphic conditions were soon replaced by much lower-temperature greenschist facies conditions. The path of heat distribution within the hydrothermal system, however, is discernible from the formation of typical Ca-Si-Fe skarn deposits in amygdales containing early limonite ($Fe_2O_3(OH)_x$). The limonite apparently dehydrated to hematite (Fe_2O_3) everywhere within the contact aureole and subsequently reduced to magnetite (Fe_3O_4) (e.g. fig. 6.16). The oxygen buffer redox reaction involved is : $3Fe_2O_3 \rightarrow 2Fe_3O_4 + 1/2\ O_2$. The oxygen fugacity thus decreased in the contact aureole across the hematite-magnetite curve at some temperature. Only within those amygdales containing early limonite are $hedenbergite_{ss}$ and andradite found suggesting that the establishment of the $hedenbergite_{ss}$ - andradite assemblage depended on the presence of early limonite (later magnetite). The principal reactions involved are:

$$cc+qtz+mt = and+mt+qtz+CO_2 = hd_{ss}+CO_2$$

Hedenbergitic pyroxenes and garnets are typical gangue minerals of skarn deposits world-wide. The compositional range of the secondary pyroxenes and the garnets from the Geitafell contact aureole are shown in figure 10.2, using the diopside-hedenbergite-johannsenite and

Figure 10.2

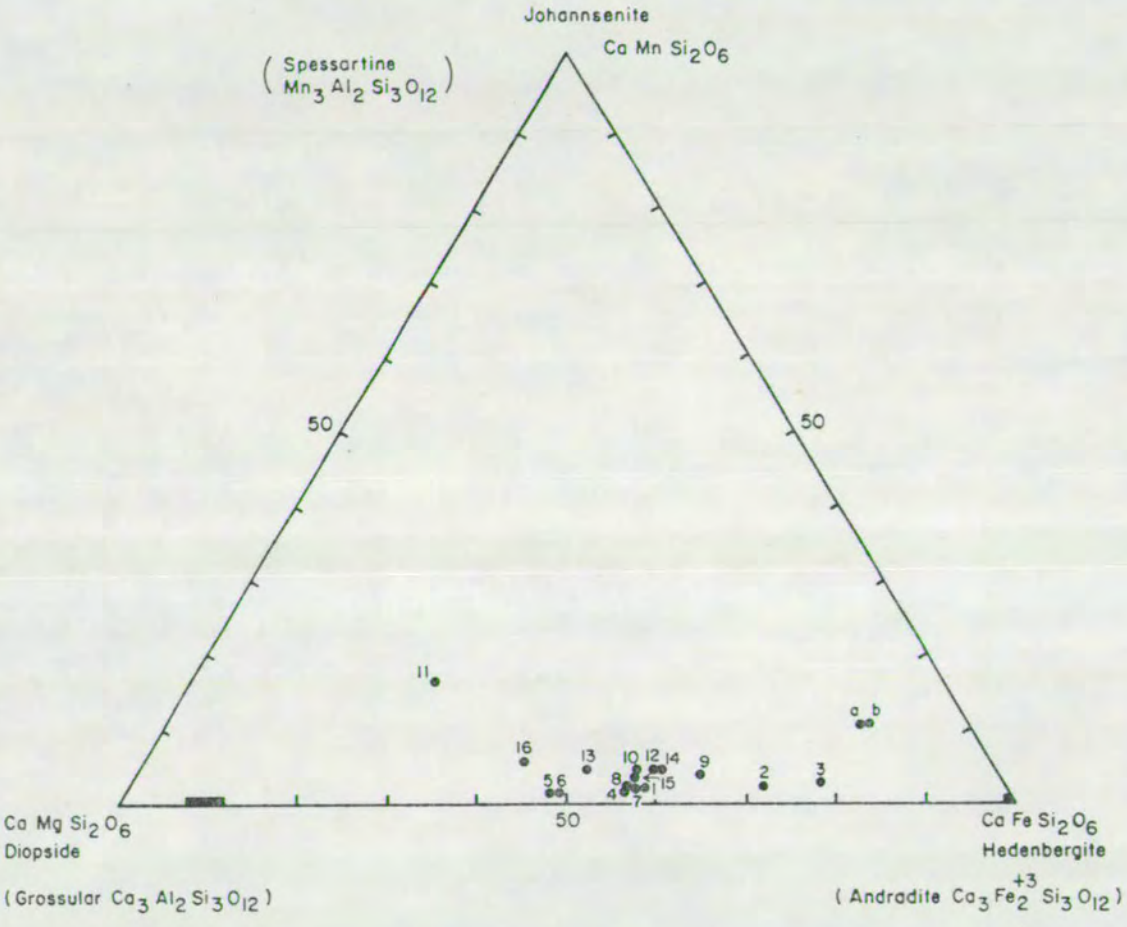

1 - 11	Geitafell gabbro contact aureole.
12 - 13	Kraksgil gabbro contact aureole.
14 - 16	Vidbordsfjall gabbro contact aureole.
▬	Garnet composition. Grossular from Geitafell gabbro contact aureole.
a, b	Vein centre pyroxene from intrusive phase 3 in the Geitafell gabbro metamorphic hornfels.

the andradite-grossular-spessartine diagrams respectively in the same triangle. Microprobe analyses and mineral calculations are provided in tables 2 and 3 in appendix I. Compared to Einaudi and Burt (1982) the Geitafell skarn minerals resemble iron skarn deposits. Skarn deposits have not previously been described from Icelandic hydrothermal systems, but their presence in the Geitafell volcano may demonstrate the path of heat distribution and fluid conditions during hydrothermal fluid - magma interaction. The apparent manner of their formation, from both field and mineralogical studies, is summarized below:

1) Early amygdale deposits in the Geitafell gabbro contact aureole are : limonite, opaline silica, jasper, quartz, smectite, $\pm$ chlorite. The hydrothermal fluid (fl_o) may have reached temperatures $\leq$ 200°C prior to the gabbro emplacement (see later discussion on min. chl temperature).

2) Gabbro injection (phase 2) provided CO_2, SO_2, Cl-gas and P_2O_5 (in apatite) and heat. Fl_o changes to $fluid_1$ (fl_1).

3) a) $fl_1 + SiO_2 \rightarrow fluid_2$ (fl_2)

b) fl_1 + lim $\rightarrow$ hm $\rightarrow$ mt + fl_2; redox reaction; HM-buffer curve was crossed at some temperature and the oxygen fugacity (f_{O_2}) dropped considerably.

c) fl_1 + sm + basalt (high fl/rock ratio) $\rightarrow$ fl_2 + chl + ab.

$fluid_2$: H_2O, CO_2, S, Cl, Ca^{2+} , SiO_2 (aqueous).

4) fl_2 + mt $\rightarrow$ hd_{ss} + fl_3 $\rightarrow$ and + cc + wai $\rightarrow$ and + qtz.

This scheme (1 $\rightarrow$ 4) is clearly very simplified. The assemblages preserved in the amygdales vary and were apparently dependent on the

volumetric relations between fl_2/mt, tentatively presented below in terms of variable fl_2/mt ratio. Therefore, the mineral assemblages resulting from the following environments are :

a) hd_{ss}-and-mt-hm-wai (low fl_2/mt environm.)

b) hd_{ss}-and-ep-wai (interm. fl_2/mt ")

c) (anisotr.)and-(turbid)wai-qtz (high fl_2/mt ")

Ep-ab-(chl/act) occurs in all vesicle walls, and andradite pseudomorphs after hd_{ss} are seen in c) above. The andradite in all environments contains numerous inclusions of hd_{ss} and calcite.

The occurrence of anisotropic garnet pseudomorphing hedenbergitic pyroxene is typical of skarn deposits (e.g. Einaudi and Burt, 1982). An extensive literature on the field relations of skarn deposits and on their topological and experimental synthesis stability relations exists, e.g. in terms of T-P_{fluid}, isobaric log f_{O_2}-T and isobaric, isothermal log f_{O_2} - log f_{CO_2}, μ_{CO_2} - μ_{O_2} and μ_{CO_2} - μ_{H_2O} diagrams. Recent papers are provided in a special issue of the Economic Geology (1982) devoted to skarn deposits. Literature review and addition of experimental data relevant to the present study are also provided by Taylor and Liou (1978). The phase relations of skarn-forming mineral paragenesis are thus fairly well-known (e.g. Burt, 1972) and have been confirmed and quantified by a number of experimental studies. Some caution, however, needs to be taken in applying these data to the interpretation of the physico-chemical relations in natural systems, as a) the experimental studies are performed in simplified systems, b) garnets in natural skarns are not pure end members, c) f_{O_2} values during skarn formation are difficult to estimate, d) other components, such as sulphur, may be significant in the

metasomatic fluid and e) equilibrium between numerous phases in skarn-forming processes may not have been attained in many cases (Taylor and Liou, 1978). Most of the experimental studies were performed at 1-2 kbar fluid pressures and their results therefore not directly applicable to the present study where the lithostatic pressures did not exceed 0.5 Kbar. The P_{fluid} in hydrothermal systems is normally only a fraction of this value, governed by the boiling curve (section 4.2). Within the gabbro aureole, however, during and shortly after the gabbro emplacement event, the hydrothermal fluid may have been superheated and T_{fluid} thereby unrelated to pressure (section 4.2). The fluid pressure in the contact aureoles may temporarily have approached the magmatic pressure - close to or slightly above the lithostatic pressure as suggested by the uplift of the volcano asssociated with the gabbro emplacement. P_{fluid} during the skarn mineral formation may thus have been in the range 0.3-0.5 kbar.

Experimental studies on hedenbergite, andradite, magnetite, quartz in the system Ca-Fe-Si-C-O-H (e.g. Kursakova, 1971, Gustafsson, 1971, 1974, Liou 1974) show that and-qtz-mt is stable at relatively high f_{O_2} values in the temperature range of 400-900°C, and the and-hd_{ss}-qtz assemblage is stable within a well-defined T-f_{O_2} range. It is clear that many mineral reactions involving andradite take place in fluids containing carbon, oxygen, hydrogen and sulphur, which are simultaneously decarbonation, redox and sulphidation reactions. Therefore, minor variations in fluid composition or in f_{O_2}, f_{S_2} may markedly affect the temperatures and pressures at which the reactions take place (e.g. Taylor and Liou, 1978, Gamble, 1982, Burton et al. 1982).

The effect of various P_{fluid} on univariant reaction relationships

was calculated from thermodynamic data by Taylor and Liou (1978) for the reaction :

3 qtz + 3 cc + 1/4 hm + 1/2 mt + 1/8 O_2 = and + CO_2

at f_{O_2} defined by the hematite-magnetite (HM) buffer, demonstrating the role of P_{fluid} on the position of univariant curves in a T-X_{CO_2} field (figure 10.3 a, X_{CO_2} = mole CO_2 / mole H_2O + mole CO_2). Other univariant and invariant relationships would similarly have been displaced in T-X_{CO_2} field with variation in P_{fluid}. The role of variable X_{CO_2} was similarly investigated by Taylor and Liou (1978) as shown in simplified form in figure 10.3 b. Also shown in this figure is the position of the qtz-cc-wollastonite(wo) reaction from Greenwood (1967) and the hd-and-qtz-mt equilibrium from Gustafsson (1974) and qtz-and-hd-wo equilibrium from Liou (1974). The role of variable X_{CO_2} on f_{O_2} and temperature is clearly shown in this figure, the andradite being stable at lower temperatures in H_2O richer fluids. Furthermore the position of the univariant curve involving hedenbergite below the HM-buffer curve is shown, suggesting that the f_{O_2} values in the Geitafell gabbro contact aureole lay below values determined by the HM-buffer, while the apparent presence of both hematite and magnetite in the vesicles suggests that the mineral assemblage was buffered by hm-mt. Hematite, however, might relate to subsequent oxidation, while the presence of iron-oxide almost inevitably buffered the reactions restricted to limonite bearing vesicles.

The study of andradite stability by Taylor and Liou (1978) gave them reason to conclude (after comparing their results with the stability field of grossular in C-O-H fluids determined by Gordon and Greenwood, 1971), that relative to the stability field of grossular, andradite is stable with fluids richer in CO_2 at a given pressure and

Figure 10.3

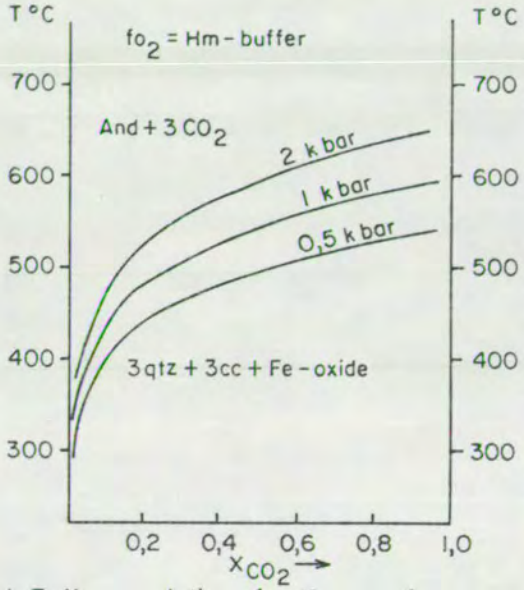

ⓐ Calculated T-X_{CO_2} relation for the reaction qtz + cc + Fe-oxides = andradite + CO_2 (from Taylor and Liou 1978).

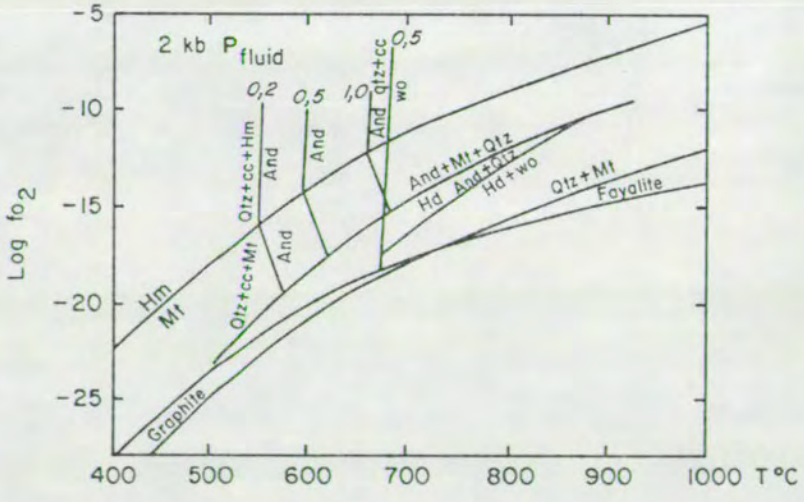

ⓑ Log fo_2-T diagram simplified from Taylor and Liou, 1978. Position of Qtz + cc + Fe-oxide = andradite + CO_2 curves at X_{CO_2}: 0,2 ; 0,5 ; 1,0 are shown from data of Taylor and Liou (1978) and Gustafson (1971). qtz + cc = wo reaction at X_{CO_2} = 0,5 from Greenwood (1967) and Hd-And-Qtz-Mt equilibrium from Gustafson (1974), And-Qtz-Hd-wo equilibrium from Liou (1974).

temperature for all values of f_{O_2}, although the temperatures of reactions which delineate the stability field of andradite are sensitive to slight changes in X_{CO_2}, f_{O_2} or both. They also deduced that the experimental results indicated that andradite is restricted to H_2O-rich fluids at temperatures below 400°C.

The results from Taylor and Liou's work are tentatively applied to the Geitafell hydrothermal system, outside the contact aureoles - where the fluid temperatures were governed by the boiling curve. Both within the andradite- and the actinolite zone, the development of andradite may have been restricted to extremely low X_{CO_2}-values. The restricted grossular occurrence within the Geitafell gabbro contact aureole, irrespective of temperature, may thus also have been restricted to lower X_{CO_2}-values than was andradite within the same rock.

A similar dependency of X_{CO_2} on a univariant reaction curve, of similar shape to that in figure 10.3 a, but principally involving:

$$\text{actinolite} + CO_2 \rightarrow \text{chlorite} + \text{calcite} + \text{quartz}$$

was also found by Best (1978). The chlorite-calcite pair sited at the low T - high X_{CO_2} side of the univariant curve, restricting the low-temperature stability field of actinolite to H_2O-rich fluids. Best's result thus suggests that the actinolite development within the presently recognized actinolite zone was restricted to X_{CO_2}-poor fluids in the environments where fluid temperature was controlled by the boiling curve.

While the discussion above not only relates to the hydrothermal system in general but also to the contact aureoles, a recognition of the possible physico-chemical conditions within the contact aureoles is left with figure 10.4 (slightly modified from figure 12 of Shimizu and Hyama, 1982). The principal constituents of skarns in the

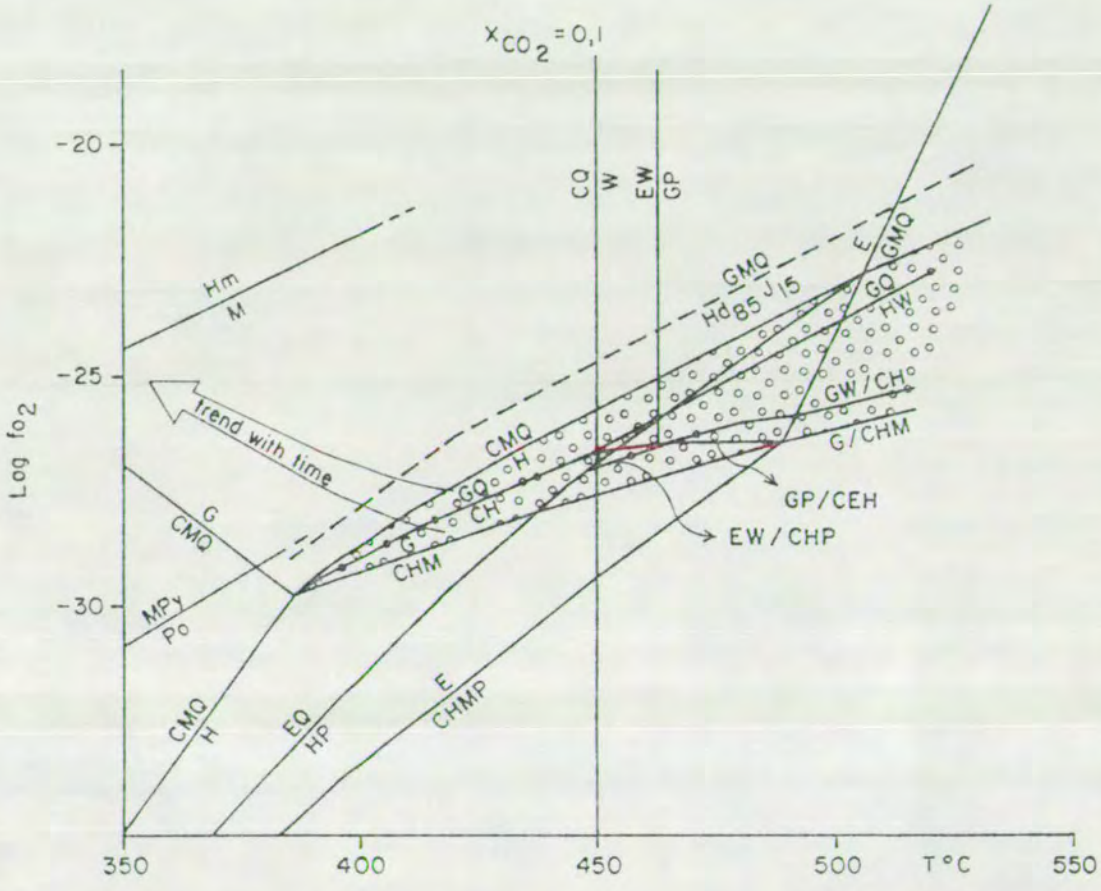

Figure 10.4

Temperature – oxygen fugacity diagram in the system $CaO - FeO - Fe_2O_3 - Al_2O_3 - SiO_2 - H_2O - CO_2$ at $X_{CO_2} = 0,1$ and P=0,3 k bar, from Shimizu and Hyama (1982). The position of the broken curve is shown approximately from data provided by Burton et al. (1982). Abbreviations : C : calcite, E : epidote, G : andradite, H : hedenbergite, Hm : hematite, J : johannesite, M : magnetite, P : plagioclase, Po : pyrrhotite, Py : pyrite, Q : quartz, W : wollastonite. See text for further explanation.

Nakatatsu mine, central Japan, are clinopyroxene partly replaced by garnet, preceeding ore deposition. Shimizu and Hyama (1982) used data from Kursakova (1971), Liou (1973,1974) and Gustafsson (1974) on the stability fields of hedenbergite, andradite, epidote, and other related minerals, recalculated and summarized by Helgeson et al. (1978), to calculate phase relations in the system $CaO-FeO-Fe_2O_3-Al_2O_3-SiO_2-H_2O-CO_2$ at 0.3 kbar total pressure and $X_{CO_2} = 0.1$, plotted in a T-f_{O_2} diagram (fig. 10.4). The pressure estimate of 0.3 kbar is similar to that in the Geitafell area which makes their T-f_{O_2} diagram applicable to the present study.

The stippled area in figure 10.4 shows the field of coexistence of andradite and hedenbergite. The hedenbergite-andradite assemblage in the Geitafell contact aureole may thus possibly have been formed at temperatures below 400°C at f_{O_2} value as low as 10^{-30}, and evidently at higher T-f_{O_2} values within the stippled field. Experimental studies by Burton et al. (1982) to evaluate the effect of Mn on the hedenbergite oxygen-buffering reaction showed, that addition of 15 mole percent johannsenite to the clinopyroxene raised the stability field of hedenbergite by about 1 log f_{O_2}-unit over the temperature range of interest. This effect is shown by the broken line in figure 10.4. The existence of manganese-rich pyroxene inclusions in the andradite from the Geitafell gabbro contact aureole (point 11 in fig. 10.2) may suggest that the oxygen fugacity rose upon cooling within the contact aureole, the direction of which in time is shown in figure 10.4.

By comparing the direction of effects upon variable X_{CO_2}, f_{O_2}, T, and P_{fluid} in figures 10.3a,b and 10.4 it is concluded that f_{O_2} in the contact aureole dropped considerably and below values

determined by the HM-buffer curve upon the gabbro intrusion. The hedenbergite$_{ss}$-andradite (mt,cc,qtz) may have been formed at temperatures above 380°C up to ca. 600°C, the stability field of andradite increasing with fall in X_{CO_2}. Both the temperature and pressure estimates are above critical point values (T :374,15°C, P : 221,2 bars for pure water), and the hydrothermal fluid was in a supercritical condition. Recognition of hydrothermal fluids at supercritical temperatures in an Icelandic hydrothermal system, demonstrates the path of heat distribution from shallow level magma bodies into a hydrothermal system, both as one of the primary causes for the establishment and maintenance of the latter. The apparent course of events is:

1) P_{fluid} in the contact aureoles may have approached $P_{lithostatic}$
2) Fluids at supercritical temperatures existed for some time in the vicinity of large magma bodies.
3) The pre-existing hydrous fluid must have undergone boiling and phase separation, driving gases (CO_2 , SO_2) out of the contact aureole systems. The boiling of the hydrothermal fluids would necessarily proceed outwards from the heat source and subsequently inwards upon cooling.
4) The supercritical fluids were CO_2-poor and reducing, f_{O_2} - values ranging between 10^{-30} - 10^{-15}.
5) Within the contact aureoles well-developed fluid-rock reaction zones were developed in environments of high fluid/rock character, driving Ca^{2+} and probably all other elements not participating in rock replacement by chlorite-albite into solution.
6) Upon cooling the hydrothermal fluid oxidised and f_{O_2}-values crossed the HM-buffer curve as the fluid adjusted to ambient

hydrostatic P-T values.

High-temperature fluids at pressures far below 221.2 bars may alternatively have arisen from heating of dry steam. The former presence of superheated dry steam seems necessary to explain the high-temperature assemblages (actinolite-sphene) within shallow-level sheets of intrusive phase 5, for instance, sited only 100-200 m below the palaeosurface. The hydrous fluid adjacent to the hot intrusion(s) would need to have boiled until all liquid water was evaporated, and the dry steam then heated further, entering the hot intrusive rock to cause low-pressure superheated dry steam - rock alteration. Evidently, such superheated dry steam could also exist in the gabbro contact aureoles and hydrous fluid at supercritical conditions does not necessarily provide the only possibility for explaining the skarn mineral paragenesis. In fact, the fluids in the Geitafell gabbro contact aureole may have passed through both supercritical and superheated fluid regions, eventually adjusting to conventional hydrothermal hydrostatic values.

CHAPTER 11

COMPARISON WITH ACTIVE HYDROTHERMAL SYSTEMS

Most of the active high-T hydrothermal systems in Iceland lie within volcanic centres (fig. 1.1, and chapter 1). The active high-T fields studied by deep drilling are restricted to 4 areas at the Reykjanes peninsula (Reykjanes, Svartsengi, Krísuvík and Hengill, fig. 1.1.) in SW-Iceland, and 2 areas in NE-Iceland (Namafjall and Krafla). Only three of these fields strictly relate to central volcanoes, i.e. the Hengill volcano, and the Namafjall and the Krafla fields of the Krafla volcano. The other three fields lie within the centres of volcanic fissure swarms at the Reykjanes peninsula.

The Krafla volcano is the more mature of the two central volcanoes studied by deep drilling, and experienced, for instance, a candera collapse during the last interglacial period (Bjornsson et al. 1977), while a caldera has not developed in Hengill. The Krafla volcano is thus suitable for a short comparison with the Geitafell volcano. Common to all the active high-T fields studied, however, is a depth-related secondary mineral zonation, with increasing depth : (i) smectite/zeolites (Sm/Z-zone), (ii) mixed layer clay minerals (MLC-zone), (iii) chlorite/epidote (Chl/Ep-zone) and (iv) chlorite/actinolite (Chl/Act-zone) (Kristmannsdottir, 1979, 1981; Palmason et al. 1979). The depths to the zonal boundaries and the thickness of the zones are variable from field to field, and only in the Krafla field has the fourth zone been postulated by the fairly zommon occurrences of actinolite at depths. Actinolite occurrences, however, are known from other fields.

Figure 11.1 shows a simplified map of the Krafla volcano, which

Figure 11.1.

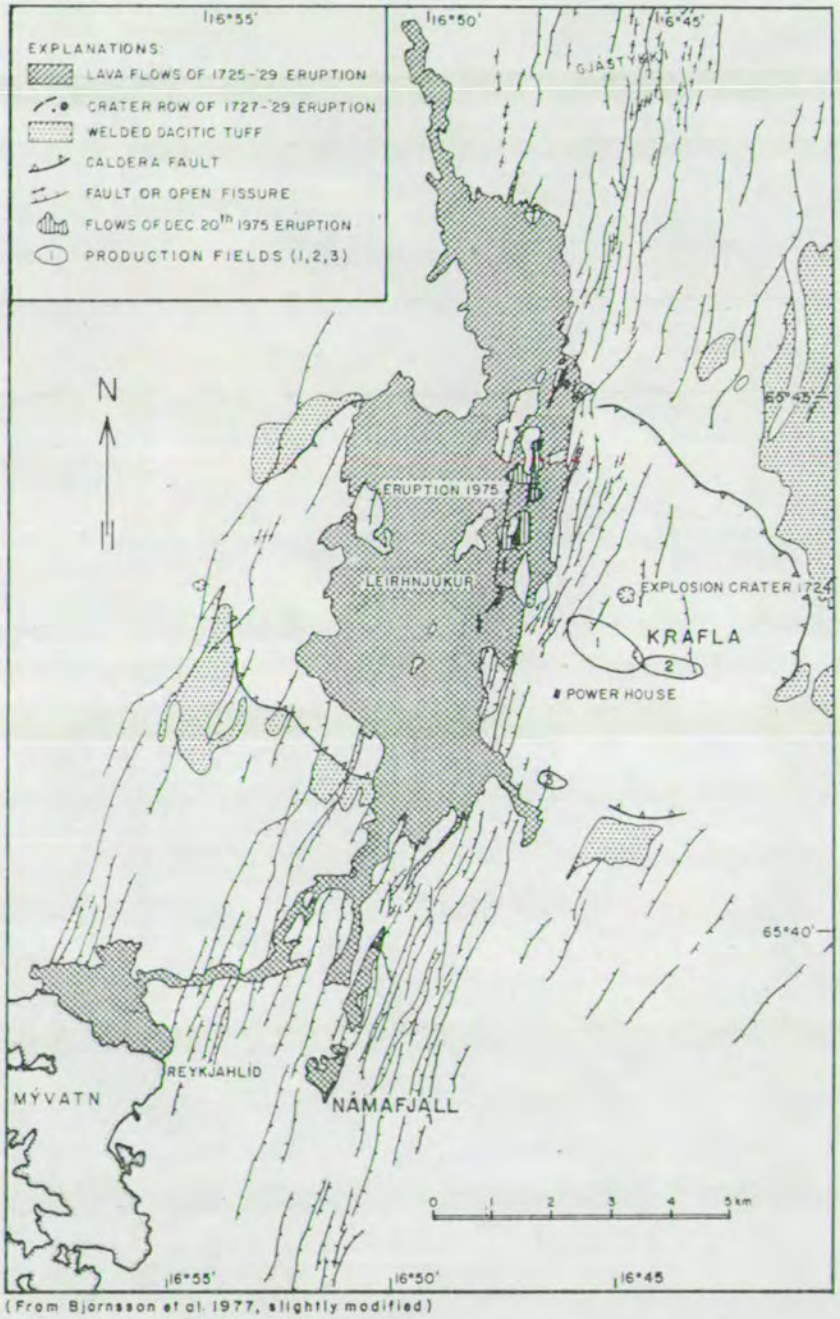

(From Bjornsson et al. 1977, slightly modified)

SIMPLIFIED MAP OF THE KRAFLA CENTRAL VOLCANO.

lies within the central portion of a 100 km long fissure swarm, part of which is shown in fig. 11.1. The caldera measures ca. 8x10 km, and is nearly filled to the rim by young volcanics, subglacially formed hyaloclastite ridges and postglacial lava flows. Major silicic eruptions have not occurred in postglacial time, while four silicic eruptions, during the last glacial period, produced large domes and ridges within and around the caldera (Bjornsson et al. 1977).

Knowledge of the subsurface geology of the Krafla volcano is restricted to the limits of the production fields (c.f. fig. 11.1). The general characteristics of production field 1 have been described by Stefansson (1981), Kristmannsdottir (1979,1981) and Armannsson et al. (1981). Production fields 2 and 3, however, were opened in 1980 and in 1982 respectively, and publications thus restricted to preliminary progress reports at NEA (in Icelandic). Due to the author's involvement in the subsurface geological research, during 1975-1977, and since 1981, selected information from fields 2 and 3 can be provided. However, as the Krafla research is still in progress, the discussion below is necessarily restricted to a general description.

The host rock stratigraphic division includes two major units of basaltic hyaloclastites above ca. 800-1000 m depth, separated by an approximately 200 m thick basalt lava unit (ca. 300-500 m depth), and underlain by a basalt lava formation, extensively intruded by sheeted dykes.

Below ca. 400 m depth, basaltic intrusions become increasingly more common and approach 100% of the sections below ca. 1500 m depth. A continuous gabbro intrusion is reached below ca. 1900 m depth within production field 2.

The basaltic intrusive rocks include fine-grained aphyric basalt,

porphyritic basalt, dolerite, porphyritic dolerite and gabbro. Medium to coarse-grained dolerites are the most common. The majority of the basaltic intrusions range in thickness from less than 2 m up to 10 m, as seen by rock-cutting analyses (2 m sampling frequency). This suggests that most of the intrusions are in the form of inclined sheets, while some of the near vertical drillholes penetrated sub-vertical dykes for several tens of metres. The strike/dip relation of the sheeted complex is unknown.

While intrusions of intermediate chemical composition have been found, acid intrusions occur within all the production fields. Their frequency within the vertical sections varies greatly. A thick (tens of metres) subhorizontal acid intrusive formation is sited within the lower hyaloclastite unit in field 2. Elsewhere, the acid intrusives chiefly occur below 1500 m depth, and generally range in thickness from ca. 1-20 m. The acid rocks range from poorly crystalline altered felsitic rock, via felsite, to granophyre.

Due to the exclusive use of tricone drill bits a detailed knowledge of the magmatic evolution (as well as the hydrothermal evolution) is lacking from the Krafla fields. Still it is clear from the stratigraphic relationships that the intrusive rocks range in age. The intrusive rock alteration varies greatly, from virtually unaltered rocks to extensively altered ones. Most commonly, however, the extent of secondary replacement of the dense intrusives, is confined to the interstitial matrices and marginal replacement of the primary minerals. Chlorite, albite, actinolite and pyrite are amongst the common replacement minerals in the basaltic intrusives, while quartz, epidote and pyrite are the most common replacement minerals of the acid rocks.

The production fields in Krafla are situated within hydrothermal

upflow zones. Surface alteration is widespread and active fumaroles, boiling mud pits and hot springs exist locally within the fields. Some of the drillholes thus penetrate extensively altered rocks from the surface down, e.g. where all volcanic glass is replaced by secondary products. In drillholes sited near the flanks of the production fields, however, fresh volcanic glass may be encountered to several hundred metres depth.

In mapping of the secondary mineral distribution within the Krafla fields, a fourfold zonal division has been used and correlated with downhole temperature (see fig. 11.2 b, and later discussion). The overall characteristics of these mineral zones are discussed by Kristmannsdottir (1979) but basically they involve a prograde transformation of clay minerals from smectite to chlorite, and then the additional appearance of actinolite in chlorite-bearing assemblages. Of concern to the present discussion is the type of the associated mineralogy in each zone, and the zonal patterns.

The Sm/Z - zone. This zone reaches from near the surface down to various depths. In some of the drill hole sections, the zone may reach down to ca. 700 m depth, while more commonly only the upper 100-300 m of the sections fall within this category. Iron-saponitic smectite is the most common secondary product, chiefly replacing volcanic glass, but is also deposited in vesicles and veins. In the upper part of the zone, low-T zeolites are encountered, including some of the following minerals : chabazite, stilbite, epistilbite, heulandite, scolecite/mesolite, thomsonite and mordenite. Their distribution within the production fields, however, is irregular, and

commonly only 1-3 species are present within the drillhole sections. With an increase in depth and temperature, all the low-T zeolites disappear and laumontite may appear instead. In the lowest part of the zone, laumontite may be absent, while wairakite is sometimes present. Other common minerals include : opaline silica and chalcedony at upper levels, along with pyrite and calcite, with the addition of quartz at deeper levels.

The MLC-zone. The transition to this zone is marked by the disappearance of smectite, and the incoming of mixed-layer smectite/chlorite. Wairakite is sometimes encountered throughout this zone. The presence of quartz, pyrite and calcite is continuous. At the deepest levels in the zone prehnite is sometimes present. The thickness of the MLC-zone varies within the fields, from ca. 100-400 m.

The Chl/Ep - zone. The boundary to this zone is marked by the first appearance of epidote. Mixed layer clays of sm/chl are no longer involved, and chlorite has become the chief phyllosilicate. From this level, chlorite and epidote occur more or less continuously to the base of the drillhole sections, along with quartz and pyrite. Feldspar replacement by albite and ilmenite replacement by sphene become pronounced. K.feldspar may be found. Wairakite may be present, normally only within the upper 300-400 m of the zone. Prehnite may be present within the upper 1000 m of the zone, as well as calcite, which locally may be exceedingly abundant. At the deepest levels, and now within the Chl/Act - zone, all three (wai,pr,cc) are commonly absent.

The depth to the MLC-Chl/Ep zone boundary varies considerably, in accordance with the thicknesses of the overlying mineral zones.

At the flanks of the production fields the boundary may be sited as deep as 800-1000 m. In general, however, the zonal boundary rests at ca. 600 m depth within production field 1, and at approximately 300 -350 m depth in production fields 2 and 3. The boundaries of the mineral zones above thus take the form of a landscape, with rises in the main upflow zones.

The Chl/Act - zone. The boundary to the Chl/Act-zone in Krafla has not been rigidly defined, but may possibly be set close to 1000 m depth, from where the actinolite occurrences become fairly continuous to the base of the sections. However, actinolite is found locally from ca. 500 m down, within the Chl/Ep-zone, but apparently related to basaltic intrusive rocks. The high-level actinolite occurrences in Krafla may thus be the counterpart of those found associated with the I.P.5 sheets within the epidote zone in Geitafell, or vice versa.

Occasionally, the skarn minerals hedenbergite, andradite, magnetite and wollastonite are found at or near the contacts of basaltic dykes in Krafla, and apparently formed by a metamorphism of earlier qtz-cc-py veins (Kristmannsdottir, 1978, 1981) Apart from wollastonite, the skarn minerals reported from Krafla are related by type to those in the gabbro contact aureoles in the Geitafell volcano. In both cases, a genetic relationship to hot intrusive rocks is comparable. The contact skarns in Krafla are encountered from ca. 500 m down.

The first reported wollastonite occurrence in Iceland is from Krafla (H. Kristmannsdottir, 1978, 1981). The white fine-grained wollastonite grows in a fibrous habit, commonly radiating from tiny white cores sitting on earlier epidote, quartz or calcite. The

wollastonite appears fairly wide-spread in the cutting samples, but it is seldom found (or noticed) in thin sections. A two-fold origin for the wollastonite occurrence in Krafla has been proposed, (i) a contact metamorphic origin, growing at the expense of qtz+cc, and (ii) a hydrothermal origin, below ca. 1000 m depth in Krafla, where fluid temperatures exceed 300°C (Kristmannsdottir, 1981).

Andradite is found sporadically at deep levels in Krafla, and in some cases clearly related to contact metamorphism (Kristmannsdottir, 1978). In Geitafell, the andradite distribution is confined to amygdales and veins. Both contact metamorphic and hydrothermal origins are proposed. Whether the same applies to the Krafla volcano is unknown.

Amongst minerals of rare, sporadic or local occurrences in Krafla, and not previously mentioned, are : pyrrhotite, goethite, maghemite, chalcopyrite, rutil (Steinthorsson and Sveinbjornsdottir, 1981), leucoxene, illite, talc, vermiculite, anhydrite, gyrolite, truscottite and reyerite (Kristmannsdottir, 1983). Only some of these have been found in the Geitafell volcano.

From the above description it is evident that the Krafla and the Geitafell volcanoes have quite a few geological and hydrothermal features in common. The large scale stratigraphic division happens to be similar, both are predominantly constructed by basaltic volcanics, late acid extrusive rocks and calderas are encountered in both, and in general, their shallow level intrusive complexes appear to be of similar nature.

The depth-contoured zonal boundaries in the active system are of interest with respect to the shape of the mineral zones in the Geitafell volcano. The epidote distribution, for instance, within

the upper-part of the Ep-zone in Geitafell, is restricted to local occurrences, a feature probably reminiscent of former hydrothermal upflow zone, as has been proposed, e.g. for the caldera fault vicinity.

The counterparts of the Sm/Z- and the MLC - zones in Krafla, may be represented by the flank rock alteration products and the Chl-zone in Geitafell during the peak-activity period, and - evidently - by part of the superimposed zeolite bearing assemblages during the cooling period of the extinct system. Difficulties, however, arise as to the distribution of the MLC-clays in Geitafell, while both the optical and the chemical analyses are suggestive of their presence, particularly within the Chl-zone in Geitafell.

The Chl/Ep- and the Chl/Act-zones in Krafla have similar mineralogy as the Ep- and the Act-zones in Geitafell. The chief difference relates to the superimposition of late hydrothermal products upon earlier in the extinct Geitafell volcano.

The production characteristics from within production field 1 have been described by Stefansson (1981). Two geothermal zones are encountered, (i) an upper zone, between ca. 200-1100 m depth, with a mean temperature of 205°C (range 195-215), and (ii) a lower zone below ca. 1100-1300 m depth to at least 2200 m (deepest well), with temperatures from 300-350°C close to the boiling curve values with depth. The production characteristics are different, as boiling in the lower zone occurs within the strata, yielding a two-phase mixture into the wells. In the upper zone boiling occurs within the wells (water dominated system). The two zones are connected by an upflow channel, surfacing in Hveragil, which also separates procuction fields 1 and 2.

In production field 2, the wells are fed from a single geothermal zone. Temperatures at shallow depths are much higher, above 200°C at 500 m depth, ca. 260°C at 700 m, being close to boiling curve values to

depths, of ca. 330°C at 2 km depth (Stefansson et al., 1982). As with the lower zone in field 1, boiling occurs within the strata in production field 2.

The fluid composition from the three geothermal zones above are quite variable (see 1-3, table 13, appendix 1). The fluid from production field 3, above 1200 m depth, has yet another character (4, table 13), while a rock temperature profile is not available at present.

If the present-day rock temperature profiles are compared to the position of temperature correlated mineral zones (see later discussion), e.g. at the MLC-Chl/Ep zone boundary, it appears that the epidote formation in the upper 200-400 m of the Chl/Ep-zone must be fossil. Scattered data from the cutting analyses suggest that epidote is being overprinted by wairakite and calcite in this interval (e.g. Stefansson et al. 1982, and later preliminary reports). However, the lack of core samples results in lack of detail.

Typical fluid chemistries, as sampled at well heads from the three production fields in Krafla, are shown in table 13, appendix 1 (anal. 1-4, NEA data), including well head pressure during collection and calculated entalphy of total flow. For comparison, a mean from 17 analyses from well Rn-8 sunk into the Reykjanes brine system is shown by anal. 5, table 13, which reflects the marked chemical differences between the meteoric- and the oceanic fed hydrothermal systems. Other chemical components, like iron and alumina, are not included in the routine analyses, partly due to analytical difficulties at the low metallic concentrations involved (Armannsson, pers. comm.). Analytical data on iron and alumina, and all other dissolved solids not shown in the tables, is thus sparse, but included in the TDS-figure. Calculations of mineral--solute equilibria, involving iron and alumina, for example, are thus not available at present, an additional constraint exerted by a lack of thermodynamic data on the iron bearing mineral assemblages involved in the active systems, while improvements may be in sight (Kristmannsdottir,

pers. comm.). In addition, the two phase condition (steam and water) within parts of the Krafla reservoirs, make calculation of the deep fluid chemistry somewhat uncertain (Kristmannsdottir, pers. comm.) partly due to the variable flow properties of the steam and the liquid, to an extent governed by the steam fraction, which changes upon exploitation of the wells (see general discussion in chapter 4, p. 114-115).

Accordingly, studies of the fluid chemistry in the active fields - as yet - do not provide exclusive information on the mineras assemblages presently being formed in the Krafla system. However, information on the solubility relationships between the present-day fluids and carbonates, sulphides, iron-oxides and simple silicates exists for Krafla, as well as on the overall effect related to the active volcanic episode in Krafla, since 1975 (e.g. Armannsson et al. 1981), briefly mentioned on p. 105. At present, however, a case history from the Krafla volcano does not add much information to the extinct system in Geitafell, while the large scale geological and mineralogical similarities are in evidence. However, there is a profound variation in the gas composition of the deep fluids from the three production fields (table 13, anal. 2-4), which in the case of field 1 is to a large extent related to the presently active volcanic episode (Armannsson et al. 1981), locally disturbing the open hydrothermal system for an unknown length of time.

In studies of active hydrothermal fields in general, rock and fluid temperatures have long been regarded as the most important factors governing the grade of alteration, while more recent geothermal studies have demonstrated that permeability and fluid composition are usually at least as important as temperature (e.g. Browne, 1978). Within active hydrothermal systems throughout the world, a fairly consistent correlation between down-hole temperatures and secondary mineral zoning has been observed. Despite age differences between the various hydrothermal systems, the number of fields studied is sufficiently large to warrant the establishment of schemes of minimum temperatures/mineral occurrences. In many cases also the presence of

late alteration events superimposed upon earlier have been evaluated prior to such presentations. A minimum temperature-mineral zoning scheme for Icelandic hydrothermal fields has recently been published by Kristmannsdottir and Tomasson (1978) and Palmason et al. (1979). These are shown in figure 11.2 a, b.

The discussion below on the relation between mineralogy - temperature is summarized from Kristmannsdottir and Tomasson, 1978, Palmason et al. 1979, Kristmannsdottir, 1979, 1981, and Stefansson, 1981. Figure 11.2 a shows the zonal arrangement of zeolite occurrences correlated with temperature. Most of the zeolites appear to have formed at temperatures below 100°C. At temperatures between 100-120°C laumontite replaces other zeolites, except mordenite which may persist up to ca. 200°C. At 180°C wairakite appears instead of laumontite, and all zeolites except wairakite (and analcime) have disappeared by ca. 200°C. Wairakite is recorded at temperatures up to 300°C.

Chalcedony precipitates at temperatures below 100°C, while quartz forms at all higher temperatures. Calcite is common at all depths at temperatures up to 270-300°C.

The mineralogical transition at approximately 200°C marks a division between low- and high-temperature hydrothermal systems in Iceland. This transition is marked by the appearance of wairakite at the expense of laumontite, or deposited directly from fluid, and smectite is transformed to mixed-layer clay minerals (figure 11.2b) which in turn converts to chlorite at higher temperatures. Between 230-250°C, chlorite becomes the dominant sheet silicate, and is commonly accompanied by the appearance of epidote at ca. 230-260°C. Prehnite is found at similar depths to epidote in most areas, but no reliable temperature estimates have been established. In the upper

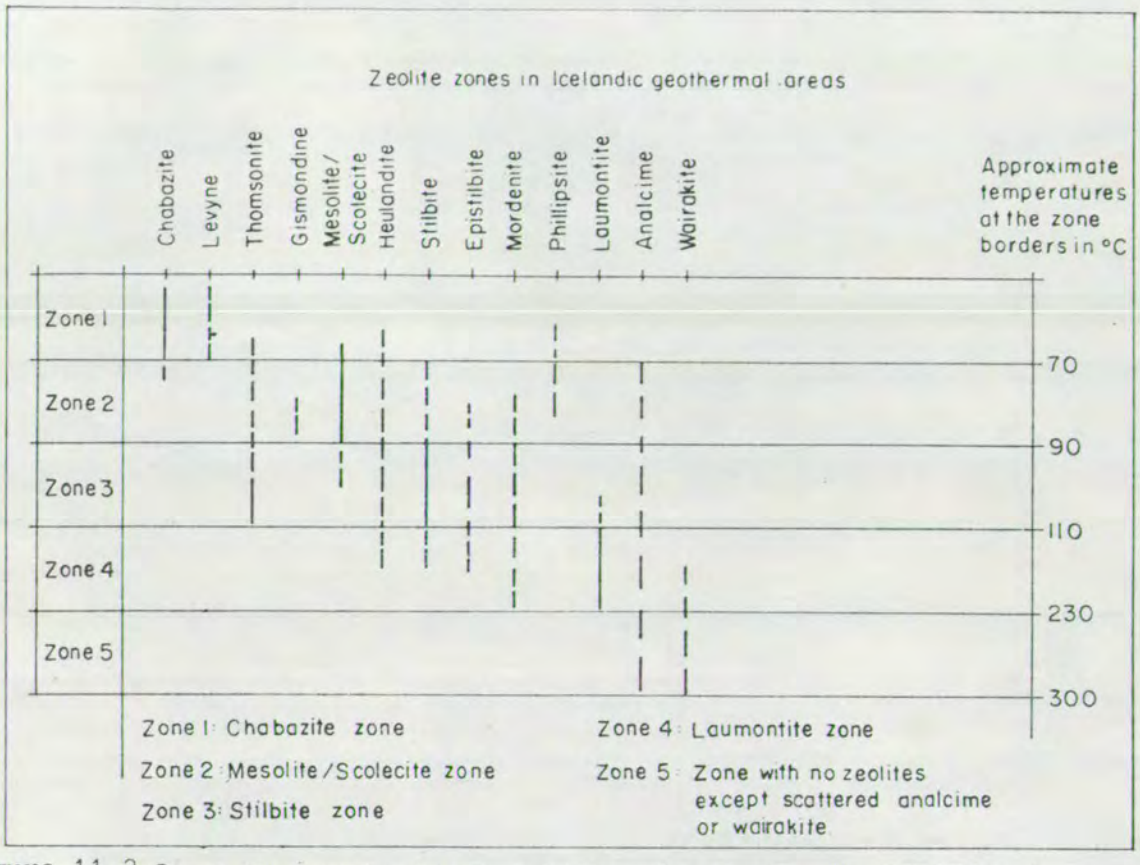

Figure 11.2 a. Zeolite zones found in the Icelandic geothermal areas. The distribution of individual zeolite species within the zones is indicated. Also shown in the approximate temperature at the zonal boundaries. (From Kristmannsdottir and Tomasson, 1978).

Correlation of alteration zones with rock temperature in high-temperature geothermal fields

Rock Temperature °C	Alteration zones	Index minerals	Mineralogical Characteristics	Regional Metamorphic Facies
50	I a	Smectite Zeolites	Low temperature zeolites and smectite forms	Zeolite Facies
100	I		Low temperature zeolites → laumontite	
150	I b		Smectite interlayered	
200			Laumontite → wairakite Smectite → mixed-layer clay minerals	
	II	Mixed-layer clay minerals		
250	III	Chlorite Epidote	Mixed-layer clay minerals → chlorite Epidote-continuous occurrence	
300	IV	Chlorite Actinolite	Actinolite forms Plagioclase commonly albitized	Greenschist Facies

F16886

Figure 11.2 b. Successive alteration zones observed with increasing depth and temperature in active high-temperature areas in Iceland. A correlation is made with rock temperature and regional metamorphic facies. Also shown are the index minerals and mineralogical changes characterizing each of the zones. (From Palmason et al., 1979).

range of the temperature scale, actinolite appears at temperatures above 280°C, wollastonite and andradite at temperatures above 300°C and hedenbergite and magnetite have been detected. Wollastonite is regarded as forming hydrothermally at temperatures above 300°C, but may also be related to contact metamorphism at dyke margins, together with andradite, hedenbergite and magnetite. Pyrite also and, more rarely, pyrrhotite occurs over the whole hydrothermal temperature range. The highest recorded fluid temperature (345°C) in Iceland is from within the Krafla geothermal field.

By comparing the zonal sequence in figure 11.2a,b, to the present study, it is obvious that the Geitafell hydrothermal system passed through all these zones with time. Using the temperature correlation in the figure the high-temperature system in Geitafell was probably established at temperatures above 200°C, and the transition from the epidote zone into the andradite- and actinolite zones is tentatively set at ca. 300°C. From the regular depth related distribution of both andradite and actinolite (map II, figs. 4.3, 4.4, 4.5) it can further be concluded that both these minerals formed hydrothermally, apparently above 300°C. The retrograde transition from high- to low-temperature systems after the caldera event can similarly be set at ca. 200°C, marked by the replacement of wairakite by laumontite. The emplacement of stilbite, heulandite and other common zeolites is deduced to have occurred at fluid temperatures below ca. 120°C.

An upper temperature limit can not be established from the secondary mineral assemblages in Geitafell. In conventional liquid--dominated active hydrothermal systems, the upper temperature limit is normally controlled by the boiling curve, which allows for slightly higher fluid temperatures in saline systems (section 4.2). Most

systems explored this far have reservoir temperatures below 280°C (Browne,1978), while higher temperatures are recorded, e.g. from Iceland (see above), Salton Sea California, up to 360° (Palmer, 1975) and Cierro Prieto, Mexico, up to 388°C (Mercado, 1969), but still within limits controlled by the appropriate boiling curves.

The hydrothermal fluid temperatures at Geitafell would probably have followed the same pattern during the longer "dormant" periods. During the shorter intrusive injection episodes, however, hydrothermal fluids at superheated and supercritical temperatures appear to have existed within the system for unknown periods. From the study of intrusive- and contact rock alteration two such major episodes can be recognized, accompanying intrusive phases 2-6, and intrusive phase 10 respectively.

Extensive experimental studies on the stability relations amongst zeolites have been undertaken, e.g. by Liou (1970, 1971 a,b, c,d), Thompson (1970,1971 a,b), the results of which are in fairly good agreement with the temperature correlation scheme for Icelandic zeolites presented by Kristmannsdottir and Tomasson (1978). The experimental data thus supports the temperature estimates made for the Geitafell hydrothermal system.

In general agreement with the discussion above, wairakite is regarded as the highest-grade zeolite formed in low-pressure environments of hydrothermal fields (e.g. Liou, 1979), whereas prehnite forms assemblages with both laumontite and wairakite its formation generally occurs at higher pressures than wairakite (e.g. Liou, 1971a). However, in low-CO_2 environments where CaO is present in excess ($CaO/Al_2O_3 > 1$) relative to the wairakite composition, prehnite may be stable in geothermal areas (Liou, 1971 a). Thompson (1971 a) also

considered the effect of variable partial pressure of CO_2 (p_{CO_2}) in low-grade metamorphism in the system $CaO-Al_2O_3-SiO_2-H_2O-CO_2$, and concluded that (a) stability of zeolite assemblages was limited to low p_{CO_2} and (b) zeolites were only stable with respect to calcite, clay minerals and quartz if X_{CO_2} was less than 0.0075 (for $P_{fluid} = P_{total}$ = 2 kbar). Calculations of reactions producing prehnite from zeolite+calcite suggested an equilibrium p_{CO_2} of ca. 30-40 bars ($P_{fluid} = P_{H_2O} + P_{CO_2}$ = 2000 bars, i.e. X_{CO_2} : ca.0.015-0.02). The common association of zeolites and calcite in low-grade metamorphic and hydrothermally altered rocks may therefore reflect univariant equilibrium conditions or in some cases, disequilibrium precipitation (Thompson, 1971 a). The same general principle noted by Taylor and Liou (1978) for mt+cc+qtz → andradite, and chl+cc+qtz → actinolite (Best 1978) in relation to X_{CO_2} thus appears to apply to most of the hydrothermal minerals occurring in the Geitafell hydrothermal system (i.e. zeolites, epidote, prehnite, garnets, actinolite), namely that these minerals may be formed under univariant equilibrium conditions within some definite P-T field at low X_{CO_2}. The temperature estimates from active hydrothermal systems may thus give information on the location of such curves at low fluid pressures (ca. $\leq$ 200 bars) in natural systems. A simplified P_{fluid}- T diagram from Liou (1979) is shown in figure 11.3. The stability fields of laumontite and wairakite at low-fluid pressures coincide with the temperature estimates for these two minerals from active hydrothermal fields. The P_{fluid} - T field of occurrences of laumontite, wairakite, prehnite, epidote, andradite and actinolite in Icelandic hydrothermal systems are also shown in figure 11.3 in accordance with the discussion above.

The effect of permeability on alteration mineralogy has already

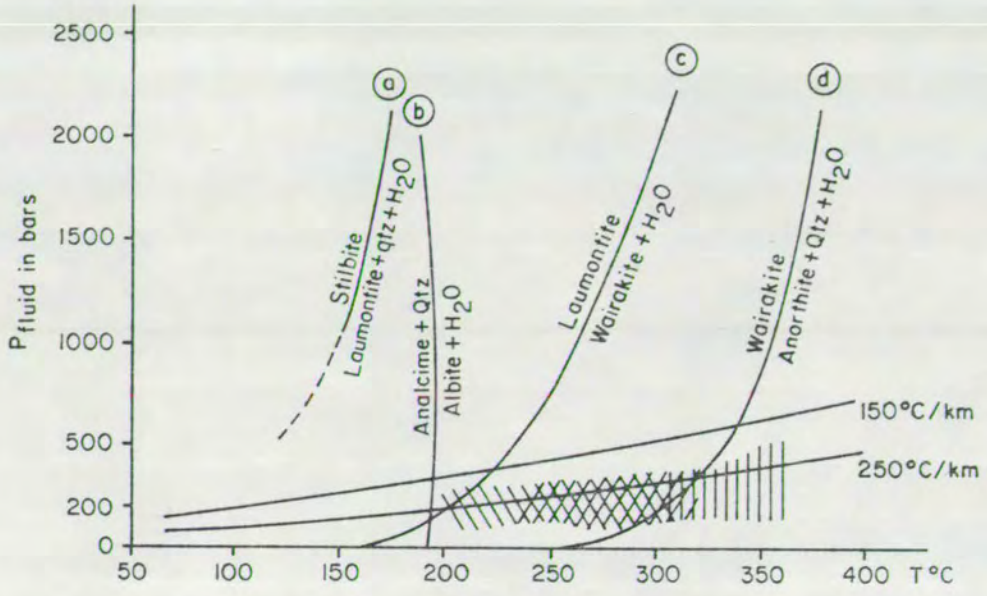

Figure 11.3

P_{fluid} - T diagram simplified from Liou (1979). Curve (a) from Liou (1971, b), (b) from Thompson (1971, b), Liou (1971, d) (c) Liou (1971, c) (d) Liou (1970). Geothermal gradients of 150°C/km and 250°C/km shown. The field of occurrence of :

prehnite, wairakite

prehnite, wairakite, epidote

epidote, andradite, actinolite

are also shown based on data from Palmason et al. 1979, Liou 1974, Taylor and Liou 1978.

been discussed in chapter 4. Apart from the metastable persistence of the primary minerals in rocks of low permeability, the correlation between secondary feldspars and high permeability made by Browne (1970) is regarded as additional evidence for movements of large volumes of fluid in the vicinity of the Geitafell caldera fault.

The relationship between fluid compositions and hydrothermal mineralogy has been discussed by Ellis and Mahon, 1977; Browne, 1978 and Fournier, 1981: A short review is provided below. While the chemical processes leading to hydrothermal alteration have been qualitatively understood for years (e.g. Fenner, 1936), it is only in the last decade or so that sufficient analytical data has become available for quantitative evaluation. The use of the silica geothermometer, for instance, to estimate deep fluid temperatures, depends on equilibrium between silica in the fluid and a silica mineral (Mahon, 1966; Fournier and Rowe, 1966; Arnorsson, 1975; Arnorsson et al. 1982 c). Similarly, successful use of Na-K and Na-K-Ca geothermometers requires that the solutions are in equilibrium with albite and K-feldspars (Ellis and Mahon, 1967; Fournier and Truesdell, 1973; Arnorsson et al. 1982 c). Chemical studies of geothermal fluids have shown that equilibrium with quartz, chalcedony and Na- and K-feldspars is attained, or closely approached, in liquid-dominated geothermal reservoirs. Knowledge of the solubilities of hydrothermal minerals and of the chemical equilibria between minerals and solutions through determination of the activities of aqueous species is essential for vigorous evaluation of hydrothermal systems. Isothermal activity - activity diagrams are conventionally used for presentation of mineral-aqueous solution equilibria. Such diagrams have been used to compare observed mineral assemblages with fluid composition, e.g. for

the Broadlands and Wairakei geothermal fields, New Zealand (Browne and Ellis 1970; Ellis and Mahon 1977), to show (a) close correlation of mineral assemblages with fluid compositions, (b) the change in mineral assemblages upon cooling of the geothermal fluids and (c) the trends with compositional changes of the fluids, e.g. with respect to CO_2. The latter demonstrates the critical role of CO_2 in determining stability relations of Ca-bearing minerals - in much the same way as has already been discussed for andradite and actinolite.

The large number of ions, ion pairs, variation in valency and presence of complexes in solutions have necessitated the use of computer programs for derivation of the activities of species at elevated temperatures. Various computer programs are now available (e.g. Arnorsson et al. 1978, 1982 a,b,c,). Calculations of mineral/solution equilibria at elevated temperatures are thereby available provided analytical data on fluid chemistry and temperatures exist for the studied hydrothermal system. Clearly it should soon be possible to reverse the calculations from mineral assemblages and inclusion--temperatures to depict, on a sample basis, the apparent fluid composition. The effects of cooling on the alteration mineralogy and of hydrothermal boiling on phase separation have also been evaluated. The drastic changes in fluid composition upon boiling, for instance, are discussed for Icelandic thermal waters by Arnorsson (1978, et al. 1982 b). The most significant changes involve pH of the fluids, and degassing of CO_2 and sulphur species . The Icelandic thermal fluids are normally close to saturation with respect to calcite. During boiling, CO_2-content of the liquid phase is controlled (a) by degassing during phase separation and (b) by supersaturation of the liquid with respect to calcite causing calcite precipitation. Similar

controls on the sulphur content of the thermal fluids involving sulphide deposition are discussed by Arnorsson et al., (1982 b). The consequent changes in fluid compositions may lead to precipitation of silicates accompanied with still further changes in fluid chemistry. The fluid composition thus changes between the stability fields of the various secondary minerals.

Application of a modification of Gibb's phase rule allowed Arnorsson et al. (1982 b) to predict that 10 alteration minerals would form at equilibrium in geothermal water-basalt systems (and 11 minerals at each P-T during alteration of acid rocks when equilibrium is attained). From the number of secondary minerals formed somewhere within the rocks within each mineral zone during each period in the Geitafell system, mineral/solution equilibria may well have been approached. Accordingly, it should be possible to infer the fluid composition from the mineral assemblages (on a sample basis) during each time period - provided the temperature is known to fit the appropriate phase diagram.

Evidently this can not be done at present for the Geitafell hydrothermal system due to lack of data, since the temperature estimates overlap and extend the entire fields of the hydrothermal systems - except at selected temperatures and for specific examples within the samples. However, studies in line with the above can be undertaken within active fields. It is, however, essential to obtain core samples from the active fields to provide the necessary mineralogical data (e.g. Browne 1970 ; Fournier, 1981). While core samples from Icelandic high-temperature fields are rare, the present study hopefully shows the necessity of core sampling in the active fields. Through core samples the latest mineral deposits in veins and ves-

icles, and associated wall-rock alteration zones can be determined and compared with the fluid chemistry. The conclusions from such studies have economic value in the exploitation of active hydrothermal fields, as well as scientific value.

CHAPTER 12

SUMMARY AND CONCLUSIONS

Summaries of this study on the Geitafell Central Volcano and its hydrothermal system are presented in table 2.1 (p.45), table 3.1 (p.95), table 5.1 (p. 158), chapter 5.3 (pp. 181-183), chapter 6.3 (pp.213-216), chapter 7.3 (pp. 226-227),chapter 8.3 (pp.240-254, table 8.1, p. 254), and figure 9.3 (p. 274). Discussions on the physico--chemical constraints on the formation of secondary minerals and mineral assemblages and a comparison with active hydrothermal systems are given in chapters 10 and 11.

From the stratigraphic and structural study a central volcano (Geitafell Volcano) is recognized, predating the SE-Iceland flexure zone. The volcano is separated into 7 major stratigraphic units (table 2.1) with an aggregate thickness of ca. 2700 m of which the uppermost 600 m may have originated outside the volcano itself. The total thickness of the extrusive rocks, however, is somewhat variable, mainly as a result of the localized distribution of the two hyaloclastite units (H-I, H-II) which account for ca. 600 m within the central area. The volcano is predominantly composed of tholeiitic basic rocks. However, intermediate rocks also occur to a subordinate extent together with two rhyolite units (R-I, R-II).

From radiometric dating in SE-Iceland and comparison of palaeomagnetic profiles with a recent study by Torfason (1979) of the area NE of the Geitafell Volcano, it is concluded that the volcano may have been active from ca. 6 to 5 m.y. However, new radiometric dating from unit R-II and intrusive phase 12 (Albertsson, pers.comm.) may suggest the volcano is ca. 1 m.y. older, and further studies are clearly needed.

Mio-Pliocene glaciation occurred in the area, leading to the subglacial formation of units H-I and H-II, whose distributions are of more than local significance, although they were erupted from within the central volcano. The earliest tillite in the area occurs at the base of unit H-II. At the time of its activity the Geitafell Volcano is inferred to have lain in an active rift zone at roughly the position of the modern Grimsvotn-Kverkfjoll Volcanoes which underlie the Vatnajokull ice-sheet (fig. 1.1). Development of large high-ground area ice-sheets in central Iceland may thus date as far back as ca. 6 m.y., in general agreement with Jonsson's (1954) conclusion regarding upper Miocene and early Pliocene glaciation in SE-Iceland.

The overall time relationship between the major structural- and intrusive events and the stratigraphic units is shown in tables 2.1 and 3.1. Three major structural events are distinguished, (i) an episode of uplift, (ii) caldera subsidence and (iii) flexuring of the volcano. Twelve intrusive phases (I.P.) are similarly distinguished in a chronological order from 1-12 :

I.P.1 : NE-SW dykes, mainly composed of fine-grained tholeiitic basalt, although a few dykes of intermediate composition are recognized. I.P.1 comprises a feeder dyke system of the volcanogenic strata up- and into unit H-II.

I.P.2 : Central gabbros

I.P.3 : Radial fsp-phyric dolerite dykes

I.P.4 : Granophyre- and felsite veins and few sheets in the central gabbro vicinity

I.P.5 : Dolerite cone-sheets, sparsely fsp-, px-phyric

I.P.6 : Fsp-phyric dolerite cone-sheets

I.P.7 : Dolerite dykes (commonly fsp-phyric)

I.P.8 : Fine-grained basalt cone-sheets

I.P.9 : NE-SW fine-grained basalt dykes

I.P.10: Marginal gabbros (close to the caldera fault) and associated fsp-phyric dolerite cone-sheets, and NE-SW coarsely fsp-phyric dolerite dykes

I.P.11: Granophyric- and felsite intrusions and veins, and NE-SW felsitic dykes

I.P.12: NE-SW dolerite dykes ('brown dolerite dykes'), characteristically much thicker than earlier dykes, and accompanying the flexuring of the volcano.

Some of the unit H-II rocks are distinctively fsp-phyric - in marked contrast to the typically aphyric rocks of older stratigraphic units - and may be correlated with some of the fsp-phyric intrusives (e.g. I.P.3,6 or 7). The extrusive acid rocks of unit R-II were fed by I.P.11, while the lower parts of basalt lava unit III (B-III) were fed by late members of I.P.10 and I.P.12. Constructional unconformity is found within unit B-III in Grasgiljatindur-Gjanupstindur, the upper part of B-III slightly postdating the flexuring of the volcano.

The E-Iceland rift zone was probably active without major breaks for ca. 13 m.y. with the locus of maximum spreading moving southwards with time (Walker, 1975 c). The spreading rate during the accumulation of the Geitafell Volcano, however, may have been relatively slow, particularly during the emplacement of I.P.2-6, which was accompanied by uplift (with development of the reverse fault) leading to the development of a radial-dyke system (I.P.3) and two regular cone-sheet systems (I.P.5 & 6). The flexure zone, however, slightly postdating the caldera subsidence (and the emplacement of I.P.10,11 and unit R-II), may have formed as a result of a relatively fast

spreading rate, as seen from a marked dilational fracturing and the much thicker I.P.12 dykes accompanying the flexuring. An increased spreading rate in the E-Iceland rift zone ca. 5-6 m.y. ago may thus have caused the flexuring - preceeding a shift in volcanic activity from the extinct NW-Iceland rift zone to the presently active NE-Iceland rift zone some 4 m.y. ago (as proposed by Ward, 1971, and Saemundsson, 1974).

The stratigraphy and its relation to the intrusive- and structural events provides information essential to the study of the hydrothermal alteration within the volcano. For example, by knowing the approximate elevation of the volcano's palaeo-surface during the active lifetime of the hydrothermal system, both lithostatic and hydrostatic pressure estimates were obtained, and knowledge of the chronology of the intrusive- and structural events provided a reference to which any metamorphic- or hydrothermal event could be fitted through studies of vein- and amygdale sequences - both with respect to time and possible origin. Similarly, recognition of the volcano's palaeo-position and glacial history provided information bearing on the origin of the hydrothermal fluid. The latter is regarded as being of meteoric origin, a conclusion supported by the formation of botryoidal limonite within amygdales prior to the establishment of an active high-temperature hydrothermal system. Furthermore the high-T hydrothermal system was established at shallow levels following the emplacement of the early central gabbros (I.P.2). The possible relationship between I.P.3, 6 or 7 and the upper part of the extrusive unit H-II also suggests that an ice-sheet (of unknown thickness) covered the volcano during the early stages of the high-T

hydrothermal system. The situation within the Geitafell Volcano may thus have been analogous to that pertaining within the present-day Grimsvotn-Kverkfjoll Volcanoes. The presence of an ice-sheet would evidently increase both the lithostatic and hydrostatic pressures. The formation of the voluminous R-II unit during the de-glaciation period is also of some interest with respect to isostatic re-equilibration whose extent would evidently depend on the (unknown) regional extent and thickness of the former ice-sheet.

The study of mineral veins and amygdales with respect to the twelve intrusive phases shows that the establishment of a high temperature hydrothermal system directly relates to hot intrusive rocks interacting with ground waters. Early interactions between hot intrusions and host rock fluids show distinctive metamorphic- and hydrothermal mineralogical characters, which include metamorphic hornfelses and skarn deposits within gabbro contact aureoles, and high--grade mineral assemblages within the intrusive rocks foreign to the host rocks. Evidence for hot intrusive - fluid interaction is found within I.P.2,3,5,6,10 & 12. Furthermore, the study of vein- and amygdale mineral infilling sequences show that a close relationship existed between the fracture- and porosity controlled fluids. Basically the mineral infilling sequences show :

(i) progressive evolution of a cold ground-water system into an active high-temperature system,

(ii) depth related evolution of the high-T system

(iii) regressive cooling sequence of the high-T system,

(iv) regional zeolitization related to a low-T system.

The earliest mineraloids and mineral infillings related to (i) pro-

gressively altered in relation to (ii), and part of the minerals related to (ii) show retrograde alteration in relation to (iii). Evidently the earlier infilling minerals were superimposed by the later. The hydrothermal history is discussed below.

Prior to the emplacement of I.P.2 (the central gabbros), cold, oxidizing ground-waters percolated through the volcanogenic strata. During this period, which may have lasted throughout the accumulation of the lavas and hyaloclastites (possibly 7-8 x 10^5 yr), layered mud deposits and botryoidal limonite settled within vesicles, joints and other rock cavities, establishing the earliest amygdale fillings and the first vein system within and beyond the area of the volcano. At the same time primary ore minerals were partly oxidized and volcanic glass was palagonitized. Dykes of I.P.1 intruded the volcano during this period, and while these presumably provided some heat to the groundwater, no evidence has been found for hot intrusive - water interaction in the few dykes of I.P.1 studied, which are cross-cut by early jasper veins. With time however, the ground-water system was slowly heated, gradually resulting in the deposition of amorphous silica (opaline, jasper and chalcedony) within vesicles and veins, establishing the second vein system within the volcano, and host rock glasses replacement by smectite, although smectite formed later than the silica deposits in amygdales.

Still prior to the central gabbro emplacement, chlorite appears to have formed at deeper levels, suggesting that fluid temperatures at ca. 1 km depth may already have been close to 200°C. It is not clear whether any low-temperature zeolites were formed from the primitive low-temperature hydrothermal system, since no early zeolite pseudomorphs have been observed.

All these early minerals became hydrothermally altered by later events, to an extent dependent upon their spatial distribution within the later high-temperature hydrothermal system.

After the emplacement of the central gabbros the previous low-T hydrothermal system changed abruptly to an active high-temperature system and lava hornfelses were formed alongside the gabbro margins, establishing an inner contact aureole. The andesine, augite, ore which replaced the primary minerals of the hornfelses also formed in the lava vesicles. The hornfelses are cut by unchilled fsp-, px-phyric felsite veins (I.P.4), suggesting that the metamorphic temperatures were close to magmatic. Accordingly the hornfelses are grouped within the sanidinite facies of contact metamorphism, formed at temperatures above ca. 800°C. Mineral veins, deposited from metasomatic/metamorphic fluid within a dyke of I.P.3 cross-cutting the hornfels, show transition from hornfels augite within vein wall-rock zones to salite, ferroaugite, ferrohedenbergite and hedenbergite towards the centre of the vein. Beyond the hornfelses but within an outer contact aureole, vesicle limonite was metamorphosed via hematite to magnetite, which further reacted with fluid to produce a typical skarn mineral assemblage, hedenbergite_{ss} - andradite. Following retrograde conditions the pyroxene was partly replaced by andradite (containing inclusions of calcite and Mn-rich pyroxene). This forms an assemblage with wairakite, $\pm$ quartz and epidote. From experimental data (chapter 10) the lowest formation temperature at 0.3 kbar fluid pressure for the stable co-existence of the skarn minerals hedenbergite_{ss} - andradite appears to be ca. 400°C, while their upper stability limit may lie in the range 600-800°C. The low temperature condition requires extremely CO_2-poor fluid and an oxygen fugacity of ca. 10^{-30}.

The fluid pressure within the contact aureole is estimated from the lithostatic load of ca. 1 km and the uplifting episode accompanying the gabbro emplacement to have been ca. 0.3 kbar. This together with the minimum temperature estimate, implies that the hydrothermal fluid within the contact aureole was supercritical for some time. Therefore, the hydrothermal fluid must have evolved through a boiling episode which proceeded outwards and apparently caused an extensive formation of calcite within the host rocks outside the gabbro contact aureole. Within the aureole itself, fluid-rock interactions took place to an extent dependent on the permeability At least one, but perhaps two types of vesicle wall-rock alteration zones formed during this time. Well-developed vesicle wall-rock replacement by chlorite-albite clearly demonstrates a marked Ca-leaching from the rocks. The Ca-enrichment of the fluid may have led to the deposition of calcite outside the contact aureole, and the development of Ca-bearing minerals, e.g. actinolite and sphene elsewhere within the contact aureole and the gabbro itself. For example, at some stage during the early cooling history of the gabbro, actinolite and sphene were formed in mineral veins which were possibly deposited directly from fluid, but also produced from augite-ilmenite--fluid reactions. An actinolite-sphene-producing fluid pervaded the entire Geitafell gabbro body, while the extent of secondary replacement depended on the permeability. It is not clear at which temperature, for instance, the actinolite-sphene formation took place, but the assemblage may apparently form hydrothermally at temperatures as low as ca. 300°C at low X_{CO_2} -values. The permeation of later hydrothermal fluids, however, was of different nature and the hydrothermal alteration of the gabbro was chiefly confined to vein wall-

-rock alteration zones, the vein relations being the same as those in the surrounding hydrothermally altered rocks.

A high-temperature hydrothermal system was clearly established within the volcano following the central gabbro emplacement. Heat and gases (CO_2, SO_2 , Cl) were supplied to the hydrothermal fluid by the magmas, and other components were supplied by fluid-rock interactions at all levels. Heat was distributed within the hydrothermal system by fluid convection, but additionally provided by two widespread cone-sheet systems (I.P. 5 and 6). Interactions between hot intrusions and water took place at all depths within and below the epidote zone. Foreign to the host rock replacement assemblage in the epidote zone, the characteristic early replacement assemblage of the intrusive rocks (I.P.5 and 6) is actinolite-sphene, the minimum temperature of which is tentatively set at ca. 300°C at low X_{CO_2} -values. From this early replacement assemblage within the I.P.5 sheets, emplaced at 100-200 m below the palaeo-surface, it is postulated that the hydrothermal fluid passed through a boiling phase and that the alteration was caused by superheated steam. However, if an ice-sheet, a few hundred metres thick, had been present the pressure estimates would need to be re-evaluated - and thereby the phase relations of the fluid phase. The apparent production of supercritical fluids within the gabbro aureoles, however, would imply the likely presence of formerly superheated fluids within the system as the hydrothermal fluid adjusted to hydrostatic values upon cooling.

With time the hydrothermal system cooled and adjusted to hydrostatic values - where maximum temperatures were controlled by boiling of the open fluid system. The rocks responded to the hydrostatically controlled fluid system by the development of a distinctive depth-

-related index mineral zonal sequence (map II) confined to the propylitic core of the volcano and crudely concentric around its centre and the central gabbros (I.P.2). In addition however, the zonal distribution shows a relation with the much later marginal gabbros (I.P.10) and the caldera fault. With increasing grade the index minerals of the various zones are (i) chlorite, (ii) epidote, (iii) andradite, and (iv) actinolite. By comparison with temperature correlated zonal sequences in active high-temperature hydrothermal systems in Iceland and experimental data (chapters 10 & 11), the minimum fluid temperatures for the epidote formation is taken as ca. 230-260°C, and the minimum temperatures for actinolite and andradite crystallization are tentatively set at ca. 300°C. The fluid composition, however, also plays a part in the formation of the index minerals. From the experimental data it appears that both andradite and actinolite form at their lowest temperatures in CO_2-poor fluids. In open hydrothermal systems the CO_2-content of the hydrothermal fluids is controlled by phase separation upon boiling - driving CO_2 into the steam phase - and by precipitation of calcite. Consequently the low-temperature conditions to form both andradite and actinolite are attainable within liquid dominated hydrothermal systems at ca. 1 km depth.

From the stratigraphy in the Geitafell volcano it is clear that the actinolite- and andradite zones were developed at depths $\geq$ 1 km. Within the gabbro aureoles however, these zones may reach slightly shallower levels - the index mineral development there being related to gabbro-contact rock alteration. Actinolite replaces the host- and intrusive rocks along with other greenschist facies minerals within the actinolite zone. The denser-rock replacement by secondary minerals

within the zone is commonly incomplete while the more porous-rock replacement is usually complete. Actinolite was similarly precipitated within mineral veins and amygdales, additionally replacing earlier chlorite and limonite in the latter. The actinolite formation within the most of the zone in the NE-part of the volcano seems to have begun in direct continuation of the emplacement of intrusive phase 5, and to have continued, with or without breaks, until after the emplacement of intrusive phase 10. A complex vein system (3-a), with several sub-systems (vein fluid generations), formed within the zone during this time, with epidote as a common mineral in all the vein mineral assemblages of system 3-a. Garnets, commonly pure andradite, were also formed hydrothermally within the actinolite zone. The andradite occurrence, however, is restricted to the vein and amygdale deposits, additionally replacing earlier chlorite and limonite in the latter. Furthermore, andradite occurs in amygdales above and beyond the zone in which actinolite occurs within host rocks, veins and amygdales so that an andradite zone envelopes the actinolite zone, and forms a boundary between the epidote- and the actinolite zones.

The host rock alteration within the epidote zone is more or less identical to that in the underlying actinolite zone, except for the complete absence of actinolite from the secondary mineral assemblages, and the absence of garnet from veins and amygdales. Chlorite however, is common throughout the epidote zone. The chlorite however, extends to levels higher and further out than epidote, and therefore a division between the two index minerals is useful in showing the direction of an 'up-grade' zonal sequence. The chlorite zone thus marginally envelopes the epidote zone indicating the outer and upper

limits of chlorite occurrence in the absence of epidote. With this in mind, two principal high-temperature hydrothermal zones are recognized, (a) an epidote zone at upper stratigraphic levels and (b) an actinolite zone at lower stratigraphic levels.

The epidote zone can be divided into upper and lower sub-zones. Within the upper sub-zone, the epidote is more or less confined to veins and vein wall-rock alteration zones and wairakite is absent from the rock replacement-, vein and amygdale assemblages. However, several generations of quartz and calcite deposition characterize the hydrothermal alteration products and sulphide deposits (pyrite and chalcopyrite) are particularly common locally - a feature shown by the superimposed sulphide zone in map II. The hydrothermal fluid temperatures may have been below ca. 230°C during most of the active lifetime of the high-temperature hydrothermal system.

Within the lower sub-zone, epidote is common in rock replacement-, vein and amygdale assemblages, along with chlorite, albite, K.feldspar, calcite, quartz, prehnite and wairakite. Vein and amygdale filling sequences suggest that epidote and chlorite were amongst the earlier hydrothermal products from the high-T system and wairakite and prehnite amongst the later. The hydrothermal fluid temperatures may have ranged from ca. 230-300°C towards the boundary of the andradite- and actinolite zones.

A second thermal boost accompanied the emplacement of intrusive phase 10 (marginal gabbros, local cone-sheets and NE-SW dykes). This produced a second generation of hornfelses at the gabbro margins within the Vidbordsfjall gabbro complex and an aureole of skarn mineral deposits in amygdales around both the Vidbordsfjall and the Kraksgil gabbros. Actinolite- and andradite-bearing contact aureoles

also developed at the gabbro margins at high levels. Large quantities of high-T fluid appear to have passed upwards in the highly permeable caldera fault zone resulting in extensive hydrothermal rock alteration. At low levels within the actinolite zone (in Kraksgil) some of the lavas became completely altered to greenschist facies assemblages. At higher levels within the actinolite zone along the fault, albite-adularia amygdale deposits developed extensively. At higher levels along the fault, within the lower epidote sub-zone, garnet developed locally in amygdales - accounting for the superimposed andradite zone (map II), and at the highest stratigraphic levels within the upper epidote sub-zone, I.P.10 dykes and adjacent host rock replacement by epidote and prehnite is particularly intense in the fault region - apparently formed only 200 m below the palaeo-surface.

The chief effect of the second thermal boost to the hydrothermal system was to maintain the high-temperature hydrothermal activity for some length of time, after which cooling of the hydrothermal system began - proceeding downwards with time. The lifetime of the high--temperature hydrothermal system is estimated at ca. 2-3 x 10^5 yrs. The latest memebers of I.P.10 and 11 only suffered low-grade hydrothermal alteration. Flexuring appears to have coincided with the cooling, and may possibly have induced cooling by extensive fracturing. Thick calcite veins typically formed at this period, particularly inside the volcano, but also in the flank areas.

Wairakite and prehnite, along with quartz, calcite and chlorite, may have been forming within the lower epidote sub-zone early in the cooling history while late formation of prehnite and wairakite took place within the actinolite zone. With cooling laumontite (± quartz, calcite, smectite) became deposited within veins, and partly replaced

earlier wairakite in amygdales, probably at temperatures between 200-120°C. Below this temperature heulandite (along with other low-T zeolites, calcite, quartz, smectite) was formed in veins and partly replaced earlier laumontite in amygdales. A similar cooling sequence is superimposed upon all the high-temperature hydrothermal system.

Prior to the I.P.12 (flexure-related) dykes, the formerly high-T system had cooled so that only low-grade alteration occurred within the I.P.12 dykes, giving rise to partial replacement of feldspar by calcite and zeolites, and replacement of glass by smectite (iron saponite), calcite, (siderite) and pyrite. Amygdales within I.P.12 dykes are composed of calcite (and locally siderite), quartz, smectite (iron saponite), pyrite and low-temperature zeolites within the volcano, and cross-cutting veins are composed of calcite, quartz, low-T zeolites, smectite and pyrite. Outside the volcano in the flank areas the I.P. 12 alteration by zeolite deposits and smectite replacement of glass is similar, while the feldspar replacement by calcite and the deposition of calcite, quartz and pyrite is by far less extensive than inside the volcano - implying that the hydrothermal system within the volcano was not extinct during intrusive phase 12.

It is concluded therefore that the flexure zone was formed during the cooling history of the Geitafell volcano hydrothermal system. Both the flexure and the volcano then became buried by younger tholeiite and olivine tholeiite lava flows (upper part of unit B-III), erupted to the northwest. A regional zeolitization was then superimposed upon all the earlier formations. Three discordant zeolite zones are recognized, (a) chabazite-thomsonite, (b) analcime and (c) mesolite-scolecite. The former two are sited within unit B-III, the third within and below unit H-II in the eastern area, but

extending further upwards into unit B-III in the western area.

The Geitafell Volcano became deeply eroded during Pleistocene glaciation and a glacial valley was carved down to the present-day 200 m level in the centre of the volcano. Further eruptive products emanating from the northwest gave rise to the Svinafellgoltur palagonite formation, which rests unconformably on the older strata on a fluvioglacial valley floor. Subsequently the volcano was further eroded during Pleistocene and Holocene glaciation to below sea-level, causing catastrophic floods from the ice-marginal lake (Gjanupsvatn) throughout historical time. At the present-day the glacier remnant, Hoffellsjokull, is at a regression stage.

ACKNOWLEDGEMENTS

I am most grateful to my 1st supervisor, Professor Brian G.J. Upton, for his lively interest and supervision throughout this research, his careful reading and constructive criticism of the manuscript, and the hospitality he and his wife, Bodil, showed my family during our stay in Edinburgh. I would also like to thank my 2nd supervisor, Dr. Ben Harte, for various and valuable assistance and critical reading of early drafts of chapters 4-8. Dr.John E.Dixon receives special thanks for his most valuable contribution to the revised planning of this research, 'where first things come first', his keen interest and valuable assistance.

I am indebted to the academic and technical staff of the Grant Institute, in particular Dr. P.G. Hill and Mr. C. Begg for their assistance in using the electron microprobe, and Mr. C. Chaplin for his ready help with the photographic work. Those and others ummentioned, as well as the research students, are thanked for inspiring discussions and cheerful companionship.

Professor S. Bjornsson at the University of Iceland is sincerely thanked for critically reading the sections on the hydrothermal systems, for valuable suggestions and lively interest in this research. Dr. K. Albertsson at the University of Iceland is thanked for his visit to the field area to include several samples for age-dating to his research, and for lively discussions. Similarly I thank Professor Th. Sigurgeirsson for allowing access to his then unpublished aeromagnetic data on SE-Iceland.

This research was financed by the Icelandic Student Loan Fund, while the field work was financed by the Geothermal Division of the National Energy Authority (NEA) under the direction of Dr. G. Palmason.

This is greatly acknowledged. I also thank my numerous colleagues at NEA for many fruitful discussions and moral support, not the least Mr. J. Tomasson and Dr. H. Franzson. Similarly, I thank the technical staff at NEA for various assistance, not the least all the lovely girls who masterly drew many of the maps and figures.

Dr. I.B. Fridleifsson is thanked for his help in selecting an appropriate field area for this research and assistance in the field at the very beginning. Not the less I thank him and his wife, Thordis, for masterly taking care of my family's financial matters during our stay in Edinburgh, and their encouragement throughout.

My parents in law, Inga and Jakob, receive my sincere thanks for their everlasting assistance and care for my family.

I am indebted to the inhabitants in the Hornafjördur district for their assistance during field work, in particular Hólmfríður and Þrúðmar Sigurðsson and their family at Midfell, and Álfheiður and Gísli Arason in Höfn, for exquisite hospitality and friendship.

The thesis is typed by Mrs. L. Begg in Edinburgh, Mrs. Th. Thorleifsdóttir and finally Mrs. S. Valdimarsdóttir at the NEA in Iceland. Their effort is greatly acknowledged. Similarly I thank Mr. J. Volker in Edinburgh and Dr. H. Franzson at the NEA for reading the final versions of the manuscript for corrections, and interesting discussions.

Last but not the least I thank my wife, Sigrún, for her endless patience and support throughout this research.

APPENDIX I : REPRESENTATIVE MICROPROBE ANALYSES OF SECONDARY MINERALS.

TABLE 1 : Representative microprobe analyses of hornfels pyroxene.

	1	2	3	4	5	6	7	8	9*	10	11	12*	13	14	15*
SiO_2	52.34	52.43	49.12	53.20	53.67	53.30	52.31	51.50	50.14	47.94	51.50	49.88	51.52	51.03	51.76
TiO_2	0.69	0.54	1.14	0.45	0.31	0.11	0.17	0.33	n.d	n.d	n.d	0.14	0.44	1.14	0.12
Al_2O_3	0.88	1.04	1.23	0.89	0.73	n.d	3.59	1.67	2.77	1.03	n.d	0.45	1.48	3.28	2.00
Cr_2O_3	n.d	n.d	n.d	n.d	n.d	0.14	n.d	n.d	n.d	n.d	n.d	n.d	n.d	0.21	n.d
FeO	12.30	11.76	13.19	11.80	10.96	14.74	12.99	12.45	18.47	24.07	22.87	23.02	12.32	7.54	25.62
MnO	0.34	0.54	0.42	0.18	n.d	0.41	0.36	0.40	1.27	0.63	3.54	3.04	0.33	0.18	0.56
MgO	14.39	13.60	12.64	14.26	13.69	10.01	9,49	11.40	6.76	3.05	1.70	1,93	13.08	15.67	7.59
CaO	19.17	20.53	21.60	20.20	21.32	20.43	20.71	21.18	19.15	21.68	22.05	22.82	20.03	21.09	11.98
Na_2O	n.d	n.d	n.d	n.d	n.d	1.24	1.09	n.d	n.d	n.d	n.d	n.d	n.d	n.d	n.d
Total	100.11	100.44	99.34	100.98	100.68	100.38	100.71	98.93	98.88*	98.40	101.66	101.49*	99.20	100.14	99.98*
						CATIONS BASED ON 6 OXYGENS									
Si	1.965	1.965	1.896	1.976	1.994	2.030	1.965	1.970	1.974	1.968	2.043	1.995	1.959	1.888	2.025
Ti	0.020	0.015	0.033	0.013	0.009	0.004	0.005	0.010	0.000	0.000	0.000	0.005	0.013	0.032	0.004
Al	0.039	0.046	0.056	0.039	0.032	0.000	0.159	0.076	0.129	0.050	0.000	0.021	0.066	0.143	0.093
Cr	0.000	0.000	0.000	0.000	0.000	0.005	0.000	0.000	0.000	0.000	0.000	0.000	0.000	0.006	0.000
Fe^{+2}	0.386	0.369	0.426	0.367	0.341	0.470	0.409	0.399	0.608	0.827	0.759	0.770	0.392	0.234	0.838
Mn	0.011	0.017	0.014	0.006	0.000	0.014	0.012	0.013	0.043	0.022	0.119	0.103	0.011	0.006	0.019
Mg	0.806	0.760	0.728	0.790	0.758	0.569	0.531	0.650	0.397	0.187	0.101	0.116	0.742	0.864	0.443
Ca	0.771	0.825	0.894	0.804	0.849	0.834	0.834	0.868	0.808	0.954	0.937	0.987	0.816	0.836	0.502
Na	0.000	0.000	0.000	0.000	0.000	0.091	0.080	0.000	0.000	0.000	0.000	0.000	0.000	0.000	n.d
Total	4.002	3.991	4.049	3.998	3.983	4.018	3.997	3.989	3.978*	4.008	3.963	3,977	4.001	4.012	3.946*
Wo	39.1	41.9	43.4	40.9	43.6	44.2	46.7	45.0	43.5	40.2	48.9	49.7	41.9	43.1	27.9
En	40.8	38.5	35.3	40.2	38.9	30.2	29.7	33.7	21.4	7.9	5.3	5.9	38.0	44.5	24.6
Fs	20.1	19.1	21.3	18.9	17.5	25.6	23.6	21.3	35.1	51.9	45.8	44.4	20.1	12.4	47.5

1-3 representative analyses of hornfels augite in matrix and 4-6 in vesicles (sample 215). 7-15 sample 216, intrusive phase 3,

7-8: pyroxene in vein wall rock zone; 9-10: pyroxene in brown rim between wall rock zone and vein centre; 11-12: pyroxene in vein centre.

Primary augite in matrix (13) and phenocryst (14) for comparison. 15: ferroaugite in vein centre (narrow vein).

9* contains 0.19% K_2O; K: 0.01; and 0.13% Cl; Cl: 0.009. 15* 0.15% K_2O; K: 0.008; and 0.20% Cl; Cl: 0.014.

12* contains 0.21% NiO; Ni: 0.07. Analysis 11: X_{hed}: 0.775; X_{joh}: 0.122; X_{di}: 0.103 and Analysis 12: X_{hed}: 0.779; X_{joh}: 0.104; X_{di}: 0.117.

TABLE 2 : Representative microprobe analyses of skarn pyroxene.

	1	2	3	4	5	6	7	8	9	10*	11*	12	13	14	15	16
SiO_2	51.68	50.54	50.26	51.31	53.44	51.96	52.07	52.41	51.22	48.45	52.38	51.21	51.83	51.38	51.15	51.93
Al_2O_3	n.d	1.36	n.d	0.44	0.16	0.39	n.d	n.d	n.d	0.24	n.d	0.65	1.36	0.76	1.40	0.64
Cr_2O_3	0.13	n.d	0.12	n.d	n.d	0.13	0.19	n.d	n.d	n.d	n.d	n.d	n.d	n.d	n.d	0.12
FeO	18.08	21.99	23.48	18.24	14.89	15.05	17.36	17.57	19.37	17.08	8.73	17.64	14.82	17.42	16.21	12.91
MnO	0.62	0.62	0.76	0.49	0.43	0.41	0.62	0.63	1.17	1.41	5.11	1.28	1.21	1.28	1.00	1.67
MgO	7.02	4.73	3.50	7.88	8.98	8.67	7.37	7.47	5.75	6.92	10.18	6.55	7.61	6.29	6.69	8.86
CaO	23.72	22.07	23.12	23.55	23.84	23.97	23.94	23.85	23.51	26.60	25.20	23.37	23.03	23.67	23.98	24.15
Na_2O	n.d	n.d	n.d	n.d	n.d	0.26	0.27	n.d	n.d	n.d	n.d	n.d	n.d	n.d	n.d	n.d
Total	101.24	101.30	101.24	101.91	101.74	100.84	101.81	101.93	101.01	100.86	101.41	100.70	99.86	100.79	100.42	100.28
CATIONS BASED ON 6 OXYGENS																
Si	2.000	1.981	1.998	1.973	2.018	1.992	1.999	2.007	2.004	1.920	1.986	1.993	2.000	2.000	1.983	1.992
Al	0.000	0.063	0.000	0.020	0.070	0.018	0.000	0.000	0.000	0.012	0.000	0.030	0.062	0.035	0.064	0.030
Cr	0.004	0.000	0.004	0.000	0.000	0.004	0.006	0.000	0.000	0.000	0.000	0.000	0.000	0.000	0.000	0.004
Fe^{+2}	0.585	0.721	0.781	0.587	0.471	0.483	0.585	0.563	0.634	0.564	0.282	0.574	0.479	0.566	0.526	0.415
Mn	0.020	0.021	0.026	0.016	0.014	0.014	0.021	0.021	0.039	0.048	0.168	0.042	0.040	0.042	0.033	0.055
Mg	0.405	0.276	0.208	0.452	0.506	0.496	0.422	0.427	0.335	0.408	0.576	0.380	0.438	0.364	0.387	0.507
Ca	0.984	0.927	0.985	0.970	0.965	0.985	0.985	0.979	0.986	1.128	1.020	0.974	0.953	0.985	0.996	0.993
Na	0.000	0.000	0.000	0.000	0.000	0.020	0.021	0.000	0.000	0.000	0.000	0.000	0.000	0.000	0.000	0.000
Total	3.998	3.989	4.002	4.018	3.984	4.013	4.014	3.999	4.002	4.122	4.056	3.994	3.975	3.987	3.991	3.997
X_{hed}	0.579	0.708	0.769	0.556	0.475	0.486	0.569	0.557	0.629	0.553	0.275	0.576	0.500	0.582	0.556	0.425
X_{joh}	0.020	0.021	0.026	0.015	0.014	0.014	0.020	0.021	0.039	0.047	0.164	0.042	0.042	0.043	0.035	0.056
X_{di}	0.401	0.271	0.205	0.429	0.511	0.500	0.411	0.422	0.332	0.400	0.561	0.382	0.458	0.375	0.409	0.519
Wo	49.3	47.7	49.2	47.9	49.3	49.8	49.6	49.3	49.4	52.5	49.9	49.4	49.9	50.3	51.3	50.4
En	20.3	14.2	10.4	22.3	25.9	25.1	21.2	21.3	16.8	19.0	28.1	19.3	22.9	18.6	19.9	25.7
Fs	30.4	38.1	40.4	29.8	24.8	25.1	29.2	29.4	33.8	28.5	22.0	31.3	27.2	31.8	28.8	23.9

Analyses 1-11 from Geitafell gabbro contact aureole (sample 134). Analyses 12-13 from Kráksgil gabbro contact aureole (sample 222).

Analyses 14-16 from Vidbordsfjall gabbro contact aureole (sample 9 23/8 '77).

10^* contains 0.15% NiO; Ni: 0.006. 11^* Pyroxene inclusion in andradite. n.d. not detected.

X_{hed}, X_{joh}, X_{di}: Calculated in terms of mole fractions of the three endmembers, hedenbergite, johannsenite, diopside.

Wo: Wollastonite ($CaSiO_3$). En: Enstatite ($MgSiO_3$). Fs: Ferrosilite ($Fe(+Mn)SiO_3$).

TABLE 3 : Representative microprobe analyses of garnets.

	1	2	3	4	5	6	7	8	9	10	11	12	13	14	15	16	17
SiO_2	35.76	35.51	35.28	32.82	36.08	35.94	35.72	35.64	36.36	35.71	35.82	39.96	40.02	39.89	39.91	39.81	39.64
AlO_3	n.d	n.d	n.d	n.d	n.d	0.15	0.16	n.d	n.d	n.d	0.33	20.51	20.57	21.04	20.49	20.78	19.85
Cr_2O_3	n.d	0.12	0.12	n.d	0.19	n.d	0.14	n.d	0.15	0.18	n.d	n.d	0.15	0.22	0.21	0.21	0.19
Fe_2O_3	31.22	31.76	31.66	30.58	31.40	30.97	32.16	31.31	31.32	31.40	30.56	3.59	2.81	3.22	3.22	2.60	3.98
MnO	0.24	0.41	0.40	n.d	0.23	0.12	0.21	0.28	0.35	0.25	0.15	0.16	n.d	0.11	n.d	n.d	n.d
MgO	0.34	n.d	n.d	n.d	n.d	0.23	n.d	n.d	n.d	n.d	0.36	n.d	n.d	n.d	n.d	n.d	n.d
CaO	33.38	32.94	32.62	33.13	32.73	33.38	33.58	32.67	33.23	33.02	33.50	37.43	37.35	37.10	37.64	37.50	37.39
Total	100.94	100.74	100.08	99.53	100.63	100.79	101.97	99.90	100.41	100.56	100.72	101.65	100.90	101.58	101.47	100.90	101.05
CATIONS BASED ON 12 OXYGENES																	
Si	2.996	2.987	2.987	3.034	3.026	3.009	2.969	3.015	3.027	3.004	3.008	2.988	3.006	2.978	2.988	2.991	2.989
Al	0.000	0.000	0.000	0.000	0.000	0.015	0.016	0.000	0.000	0.000	0.011	1.808	1.821	1.852	1.809	1.840	1.765
Cr	0.000	0.008	0.008	0.000	0.013	0.000	0.009	0.000	0.010	0.012	0.000	0.000	0.009	0.013	0.012	0.012	0.012
Fe^{+3}	1.968	2.010	2.017	1.950	1.982	1.952	2.012	1.993	1.962	1.988	1.932	0.202	0.159	0.181	0.182	0.147	0.226
Mn	0.017	0.029	0.029	0.000	0.016	0.009	0.015	0.020	0.025	0.018	0.011	0.010	0.000	0.007	0.000	0.000	0.000
Mg	0.042	0.000	0.000	0.000	0.000	0.029	0.000	0.000	0.000	0.000	0.024	0.000	0.000	0.000	0.000	0.000	0.000
Ca	2.996	2.969	2.960	3.007	2.941	2.995	2.991	2.961	2.964	2.976	3.015	2.999	3.006	2.968	3.020	3.020	3.020
Total	8.019	8.003	8.001	7.991	7.978	8.009	8.012	7.989	7.988	7.998	8.001	8.007	8.001	7.999	8.011	8.010	8.012
Andradite	100	100	100	100	100	99.2	99.2	100	100	100	99.4	10.1	8.0	9.1	9.1	7.3	11.3
Grossular	0	0	0	0	0	0.5	0.3	0	0	0	0.3	89.6	92.0	90.7	90.9	92.7	88.7
Spessartine	0	0	0	0	0	0.3	0.5	0	0	0	0.3	0.3	0	0.2	0	0	0

Analyses 1-7 (sample 134) and 11-17 (sample 1 11/7 '77) are from the Geitafell gabbro contact aureole. Analysis nr 8 (sample 222) from Kráksgil gabbro contact aureole and analyses 9-10 (sample 9 23/8 '77) from Vidbordsfjall gabbro contact aureole. Total iron calculated as Fe^{+3}; Cr (to uvarovite) and Mg (to pyrope) are ignored, and the garnets listed as end-member andradite if Al was not detected.

TABLE 4: Representative microprobe analyses of smectites and sheet silicates

	(1)	(2)	(3)	(4)	(5)	(6)	(7)	(8)	(9)
SiO_2	35.28	40.54	42.97	44.68	50.43	38.93	55.67	55.29	57.10
TiO_2	0.14	0.50					0.48	0.47	0.22
Al_2O_3	9.83	9.64	3.87	3.68	17.82	11.94	1.88	2.41	14.22
FeO	30.91	23.08	20.61	26.44	10.35	18.24	22.06	21.68	9.70
MnO		0.16	0.19	0.63					
MgO	8.17	8.06	5.48	5.99	2.42	18.94	4.68	4.50	5.07
CaO	2.30	2.32	2.61	3.40	2.97	1.51			1.45
Na_2O									3.12
K_2O	0.84	1.56	0.19	0.30	0.47	0.14	9.94	9.76	6.07
	*	*	*	*	*				
Total	88.32	85.94	76.44	85.63	84.95	89.69	94.71	94.10	96.95
	Number of Cations on Basis of 22 oxygens								
Si	5.94	6.67	7.74	7.46	7.44	5.96	8.34	8.32	7.68
Ti	0.02	0.07					0.07	0.07	0.04
Al	1.96	1.87	0.88	0.73	3.10	2.15	0.35	0.44	2.27
Fe^{+2}	4.36	3.19	3.10	3.70	1.28	2.33	2.77	2.73	1.10
Mn		0.04	0.04	0.11					
Mg	2.05	1.98	1.47	1.50	0.55	4.30	1.06	1.01	1.03
Ca	0.42	0.42	0.51	0.62	0.48	0.09			0.22
Na									0.81
K	0.18	0.33	0.04	0.07	0.09	0.05	1.89	1.87	1.06
Total	15.16	14.67	13.93	14.32	13.11	15.07	14.56	14.52	14.26

Total iron as FeO: Samples 1-6 are brown to green smectites.
Sample 1: 207 lava; Sample 2: 208 lava; Sample 3: 127A: IP12 dyke, glass replacement; Sample 4: 127A: IP12 amygdales; Sample 5: 127B: late veins in IP12; Sample 6: 115: gabbro, late vein.
Samples 7-9: Celadonite; Sample 7&8: 159: acid rock: green celadonite replacing glass, fsp, px.; Sample 9: 150: IP10 dyke: red brown K-rich clay in amygdales and replacing matrix glass.

*
1: Contains 0,11 S (0.78%) and 0,04 Cl (0.08%); 2: Contains 0.04 Cl (0.08%); 3: Contains 0.07 S (0.48%) and 0.02 Cl (0.06%); 4: + 0.04 S (0.29%) and 0.04 Ni (0.22%); 5: 0.07 S (0.51%).

TABLE 5: Representative microprobe analyses of the up-grade alteration of the phyllosilicates

	(1)	(2)	(3)	(4)	(5)	(6)	(7)	(8)	(9)	(10)	(11)	(12)
SiO_2	34.29	31.36	31.18	31.13	32.32	32.93	28.88	28.82	28.43	28.35	29.21	29.11
Al_2O_3	19.19	17.57	15.66	15.64	18.74	18.87	17.34	17.28	15.98	17.47	17.63	18.26
FeO	20.55	23.97	24.50	25.01	23.32	22.15	28.45	29.02	26.13	20.86	21.50	20.37
MnO	0.21	0.26	0.22	0.26	0.18	0.18	0.11	0.17	0.31	0.60	0.27	0.44
MgO	12.95	13.43	15.72	16.24	10.24	10.03	12.34	12.65	15.49	18.50	18.74	19.64
CaO	0.61	0.72	0.56	0.34	0.59	0.46	0.52	0.58	0.09	0.35	0.08	0.20
K_2O	1.12	0.80	0.31	0.46	1.32	1.82	0.07					
	*	*					*					
Total	89.78	88.50	88.16	89.08	86.69	86.45	87.84	88.52	86.44	86.14	87.43	88.02
	Number of Cations on Basis of 28 oxygens											
Si	6.78	6.47	6.50	6.44	6.75	6.86	6.16	6.13	6.10	5.95	6.02	5.93
Al	4.68	4.26	3.84	3.81	4.62	4.65	4.37	4.34	4.05	4.32	4.29	4.39
Fe	3.42	4.14	4.26	4.31	4.09	3.86	5.07	5.15	4.69	3.66	3.71	3.47
Mn	0.06	0.06	0.06	0.06	0.06	0.06	0.03	0.06	0.06	0.11	0.05	0.08
Mg	3.81	4.12	4.87	5.01	3.19	3.14	3.92	4.00	4.96	5.78	5.76	5.97
Ca	0.14	0.17	0.14	0.08	0.14	0.11	0.14	0.14	0.02	0.08	0.02	0.05
K	0.31	0.22	0.08	0.14	0.36	0.50	0.03					
Total	19.26	19.60	19.85	19.94	19.32	19.26	19.85	19.94	19.88	19.90	19.84	19.89

1-4 : Sample: 146; 1-2 brown clay; 3-4 green clay; *1 contains 0.03 Cl(0.06%); 2 contains 0.08 S(0.4%)
5-8 : Sample: 5 24/8/77; 5-6 brown "chl"; 7-8 green chl; *7 contains 0.03 Ti(0.08%)
9-10: Sample: 222; 9 green chlorite; 10 brown chlorite
11-12: Sample: 1 11/7/77; 11 green chlorite; 12 brown chlorite
Total iron as FeO

TABLE 6: Representative microprobe analyses of chlorites

	(1)	(2)	(3)	(4)	(5)	(6)	(7)	(8)	(9)	(10)	(11)	(12)
SiO_2	28.83	28.81	28.10	27.20	28.45	25.56	27.12	27.95	28.46	28.53	29.67	29.40
Al_2O_3	13.69	16.73	16.89	17.32	17.52	18.11	17.77	18.01	17.04	16.56	16.84	17.54
FeO*	29.09	26.52	24.16	29.40	27.17	31.34	29.71	27.26	24.49	24.03	19.72	14.74
MnO	0.31	0.25	0.24	0.36	0.30	0.47	0.48	0.39	0.34	0.18	0.16	0.45
MgO	14.67	15.50	16.48	13.44	13.68	11.80	11.98	15.43	17.45	17.23	21.09	24.28
CaO		0.15				0.16					0.35	0.14
Total	86.59	87.95	85.86	87.72	87.11	88.44	87.06	89.04	87.77	86.53	87.83	86.58
	Number of Cations on Basis of 28 Oxygens											
Si	6.29	6.07	6.01	5.86	6.07	5.74	5.90	5.85	5.96	6.04	6.04	5.93
Al	3.52	4.16	4.26	4.40	4.41	4.62	4.56	4.44	4.20	4.13	4.04	4.18
Fe	5.31	4.68	4.32	5.30	4.85	5.67	5.40	4.77	4.29	4.26	3.36	2.48
Mn	0.06	0.05	0.04	0.07	0.06	0.09	0.09	0.07	0.06	0.03	0.03	0.08
Mg	4.77	4.87	5.25	4.32	4.35	3.80	3.88	4.81	5.44	5.44	6.40	7.29
Ca		0.03				0.04					0.08	0.03
Total	19.95	19.85	19.87	19.94	19.73	19.54	19.83	19.94	19.95	19.90	19.94	19.99

1-2 : Epidote zone: outer margin at low stratigraphic levels; (samples:1 5/7/77,1 30/6/77)
3-5 : - " - : upper part; (samples: 165, 164, 019)
6-7 : - " - : lower part; (samples: 010, 5 12/7/77)
8 : Andradite zone; (sample: 085)
9-12: Actinolite zone; (samples: 047, 134, 213, 9 23/8/77)

*Total iron as FeO

TABLE 7: Representative microprobe analyses of amphiboles.

	(1)	(2)	(3)	(4)	(5)*	(6)	(7)*	(8)	(9)	(10)	(11)	(12)	(13)
SiO_2	53.79	48.94	50.81	54.69	53.86	52.88	51.75	54.04	51.73	55.46	51.04	50.36	51.61
TiO_2			0.14		0.11				0.17	0.26	0.32	0.89	0.53
Al_2O_3	4.33	3.95	2.40	5.48	1.38	2.49	2.34	2.03	3.13	0.38	2.47	5.05	3.01
FeO	19.88	25.83	25.66	14.39	15.68	15.28	25.36	16.73	17.53	11.98	20.50	15.52	16.59
MnO	0.46	0.54	0.56	0.64	0.44	0.41	0.41	0.26	0.35	0.43	0.52	0.30	0.51
MgO	8.06	5.58	6.93	10.33	12.72	12.78	6.79	12.96	12.77	17.50	10.56	13.77	12.90
CaO	10.84	11.91	11.54	11.98	12.24	12.11	12.04	12.13	12.44	7.34	11.29	11.72	11.36
Na_2O	0.91									3.70		0.94	
K_2O	0.17					0.09				0.70	0.11		0.12
Chlorine	0.09		0.08				0.05	0.06			0.29		0.21
Total	98.52	96.75	98.11	97.50	97.01	96.03	99.09	98.09	98.10	97.74	97.08	98.54	96.83
	Number of Cations on Basis of 23 oxygens												
Si	7.89	7.61	7.76	7.87	7.91	7.83	7.81	7.86	7.60	7.96	7.70	7.32	7.65
Ti			0.02		0.01				0.02	0.03	0.04	0.10	0.06
Al	0.75	0.72	0.43	0.93	0.24	0.43	0.42	0.35	0.54	0.06	0.44	0.87	0.53
Fe^{+2}	2.44	3.36	3.28	1.73	1.93	1.89	3.20	2.02	2.15	1.44	2.59	1.89	2.06
Mn	0.06	0.07	0.07	0.08	0.06	0.05	0.05	0.03	0.05	0.05	0.07	0.04	0.06
Mg	1.76	1.29	1.58	2.22	2.79	2.82	1.53	2.81	2.80	3.74	2.38	2.99	2.85
Ca	1.70	1.98	1.89	1.85	1.93	1.92	1.95	1.89	1.96	1.13	1.83	1.83	1.81
Na	0.26									1.03		0.27	
K	0.03					0.02				0.13	0.02		0.02
Total	14.91	15.03	15.05	14.69	14.93	14.97	15.03	14.99	15.12	15.57	15.11	15.30	15.09
Cl	0.02		0.02				0.05	0.02			0.07		0.05

5*: 0.20% Cr_2O_3 (Cr 0.02); 7*: 0.60% Cr_2O_3 (Cr 0.07)

Analyses 1-5 og amygdale amphiboles; 6 of matrix amphibole; 7-8: vein amphibole; 9-13: amphiboles replacing pyroxene.

1: sample 2 19/7/77; 2-3: sample 222; 4: sample 9 23/8/77; 5-6: sample 050; 7: sample 051;

1-7: from lavas; 8-9: sample 213: IP2 gabbro; 10-11: IP4 acid rocks: samples 215 and 171; 12: sample 129: IP5; 13: sample 125: IP6.

TABLE 8: Representative microprobe analyses of epidote

	(1)	(2)	(3)	(4)	(5)	(6)	(7)	(8)
SiO_2	38.18	38.02	38.59	37.40	37.44	37.90	38.14	38.44
Al_2O_3	20.80	25.82	24.75	23.12	17.37	22.79	22.53	24.18
Fe_2O_3	16.43	9.50	11.04	12.71	20.37	13.43	13.89	12.32
CaO	22.75	23.37	23.36	23.69	22.99	23.47	23.67	23.38
MnO			0.25	0.60				
Cr_2O_3							0.14	
Total	98.17	96.71	97.98	97.52	98.16	97.60	98.36	98.32
	Number of Cations on Basis of 12.5 oxygens							
Si	3.06	3.02	3.04	3.00	3.05	3.03	3.03	3.03
Al	1.96	2.42	2.30	2.19	1.67	2.15	2.11	2.25
Fe^{3+}	0.99	0.57	0.65	0.77	1.25	0.81	0.83	0.73
Ca	1.95	1.98	1.97	2.03	2.01	2.01	2.01	1.98
Mn			0.02	0.04				
Cr							0.01	
Total	7.96	7.99	7.98	8.03	7.98	8.00	7.99	7.99
Ps	33.56	19.06	22.03	26.01	42.81	27.36	28.23	24.50

Total iron as Fe_2O_3.

Analyses: 1: sample 164; 2: sample 165; 3: sample 010; 4: sample 124; 5-6: sample 1 11/7/77; 7: sample 050; 8: sample 134.

TABLE 9: Representative microprobe analyses of prehnites

	(1)	(2)	(3)	(4)	(5)	(6)	(7)	(8)
SiO_2	43.86	44.03	43.40	43.44	44.13	42.98	42.99	42.86
TiO_2							0.13	0.62
Al_2O_3	24.16	22.30	24.18	21.35	24.15	22.55	21.54	20.12
Fe_2O_3		2.74		3.83	0.20	1.90	3.45	6.04
MgO								0.41
CaO	26.73	26.52	27.13	26.59	26.98	26.57	26.07	25.80
Total	94.75	95.59	94.71	95.21	95.46	94.00	94.18	95.85
Structural formula on the basis of 11 oxygens								
Si	3.04	3.02	3.01	3.05	3.04	3.02	3.03	3.00
Al^{iv}	0.96	0.98	0.99	0.95	0.96	0.98	0.97	1.00
ΣZ	4.00	4.00	4.00	4.00	4.00	4.00	4.00	4.00
Al^{vi}	1.02	0.84	0.99	0.80	1.00	0.89	0.82	0.66
Ti							0.01	0.03
Fe^{3+}		0.14		0.20	0.01	0.10	0.18	0.32
ΣY	1.02	0.98	0.99	1.00	1.01	0.99	1.01	1.01
Mg								0.04
Ca	1.99	1.97	2.02	1.98	1.99	2.00	1.97	1.93
ΣX	1.99	1.97	2.02	1.98	1.99	2.00	1.97	1.97

Total iron as Fe_2O_3. 1-2: sample 010; 3-4: sample 125; 5: sample 053; 6-7: sample 165; 8: sample 009.

1 and 5: amygdale prehnite

3 and 6: vein prehnite

2, 4, 7: prehnite replacing feldspar

8 : - " - replacing glass

TABLE 10. Representative microprobe analyses of zeolites.

	(1)	(2)	(3)	(4)	(5)	(6)	(7)	(8)	(9)	(10)	(11)	(12)
SiO_2	54.71	54.72	51.97	52.06	56.35	58.44	56.10	58.01	44.06	44.72	56.82	65.13
Al_2O_3	22.61	22.86	21.00	21.78	15.83	14.61	17.23	16.66	24.20	24.52	22.01	12.33
Fe_2O_3								0.15	0.18		0.31	
CaO	12.57	12.68	11.41	11.40	6.91	6.99	8.41	7.99	12.89	12.75	0.94	2.77
Na_2O					0.24	0.31			0.35	0.48	10.44	1.01
K_2O			0.13	0.20	0.24	0.14						1.64
			x	x						x		x
Total	89.91	90.26	84.57	85.49	79.56	80.48	81.74	82.81	81.67	82.66	90.52	83.48
Number of Cations:			12 oxygens			18 oxygens			10 oxygens		6 oxygens	48 oxygens
Si	4.03	4.02	4.07	4.03	6.84	7.00	6.66	6.77	3.04	3.04	2.07	19.80
Al	1.96	1.98	1.94	1.99	2.27	2.07	2.41	2.30	1.97	1.97	0.95	4.42
Fe^{+3}								0.02	0.01		0.01	
Ca	0.99	1.00	0.96	0.95	0.90	0.90	1.07	1.00	0.95	0.93	0.04	0.90
Na					0.07	0.07			0.05	0.06	0.74	0.60
K			0.02	0.02	0.05	0.04						0.64
Total	6.99	7.00	7.07	7.08	10.21	10.15	10.14	10.09	6.02	6.02	3.82	26.64

3*: Chlorine 0.07% (Cl 0.01); 4*: Chlorine 0.06 (Cl 0.01); 10*: Cr_2O_3 0.19% (Cr 0.02); 12*: MgO 0.60% (Mg 0.28).

Analyses: 1-6: sample 010, same amygdale, 1-2: wairakite, 2-4: laumontite, 5-6: heulandite; 7-8: samples 090A and 125, stilbites replacing feldspars; 9-10: sample 1 30/6/77, scolecite, 9: from vein, 10: replacing feldspar; 11: sample 090B: IP5, analcime replacing feldspar; 12: sample 053, mordenite in lava amygdale.

TABLE 11. Representative microprobe analyses of secondary feldspars and sphene.

	(1)	(2)	(3)	(4)	(5)	(6)	(7)	(8)	(9)	(10)
SiO_2	65.85	64.48	65.27	66.54	68.17	69.53	30.95	31.24	28.51	32.72
TiO_2					0.15		32.79	35.34	36.30	32.08
Al_2O_3	18.12	18.05	18.45	20.53	19.62	19.97	2.08	1.99	2.57	3.89
FeO		0.21	0.21	0.84	0.28		3.13	1.63	3.34	1.70
CaO		0.14	0.54	1.73	0.64	0.38	27.96	27.72	26.73	27.93
Na_2O			0.75	10.45	11.07	11.83				
K_2O	16.19	16.05	15.36	0.09						0.24
BaO	0.24	0.36								
Total	100.40	99.29	100.58	100.17	100.44	101.71	96.91	97.91	97.45	98.57
Number of Cation:				32 oxygens			18 oxygens			
Si	12.10	12.03	11.97	11.69	11.95	11.95	3.78	3.74	3.48	3.87
Ti					0.02		3.01	3.19	3.33	2.86
Al	3.93	3.97	3.99	4.25	4.03	4.05	0.30	0.28	0.37	0.54
Fe		0.03	0.03	0.12	0.04		0.32	0.16	0.34	0.17
Ca		0.03	0.11	0.33	0.12	0.07	3.66	3.56	3.49	3.54
Na			0.27	3.56	3.73	3.94				
K	3.80	3.82	3.60	0.02						0.04
Ba	0.02	0.03								
Total	19.84	19.91	19.97	19.98	19.89	20.06	11.07	10.94	11.01	11.02
An:	0	0.8	2.8	8.4	3.1	1.8				
Ab:	0	0	6.8	91.1	96.9	98.2				
Or	100	99.2	90.4	0.5	o	0				

1-3: K feldspar; 4-6: albite; 1: sample 090A; 2: sample 216; 3: sample 222; 4: sample 4 12/7/77; 5: sample 050; 6: sample 215.

7-10: Sphene; 7: sample 050, sphene in matrix; 8: sample 4 12/7/77, sphene replacing feldspar; 9: sample 153, sphene replacing ilmenite; 10: sample 123, sphene replacing ilmenite.

TABLE 12. Microprobe analyses of talc, Al-rich clay and apatite.

	(1)*	(2)*	(3)	(4)	(5)	(6)
SiO_2	61.15	60.72	53.27	52.21		
TiO_2		0.15				
Al_2O_3	0.61	1.54	26.44	27.16		
FeO	1.77	4.36	1.35	1.81	0.48	0.35
MgO	29.52	28.62	2.13	1.97	0.29	
CaO	0.48	0.32	3.73	2.40	55.15	54.38
Na_2O				0.47		
K_2O			0.91	1.94		
P_2O_5					41.14	41.18
Chlorine	0.08				0.26	0.18
Total	93.74	95.87	87.83	87.94	97.33	96.10
Number of Ions			23 oxygens		25 oxygens	
Si	8.30	8.17	7.55	7.45		
Ti		0.02				
Al	0.12	0.25	4.42	4.57		
Fe	0.21	0.51	0.16	0.22	0.07	0.05
Mg	5.98	5.73	0.45	0.42	0.07	
Ca	0.09	0.05	0.57	0.37	10.05	10.00
Na				0.13		
K			0.17	0.35		
P					5.92	5.98
Cl	0.02				0.07	0.05
Total	14.81	14.84	13.32	13.50	16.18	16.08

Total iron as FeO. 1*: 0.14% sulphur (S:0.02);
2*: 0.15% sulphur (S:0.02)

1-2: talc replacing hypersthene, sample 115
3-4: unidentified Al-rich white clay repl. fsp; sample 130A and 130B.
5-6: Apatite, sample 215.

TABLE 13 : Fluid analyses from active hydrothermal systems.

	(1) KG-8	(2) KJ-15	(3) KJ-14	(4) KJ-21	(5) RN8	(St.dev.%)
Date	810307	820209	820704	821127		
Sample	1004	1005	1044	1124		
P_o	2.5	13.5	10.6	17.5	9.0	(67.5%)
H_o	925	2676	2602	1528	1184	
SiO_2	334	43	60	429	588	(20.3%)
Na	191	20	16	119	9522	(10.3%)
K	20.5	4.0	3.1	20.6	1378	(9.7%)
Ca	1.5	0.2	0.0	0.7	1578	(5.3%)
Mg	0.01	0.01	0.00	0.00	1.43	(46.6%)
SO_4	57.8	3.8	0.5	15.8	40.8	(32.0%)
Cl	39	3	8	120	19200	(5.3%)
F	0.99	0.17	0.35	0.49	0.15	(25 %)
TDS	869	93	108	764	33282	(6.8%)
GASES						
CO_2	303	55884	16380	1700	1930	(77.1%)
H_2S	73.5	1660	753.2	303.3	36.5	(68.5%)
H_2	0.28	0	12.26	2.28	0.24	(88.9%)
CH_4	5.36	0.0	0.59	0.82	0.49	(82.6%)
N_2	19.23	1620.57	15.41	3.97	10.80	(96.2%)

(1) Upper zone, Production field 1, Krafla

(2) Lower zone, Production field 1, Krafla From H. Ármannsson

(3) Suðurhlíðar, Production field 2, Krafla NEA (pers. comm.).

(4) Hvíthólar, Production field 3, Krafla

(5) Deep water Rn 8 Reykjanes (mean from 17 analyses) (from T.Hauksson, 1981. Reykjanes, Styrkur efna í jarðsjó, OS81015/JHD 10).

P_o Well head pressure

H_o Calculated enthalpy of total flow

TDS Total dissolved solids

Chemical constituents in mg/kg.

APPENDIX II. LIST OF SAMPLES.

A list of samples is provided below including a simple description- and location-key ; I.P.: intrusive phase ; A.E.: approximate elevation in metres ; T.S.:thin-section ; P.S.:probe-section ; XRD:XRD-analyses.

HOFFELLSFJALL, from farms into Kraksgil:

SAMPLE CODE	T.S.	P.S.	XRD	A.E.	SAMPLE-KEY:
1 30/6/77	x	x	x	400	Fsp-phyric lava
1 4/7/77	x			250	lava
2 " A/B	x	x		300	conglomerate
1 29/8/77	x				lava, near farms
2 "	x				I.P.5 " "
3 "	x				I.P.5 " "
4 "	x				I.P.11 " "
5 "	x				lava " "
6 " A	x				scoria " "
6 " B	x				" " "
7 "	x				intrusion " "
060	x				I.P.5 " "
7960	x		x	350	lau-vein

HOFFELLSFJALL-HOFFELLSDALUR :

1 5/7/77	x	x	x		Storaskridugil, lava, B-I
2 "	x		x		" acid tuff
1 20/7/77			x	930	Amygdales in B-II lavas
2 "			x	800	" " " "
3 "			x	950	scoria in B-II
4 "	x				lava, at peak
5 "	x	x	x	700	lava, B-II
1 10/8/77	x			200	scoria, B-I, Urdaskridugil
2 "	x			200	lava " "
110			x		celadonite, Djöflaey
180 A/B	x/x			980	lava/scoria
181	x			850	fsp-phyric dyke
182				800	I.P.5?
183	x			750	lava/scoria
184	x			700	scoria
190	x			250	scoria below H-I
191	x			250-400	H-I collection
192 /A	x/	/x		550	R-I rock, vesicular
193 A/B	x/x	/x		580	R-I. felsite/granophyre
194	x			575	B-I tholeiite lava
195	x				I.P.9 & veins in B-I
196 A	x			500	B-I, lava
196 B	x			300	B-I, fsp-phyric lava
197	x			300	" " " "
223	x			650	I.P.5 : fine-gr.gabbro/dol.
224				680	lavas, ep-check
225				680	lava/amygdale/veins
226				250	Iceland-spar at I.P.9
7965					Djöflaey,R-II batch for dating
7966					" " " " "
7967					" " " " "

KRAKSGIL :

SAMPLE CODE	T.S.	P.S.	XRD	A.E.	SAMPLE-KEY :
3 4/7/77	x			350	lava, opposite gabbro
4 "	x			350	scoria " "
047	x	x			I.P.6, ravine front
048	x				I.P.11 - veins
049	x			150	I.P.5 or I.P.6
050	x	x		150	lava
051	x	x		150	scoria
052	x			200	lava at contact with I.P.12
052 A	x			"	" " " " "
052 B	x			"	" " " " "
053	x	x		"	" " " " "
054	x				lava
055	x				felsite intrusion I.P.11
056	x				dolerite-gabbro I.P.10
057	x				gabbro-diorite I.P.10
058	x				I.P.11 breccia
059	x				I.P.11 apophysis
167	x				lava,gt in veins
168	x				I.P.5, very altered
169 A/	x/	x			I.P.5, altered & veins
170					scree collection
222	x	x		450	lava & gt , caldera-fault
7905	x			100	veins in I.P.3
7906	x			"	veins in lava host, loc.1
7908	x			"	" " " " "
7909	x			"	" " " " "
7910	x			"	" " " " "
7911	x			"	" " " " "
7912	x				lava free of veins
7913	x				veins in host-rock
7914	x		x		" " " "
7915					gabbro
7916					felsite-veins in gabbro
7917	x				lava, close to gabbro, veins
7918	x		x		" " " " "
7919			x		veins in gabbro
7920	x				breccia
7921	x			150	amygdale
7922	x		x	"	late-vein collection
7923	x			250	vesicular zone in I.P.6
7924				280	stb.amygdale
7925				300	felsite layer, collection
7926	x			130	veins, locality 1
7927	x			"	" "
7928	x		x	"	" "
7929	x		x	"	" "
7930	x		x	"	" "
7931	x			"	an amygdale
7932					late-vein alongside I.P.3
7933 A	x			200	mixed breccia
7933 B	x			"	" "
7933 C	x			"	" "
7933 D	x			"	" "
7933 E	x			"	" "

KRAKSGIL : cont.

SAMPLE CODE	T.S.	P.S.	XRD	A.E.	SAMPLE-KEY :
7934	x			150	I.P.11 veins
7935	x			"	lava & veins
7936	x			"	I.P.5 & "
7937	x		x	"	I.P.12 & "
7938	x			130	jasper vein etc.
901	x				Diorite I.P.10

TUNGUFELL :

3 11/7/77	x			260	lava scoria
4 "			x	"	" "
5 "	x			"	felsitic layer
1 19/7/77	x	x		190	I.P.6
2 "	x	x		210	an amygdale
3 "	x			300	felsitic layer I.P.4?
4 "	x			250	I.P.11 apophyse
5 "	x			"	I.P.11 felsite intrusion
6 "	x			"	" " " ,top
080	x			400	tholeiite lava
081				"	clay-like veins
082				"	veins
083				"	"
084				"	an amygdale
085	x	x		450	lava
086	x			"	lava
087 A				530	rocks at fault
087 B	x			"	" near fault
087 C				"	jasper
088	x			550	fsp-phyric lava
089	x	x		700	scoriaceous lava
166	x			100	amygdales

MIDFELLSGIL :

1 11/7/77	x	x		100	scoria, andradite & grossular
2 "	x	x	x	"	" " "
1 12/7/77			x	150	vein
2 "	x			"	granophyre sheet, I.P.4?
3 "	x			"	scoria below
4 "		x		"	lava below
029	x			100	scree collection
030				"	lava
031				"	amygdale
032	x			"	intr.sheet
033	x	x		"	lava & amygdales
034				"	amygdales
035				200	amygdales
036	x			"	flow-banded basaltic tuff

MIDFELLSGIL : cont.

SAMPLE CODE	T.S.	P.S.	XRD	A.E.	SAMPLE-KEY :
037	x			200	I.P.12 apophysis
038	x			"	lava & veins
039	x			"	" " ,gt-zone margin
040				250	amygdales
041				"	" & lava
042				270	"
043	x			300	I.P.11 dyke
044	x			"	amygdales
045	x			"	I.P.12 cross-cuts 043
046	x			400	felsitic layer, T-side
7961			x	100	stilbite
7962	x				composite sheet (I.P.4?)
7963			x		stb-qtz-cc vein in I.P.12
7964	x			180	lava
7964 B	x			480	fsp-phyric lava,
7964 C	x			720	lava

MIDFELL :

068	x			400	fsp-phyric lava
069	x			500	lava
070	x			650	lava
071	x			650	amygdales
072 A/B	x/x			700	lava/scoria
073	x				I.P.12 at caldera fault
074 A	x			750	lava, east of fault
074 B	x			"	" " " "
074 C	x			"	" " " "
075	x			700	fsp-phyric sheet contact
076 A/B	x/x			650	lava/tuff, Geitafellgil-side
077	x			"	I.P.10 & vein at fault " "

GEITAFELL GABBRO :

000	x				I.P.2 & I.P.4
001					I.P.2 xenolith in I.P.5
002	x				I.P.2 xenolith in I.P.5,G-gil
021	x				I.P.2 in Efstafellsgil
026					" " " , altered
027					" " " I.P.4-contact
091					I.P.2 or I.P.3 dyke in G-gil
111 A/B	x/x	x/			I.P.2, loc.2 veins 2,3,6 & 7
112	x		x		I.P.2 vein of system 7
113	x				I.P.2 close to I.P.5 or I.P.7
114	x				I.P.5 or I.P.7 in I.P.2
115	x	x			I.P.2, effect from I.P.12
116	x				" " " "
118	x				" at contact with I.P.6
119 A/B	x/x				I.P.6/I.P.9 in I.P.2
153 A/B	x/x	x			I.P.2 altered in E-gil
154	x				I.P 2 porphyritic gabbro,E-gil
171	x	x			I.P.2 and I.P.4 veins
172	x				I.P.2 & veins of systems 2, 3.
173 A/B	x/x				I.P.2 & " " " 3, 6.
174	x	x			basaltic vein (4) & younger veins
175	x				I.P.2

GEITAFELL GABBRO : cont.

SAMPLE CODE	T.S.	P.S.	XRD	A.E.	SAMPLE-KEY :
213	x	x			I.P.2 & vein of system 3
217 A/B/C	x/ /x				I.P.2 & late qtz-cc veins
7901 A/B	x/x				I.P.5 in I.P.2 cut by acid vein and containing I.P.2 xenolith.
7902	x				basalt vein & 2 ep-veins in I.P.2
7903	x				I.P.2 & vein of system 7
7904	x				I.P.2 & veins of system 6

GEITAFELL GABBRO CONTACT AUREOLE :

1 14/7/77			x		late vein alongside I.P.12
1 16/8/77			x		veins in lava host
2 "	x				lava host
3 "			x		veins in host
4 "	x				lava host
5 "	x		x		veins
6 "	x				fault breccia & late vein
7 "	x				I.P.5 altered
8 "	x		x		vein alongside I.P.9
012 A/B	x/x				I.P.3 contact/host rock
013	x				lava host close to I.P.3
014	x				" " " " I.P.5
015	x				" "
016					" "
017	x				" "
018 A/B	x/x				" " /scoria host
028	x				" "
090 A	x	x			I.P.3
090 B	x	x			I.P.5
090 C	x				host
120					I.P.5
121	x				I.P.6
123	x	x	x		veins , locality 3 (and below)
124	x	x			host & veins
125 A/B	x/x	/x	/x		I.P.6/lau-stb vein in I.P.6
126 A/B	x/x		x/		vein /I.P.9
127 A	x	x	x		I.P.12 & veins
127 B	x	x			" "
127 C	x				" "
128			x		vein between I.P.7 and I.P.9
129	x	x			I.P.5 effect from vein
130					veins & host
130 A/B	x/x	x/x			I.P.4&I.P.5/I.P.3
131	x	x			scoriaceous host
132 A/B	x/x				I.P.3/I.P.2
133	x				I.P.5 fine-grained
134	x	x			lava
135	x	x			porphyritic sheet
214	x				hornfels scoria
215	x	x			hornfels lava & I.P.4 vein
216	x	x			I.P.3 & metam. veins

GEITAFELLSGIL (G-gil) :

SAMPLE CODE	T.S.	P.S.	XRD	A.E.	SAMPLE-KEY :
5 12/7/77	x			200	lava
6 "	x			"	lava
7 "	x			"	scoria between
2 14/7/77			x	150	amygdales
3 "			x	"	late veins (5-15 cm)
4 "	x			"	scoria close to vein
1 25/8/77 A/B	x/x			370	H-I rocks
2 "	x		x	"	lava amygdales
3 "	x				acid tuff in H-I base
4 "			x		amygdales
5 "	x				I.P.11 intr.brccia R-II feeder
6 "	x			700	R-II rocks
7 "	x				brown rock below tillite
8 "	x		x		B-II lava
9 "	x			500	I.P.11 feeder to R-II
10 "	x			300	R-I lava
11 "	x			"	B-I lava
003	x				fine-grained basalt dyke &jasper
004				300	vesicular lava below R-I
005				"	vein, cc,stb,clay
006	x			"	lava adjacent to 005
007	x				I.P.4?
008	x			300	Interm.sheet ? older than I.P.12
009	x	x			lava & clay
010	x	x			amygdale & lava
011	x				fine-grained sheet I.P.8?
078					amygdale
079				500	amygdales
176	x				lava
211 B				440	B-II base
212	x			500	B-II lava
218					R-I? felsite breccia in H-I
219	x			480	R-I felsite in H-I
220	x				I.P.5? in H-I
221	x			340	scoriaceous lava

GEITAFELL :

061	x			600	I.P.6
062	x		x	840	lava
063	x		x	900	veins in H-II
064 /A	x/x		x/x		amygdales in B-II,M-fell-peak
065	x		x		I.P.11 dyke " "
066	x				oxidized dyke " "
067					I.P.10 " "
092				350	vesicular acid rock
092x	x			400	I.P.5 & veins
093	x			500	I.P.6. & vein
094				750	I.P.6
095	x			760	lava, B-II
096	x			"	" "
097	x			800	" "
098	x			"	I.P.6?
099	x			"	I.P.10?
100 A/B	x/			"	I.P.5/collection
101	x				I.P.1 ?, fine-grained basalt
102	x			850	scoriaceous lava, B-II

GEITAFELL : cont.

SAMPLE CODE	T.S.	P.S.	XRD	A.E.	SAMPLE-KEY :
103	x			850	scoriaceous lava, B-II
104	x			650	felsitic rock in H-I
105					zeolite
106	x			650	I.P.8 -type
107	x			600	I.P.1 ?
108 A/B	x/x				I.P.1 & veins /I.P.8 cuts
109	x			330	amygdale
136 A/B	x/x			460	I.P.10 margin/centre,E-gil side
137	x			600	H-I mixed " "
138	x			600	I.P.10?
139	x			620	scoria
140	x			640	lava
141	x			"	amygdale
142	x			"	lava, B-II
155 /	x/x		/x	850	ol-basalt/amygdale
156			x	1000	vein in B-III
157				1000	B-III amygdales
158					B-III base E-gil-botn
160x	x			300	I.P.10

EFSTAFELLSGIL (E-gil) - Efstafellsnes :

1 21/8/77	x			100	tholeiite lava
2 "	x	x		"	" "
3 "				"	amygdale & vein
4 " A/B	x/x	x		170	pillow/tuff
5 "	x			"	hyaloclastite
019	x	x		150	fsp-phyric lava
020	x			"	blue tuff
022	x			"	hyaloclastite
023	x			"	breccia, contact to I.P.9
024	x	x		"	collection from sulphide pond
025	x	x		"	scoriaceous basalt " "
7939			x	150	two cc-veins
7940	x			"	I.P.2-I.P.3
7941 A/B	x/x			"	I.P.2 & veins, locality 5
7942			x	"	vein at I.P.12 margin
7943	x			"	I.P.2 & veins
7944	x			"	" "
7945	x			"	jasper amygd.I.P.5/I.P.7 junct.
7975	x			450	I.P.5, river exposures
7979			x	370	platy cc-qtz at caldera fault
7980	x			300	I.P.10
7982			x	150	I.P.2 & lau-py zone

GJANUPSVATN - EFSTAFELLSNES :

160	x			200	rusty zone/H-II scoriaceous
161	x			"	" " contact to H-II host
162	x			"	tuff, H-II
163	x			"	breccia
164	x	x		"	lava host
165	x	x		"	I.P.10 sheet

GJANUPSVATN - EFSTAFELLSNES : cont.

SAMPLE CODE	T.S.	P.S.	XRD	A.E.	SAMPLE-KEY :
7970	x			200	fsp-phyric basalt host?&veins
7971 A/B	x/		/x	"	host & veins, locality 6
7972			x	"	veins, qtz,cc
7973	x		x	"	I.P.10 & veins
7974	x			"	I.P.11
7975	x			"	I.P.8
7976	x		x	"	H-II & veins
7977	x			"	I.P.10 vein-free

EFSTAFELL - GRASGILJATINDUR :

143	x			350	I.P.8? margin
144 A/B	x/x		x	470	Interm.pillow
145			x	"	" tuff?
146	x	x		500	I.P.5
147	x			"	I.P.6 or I.P.10 apophysis
148	x			"	I.P.9 or I.P.12 (-appearance)
149	x	x		550	" " & veins
150	x	x		600	I.P.10
151 A/B/C	x/X/		//x	600	H-II + vein /vein-free / vein
152	x			400	acid tuff in H-II
159	x	x		800	acid-tuff R-II
177				300	sulphide, Thvera
178	x			500	lava "
179	x			550	" "
200 A/B	x/x			340	H-I collection
201	x			640	H-II, brown
202	x			670	lava within H-II
205					pillow breccia collection
206	x			800	pillow at lava base
207	x	x		800	1st lava at B-III base
208	x	x		800	2nd lava at B-III base
209	x			700	R-II tuff
210	x			700	R-II felsite
211 /A	x/x			700	H-II interm?

LYNGTUNGNAFJALL - GJANUPSTINDUR :

7968	x			300	2nd lava in B-III
7969	x			300	1st lava in B-III
7981	x			500	B-III lava, analcime

SVINAFELL AREA :

230	x			100	I.P.2 to I.P.3
231	x			"	lava host
232	x			130	gabbro Öldutangi
233					
234					
235	x			200	gabbro in reworked H-II
236	x			"	basalt in breccia
237	x			"	hyaloclastite
238				"	
239				"	
240	x			"	tuff in Öldutangi
241		x		"	I.P.12 su & z
242	x				hyaloclastite
243	x				basalt in Goltur
900	x			100	I.P.5
902	x				I.P.12

VIDBORDSFJALL (south) :

SAMPLE CODE		T.S.	P.S.	XRD	A.E.	SAMPLE-KEY :
1	17/7/77	x			70	Lava, B-I, Strönd
2	"	x			"	scoria " "
3	"	x			100	lava/scoria, Vidbordssel
4	"	x			"	lava, Stóraból
5	"	x			150	scoria, B-I, Grjotargil
6	"	x			"	lava " "
1	19/8/77				200	basaltic sheet, "
2	"				300	iceland-spar "
11	23/8/77	x		x/x	400	tholeiite lava " ,N
12	"	x			320	sediment collection " "
13	"	x		x	300	lava & acid vein " "

VIDBORDSFJALL (gabbros and vicinity) :

3	18/7/77	x				gabbro, unit D (north)
4	"	x				granophyre, I.P.11
5	"	x				" "
1	17/8/77			x/x	350	red-brown vein in dyke
2	" A	x		x	"	breccia, N-contact to unit D
2	" B	x			"	" " "
3	"	x		x	"	" " "
4	" A	x	x		"	unit D "
4	" B	x			"	" "
5	" A	x			"	fsp-phyric basalt, N-contact
5	" B	x			"	" "
6	"	x			"	tuff, N-contact to unit D
7	"			x	400	clay-vein (sm/illite)
8	"			x/x	"	white veins
9	"	x			"	felsite, I.P.11
10	"	x			500	breccia at I.P.11 contact
11	"	x			"	" " "
1	18/8/77	x			500	I.P.10 dyke,S-contact to unit C
2	"	x			"	" " " "
3	"			x/x	"	collection from SW-contact "
4	"	x			"	breccia " " "
5	"	x			"	gabbro boulder " "
6	"				"	breccia " " "
7	"	x			"	" " " "
8	"	x			"	tuff " " "
9	"	x			"	breccia " " "
10	"			x/x	"	amygdales " " "
11	"			x	"	clay veins " " "
1	23/8/77	x			380	gabbro-sheet I.P.10,margin/centre
2	"				"	" " " ,chilled margin
3	"	x			360	collection between units D and C
4	"			x	"	" " "
5	"	x	x	x/x	"	" " "
6	"	x			"	lava " "
7	"			x/x	"	veins " "
8	"	x		x/x	"	collection " "
9	"	x	x	x	"	lava " "
10	"	x		x/x	450	fsp-phyric lava & amygdales
1	24/8/77			x	250	gabbro, altered,unit D, N-margin
2	"			x	300	vein " "
3	" A	x	x	x	500	collection W-contact to unit D
3	" B	x			"	" " "
4	"	x			540	lava " "

VIDBORDFJALL (gabbros and vicinity) : cont.

SAMPLE CODE	T.S.	P.S.	XRD	A.E.	SAMPLE-KEY :
5 24/8/77A	x			400	hyaloclastite, west-side
5 " B				"	" "
441	x		x	250	within unit D
442	x			"	unit D
7947	x			150	unit D, N-margin
7948	x			"	" "
7956	x			100	unit A
7957	x			150	unit B, east-contact
7958	x			"	hornfels " to unit B
7959	x			"	" " "
7951 A	x			80	Litla Dima- granodiorite
" B	x			"	" " diorite
" C	x			"	" " gabbro
" D	x			"	" " granophyre

GRAENAFELL - Haukafellsheidi :

1 18/7/77	x			100	tuff
2 "	x			"	sulphide-mineralization along dyke
7949	x			400	fsp-phyric hyalocl.H-II
7950			x	600	" " "
7953	x				pillow in H-II,Haukaf.heidi
7954	x				I.P.12 "
7955 A	x			600	intermediate lava Graenafell
7955 B	x			"	basaltic lava "

JOKULFELL AND VIDBORDSDALUR :

1 30/7/77			x	200	amygdale collection V.dalur
2 "			x/x	"	" " "
3 "	x		x/x	"	scoria " "
1 31/7/77	x			300	R-II rocks " Jokulfell
2 "	x			"	" " " "
3 "				"	" " " "
4 "	x			"	" " " "
5 "	x			"	" " " "
6 "			x	500	amygdale collection,Vidb.halsar
7 "			x	"	" " "
8 "	x			"	" " "
9 "				300	intermediate lava ? in R-II
10 "	x			200	I.P.10 boulder in H-II Jokulfell
11 "	x			"	H-II rocks "
1 1/8/77				130	scoria, pl-phyric "
2 "			x	"	pl-phyric lava in H-II "
3 "	x			"	basic apophysis " " "
4 "	x	x		"	breccia " "
5 "	x			"	tuff " "
6 "	x		x	100	pillow in H-II "
7 "	x			"	tuff " "
8 "	x			"	" " "
9 "			x	"	amygdales in pillow " "
10 "			x/x	"	" " " "
11 "	x			"	I.P.11 dyke margin " "
12 "	x			"	I.P.11 " centre " "

APPENDIX III

ANALYTICAL METHODS.

Four methods were used to identify the secondary minerals; (i) Hand-specimen study, (ii) XRD-study, (iii) Electron Microprobe study, and (iv) Microscope study.

Hand-specimen study. A preliminary identification of secondary minerals was carried out in the field with the help of a hand lens. During the first field season, a binocular magnifying microscope was kept in camp for the same purpose. The preliminary field identification of the zeolites, for instance, were confirmed by the later laboratory studies.

XRD-identification. During and after each field season sufficiently large amygdale or vein deposits were hand picked at the NEA-laboratory, or in the field, and ground for XRD-powder diffraction analyses. These specimen were included in routine XRD-analyses at the NEA - laboratory, operated by Mrs. H. Thorsteinsdottir (Philips PW1130/00/60 X-ray generator, Cu-tube, 25 mA, 35 KV). Identification was made by comparison with standard XRD-diagrams, compiled at NEA, or by the aid of powder diffraction files. The results of this study were used as an aid in the subsequent optical study of the same samples, and a few reference thin sections of zeolites, for instance, were thus prepared.

Commonly, the XRD-analysed samples of amygdales and veins included two or more mineral species. Later comparison with thin sections showed that only the most abundant minerals within such assemblages were identifiable on the XRD-diagrams, e.g. disseminated ep or py in a cc-qtz bulk sample did not show up - not surprisingly. From the later optical and chemical studies detailed separation of the amygdale and the vein deposits for further XRD-study was not considered necessary. One amygdale, however, containing the assemblage ab-K.fsp, was hand picked from a sample and XRD-analysed at the Grant Institute laboratory, confirming the K.fsp-phase as being adularia.

All the zeolites, except wairakite, were analysed by XRD at the NEA-laboratory, as well as qtz, cc, pr, aragonite, ep and py. A few reconnaisance XRD-analyses of dry, glycolated and heated clay species were also made, revealing the presence of smectite in late zeolite-bearing veins within the former high-T hydrothermal system. Due to the lack of knowledge on the extent of overprinting within the extinct hydrothermal system, at the early stage of this research, and the difficulties involved in detailed clay separation, extensive XRD studies of the clay minerals were not included in the present study of the hydrothermal evolution. The chemical analyses by the microprobe were further considered of reasonable tolerance for the most abundantly occurring clay minerals (appendix 1).

Electron microprobe analyses. The Cambridge Instruments Microscan V electron probe microanalyser of the Grant Institute was extensively used for mineral identification and chemical composition. The mineral analyses were all performed by the energy dispersive methods (EDS). After an optical study (transparent- and reflected light microscopes), the thick, transparent, polished thin sections were cleaned in an ultrasonic bath and coated with a conductive carbon film. Each batch of the polished thin sections and cobalt standards, used for calculations of the apparent elemental concentrations, were carbon coated simultaneously, and stored in a dessicator prior to analysis. A gun potential of 20 KV was used, and a nominal probe current of 6 nA, frequently monitored using a Faraday cage. The probe beam of ca 2 µm diameter was focussed on a periclase and centred on araldite. A 100 s livetime was used on a Si(Li) detector. Corrections for matrix absorptions, atomic number and enhancement (ZAF) were made on an on-line Data General computer using a program based on the work of Statham (1975). A video screen connected to the microprobe unit enabled a visual study of the chemical spectra, useful for determination of the apparent mineral phase involved, fed into the computer calculating the mineral composition. The zeolite and clay analyses were produced as unknown minerals (1 oxygen per formula unit) and calculated manually to the appropriate oxygen number per formula unit. Total iron (as FeO) was converted manually to Fe_2O_3 (1.1113xFeO) where necessary (e.g. in epidote and andradite). The sulphide composition was determined from the elemental weight %.

Representative chemical analyses of most of the secondary minerals found within the volcano are shown in appendix 1 and discussed in chapter 9. The microprobe was particularly useful in determining the fine-grained mineral assemblages within the rock matrices and in the primary mineral pseudomorphs. Similarly, a visual study of the elemental spectra was useful to check the carbonate composition within the samples, revealing the presence of siderite in one sample, in addition to the ubiquitous presence of calcite. Most of the zeolites found within the volcano were successfully analysed (appendix 1). Volatilization, shown by burn marks on zeolites, clays and apatite, was sometimes observed. A slightly defocused probe-beam was then used, often with little or no better result. In most cases, however, volatilization did not cause problems, and the analytical results, e.g. of the zeolites, proved to be fairly consistent.

Commonly, the softer minerals, like the clays or the zeolites, take poor polish. The carefully polished thin sections, however, made by Mr. K. Cameron at the Grant Institute, resulted in the apparently reliable clay mineral analyses (appendix 1).

The relatively few secondary minerals, abundantly occurring in the extinct hydrothermal system, as seen by the combined result of the XRD-, the microprobe-, and the optical study, evidently simplified the optical identification of minerals, like the zeolites for instance, as the study proceeded. Other minerals, like the secondary iron and titanium ore and the fine-grained clays, were more difficult. The samples analysed by the microprobe, however, are sufficiently widespread from within the volcano to warrant the general conclusions made, as to their distribution and their overall status (e.g. lim, hm, mt) within the hydrothermal mineral assemblages.

Microscopic identification. The number and the division of the unpolished and the polished thin sections prepared for this research are shown in appendix II. Most of the thin sections were made by Mr. K.Cameron and Mr. W.Hamilton at the Grant Institute, while quite a few sections, mainly from the last field season, were prepared by Mrs. B. Baldursdottir at the NEA. Some of the fragile samples had to be impregnated or immersed in resin prior to the thin section preparation.

While the optical identification of the secondary minerals was either supported or confirmed by the microchemical and the XRD-studies, knowledge on the secondary mineral distribution and the mineralogical evolution of the hydrothermal system was gained from the thin section study.

The distribution and the appearance of most of the common secondary hydrothermal minerals has already been discussed within the thesis, and numerous examples from thin sections of the common vein and amygdale minerals are shown by figures 6.1-6.23 and 8.1-8.4. A few comments on the most useful optical properties of the zeolites (not shown by the examples) may still be mentioned.

The distinction between the most common zeolites, wairakite, laumontite, stilbite and heulandite, was fairly straight forward. Distinctive polysynthetic twinning readily distinguishes wairakite from all the other zeolites. The oblique extinction of the tabular laumontite, its negative sign, and two cleavage directions distinguishes laumontite from both heulandite (opt.+ve) and stilbite (opt.-ve) which extinguish parallel to their 010-cleavage. In addition to the different optical signs, heulandite has much better cleavage than stilbite, which in turn commonly occurs in sheaf-like aggregates. The sometimes sheaf-like prehnite cannot be mistaken for stilbite due to their different relief and the much higher birefringence of the prehnite.

Other zeolites discussed in this thesis, but much less common, are scolecite, mordenite, thomsonite, analcime and chabazite. The first three typically form columnar, fibrous, radiating aggregates. Both the scolecite and the thomsonite usually form densely packed aggregates, while the mordenite aggregates are commonly loosely packed, composed of hair-like prisms, radiating from somewhat denser cores at the walls of veins or amygdales. Due to the loosely packed prismatic habit, other minerals, like calcite, may totally surround the mordenite prisms. Due to this, and the fact that the other fibrous zeolites may develop single-standing elongated prisms, mordenite is difficult to identify optically. The scolecite contrasts with thomsonite by its oblique extinction and its negative sign. The thomsonite (parallel extinction, opt.+ve) from within the volcano, further shows a faint brownish tint due to some minute

inclusions, and has sometimes developed narrow and clear concentric zones within the radiating aggregates, while the scolecite is usually both clear and colourless. The chabazite is optically positive, has irregular cleavage, symmetric extinction and a birefringence near nil. The isometric analcime is dark between crossed nicols, and, as far as is known, does not develop the characteristic polysynthetic twins typical of weakly birefringent wairakite.

The presence of the less common zeolites from within the volcano has in most cases been confirmed by XRD or chemical analysis.

Most of the zeolites discussed have been found in feldspar pseudomorphs, forming assemblages with albite, K.fsp and other minerals. In such a situation, the zeolites may form low-relief anhedral patches, impossible to identify, while their development varies within the pseudomorphs both on an inter- and an intrasample basis. Chemical study of the feldspar pseudomorphs, however, shows that the low-T zeolites are more or less restricted to vein wall rock zones, and the types of zeolites may thus be traceable from the mineral veins into the wall rocks.

In conclusion, the application of the four methods used for mineral identification suggests that an optical study, in most cases, is sufficiently accurate to sort out the chief mineral assemblages composing the rocks, as far as the zeolites and all the common silicates are concerned. The clay minerals and the secondary iron- and titanium oxides, however, require either or both a detail XRD- or a microchemical study. Furthermore, a microchemical study is essential to ascertain the mineral species composing the most fine-grained assemblages, as the fine-grain size hampers a detail optical study.

REFERENCES

Anderson, E.M., 1936. The Dynamics of the formation of cone sheets, ring dykes and caulderon subsidence. P.R. Soc. Ed. 56, 2, pp. 128-163.

Annels, A.E., 1967. The Geology of the Hornafjordur Region, S.E. Iceland. Ph.D. thesis. University of London, 278 p.

Annells, R.N., 1968. A geological investigation of a Tertiary intrusive centre in Vididalur-Vatnsdalur area, northern Iceland. Ph.D. thesis, Univ. of St. Andrews, 614 p.

Armannsson, H., G. Gíslason and T. Hauksson, 1981. Magmatic gases in well fluids and the mapping of the flow pattern in a geothermal system. Geochim. Cosmochim. Acta, 46, pp. 167-177.

Armstead, H.C.H., 1978. Geothermal Energy. E. & F.N. Spon Ltd., London, 357 p.

Arnason, B., 1976. Groundwater systems in Iceland traced by deuterium. Soc. Sci. Islandica, 42, 236 p.

Arnórsson, S., 1981. Mineral deposition from Icelandic Geothermal waters: Environmental and Utilization Problems. J. Pet. Tech. 33, pp. 181-187.

Arnórsson, S., A. Björnsson, G. Gíslason and G. Gudmundsson, 1975. Systematic Exploration of the Krísuvík High-Temperature Area, Reykjanes Peninsula, Iceland. Proceedings of the 2nd UN Symposium on the Development and Use of Geothermal Resources, San Francisco, California, 1975, vol. 2, pp. 859-864.

Arnórsson, S., K. Grönvold and S. Sigurdsson, 1978. Aquifer chemistry of four high-temperature geothermal systems in Iceland. Geochim. Cosmochim. Acta, 42, pp. 523-536.

Arnórsson, S. and H. Svavarsson, 1980, CO_2-gas geothermometer (in Icelandic). Abstract, Geothermal Conference, pp. 35-37, Nov. 7, 1980, Reykjavík, Iceland.

Arnórsson, S., S. Sigurdsson, and H. Svavarsson, 1982 a. The chemistry of geothermal waters in Iceland. I. Calculation of aqueous speciation from 0° to 370°C. Geochim. Cosmochim. Acta, 46, pp. 1513-1532.

Arnórsson, S., E. Gunnlaugsson, and H. Svavarsson, 1982 b. The chemistry of geothermal waters in Iceland. II. Mineral equilibria and independant variables controlling water composition. Geochim. Cosmochim. Acta (submitted).

Arnórsson, S., E. Gunnlaugsson, and H. Svavarsson, 1982 c. The chemistry of geothermal waters in Iceland. III. Chemical geothermometry in geothermal investigations. Geochim. Cosmochim. Acta (submitted).

Best, N.F., 1978. Experimental studies of greenschist and amplibolite facies metamorphism of basic rocks. Ph.D. thesis. University of Edinburgh, 76 p.

Billings, M.P., 1954. Structural geology, 2nd ed., New York, Prentice Hall Inc., 514 p.

Bischoff, J.L., and W. Seyfried, 1978. Hydrothermal chemistry of seawater from 25° to 350°C. Am. J. Sci. 278, pp. 838-860.

Björnsson, A., K. Saemundsson, P. Einarsson, E. Tryggvason and K. Grönvold, 1977. Current rifting episode in north Iceland. Nature, v. 266, pp. 318-323.

Björnsson, S., S. Arnórsson, and J. Tómasson, 1970. Exploration of the Reykjanes brine area, Geothermics, Special issue 2, pp. 1640-1650.

Björnsson, S., S. Arnórsson and J. Tómasson, 1972. Economic evaluation of Reykjanes thermal brine area. AAPG. Bull. 56, pp. 2380-2391.

Blake, D.H., 1964. The volcanic geology of the Austurhorn area, Southeastern Iceland. Ph.D. thesis, University of London, 191 p.

Bodvarsson, G., 1961. Physical characteristics of natural heat resources in Iceland. Proc. U.N. Conf. New Sources Energy, Rome, 1961, 2, 82.

Browne, P.R.L., 1970. Hydrothermal Alteration as an Aid in Investigating Geothermal Fields. Geothermics - Special issue 2, pp. 564-570.

Browne, P.R.L., 1978. Hydrothermal alteration in active geothermal fields. An. Rev. Earth Planet. Sci., 6, pp. 229-250.

Burt, D.M., 1972. Mineralogy and geochemistry of Ca-Fe-Si skarn deposits. P.D. thesis, Harward University, 256 p.

Burton, J.C., L.A. Taylor, and I-Ming. Chou, 1982. The f_{O_2}-T and f_{S_2}-T stability relations of Hedenbergite and of Hedenbergite-Johannsenite solid solutions. Econ. Geol. v. 77, no. 4, pp. 764-783.

Carmichael, I.S.E., 1961. Volcanic geology of Thingmuli eastern Iceland. Ph.D. thesis, University of London, 132 p.

Carmichael, I.S.E., 1964. The petrology of Thingmuli ; A Tertiary volcano in eastern Iceland. J. Petr. v. 5, no. 3, pp. 435-460.

Carmichael, I.S.E., 1967. The mineralogy of Thingmuli, a Tertiary volcano in eastern Iceland. Am. Mineral., v. 52, pp. 1815-1841.

Coombs, W.S., P.J. Ellis, W.S. Fyfe and A.M. Taylor, 1959. The zeolite facies, with comments on the interpretation of hydrothermal synthesis. Geochim. Cosmochim. Acta, v. 17, pp. 53-107.

Davis, S.N., and R.J.M. DeWiest, 1966. Hydrogeology, John Wiley & Sons, New York, 463 p.

Desmet, A., Cl. Gagny, H. Lapierre, and G. Rocci, 1979. Organisation spatio-temporelle du complex filionien du Troodos : Son erracinement dans la chambre magmatique. Proceedings of the International Ophiolite Symposium, Cyprus, pp. 66-72.

Dullien, F.A.L., 1979. Transport phenomena in porous media and pore structure. Academic Press, New York.

Durrance, E.M., 1967. Photoelastic stress studies and their application to the mechanical analysis of the Tertiary ring complexes of Ardnamurchan, Agyllshire. Proc. Geol. Assoc., 78, pp. 289-318.

Einarsson, P. and S. Björnsson, 1979. Earthquakes in Iceland, Jokull, special issue 29, Reykjavík, pp. 37-43.

Einaudi, M.T., and D.M. Burt, 1982. Introduction-Terminology, Classification and Composition of Skarn Deposits. Econ. Geol., v. 77, no. 4, pp. 745-754.

Ellis, A.J. and W.A.J. Mahon, 1977. Chemistry and Geothermal Systems. Academic Press, New York, 392 p.

Eskola, P., 1915. On the relation between the chemical and mineralogical composition in the metamorphic rocks of the Orijärvi region. Bull. Comm. Géol. Finlande, no. 44 (English summary pp. 109-145).

Eskola, P., 1939. Die metamorphen Gesteine, "Die Entstehung der Gesteine" (T.F.W. Barth, C.W. Correns, P. Eskola) Springer, Berlin, pp. 263-407.

Evarts, R.C., and P. Schiffman, 1983. Submarine hydrothermal metamorphism of the Del Puerto Optiolite, California. Am. J. Sci., v. 283, pp. 289-340.

Exley, R.A., 1982. Electron microprobe studies of Iceland Research Drilling Project, High-Temperature Hydrothermal Mineral Chemistry. Journ. of Geoph. Research, v. 87, no. B8, pp. 6547-6557.

Fenner, C.N., 1936. Borehole investigations in Yellowstone Park. J. Geol. 44, pp. 225-315.

Forester, R.W., and H.P. Taylor, Jr., 1976. Oxygen-18-depleted igneous rocks from the Tertiary complex of the Isle of Mull, Scotland. Earth and Planetary Sci. Lett. 32, pp. 11-17.

Fournier, R.O., 1981. Application of water geochemistry to Geothermal Exploration and Reservoir Engineering, pp. 109-143, in Geothermal Systems: Principles and Case Histories, Ed. by Rybach and Muffler. John Wiley & Sons Ltd., 359 p.

Fournier, R.O., and J.J. Rowe, 1966. Estimation of underground temperature from the silica content of water from hot springs and wet-steam wells. Am. J. Sci., 264, pp. 685-697.

Fournier, R.O., and A.H. Truesdell, 1973. An empirical Na-K-Ca geothermometer for natural waters. Geochim. Cosmochim. Acta 37, pp. 1255-1275.

Fridleifsson, I.B., 1973. Petrology and structure of the Esja Quaternary volcanic region, SW-Iceland. Ph.D. thesis. Univ. of Oxford, 208 p.

Fridleifsson, I.B., 1979. Geothermal activity in Iceland. Jokull, special issue 29, Reykjavík, pp. 47-56.

Fridleifsson, I.B., H. Furnes and F.B. Atkins, 1982. Subglacial Volcanics - on the control of magma chemistry on pillow dimensions. Journal of Volcanology and Geothermal Research, 13, pp. 103-117.

Fyfe, W.S., and F.J. Turner, 1966. Reappraisal of the metamorphic facies concept. Contrib. Mineral. Petrol., v. 12, pp. 354-364.

Fyfe, W.S., N.J. Price, A.B. Thompson, 1978. Fluids in the earth's crust (Developments in Geochemistry ; 1). Elsevier Scientific Publishing Company. (Amsterdam-Oxford-New York) 383 p.

Gale, N.H., S. Moorbath, J. Simons, and G.P.L. Walker, 1966. K-Ar ages of acid intrusive rocks from Iceland. Earth and Planetary Sci. Lett., 1, pp. 284-288.

Gamble, R.P., 1982. An experimental study of sulfidation Reactions Involving Andradite and Hedenbergite. Econ. Geol. v. 77, no. 4, pp. 784-797.

Garrels, R.M., Z.M. Dreyer and D.L. Howland, 1949. Diffusion of ions through intergranular spaces in water saturated rocks. Geol. Soc. Am. Bull., v. 60, pp. 1809-1828.

Gibson, I.L., D.J.J. Kinsman, and G.P.L. Walker, 1966. Geology of the Faskrudsfjordur area, eastern Iceland. Soc. Sci. Islandica, Greinar 2, pp. 1-52.

Gordon, T.M. and H.J. Greenwood, 1971. The stability of grossularite in H_2O-CO_2 mixtures. Am. Mineral. 56, pp. 1674-1688.

Greenwood, H.J., 1967. Wollastonite: Stability in H_2O-CO_2 mixtures and occurrence in a contact metamorphic aureole near Salmo, British Columbia, Canada. Am. Mineral. 52, pp. 1669-1680.

Griggs, D.T., and J.H. Handin, 1960. Observations on fracture and a hypothesis of earthquakes, in Griggs, D.T. and Handin, J.H., eds., Rock deformation: Geol. Soc. Am. Mem. 79, pp. 347-364.

Gustafsson, W.L., 1971. Stability relations of andradite, hedenbergite, and related minerals in the system Ca-Fe-Si-O-H. Ph.D. thesis, University of California, Los Angeles.

Gustafsson, W.L., 1974. The stability of andradite, hedenbergite, and related minerals in the system Ca-Fe-Si-O-H. J. Petr., v. 15, pp. 455-496.

Haas, J.L. Jr., 1971. The effect of salinity on the maximum thermal gradient of a hydrothermal system at hydrostatic pressure. Econ. Geol., v. 66, pp. 940-946.

Hald, N., A. Noe-Nygaard, and A.K. Pedersen, 1971. The Króksfjordur central volcano in north-west Iceland. Acta. Nat. Isl., v. 2, no. 10, pp. 1-29.

Helgeson, H.C., J.M. Delany, H.W. Nesbitt, and V.K. Bird, 1978. Summary and critique of the thermodynamic Properties of rock forming minerals. Am. J. Sci. 278-A, pp. 1-229.

Humphris, S.E., and G. Thompson, 1978. Hydrothermal alteration of oceanic basalts by seawater. Geochim. et Cosmochim. Acta, v. 42, pp. 107-125.

Jakobsson, S.P., 1972. Chemistry and distribution pattern of Recent basaltic rocks in Iceland. Lithos, v. 5, pp. 365-386.

Jakobsson, S.P., 1979. Outline of the Petrology of Iceland, Jokull, special issue 29, Reykjavík, pp. 57-73.

Johannesson, H., 1975. Structure and petrochemistry of the Reykjadalur central volcano and the surrounding areas, midwest Iceland. Ph.D. thesis, Durham University, 273 p.

Jonsson, J., 1952. Forn thursabergslog í Hornafirdi, Natturufraedingurinn, v. 4, Reykjavík.

Jonsson, J., 1954. Hoffellssandur part I: Outline of the Geology of the Hornafjordur region. Geografiska Annaler, v. 1-2, pp. 146-161.

Jonsson, J., 1955. Hoffellssandur part II: Tillite in the basalt formation in east Iceland. Geografiska Annaler, v. 2-3, pp. 170-175.

Jonsson, J., 1978. Surtarbrandslogin vid Borgarstuf. Natturufraedingurinn, 48, v. 3-4, pp. 192-195.

Kristmannsdóttir, H., 1976. Types of clay minerals in hydrothermally altered basaltic rocks, Reykjanes, Iceland. Jökull, 26, pp 30-39.

Kristmannsdóttir, H., 1978. Ummyndun berggrunns á jarðhitasvæðinu Kröflu. Mimeogr. report to NEA, OSJHD 7854, 29 p. (in Icelandic).

Kristmannsdóttir, H. 1979. Alteration of basaltic rocks by hydrothermal activity at 100-300°C. International clay conference 1978. Ed. by Mortland and Farmer. Elsevier Sci. Publ. Company, Amsterdam 1979, pp. 359-367.

Kristmannsdóttir, H., 1981. Wollastonite from hydrothermally altered basaltic rocks in Iceland. Min. Mag.,.v. 44, pp. 95-99.

Kristmannsdóttir, H., 1983. Chemical evidence from Icelandic Geothermal Systems as compared to submarine Systems. NATO-ARC series, in print.

Kristmannsdóttir, H., and J. Tómasson, 1978. Zeolite zones in Geothermal areas in Iceland. Natural Zeolites. Occurrence, Properties, Use. (ed) Sand and Mumpton, Pergamon Press, Oxford and N.Y., pp. 277-288.

Kurshakova, L.D., 1971. Stability field of hedenbergite on the log f_{O_2}-T diagram. Geochemistry Internat. v. 5, pp. 340-349.

Lambert, R. St. J., 1965. The metamorphic facies concept. Min. Mag., v. 34, pp. 283-291.

Liou, J.G., 1970. Synthesis and stability relations of wairakite. $CaAlSi_4O_{12}\cdot 2H_2O$: Contr. Mineral. Petrol. v. 27, 259-282.

Liou, J.G., 1971 a. Synthesis and stability relations of prehnite $Ca_2Al_2Si_3O_{10}(OH)_2$. Am. Mineral. v. 56, pp. 507-531.

Liou, J.G., 1971 b. Stilbite-Laumontite equilibrium: Contr. Mineral. Petrol. v. 31, pp. 171-177.

Liou, J.G., 1971 c. P-T stabilities of laumontite, wairakite, lawsonite and related minerals in the system $CaAl_2Si_2O_8$-SiO_2-H_2O. J. Petr. v. 12, no. 2, pp. 379-411.

Liou, J.G., 1971 d. Analcime equilibria. Lithos 4, pp. 389-402.

Liou, J.G., 1973. Synthesis and stability relations of epidote, $Ca_2AlFeSi_3O_{12}(OH)$. J. Petr., v. 14, no. 3, pp. 381-413.

Liou, J.G., 1974. Stability relations of andradite-quartz in the system Ca-Fe-Si-O-H. Am. Mineral. 59, pp. 1016-1025.

Liou, J.G., 1979. Zeolite facies metamorphism of basaltic rocks from the East Taiwan Ophiolite. Am. Mineral. 64, pp. 1-14.

Mahon, W.A.J., 1966. Silica in hot water discharged from drillholes at Wairakei. New Zealand. N.Z. J. Sci. 9, pp. 135-144.

McDougall, I., N.D. Watkins, and L. Kristjánsson, 1976. Geochronology and palaeomagnetism of a Miocene-Pliocene lava sequence at Bessastadaá, eastern Iceland. Am. J. Sci. 276, pp. 1078-1095.

Mehegan, J.M., P.T. Robinson and J.R. Delaney, 1982. Secondary Mineralization and Hydrothermal Alteration in the Reydarfjordur Drill Core, Eastern Iceland. Journ. of Geoph. Research, v.87, no B8, pp.6511-6524.

Mercado, S., 1969. Chemical changes in geothermal well M-20, Cerro Prieto, Mexico. Geol. Soc. Am. Bull., v. 80, pp. 2623-2629.

Newman, T.C., 1967. The geology of some igneous intrusions in the Hornafjordur region of S.E. Iceland. Ph.D. thesis, University of Manchester, 168 p.

Norton, J. and R. Knapp, 1977. Transport phenomena in hydrothermal systems: The nature of porosity. Am. J. Sci. 277, no. 8, pp. 913-936.

Ólafsson, J., and J.P. Riley, 1978. Geochemical studies on the thermal brine from Reykjanes (Iceland). Chemical Geology, 21, pp. 219-237.

Pálmason, G., S. Arnórsson, I.B. Fridleifsson, H. Kristmannsdóttir, K. Saemundsson, V. Stefánsson, B. Steingrímsson, J. Tómasson and L. Kristjánsson: The Iceland crust: Evidence from drillhole data on structure and processes. In: Deep Drilling Results in the Atlantic Ocean: Ocean Crust. Ed: M. Talwani, C.G. Harrison and D.E. Hayes. Maurice Ewing Series 2, p. 43-65, Am. Geophys. Union, 1979.

Palmer, T.D., 1975. Characteristics of geothermal wells located in the Salton Sea geothermal field, Imperial County, California. Univ. Calif. Livermore Rep. 51976, 54 p.

Phillips, W.J., 1974. The dynamic emplacement of cone sheets. Tectonoph. 24, pp. 69-84.

Price, N.J., 1966. Fault and Joint Development in Brittle and Semi-brittle Rock. Pergamon Press, Oxford, 176 p.

Robson, G.R. and K.G. Barr, 1964. The effect of stress on faulting and minor intrusions in the vicinity of a magma body. Bull. Volcanol., 27, pp. 315-330.

Ross, J.G., and A.E. Musset, 1976. $^{40}Ar/^{39}Ar$ dates for spreading rates in eastern Iceland. Nature, v. 259, pp. 36-38.

Rutten, M.G., and H. Wensik, 1960. Structure of the central graben of Iceland. Int. Geol. Cong. XXI, Session: Norden Part XVIII, pp. 81-88.

Rybach, L. 1981. Geothermal Systems, Conductive Heat Flow, Geothermal Anomalies, pp. 3-36. In Geothermal Systems: Principles and Case Histories, Ed. Rybach and Muffler, John Wiley & Sons, 359 p.

Saemundsson, K., 1974. Evolution of the axial rifting zone in northern Iceland and the Tjornes fracture zone. Geol. Soc. Am. Bull., v. 85, pp. 495-504.

Saemundsson, K., 1979. Outline of the Geology of Iceland. Jokull, special issue 29, Reykjavík, pp. 7-28.

Schilling, J.G., 1973. Iceland mantle plume : Geochemical study of the Reykjanes Ridge. Nature, v. 242, pp. 565-571.

Schwarzbach, M., 1955. Allgemeiner Überblick der Klimageschichte Islands. Neu. Jahrb. Geol. Paläontol. v. 3, pp. 97-130.

Schwarzbach, M. and H.D. Pflug, 1957. Das Klima des jüngeren Tertiärs in Island. Neu. Jahnb. Geol. Paläontol. Abh. 104.3. pp. 279-298.

Scholz, C.H., L.R. Sykes and Y.P. Aggarwal, 1973. Earthquake prediction: a physical basis. Science, 181, pp. 803-810.

Schubert, G., and J.M. Strauss, 1977. Two phase convection in a porous media. J. Geophys. Res. 82, pp. 3411-3421.

Secor, Jr., D.T., 1965. Role of Fluid Pressure in Jointing. Am. J. Sci. 263, pp. 633-646.

Seyfried, W. and J.L. Bischoff, 1977. Hydrothermal transport of heavy metals by seawater: the role of seawater/basalt ratios. Earth and Planetary Sci. Lett., 34, pp. 71-77.

Seyfried, W., and J.L. Bischoff, 1981. Experimental seawater-basalt interaction at 300°C , 500 bars. Chemical exchange, secondary mineral formation and implications for the transport of heavy metals. Geochim. Cosmochim. Acta, v. 45, pp. 135-147.

Shimizu, M. and J.T. Hyama, 1982. Zinc-Lead Skarn Deposits of the Nakatatsu Mine, Central Japan. Econ. Geol. v. 77, no. 4, pp. 1000-1012.

Sibson, R.H., J. McM. Moore and A.H. Rankin, 1975. Seismic pumping - a hydrothermal fluid transport mechanism. J. Geol. Soc. London, 131, pp. 653-659.

Sigurdsson, H., 1966. Geology of the Setberg area, Snaefellsnes, western Iceland. Soc. Sci. Islandica, Greinar 4, no. 2, p. 53-125.

Sigvaldason, G.E., 1974. Basalt from the centre of the assumed Icelandic mantle plume. J. Petr., v. 15, pp. 497-524.

Símonarson, L.A., 1979. On Climatic changes in Iceland. Jökull, special issue 29, Reykjavík, pp. 44-46.

Sourirajan, S. and G.C. Kennedy, 1962. The system H_2O-NaCl at elevated temperatures and pressures. Am. J. Sci. 260, pp. 115-141.

Statham, P.J., 1975. Quantitative "X"-ray energy spectrometry: The application of a Si(Li) detector to microprobe analysis. Unpubl. Ph.D. thesis, University of Cambridge.

Stefánsson, V. 1981. The Krafla geothermal field, Northeast Iceland. pp. 273-294. In Geothermal Systems: Principles and Case Histories. Ed. by Rybach and Muffler, John Wiley & Sons, 359 p.

Stefánsson, V. and S. Björnsson, 1982. Physical aspects of Hydrothermal Systems. In: Continental and Oceanic rifts. Geodynamic Series, v. 8, pp. 123-145. Am. Physical Union.

Stefánsson, V., A. Gudmundsson, B. Steingrímsson, G.K. Halldorsson, H. Armannsson, H. Franzson and T. Hauksson, 1982. Krafla - Hola KJ-14, borun, rannsóknir og vinnslueiginleikar. OS82061/JHD 09, 119 p. (in Icelandic).

Steinthorsson, S. and A.E. Sveinbjörnsdóttir, 1981. Opaque minerals in geothermal well no. 7, Krafla, Northern Iceland. Journal of Volcanology and Georhermal Research, 10, pp. 245-261.

Taylor, B.E. and J.G. Liou, 1978. The low temperature stability of andradite in C-O-H fluids. Am. Mineral. 63, pp. 378-393.

Taylor, Jr., H.P., 1974. Application of oxygen and hydrogen isotope studies to problems of hydrothermal alteration and ore deposition. Econ. Geol. v. 69, pp. 843-883.

Taylor, Jr., H.P., 1977. Water/rock interactions and the origin of H_2O in granitic batholiths. Jour. Geol. Soc. 133, pp. 509-558.

Thompson, A.B., 1970. Laumontite equilibria and the zeolite facies. Am. J. Sci. 269, pp. 267-275.

Thompson, A.B., 1971 a. P_{CO_2} in low-grade metamorphism; zeolite; carbonate; clay minerals; prehnite relations in the system: $CaO-Al_2O_5-SiO_2-CO_2-H_2O$. Contrib. Mineral. Petrol., v. 23, pp. 145-161.

Thompson, A.B., 1971 b. Analcime-albite equilibria at low-temperatures. Am. J. Sci. 271, pp. 79-92.

Thorarinsson, S., 1952. Ritstjórnarrabb (Editorial note). Natturu-fraedingurinn, v. 4, Reykjavík.

Tomasson, J. and H. Kristmannsdóttir, 1972. High Temperature Alteration Minerals and Thermal Brines, Reykjanes, Iceland. Contrib. Mineral. Petrol. 36, pp. 123-134.

Torfason, H., 1979. Investigations to the Structure of South-East Iceland. Ph.D. thesis, University of Liverpool, 568 p.

Toulmin, III, P., and S.P. Clark, Jr., 1967. Thermal aspects of ore formation, pp. 437-464. In Geochemistry of Hydrothermal Ore Deposits, ed. H.L. Barnes; Holt, Rhinehart and Winston, Inc., New York, 670 p.

Truesdell, A.H., and D.E. White, 1973. Production of superheated steam from vapour-dominated geothermal reservoirs. Geothermics 2, pp. 154-175.

Turner, F.J., 1981. Metamorphic petrology, mineralogical, field and tectonic aspects. 2nd edition, Hemisphere Publishing corporation, Washington, 1981.

Van Bemmelen, R.W. and M.G. Rutten, 1955. Tablemountains of Northern Iceland. Leiden, 217 p.

Viereck, L.G., B.J. Griffin, H-U. Schmincke, and R.G. Pritchard, 1982. Volcaniclastic Rocks of the Reydarfjordur Drill Hole, Eastern Iceland 2. Alteration. Journ. of Geoph. Research, v. 87, no B8, pp. 6459-6476.

Walker, G.P.L., 1959. Geology of the Reydarfjordur Area, eastern Iceland. J. Geol. Soc. London, 114, pp. 367-393.

Walker, G.P.L., 1960. Zeolite zones and dike distribution in relation to the structure of the basalts of Eastern Iceland. J. Geol. 68, pp. 5.5-528.

Walker, G.P.L., 1963. The Breiddalur Central volcano. E. Iceland. Q.J. G.S., London, v. 119, pp. 29-63.

Walker, G.P.L., 1964. Geological investigation in Eastern Iceland. Bull. Volc., v. 27, pp. 3-15.

Walker, G.P.L., 1974. The structure of Eastern Iceland, pp. 177-188. In Geodynamics of Iceland and the North Atlantic area: ed: Kristjánsson, L., D. Reidel, Amsterdam.

Walker, G.P.L., 1975 a. A new concept of the evolution of the British Tertiary intrusive centres. J. Geol. Soc. London, 131, pp. 121--141.

Walker, G.P.L., 1975 b. Intrusive sheet swarms and the identity of Crustal Layer 3 in Iceland. J. Geol. Soc. London, 131, p. 143-161.

Walker, G.P.L., 1975 c. Excess spreading axes and spreading rate in Iceland. Nature, v. 255, pp. 468-471.

Walker, G.P.L., and D.H. Blake, 1966. The formation of a palagonite breccia mass beneath a valley glacier in Iceland. J. Geol. Soc., London, 122, pp. 45-61.

Ward, P.L., 1971. New interpretation of the geology of Iceland. Geol. Soc. Am. Bull., v. 82, pp. 2991-3012.

Watkins, N.D., L. Kristjánsson and I. McDougall, 1975. A detailed paleomagnetic survey of the type location for the Gilsá geomagnetic polarity event. Earth and Planetary Sci. Lett., 27, pp. 436-444.

Watkins, N.D. and G.P.L. Walker, 1977. Magnetostratigraphy of eastern Iceland. Am. J. Sci. 277, pp. 513-584.

Whitcomb., J.A., J.D. Garmany, and D.L. Anderson, 1973. Earthquake prediction: variation of seismic velocities before the San Fernando earthquake. Science, 180, pp. 632-641.

White, D.E., 1957 a. Thermal waters of volcanic origin. Geol. Soc. Am. Bull., v. 68, pp. 1637-1658.

White, D.E., 1957 b. Magmatic, connate, and metamorphic waters, Geol. Soc. Am. Bull., v. 68, pp. 1659-1682.

White, D.E., 1973. Characteristics of Geothermal Resources, pp. 69-94. In: Geothermal Energy, Resources, Production, Stimulations, ed. P. Krüger and C. Otte, Stanford University Press, Stanford, California.

White, D.E., 1974. Diverse origin of hydrothermal ore fluids. Econ. Geol., v. 6, pp. 954-973.

White, D.E., L.J.P. Muffler and A.H. Truesdell, 1971. Vapour-dominated hydrothermal systems compared with hot-water systems. Econ. Geol., v. 66, pp. 75-97.

White, D.E. and M. Guffianti, 1979. Geothermal systems and their energy resources. Reviews Geophysics and Space Physics 17, no. 4, pp. 887-902.

GEOLOGICAL MAP OF THE GEITAFELL CENTRAL VOLCANO

Southeast Iceland

By Guðmundur Ómar Friðleifsson
1978 & 1979

Partly based on maps from
Annels (1967) & Newman (1967)

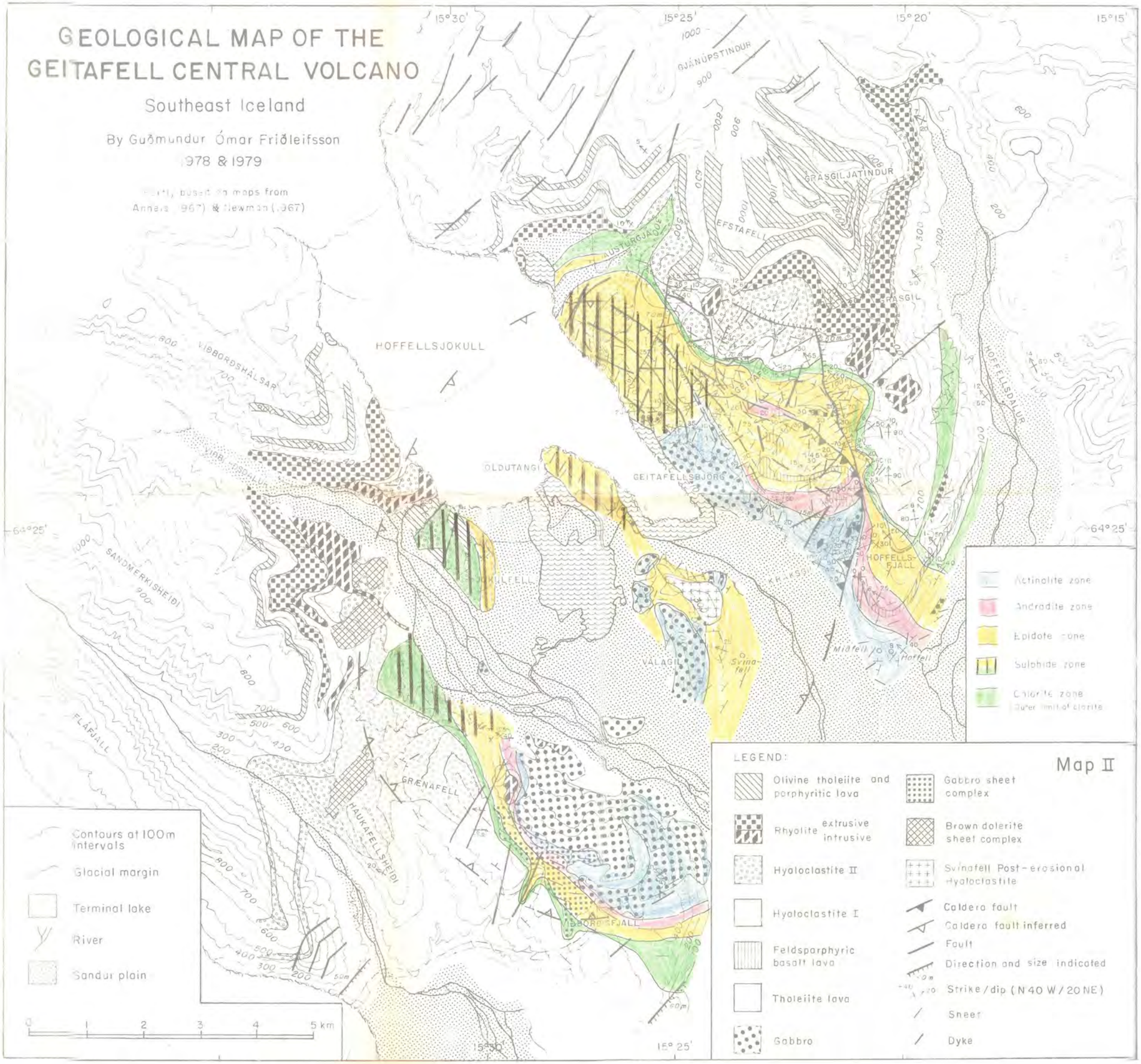

GEOLOGICAL MAP OF THE GEITAFELL CENTRAL VOLCANO

Southeast Iceland

By Guðmundur Ómar Friðleifsson

1978 & 1979

Partly based on maps from
Annels (1967) & Newman (1967)

MAP I

LEGEND:

- Olivine tholeiite and porphyritic lava
- Rhyolite extrusive / intrusive
- Hyaloclastite II
- Hyaloclastite I
- Feldsparphyric basalt lava
- Tholeiite lava
- Gabbro
- Gabbro sheet complex
- Brown dolerite sheet complex
- Svínafell Post-erosional Hyaloclastite
- Caldera fault
- Caldera fault inferred
- Fault
- Direction and size indicated
- Strike/dip (N 40 W / 20 NE)
- Sheet
- Dyke
- LINE OF SECTION

- Contours at 100m intervals
- Glacial margin
- Terminal lake
- River
- Sandur plain

0 1 2 3 4 5 km

15°30' 15°25' 15°20' 15°15' 64°25'